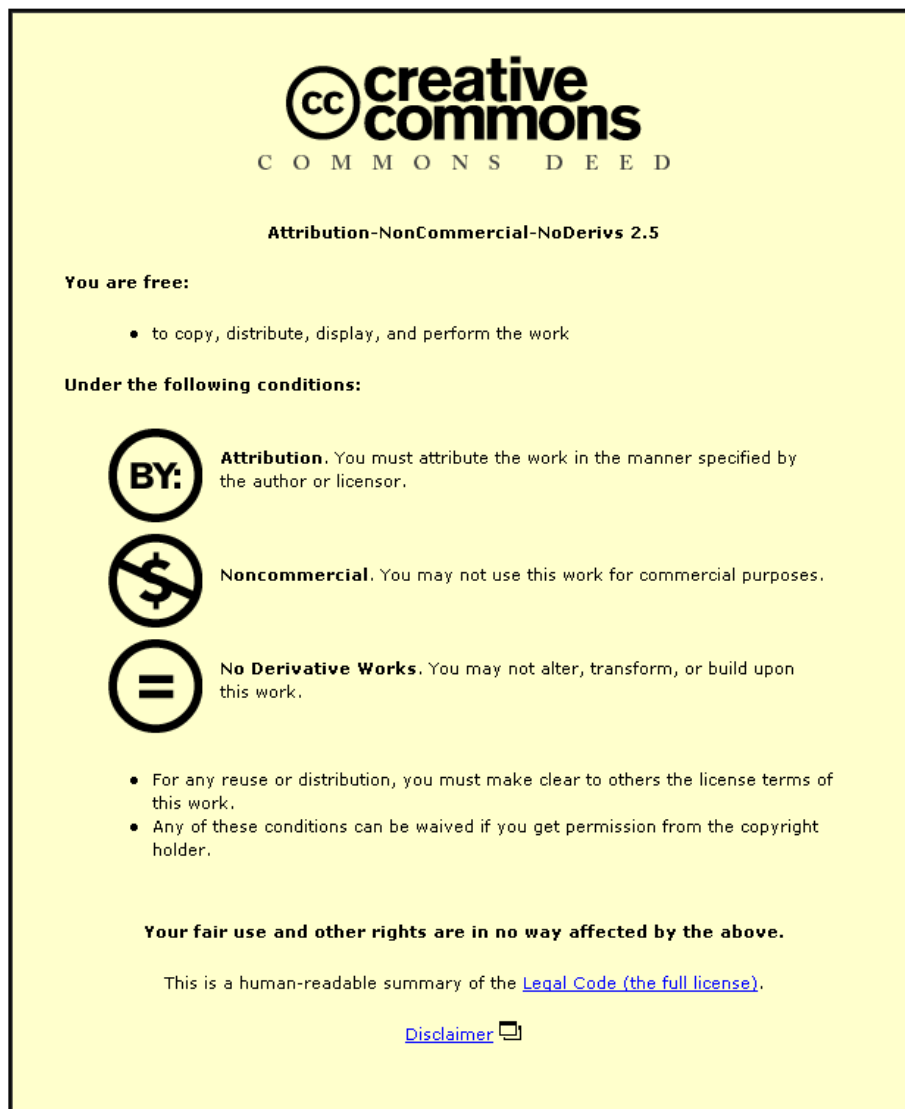


This item was submitted to Loughborough University as a PhD thesis by the author and is made available in the Institutional Repository (<https://dspace.lboro.ac.uk/>) under the following Creative Commons Licence conditions.



For the full text of this licence, please go to:
<http://creativecommons.org/licenses/by-nc-nd/2.5/>



Pilkington Library

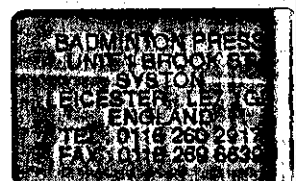
Author/Filing Title COTTAM

Vol. No. Class Mark T

**Please note that fines are charged on ALL
overdue items.**

LOAN COPY

0402086449



TEA CO₂-Laser Treatment of Coated and Corroded Metals

by

Christopher Andrew Cottam

A Doctoral Thesis

Submitted in partial fulfilment of the requirements for the award of Doctor
of Philosophy at Loughborough University

August 1998

© by C. A. Cottam 1998

 Loughborough University Physical Library
Date Jy 99
Class
Acc No. Q40 208644

K2644306

Acknowledgements

I would like to thank all the people at Loughborough University physics department who have provided a warm and friendly environment in which to complete my studies.

Special thanks go to the members, past and present, of the optoelectronics department, who added colour to even the greyist of days.

Special thanks also go to my supervisor, David Emmony, for providing me with the opportunity to enter a unique and interesting field of research.

I would also like to acknowledge the contribution made by the National Museums and Galleries on Merseyside in sponsoring and supporting the project.

The contributions of Gary Critchlow and Ana Cuesta merit special attention and it has been a great pleasure to collaborate with two such gifted scientists.

Finally, I would like to acknowledge the support provided by the technicians without which this project would not have been possible. In particular, John Oakley has been essential to this project and never failed to meet an unreasonable deadline!

Abstract

A selection of corroded, painted and lacquered metals have been subjected to high-powered, pulsed TEA CO₂-laser radiation to investigate self-limiting cleaning and treatment processes. Changes in the surface chemistry were observed and recorded using a variety of surface analysis techniques including X-ray Powder Diffraction, Auger Electron Spectroscopy and X-ray Photoelectron Spectroscopy. Changes in surface appearance were recorded using colour macro-photography and Scanning Electron Microscopy. The effects of both plasma and sub-plasma laser fluences were investigated.

Results from naturally and artificially corroded metals show that the ability of the laser to remove or modify corrosion products depends upon their precise composition. All paints and lacquers tested were susceptible to ablation at sub-plasma fluences. Aged paints, resilient to removal by volatile solvents, could also be removed by the laser. Modification of metal surfaces at plasma fluences produced a significant increase in the bond durability of adhered metal coupons.

The potential for the laser to be used in the fields of sculpture conservation, industrial paint removal, and metal adhesion pretreatments are discussed and conclusions presented.

TEA CO₂-Laser Treatment of Coated and Corroded Metals

Contents

Introduction

Chapter 1: Corrosion and Conservation of Metals

Introduction	i
1.1 General Metallurgy	1
1.1.1 Atomic structures of metals	2
1.1.2 Micro-structures of metals	3
1.1.3 Alloy structures	5
1.1.4 Corroded micro-structures	9
1.1.5 Optical properties of metals	10
1.2 Metals in Sculpture, Historical Artifacts and Modern Industry	14
1.2.1 Introduction	14
1.2.2 Cast metals	14
1.2.3 Worked metals	19
1.2.4 Present day metals and alloys	20
1.3 Corrosion and Patination	22
1.3.1 The corrosion process	23
1.3.2 Factors affecting metal corrosion	26
1.3.3 Species of corrosion product	30
1.3.4 The value of corrosion	39

1.4	Organic Coatings	43
	1.4.1 Constituents of organic coatings	43
	1.4.2 Types of organic coatings	44
	1.4.3 Methods of protection	46
	1.4.4 Deterioration of coatings	46
	1.4.5 Removal of organic coatings	48
	1.4.6 Accelerated ageing techniques	49
1.5	Metal Conservation	49
	1.5.1 Large, outdoor sculpture	50
	1.5.2 Small, metal artefacts	51
	1.5.3 Patina stabilisation	53
	1.5.4 Re-patination	54
	Summary	55
	References	56

Chapter 2: CO₂-Laser Cleaning Methodology and Monitoring

2.1	Laser Cleaning	60
	2.1.1 Principles of TEA CO ₂ -lasers	61
	2.1.2 Laser interaction with materials	62
	2.1.3 Factors affecting ablation characteristics	64
	2.1.4 Plasma/sub-plasma cleaning effects	68
	2.1.4.1 Temporal beam profile (TBP) measurements	70
	2.1.5 Beam delivery	72
	2.1.6 The CO ₂ -laser cleaning system	74

2.2	Surface Chemistry Analysis	75
2.2.1	X-ray powder diffraction analysis (XRD)	75
2.2.2	X-ray photoelectron spectroscopy (XPS)	80
2.2.3	Auger electron spectroscopy (AES)	81
2.2.4	Contact angles	83
2.3	Surface Topographical Analysis	85
2.3.1	Colour photography	85
2.3.2	Embedded cross-section	85
2.3.3	Scanning electron microscopy (SEM)	87
2.4	In-line Laser Observations	87
2.4.1	Surface temperature measurement	87
2.4.1.1	Bulk temperature measurement during ablation	90
2.4.2	In-line laser induced breakdown spectroscopy (LIBS)	95
2.4.3	Acoustic monitoring	97
	Summary	100
	References	101
	Colour Photographs	103

Chapter 3: Sub-plasma Laser Cleaning and Treatment

3.1	Artificially patinated samples	104
3.1.1	Experimental	105
3.1.2	Case 1a	108
3.1.3	Case 2a	109
3.1.4	Case 3a	111
3.1.5	Case 4a	113
3.1.6	Case 5a	114
3.1.7	Case 6a	115
3.1.8	Case 7a	117
3.1.9	Case 8a	119
3.1.10	Case 9a	122
3.2	Naturally Patinated Samples	124
3.2.1	Case 1n	124
3.2.2	Case 2n	128
3.2.3	Case 3n	130
3.2.4	Case 4n	134
3.2.5	Case 5n	137
3.2.6	Case 6n	138
3.2.7	Case 7n	139
3.2.8	Case 8n	141
3.2.9	Summary of results	142
3.3	Organic Coatings	148
3.3.1	Fresh paint	148
3.3.2	Fresh lacquers	150
3.3.3	Aged and weathered coatings	151

3.3.4 Residual layers	158
References	161
Colour Photographs	163
 Chapter 4: Plasma Laser Cleaning and Treatment	
4.1 Plasma effects	175
4.1.1 Plasma cleaning mechanisms	175
4.1.2 Initiating and sustaining plasma	176
4.1.3 Plasma observations	179
4.1.4 Plasma cleaning	180
 4.2 Cleaning and adhesion	 184
4.2.1 Aluminium	186
4.2.2 Steel	192
4.2.3 Hot-dip Galvanised (HDG) mild steel	197
4.2.4 Summary of results	202
 References	 204
 SEM Micrographs	 206

Chapter 5: Conclusions and Further Work

5.1	Conclusions	209
	5.1.1 Metals without a coating	209
	5.1.2 Metals with inorganic coatings	211
	5.1.3 Metals with organic coatings	216
5.2	Further Work	217
5.3	Laser Safety	219
	References	221
	Appendices	222

Introduction

The ability of high-powered laser radiation to alter solid surfaces has been known since the first high-powered lasers were produced. This property has been exploited in many areas of surface cleaning and surface treatment. This thesis explores two areas of TEA CO₂-laser treatment that have thus far received little attention:

- The laser cleaning and treatment of coated and corroded metals at sub-plasma fluences, eg for the cleaning of metal sculpture.
- The laser cleaning and treatment of metals at plasma-fluences, e.g. for adhesive pretreatments.

The use of lasers in the cleaning of sculpture and objects of historical and cultural interest has grown in popularity over recent years. When conditions are favourable, the laser may remove dirt and detritus from a target without damaging or altering the underlying material, thus offering a worthwhile improvement on conventional cleaning techniques. Whilst lasers have gained acceptance in the cleaning and treatment of materials such as stone and paper, there remains much work to be done in the area of metals. This thesis looks at the potential of TEA CO₂-lasers to clean and treat corroded and coated metals, and assesses the value of the laser as a conservation tool.

The growing concerns over recent years as to the environmental impact of volatile solvents has provided industry with a strong impetus to develop environmentally-friendly methods of cleaning metal surfaces. A field where surface cleanliness is of considerable importance is in metal adhesion where large amounts of volatile solvents are required to degrease the surface of the metal adherends. This thesis shows that using the TEA CO₂-laser at plasma fluences offers an effective and environmentally-friendly alternative to volatile solvents to clean the surface of metal adherends.

In writing-up this thesis, it was considered to be most effective to keep the results as a collection of case studies and present them in Chapters Three and Four, for targets

treated below and above the plasma fluence respectively. This left Chapters One and Two for an introduction and overview of the methodology employed, and Chapter Five for conclusions and further work. Additional details are given below:

Chapter One: 'Corrosion and Conservation of Metals' provides a detailed introduction to metallurgy and both organic and inorganic coatings that exist on old and new metals. A review of existing conservation methods and objectives are described together with the shortfalls that still exist in modern techniques. A large proportion of this chapter is devoted to the complex field of metal corrosion, its causes and its consequences. The optical properties of metals is also explored with reference to why the TEA CO₂-laser was considered the most appropriate in this field.

Chapter Two: 'CO₂-Laser Cleaning Methodology and Monitoring' describes how the laser was applied to clean and treat the target surfaces. The difference between using the laser at plasma and at sub-plasma fluences is investigated. Various methods of surface analysis are explained and demonstrated to provide a scientific basis on which to assess the laser treatment results. In-line surface monitoring experiments are described that provide the user with instant feed-back as to how the laser treatment is proceeding.

Chapter Three: 'Sub-plasma Laser Cleaning and Treatment' presents the empirical data obtained from the laser treatment of a wide variety of metal systems. Artificially patinated, naturally patinated and metals with organic coatings were used as target materials to explore the effect that sub-plasma fluences had on them. Where possible, targets were chosen or created that were directly applicable to problem areas of metal conservation. Results were obtained using the surface analysis methods described in Chapter Two. A summary of results is presented at the end that phenomenologically classifies the effects of the laser into five categories.

Chapter Four: 'Plasma Laser Cleaning and Treatment' explores the application of the laser, when used above the plasma fluence, to metal cleaning and adhesive pretreatments. Three different metal targets are considered, and a comparative study is

carried out on each such that the laser treatment can be assessed in relation to their respective conventional surface pretreatments.

Chapter Five: 'Conclusion and Further Work' offers conclusions that encompass the results presented in Chapters Two, Three and Four. The laser is assessed in terms of its potential to be used in the specific areas of metal sculpture conservation and metal adhesive pretreatment, as well as its effect on metals systems in general. Some ideas for further work that could be beneficial in this area are also forwarded. Finally, some basic safety considerations are described that have been encountered over the duration of this work.

CHAPTER 1

Corrosion and Conservation of Metals

Introduction

This chapter reviews the three basic physical components of sculpture and manufactured metal objects; the metal or alloy from which it is made; the inorganic layers of corrosion or patination; and the possible presence of organic layers applied for protection or decoration. An introduction is given to the various contemporary attitudes and practices in metal conservation and some of the limitations of modern and conventional methods are described. Deterioration of both modern and historic objects are considered. The scope of study is far broader than detailed here as omissions have had to be made for the sake of brevity.

Metal conservation requires considerable knowledge of the physical and chemical processes behind corrosive systems and also an understanding of aesthetics and artistic integrity. It is immediately apparent that the conservator has three fundamental problems: (i) corrosion processes are not fully understood and existing models can be simplistic and unreliable, (ii) aesthetic qualities are largely subjective; varying with time, culture and the personal tastes of the observer and (iii) where they conflict, resolving whether aesthetics or preservation of the object takes precedence in deciding the most effective form of treatment.

1.1 General Metallurgy

"Metallurgy is one of the oldest of the arts, but one of the youngest of sciences",^[1]

What is a metal?

Metals can be defined as elements with atomic electrical conductivities (i.e. for one mole of atoms) greater than $3 \times 10^{-4} \text{ohm}^{-1} \text{cm}^{-4}$ whose electrical conductivities decrease with increasing temperature^[2]. This reveals little about the common properties of metals, however, which go far beyond simply having good electrical conductivities.

1.1.1 Atomic structure of metals

Metals have metallic-bonded crystal structures, the atoms forming a crystal lattice which is, in the classical model, suffused by a 'cloud' of delocalised electrons. The high electrical conductivities of metals can be assigned to the delocalised nature of the electrons. The various crystal structures, as shown in *Fig.1.1.1a*, can be hexagonal close-packed (e.g. magnesium or zinc), face-centred cubic (e.g. aluminium, nickel, copper and lead) or body-centred cubic (e.g. sodium and chromium). Such structures have a high coordination number of 8 (body-centered cubic) or 12 (hexagonal close-packed and face-centered cubic).

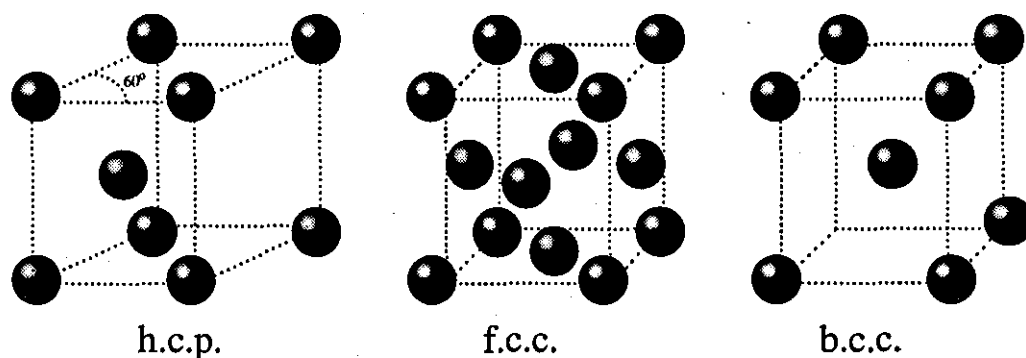


Fig. 1.1.1a: Lattice structures for metal crystals can be hexagonal close-packed (h.c.p.), face-centered cubic (f.c.p.) or body-centered cubic (b.c.p.).

1.1.2 Micro-structure of metals

Apart from having an atomic crystalline structure, metals also form a micro-structure that evolves during solidification and can influence its physical and chemical properties significantly.

Metal solidification is not an instantaneous process and will be initiated at various 'nucleation' sites within a melt as it cools. These sites are produced by the random movement of atoms which form clusters that have crystalline order and become stable when the temperature drops below the melting point. Once stable nuclei form in a liquid their growth is fuelled by atoms from the surrounding liquid.

Dendrites

Each nucleation site acts as a seed for dendritic (a Greek word meaning 'treelike') growth that tends to follow directions determined by the structure of the unit cell, for example, f.c.c and b.c.c. crystals tend to form branches at right-angles to each other as shown in *Fig. 1.1.2a*.

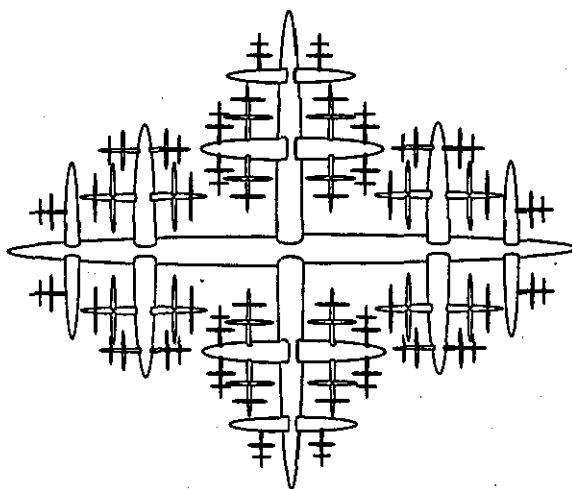


Fig. 1.1.2a: Dendritic growth during metal solidification.

Grains

Grain boundaries are formed at the intersection of colliding dendritic growths; thus the faster the cooling rate, the greater the density of nucleation sites, and the smaller the grain size^[3]. Although often referred to within the context of the microstructure of the metal, grains can sometimes be seen with the naked eye and may even form as large as a few centimetres across. Under controlled conditions, it is possible to form single crystal solids by only allowing one nucleus to grow. Small grains contribute to the hardness of the metal, a fact exploited by using a 'chill' mould shown in *Fig. 1.1.2b*.

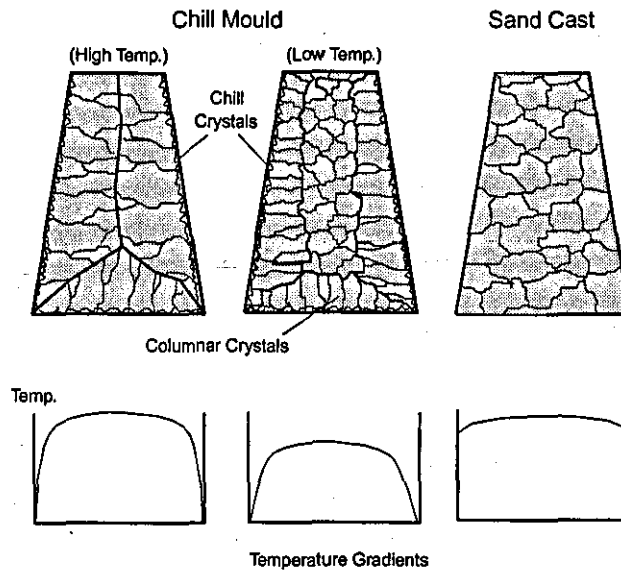


Fig. 1.1.2b: The effect of mould design on crystal formation in casting. The graphs show the temperature distribution through a cross-section of the above melts.

Polymorphism

Some metals adopt different crystal structures depending on the temperature they are exposed to; a phenomena known as 'polymorphism'. For example, polymorphism is exhibited by iron which is b.c.c. below 910°C (α -Fe), f.c.c. between 910 °C and 1400°C (γ -Fe), and reverts back to b.c.c. above 1400°C (δ -Fe).

1.1.3 Alloy structures

An alloy is a mixture of two or more elements, the principal components being metals, such that the resultant mixture exhibits metallic properties. Alloying can be used to greatly alter the mechanical and physical properties of metals and most commercially available metals are alloyed to some degree. The micro-structures of alloys can be far more complicated than those of pure metals.

Phase mixtures

Unlike pure metals, alloys freeze over a range of temperatures and progress from a liquid state, through a liquid + solid state, to a solid state. Phase diagrams (e.g. *Fig 1.1.3a*) are used to describe the solidification of binary alloys and show how the liquid/solid composition varies throughout the process.

Solid-solutions

If the constituents of an alloy are chemically indifferent to each other and the alloy is cooled slowly, the melt forms a solid-solution in which the crystal structure is identical to that of the parent metal. In a substitutional solid-solution the alloying metal (the solute) atoms take the place of the parent metal (the solvent) atoms in the crystal lattice (e.g. brass). In an interstitial solid-solution the alloying metal atoms can fit in between the spaces in the crystalline lattice of the parent metal without altering its structure (e.g. steel).

If the alloy is cooled quickly, dendritic growth can cause segregation due to the different melting points of the metal constituents. For example, an alloy melt cooled at a high rate consisting of copper (m.pt of 1356K) and nickel (m.pt of 1431K) would solidify by dendritic segregation as shown in *Fig.1.1.3a*. For composition C, solidification starts at T_1 and nickel-rich (due to its higher melting point) dendrites start to form of composition

a, leaving the remaining mixture with an increasing copper concentration. The composition of the solid and the liquid at a given temperature is given by the intersection of the isotherm with the solidus and liquidus lines respectively. As the melt cools to T_2 , the composition of liquid becomes *d* and that of the solid becomes *b*. In this way a 'coring' effect is produced where the cores of the dendrites are rich in the high-melting point metal and the outer parts are rich in the lower-melting point metal. When T_3 is reached, the remaining copper-rich mixture solidifies to form the inter-dendritic alloy of composition *e*.

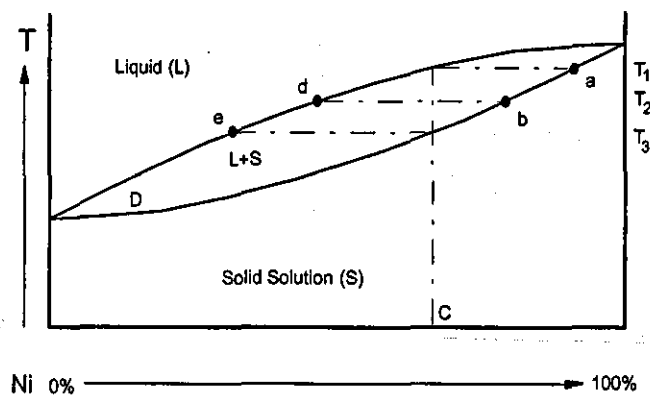


Fig. 1.1.3a: Dendritic segregation in rapidly cooled, Cu/Ni system.

Solid-state diffusion: the above example describes solidification for a rapidly cooled solid solution. If the solution is cooled slowly, the process of solid-state diffusion allows atom migration in the solid-state when near the melting point. This enables the melt to reach equilibrium and a homogenous solid is formed. For example, an alloy cast using a 'chill' mould will exhibit coring at the rapidly cooled outer surface, but a more homogenous interior as it cools more slowly.

No mutual solid solubility

Solid-solutions are uncommon; more often limited solid solubility is encountered and two-phase microstructures form of different crystalline structure. When completely

immiscible metals are alloyed they form a 'eutectic mixture' within which individual crystals of each metal occur in the form of plates, rods or particles. Within this mixture there may be pure grains of either alloying metal if either has been added in excess of the eutectic composition C as shown in *Fig. 1.1.3b*. As can be seen in the diagram, the lowest melting point is at C ('eutectic' comes from the Greek for 'easily melted') and is, for example, used to determine the ideal composition of solders.

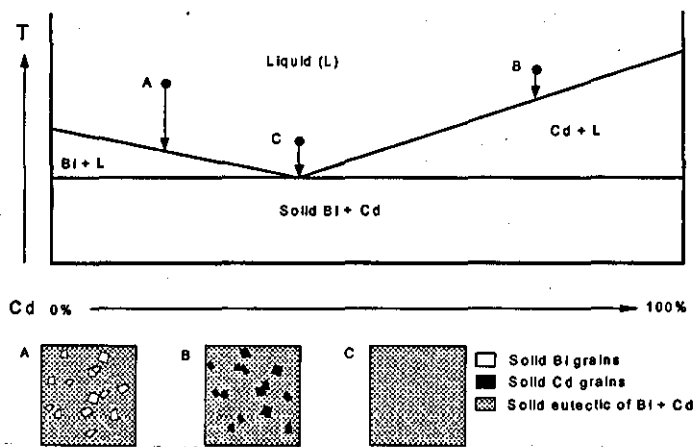


Fig. 1.1.3b: Eutectic mixtures in an immiscible Bismuth/Cadmium system.

Limited mutual solid solubility

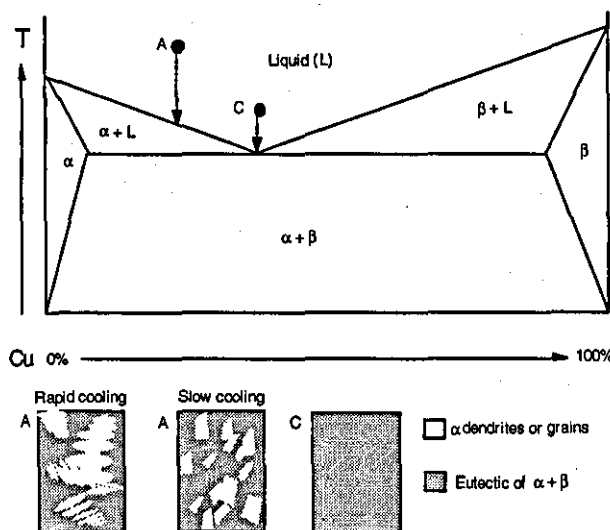


Fig. 1.1.3c: Dendritic and eutectic structures in metal solutions of limited mutual solubility

As can be expected, alloys of limited mutual solubility may contain a mixture of dendritic and eutectic structures as shown in *Fig. 1.1.3c*. Different phases are assigned a Greek-character prefix.

Other structures, that may depend on specific alloy composition or cooling factors, are briefly described below:

Eutectoid structures: for certain alloys, phase changes occur in an already existing solid solution to form eutectoid structures. For example, tin-bronze may form a delta phase of the inter-metallic compound $\text{Cu}_{31}\text{Sn}_8$. Eutectoid structures are important in determining the properties of steels. In this case, the eutectoid is formed when the gamma phase solid solution (austenite) decomposes at 727°C to form pearlite, a fine collection of plates of α -Fe (ferrite) and Fe_3C (cementite) phases, as shown in *Fig. 1.1.3d*.

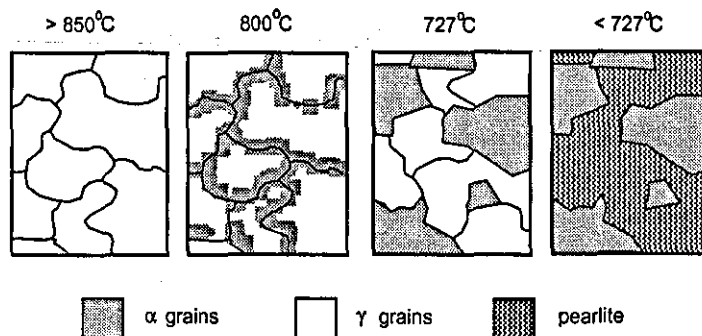


Fig. 1.1.3d: Phase structures in cooling steel.

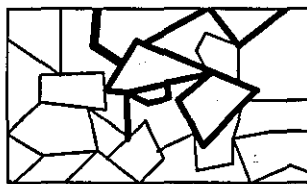
Peritectic structures: A liquid phase may react with a solid phase to form peritectic structures. Peritectic reactions may cause precipitation of a new phase within existing alpha grains or at grain boundaries, giving them rounded corners.

Martensite transformations: Martensite is a collection of fine intersecting needles that can form if an alloy is cooled very quickly.

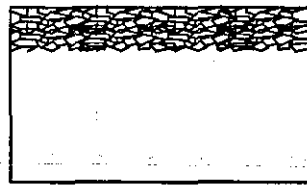
Widmanstaetten transformations: the precipitation of a solid phase at a high temperature decomposing at a lower temperature into two solid phases. This precipitation takes the form of plates or needles at the grain boundaries of the initial crystals.

1.1.4 Corroded micro-structures

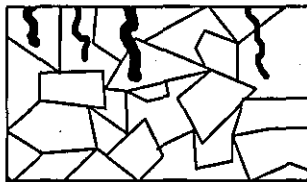
Metal microstructure can determine the nature of the corrosion processes at the surface of the metal and also how corrosion permeates into the bulk of the solid. Corrosion phenomena can be classified on this basis, as shown in *Fig. 1.1.4a*. For example, the grain boundaries may corrode preferentially by inter-granular corrosion, severely damaging the structural integrity of the metal whilst leaving the majority of the metal intact.



Inter-granular corrosion



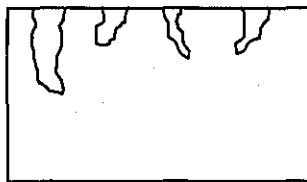
Uniform corrosion



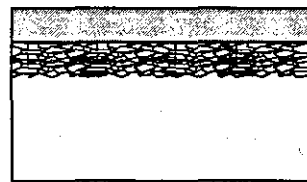
Intra-granular corrosion



Selective corrosion



Pitting corrosion



Corrosion products on surface

Fig. 1.1.4a: Examples of the microstructure of corroded metals.

1.1.5 Optical properties of metals

A thorough review of the optical properties of metals is required for this study to understand how the laser will interact with the metals studied. Classical electromagnetic theory provides a good basis for understanding the optical properties of solids. Not surprisingly, the electrical properties of a metal are closely related to its optical properties.

Skin depth: the skin depth (δ) of a metal is the distance over which the amplitude of an electromagnetic wave drops to $1/e^*$ of its value at the surface. We can derive *Eqn. 1.1*^[4]

$$\delta = 1/\alpha = (2/\omega\sigma\mu_0)^{0.5} \quad \text{Eqn. 1.1}$$

from Maxwell's equations which shows how skin depth is directly related to electrical conductivity (σ) and the frequency of incident radiation (ω); μ_0 is the permeability of free space and α is the absorption coefficient of the material. Hence, good electrical conductors are generally also highly opaque.

Plasma frequency: further manipulation of Maxwell's equations give relations between the extinction coefficient (κ), refractive index (n) and frequency of incident radiation (ω) as shown in *Eqn. 1.2* and *Eqn. 1.3*^[5].

$$n^2 - \kappa^2 = 1 - [\omega_p^2 / (\omega^2 + \tau^{-2})] \quad \text{Eqn 1.2}$$

and

$$2n\kappa = \omega_p^2 / [\omega\tau(\omega^2 + \tau^{-2})] \quad \text{Eqn 1.3}$$

where τ is the relaxation time, a constant for a given metal, and ω_p is the plasma frequency.

* e is the mathematical constant 2.718 (to three decimal places)

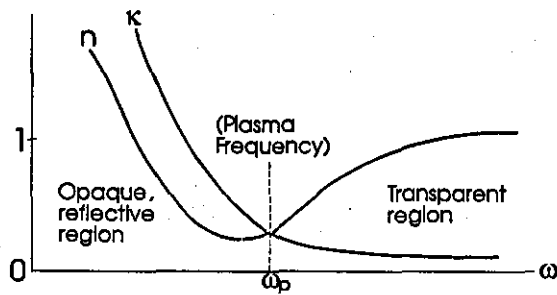


Fig. 1.1.5a: Index of refraction and extinction coefficient versus frequency for a metal.

The plasma frequency is essentially the frequency above which a metal becomes transparent, as shown in *Fig. 1.1.5a*, and can be determined, for good electrical conductors, from the equation^[6]

$$\omega_p = (Ne^2/m\epsilon_0)^{1/2} \quad \text{Eqn 1.4}$$

where N is the number of conduction electrons per unit volume, e the electron charge, m the electron mass and ϵ_0 the permittivity of free-space. Plasma frequencies for metals are typically found to be around 10^{15} s^{-1} , in the visible and near ultraviolet regions of the spectrum.

Metal	n	κ	R	R_{max}
Cu	12.8	64.0	0.984	0.9935
Ag	5.88	76.1	0.996	0.9953
Al	34.3	108	0.989	0.990
Au	8.57	75.9	0.994	0.994
Fe	7.60	27.0	0.962	-
Pb	22.3	38.5	0.956	-

Table 1.1: Calculated normal reflectance (R) for metals from n and κ values at $10.6\mu\text{m}$.

R_{max} is the maximum experimentally measured value.

Thus, metals are generally highly reflective in the infrared and have a low reflectivity in the ultraviolet. Qualitative agreement for these predictions of classical theory is particularly good for the better electrical conductors such as gold, silver and copper, as shown in *Table 1.1*^[7]. Determination of the plasma frequency of different metals allows us to predict how different types of laser radiation are likely to interact with them: heating effects from an ultraviolet laser beam incident on a metal surface will be more significant than by an otherwise identical infrared laser beam due to the decrease in reflectivity of metals in the UV region of the spectrum.

Factors affecting reflectance and absorptivity

The reflectance (R) of a metal can be approximated to^[5]:

$$R = [(1 - n)^2 + \kappa^2] / [(1+n)^2 + \kappa^2] \quad \text{Eqn 1.5}$$

In practice, metals rarely exhibit the reflectance values expressed in *Table 1.1* due to a variety of factors which influence the optical properties of a metallic surface as described below. It should be noted that an apparently small decrease in reflectance, for example, from 0.99 to 0.98, appears more significant when expressed in terms of the absorptivity ($A = 1-R$), which doubles from 0.01 to 0.02.

Surface temperature: A simple relationship can be derived for the increase in absorptivity (A) with temperature (T)^[8]:

$$A(T) = A_0 + A_1 T \quad \text{Eqn 1.6}$$

which is in good agreement with observations made on pure metals. The absorptivities of metals can double over an increase in temperature of a few hundred degrees.

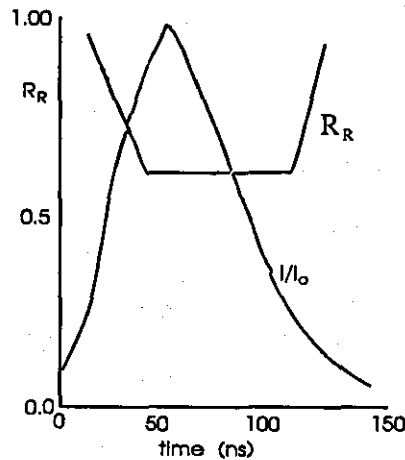


Fig. 1.1.5b: Temporal profile of normalised laser pulse (I/I_0) showing the variation in reflectivity during irradiation of prepared copper sample.

This effect is significant when treating metals with lasers, especially as the temperature at the surface can vary radically within the duration of each laser pulse, as shown in *Fig. 1.1.5b*^[7].

Surface roughness: the effect of surface roughness is to increase absorptivity by increasing the actual surface area irradiated by the beam and through causing multiple reflections in grooves and cracks. Extremely rough and complex surfaces are common on corroded metal substrates and can significantly affect their surface reflectivities. A simple expression for the estimation of reflectivity, R_r , for a surface with roughness δ , as compared with a hypothetically smooth surface, R_s , is given in *Eqn 1.7*^[9] for conditions where $\delta \ll \lambda$, the wavelength of incident radiation,

$$R_r = R_s \exp [-(4\pi\delta/\lambda)^2] \quad \text{Eqn 1.7}$$

This equation also shows how the shorter the wavelength of the incident radiation the more likely it is to be absorbed due to the extent of the surface roughness.

Impurities and oxidation: the exposure of metal surfaces to the atmosphere renders them susceptible to contamination by a variety of foreign bodies and to general oxidisation and

corrosion. The extent to which the absorptivity of the metal is increased by the presence of these species depends on their volume and optical properties.

Corrosion: prolonged exposure of metal surfaces to an aggressive environment (e.g. outside) can cause the formation of corrosion layers a few microns in thickness. Under such conditions, the optical properties of the metal can be completely shrouded by the corrosion layer which may entirely absorb the incident radiation.

1.2 Metals in Sculpture, Historical Artefacts and Modern Industry

1.2.1 Introduction

Casting is, and has always been, the most popular method for producing metal sculpture, although there are many examples of sculpture formed from metal sheet. Recent advances in metallurgy (aluminium was discovered as late as 1808 and commercial production was not until 1886), have resulted in over 20,000 alloys in present use. The metallurgy of a metal or alloy depends not only upon its composition, but also on the method of production. The properties of a cast metal will vary greatly from sheet metal.

1.2.2 Cast Metals

A brief history of copper alloys

Evidence for the smelting of copper has been dated as early as 7000BC from slags excavated from Southern Anatolia and consistent bronze production dates back as far as 2800BC in Egypt, India and Mesopotamia. Alloys of similar composition to modern gunmetals were being cast before 1000BC. Ancient Rome found many diverse applications for bronze, including cutlery, needles, jewellery, containers, coinage, knives, razors, tools, musical instruments and weaponry. Brass was not produced deliberately

until the Middle Ages due to the late discovery of zinc. Brass became particularly popular in Elizabethan times when it was exploited for its yellow coloration for purposes of ornamentation.

Casting was probably the first form of chemistry - the word chemistry is derived from the Greek 'chyma', meaning casting. Although casting techniques have a history of thousands of years, the most popular method, since it was first tried in ancient India and Egypt, has been that of lost-wax casting. Since then it has been used to create the great sculptures of the Shang, Chou and Han dynasties of China, of Nara and Mamakura in Japan, of Ife and Benin in Africa, of the Golden Age in Greece and Imperial Rome and of Renaissance Italy^[10]. Lost-wax casting is still the most popular form of casting today.

Lost-wax casting

"The skill of the Chinese bronze-worker in casting large quantities of metal is aptly illustrated by the Great Bell of Peking, reputed to weigh sixty-five tons. The bell was cast in the reign of Yung-Lo (1403-24), and it is related that the first attempts to cast it by the cannon-founder, Kuan Yu, were unsuccessful. One of Yung-lo's daughters, Ko-ia, sacrificed herself by throwing herself into the crucible just as the metal started to flow, leaving behind her shoe in the hand of an attendant who tried to restrain her. The bell was cast successfully, but when it was struck its deep note was followed by a wailing sound in which the word *hsieh* could be heard. It was Ko-ia wailing for her lost shoe."^[10]

The method of lost-wax casting does not produce a homogenous material, but one of varying constituency and grain structure on both macro and micro-scales due to the process of crystal growth in a mixture of metals during solidification. The precise composition of the alloy (very variable, especially in ancient bronzes) and the cooling conditions have a fundamental effect on the properties of the cast alloy. Although the Great Bell of Peking is an extreme example (see above), the composition of a given bronze, or any given alloy, may vary considerably. Varieties of composition may be deliberate, by means of following one of the hundreds of different alloying "recipes", or

simply by the addition of various scrap metals in times when following recipes was either too expensive, as yet unknown, or simply not bothered with. As a result, the metallurgist has to deal with alloys that vary in composition from piece to piece.

The composition of copper alloys

Sculpture is almost invariably cast in bronze, and it is for this reason that the majority of our attention shall be focused upon bronzes. The popular conception that bronze is an alloy of copper with tin is over-simplistic and, although these two metals are necessary ingredients, many more are normally present. A popular bronze used for casting sculpture, such as gun-metal bronze, may contain a cocktail of fourteen or more different ingredients (see Appendix C). Some of the more common metals found in copper alloys are described below.

Copper: although over 160 copper minerals are known, most are rare and almost all copper is extracted by smelting copper sulphide minerals. Copper is a soft metal and difficult to machine but readily forms alloys, the properties of which can be tailored to the requirements of the application to improve hardness and machinability^[11-15].

Tin: 'true' bronzes contain between 5-15% tin. Most ancient bronzes have less than 17% tin (the limit of the solubility of tin in copper-rich solid solution). A higher proportion of tin makes the bronze very difficult to work, although a high percentage of tin has been found in ancient bronzes to produce a 'white' bronze for mirrors (e.g. speculum contained up to 35% tin and was popular in Rome). The aptly named bell-metal (79%Cu, 21%Sn) has good sonorous properties.

Zinc: brass is a copper alloy with zinc as the secondary ingredient to form a hard and strong alloy. To form brass, zinc ore and copper ore are mixed and smelted together to avoid the loss of zinc, which boils at 907°C. There are basically three types of brasses (depending on the phase type): alpha-brasses with up to 35% zinc; alpha + beta brasses

with between 35% and 46.6% zinc; and beta-brasses with between 46.6% and 50.6% zinc. Gilding metals are brasses with less than 20% zinc. The brass becomes harder and more brittle as the zinc percentage increases; most ancient specimens are alpha-brasses.

Lead: lead is a common addition (typically less than 4%) to many tin-bronzes principally to infiltrate and fill pores formed by shrinkage during solidification, thus improving machinability. When cast with low-tin bronzes the lead does not alloy (i.e. is completely insoluble) with the copper or tin, but forms fine globules randomly distributed throughout the structure. The addition of lead to tin-bronzes significantly lowers the melting point of the alloy and can have a variety effects on the grain and dendritic structure.

Nickel: the inclusion of between 10% and 30% nickel to copper alloy is carried out to improve corrosion resistance, particularly to salt water. This fact, coupled with the ability for copper-nickel alloy to resist biological growth has seen its growth in the use for cladding for the hulls of ships.

Phosphorous: rarely exceeding 1% of the composition, phosphorous can increase the hardness of copper alloys.

Arsenic: the addition of arsenic to alloys containing zinc can improve corrosion resistance by preventing dezincification (the sacrificial loss of zinc in preference to copper from the surface of the alloy). Commonly found in ancient bronzes, the arsenic can segregate during casting (a process known as 'sweating') to form a silvery coating of an intermetallic arsenic compound.

Antimony: like arsenic, antimony has been found to form intermetallic silvery coatings on ancient bronze.

Manganese: added to copper alloys to increase tensile strength and also give a 'chocolate' bronze appearance to the alloy.

Gold: Japanese copper alloys, such as *shakudo*, contained up to 5% gold and its patination qualities were exploited to produce rich colours. *Tumbago* was a copper/gold alloy used for both casting and sheet-metal work in South America.

Silver: another popular Japanese alloy, *shibuichi*, comprises of copper with between 10 and 40% silver and also offers valuable patination possibilities.

Aluminium: an addition of 9-11% aluminium to modern bronzes can improve corrosion resistance and also resistance to erosion and wear.

Other metals and alloys used in sculpture and casting

Iron and steel: found applications in the manufacture of armour and armory, as well as household utensils. The precise nature of a steel is dependent on the carbon content and the cooling process. Steels increase in hardness with carbon content until the limit of solubility is obtained at 1.7%.

Pewter: ancient pewters were alloys of lead and tin, although modern pewters are alloys of lead, antimony and copper. The oxide coating that forms on exposure to the air has protective qualities and is considered desirable^[16].

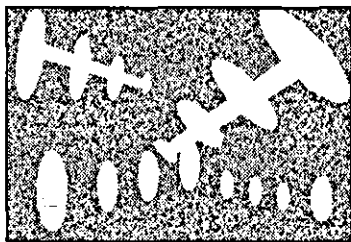
Silver: is often combined with copper as an alloying element. Sterling silver may contain up to 10% copper.

Gold: the use of gold in gilding bronze sculpture was popular in ancient Greece and Rome to provide a protective and attractive coating with the appearance of gold. Evidence of gilding rarely survives due to detachment from the base metal caused by interfacial corrosion processes and examples of its preservation are all the more valuable because of this. Gold is often alloyed with silver to form electrum for colour variation and economic purposes.

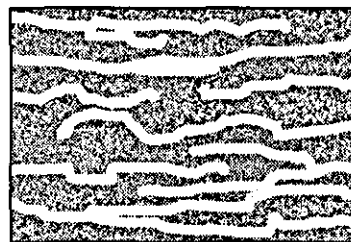
1.2.3 Worked metals

A worked metal or alloy is one that has undergone some morphological process, such as hammering, turning, drawing, and so forth, that has altered its properties. Metals may be cold-worked or hot-worked.

Cold-working: the grains that exist in a metal become deformed by cold-working processes, such as hammering, which generate dislocations in the crystal structure. Dislocations have difficulty moving across grain boundaries and therefore, if the grain size is small, the metal becomes progressively more brittle as it is 'work-hardened'.



Alpha phase dendrites with eutectic fill in typical cast alloy



Elongated dendritic remnants after heavy working

Fig. 1.2.3a: Grain structures in cast and worked alloys

Hot-working: work-hardened metals can be softened by heating the metal to a temperature between one third and one half of its melting point (a process known as annealing) to induce recrystallisation of the grains. Hot-working is a combination of the effects of cold-working and annealing and produces no work-hardening. Many forging operations use hot working to effect initial shape changes with minimum expenditure of energy followed by cold-working processes to work-harden the metal and give a good surface finish^[17]. Thus, we can expect the grain size to be much smaller, and dislocation densities much higher, in worked metals and alloys (such as sheet metal) than those that have been cast, as shown in *Fig. 1.2.3a*.

1.2.4 Present day metals and alloys

Steel: is used in applications where hardness and durability are required. Plain carbon steels contain up to 1.7% carbon and significant amounts of manganese residual from the deoxidation process. Above 910°C, pure iron has a face-centre cubic structure that can dissolve up to 1.7% carbon. Below 910°C, iron has a body-centre cubic structure that can dissolve only 0.03% carbon and thus precipitation effects create various transformations on cooling. Carbon precipitates as cementite (Fe_3C), a very hard compound that increases the hardness of the steel. The hardness of the steel determines the application to which it is best suited; structural applications, machine parts, tools, springs, blades, vehicle body-work and many other areas^[18]. Surface treatments can be applied to steels with poor engineering properties to improve the surface hardness, durability and corrosion resistance.

Aluminium and aluminium alloys: although aluminium is the most common metal on earth, its high reactivity prevents large scale production by smelting methods (small amounts were produced by reduction of sodium by the mineral bauxite from 1825) and it was not until 1886 that the electrolysis of purified alumina formed the basis for large scale production. Although casting is still performed on a large scale, most aluminium is marketed in sheet form and, to a lesser extent, as extruded bars and tubes^[19]. Aluminium is capable of dissolving elements such as copper, silicon, magnesium, manganese, zinc, titanium, cadmium, columbium, nickel, cerium, tin, lead and others which are generally added to form an alloy of increased strength and decreased ductility. The strength, lightness and corrosion resistance of aluminium has found it many applications in aerospace and transport in general, building and architecture, and domestic appliances^[20].

Copper and copper alloys: the high electrical conductivity and ductility of copper has found it many applications in the transmission of electricity and over a third of all copper produced is used in the area of electrical engineering. Another major use for copper (and copper-nickel) is in buildings due to its corrosion resistance and its potential to form

attractive patinas. Sheet copper has also been used in sculpture, such as the Statue of Liberty.

Surface treatments

The hardness, wettability, adhesive properties, corrosion resistance, and appearance of metals are all dependent to some extent on their surface properties. Modern surface treatments enable manufacturers to improve the surface characteristics of metals for their particular application without significantly altering the properties of the bulk material. It is the surface of the metal that is subjected to environmental influences and determines how the metal will behave when exposed to different conditions.

Pickling and cleaning: cleaning is the removal of oil, grease and dirt from the surface of the metal by dipping in organic solvents or hot alkali solutions. Pickling is the removal of oxide layers by the use of acidic solutions^[21]. The combination of cleaning followed by pickling is a common pretreatment in industrial processes prior to electroplating, or application of paint or adhesives, the quality and durability of which are most dependent on effective pretreatment processes.

Plating, galvanising and coating: coating a metal with a less-noble metal can offer protection to the bulk material if the coating metal is chosen such that it forms a sacrificial passivating film of corrosion. Zinc is often applied to steel surfaces by hot-dip galvanising, electroplating or spraying. The application of a suitable paint to the zinc surface can form a 'duplex system' that can further extend the life to 1.5-2.5 times that of the individual systems^[22].

Abrasive treatments: abrasives, such as sand-blasting, have the effect of cleaning-off contamination and also texturing the surface. A textured surface provides a large surface area for adhesion and may also increase the number of polar groups available for coating attachment^[23].

Laser treatments: these include laser transformation hardening (LTH), laser surface melting (LSM), laser surface alloying and cladding^[24]. LTH and melt-solidification has been shown to give stainless steel a three fold increase in fretting wear resistance^[25]. Surface structures produced by excimer laser ablation can increase surface area and adhesive properties of metals^[26]. LSM has been shown to improve wear and corrosion resistance and refines grain size^[27].

Phosphating: phosphate coatings can be applied to zinc, steel and aluminium substrates as a form of protection against corrosion and wear. They are particularly favoured as pretreatment processes for organic coatings as they provide an active surface for adhesion^[28].

1.3 Corrosion and patination

Jean-Paul Sartre once wrote of a weathered sculpture:

"He has no eyes, scarcely any nose, a beard eaten away by that strange leprosy which sometimes descends, like an epidemic, on all statues in a particular district. He looked sickly and evil."^[29]

It is clear to see how the artistic integrity of the piece has been compromised through the action of corrosion, and what was once intended to be a monument to the achievements of Impetraz, poet and writer, presents an image of something to the contrary. Since Sartre's novel, first published in 1938, the leprosy to which he refers, spawned and perpetuated by the industrial revolution, can be observed to be attacking most of the outdoor sculpture of the worlds' cities today.

1.3.1 The Corrosion Process

It is generally recognised that corrosion takes place by an electrochemical process. Faraday's Law of Electrolysis states that the chemical change produced by a steady electric current is proportional to the number of coulombs which have passed. Thus, the amount of metal deposited at a cathode or dissolved at an anode is proportional to the current and time. The current is in turn equal to E/R where E is the E.M.F. in volts (in general, this varies with time due to polarisation effects), and R is the sum of the resistances between the metallic and liquid parts of the circuit.

Thus, the normal electrode potential of a given metal defines its reactivity and general susceptibility to corrosion (see Appendix A).

Electrochemical corrosion

Bimetallic systems: corrosion in the presence of dissimilar metals is facilitated by the presence of an electrolyte (e.g. rainwater). Different metals have different affinities for electrons, a more noble metal (e.g. copper) will tend to absorb electrons from a baser metal (e.g. iron). Thus, the noble metal becomes the cathode and the base metal the anode. Anions and cations in the solution are attracted to their respective electrodes, as in an electric cell, see *Fig 1.3.1a*.

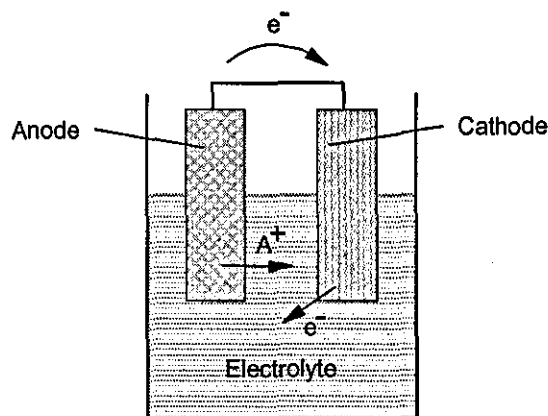


Fig. 1.3.1a: A simple electrochemical cell

At the anode: atoms of the electrode will be deprived of electrons and enter the electrolyte as cations. The oxidation state of the ions will depend on the current density (e.g. Fe^{++} ions produced at low current density, Fe^{+++} ions produced at a higher current density). These ions may form soluble or insoluble corrosion products. Unless the corrosion products form an adherent coating to stifle the reaction, the anode will be gradually eaten away.

At the cathode: the reactions at the cathode are very much dependent on the presence of dissolved oxygen in the electrolyte. With no oxygen present, the supply of electrons combine with hydrogen ions to produce hydrogen gas. In the presence of oxygen the electrons combine with it and water to form hydroxide ions. Both reactions increase the concentration of hydroxide ions in the solution and therefore can be considered as alkaline reactions; they do not produce any corrosion of the cathode in themselves.

Bimetallic systems are common in sculpture; micro-cells may evolve between alloying components and phases; or large cells may form between dissimilar metals used for repair work, welds, support bolts, or different parts of the sculpture itself. However, electrochemical corrosion does not necessarily require the presence of more than one metal.

Single-metal electrochemical action

Electrochemical corrosion occurs in single metal systems due to a potential forming between the metal anode and a cathode that may be an impurity in the metal, surface contamination, or surface corrosion products, see *Fig 1.3.1b*. The process then proceeds as with the bimetallic system. Variation in oxygen concentration in the electrolyte can also create a potential difference to facilitate electrochemical processes: aerated portions of electrolyte (i.e. submerged but near the water-line) can behave as a cathode towards the anodic, 'unaerated' portions.

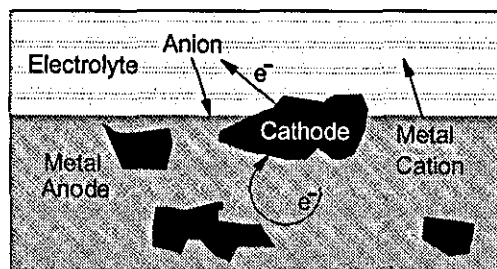


Fig. 1.3.1b: Electrochemical corrosion in single metal systems.

The effect of corrosion products on corrosion

From the onset of electrochemical corrosion a complex, dynamic system evolves, the nature of which is affected by the corrosion products that form. This complexity has provided the fuel for much research and cannot be considered here in its entirety. In general, however, for a given electrolyte, corrosion products may form passive coatings that inhibit further corrosion or aggressive coatings that perpetuate further corrosion. It should be noted, however, that terming a corrosion layer 'passive' or 'aggressive' should be done with care as its protective qualities can be very sensitive to changes in the system and most corrosion layers will have a mixture of passive and aggressive components. Some metal oxides that are insoluble in pure water will become soluble in rain-water.

Passive coatings: the term 'passive' has been subject to varying definitions and shall be used here to represent the quality of a coating that inhibits further corrosion under conditions to which it is likely to be exposed^[30]. A passive film is an insoluble film that forms through the corrosion process and presents a barrier between the electrode and electrolyte, stifling ionic (and electronic) transport between them, thus reducing the rate of corrosion as defined by Faraday's law. The influence of passive films can be extremely significant: in the case of aluminium (very low in the electrochemical series, see Appendix A), the passive alumina (Al_2O_3) film that forms on exposure to air renders it protected from certain acids that actively attack 'less reactive' metals such as iron and zinc.

Aggressive coatings: films may form that are insoluble but do not prevent ion migration. These have no significant stifling effect but may provide a cathodic region to encourage further electrochemical attack. Such coatings are responsible for low corrosion resistance of iron. When iron is exposed to water, the cations from the anodic region will pass into the solution as soluble $\text{Fe}(\text{OH})_2$. This primary corrosion product will be later oxidised (by oxygen in the water) to precipitate insoluble $\text{FeO}(\text{OH})$ (a secondary corrosion product) that is not immediately in contact with the metal surface and thus forms a friable, permeable coating responsible for the majority of the loosely adherent 'rust' commonly seen on iron structures.

1.3.2 Factors affecting metal corrosion

With few exceptions, metals are wrought from mineral deposits and it is to these that they revert on exposure to the atmosphere. The energy required to reduce metallic ore makes it energetically favourable for a metal to oxidise if placed in an oxidising atmosphere. The chemistry of corrosion products and rate of corrosion is dependent on the metal and environment, as described below:

(i) The Metal

Apart from obvious variations in the corrosion products from different metals and alloys, even very slight discrepancies in composition, grain size, impurities, surface roughness and topography can have pronounced effects on the corrosion products.

Composition: for example, even trace quantities of arsenic and bismuth can significantly encourage the growth of a protective film on sheet copper^[31].

Grain-size: there is often an epitaxial relation between the cuprite layer and the orientation of the copper alloy substrate^[32]. Nassau found that, under controlled conditions, there

existed a direct correlation between grain-size and thickness of an artificially grown patina^[33]. This is supported by observations made on the Statue of Liberty, where patination was found to be absent on copper panels with a small grain size although it was present on the rest of the structure^[34].

Impurities: provide cathodic regions for electrochemical attack. Impurities may be present in the cast metal or as particulate matter that is transferred from the atmosphere to the surface.

Surface roughness and topography: air turbulence is higher for air flow over rough or complicated surfaces, thus the transfer of corrosive species from the air to the metal is higher than for a smooth, simple surface^[35]. Surface roughness can also increase wettability, thus encouraging the presence of rain-water on the surface.

(ii) The Environment

Aerobic Corrosion

The rate of outdoor corrosion is very susceptible to weather conditions, particularly the frequency and chemistry of rain and other forms of precipitation. Of course, environments vary significantly over the world and are subject to seasonal, geographical as well as anthropogenic influences. For example, a survey by the United Nations Environment Program (1980-84) surveyed 54 cities throughout the world and found SO₂ levels to vary by a factor of 100 and Total Suspended Particles (TSP) varied by a factor of 200. In London, SO₂ and TSP levels have gradually increased from 1500 A.D. to 1900 A.D., after which they have gradually declined^[36].

Wind: Vernon^[31] observed that copper exposed to prevailing winds forms a more uniform, green layer of corrosion than sheltered copper areas, which remains green and black. Winds accelerate the transfer of particles to the surface of the metal and the rate at

which rain-water evaporates from the surface, both of which can affect the corrosion process.

Time-of-wetness: 70% humidity is required for the corrosion rate to be significant.

Corrosion by electrochemical processes is made possible by the presence of a thin film of impure water on the surface of the metal to act as an electrolyte. The time-of wetness is significantly dependent upon the relative humidity, duration and frequency of precipitation; temperature of the air and the metal; chemistry of the corrosion products; wind-speed; and hours of sunshine^[37].

Composition of surface electrolytes: clearly, the composition of corrosion products will depend on the chemical species dissolved in the electrolytes and their respective concentrations. Oxygen is responsible for high rates of cathodic reaction, its concentration becomes a maximum when the electrolyte layer becomes very thin, just before it dries. The presence of SO₂ in the atmosphere is common through the combustion of fossil fuels and it is oxidised by a series of processes to form corrosive H₂SO₄. NO₂ is a relatively inert gas but often present in significant quantities and has been shown to have a synergetic effect with dissolved sulphates by increasing the oxidising power of the aqueous environment^[38]. Whereas SO₂ delivery to the surface is strongly enhanced by the presence of water, NO₂ is essentially repelled by wet surfaces^[35]. Chlorides can be present in marine air, in the form of NaCl and KCl, or from combustion of coal or waste, in the form of HCl. Chlorides are responsible for self-perpetuating corrosion phenomena on both iron and copper alloys^[39]. Even if present in ppm, HCl can accelerate corrosion processes enormously^[40]. Ozone, ammonium and bicarbonates also influence the corrosion process.

Pollutants and suspended particles: even insoluble particles, e.g. soot, alumina and sand can affect corrosion process^[41]. Hard particulates, such as those containing silica and alumina, can 'sand-blast' the metal. Insoluble particles on the surface can act as a cathode for electrochemical attack, see *Fig.1.3.1b*. Reduced sulphur gases, such as H₂S produced

by mills, marshes and sewage treatment plants, can attack metals in the absence of water. Hygroscopic particles can enhance the deposition of atmospheric gases onto the metal surface. Large particles are prevalent on skyward facing surfaces due to the effect of gravity.

Location: the corrosivity of the atmosphere for a given sculpture depends very much on its location, whether in a urban, rural or coastal setting^[42,43]. The prevalence of emissions from industry and exhausts in urban surroundings contributes many potentially corrosive species to the environment such as $(\text{SO}_4)^{-}$, $(\text{NO}_3)^{-}$, $(\text{NH}_4)^{+}$, Cl^{-} , S^{-} , various organic acids and inert particulate matter. Concentrations tend to be much lower in rural areas, although inert particulate matter can be generated through various agricultural practices. Coastal atmospheres have a predictably high concentration of chlorides due to sea-salt. Even sculpture that has been stored for transfer to a museum environment may be subjected to chemical attack. Antiquities stored in wooden cabinets are prone to attack from acetic acid and formaldehyde derived from the woods, coatings and adhesives used in their manufacture^[44].

Temperature: the rate of chemical reactions increases with temperature in general. Temperature can vary by as much as 20°C over the surface of a sculpture at a given time^[45].

Light: non-corrosive NO_2 has been known to be converted to corrosive HNO_3 by photochemical oxidation^[37].

Anaerobic Corrosion

The exclusion of air from the surface of a metal artefact (e.g. by burial) generally retards corrosion processes. Indeed, the excavation of an object and its subsequent exposure to an oxidising atmosphere can activate redundant corrosion mechanisms and an artefact that has been buried for 2000 years can become completely destroyed 40-80 years after

excavation^[46]. As a result, many excavated objects require some form of stabilisation if the deleterious effects of moisture, oxygen and residual chlorides are to be avoided^[47]. Clearly, buried artefacts will not generally suffer the rapid, chaotic environmental fluctuations endured by those in outdoor conditions and the corrosion process is more likely to be determined by the chemical properties of the impacting material, especially the acidity/alkalinity of the soil (see Appendix F). For example, the composition of loess^{*} is responsible for the formation of a desirable lilac patina on Chinese silver from the T'ang dynasty^[48].

1.3.3 Species of corrosion product.

As can be expected from the wide variety of metals and alloys requiring conservation, and the sensitivity of corroding systems, the diversity of corrosion products is considerable, even over the surface of a single artefact. A study of sixteen bronze monuments in close vicinity to each other around Ottawa, Canada, revealed the presence of 94 different corrosion products resulting from 168 surface scrapings^[50]. Despite this complexity, generalisations can be made and certain corrosion products dominate and merit most attention. Knowledge of the type and nature of corrosion products is vital for a complete study and evaluation of conservation processes. Certain corrosion products are stable and passive and inhibit further corrosion. Others are aggressive and encourage further corrosion of the metal substrate. Clearly, the appearance and nature of corrosion products will determine whether a conservator would wish to remove or retain part or all of the corrosion layer.

Structural variations

Corrosion products can form single, homogenous layers of corrosion, such as the passive Al_2O_3 layer commonly found on aluminium. Very often, however, corrosion products can form as two or more layers, as is common with copper and its alloys, see *Fig 1.3.3a*. It is

* Loess is an alkaline soil common to north central Europe, China, the American West and other areas^[49].

not unknown for copper alloys to have been discovered with up to 75 layers of corrosion alternating between malachite and cuprite^[51].

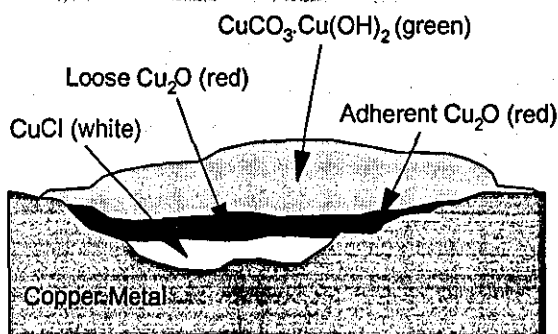


Fig. 1.3.3a: Typical corrosion layers on excavated copper artefacts.

Fig. 1.3.3a also illustrates a common feature of both excavated and outdoor corrosion processes for most metals. The external corrosion layers are typically complex compounds containing hydroxide or hydrate groups (e.g. $\text{CuCO}_3 \cdot \text{Cu}(\text{OH})_2$) whereas inner corrosion layers that form in contact with the metal are, in general, simple compounds (e.g. CuO_2)^[38].

Chemical variations

The variety of chemical compounds that have been discovered on metals is so extensive, therefore, for each balance metal considered, only the most common forms of corrosion are described. Copper shall be afforded most attention due to its presence in popular casting alloys such as bronze and brass.

A general note on oxides

Most metals (other than gold) form a thin oxide layer after brief exposure to the air. Many transition metals can form oxides of different oxidation states (and hence different solubilities), although one form usually predominates. The oxides of metals (other than

alkali and alkaline earth metals, and thallium) are sparingly soluble in pure water and hence can provide a protective coating against corrosion. Oxides of the form MO (where M is any metal) become soluble in acidic solutions, such as rainwater, although the acidity of the solution rapidly decreases in the vicinity of the anode during the corrosion process. Sesquioxides (i.e. those of the form M_2O_3) are only sparingly soluble in acids and therefore form the most effective passive oxide layers, such as alumina layers that passivate aluminium or magnetite layers on steel.

Copper

Oxides: a copper oxide layer most often forms as cuprite (Cu_2O), although tenorite (CuO) may be found under certain conditions, such as high temperatures. Oxides often form an interfacial layer between the metal substrate and more complicated external corrosion products. Oxides can form an acceptable patination layer for copper and copper alloys^[52]; a familiar example might be the oxide on the bronze lions under Nelsons Column^[53]. Oxides were particularly popular as an artificial method of patination in the 17th Century with sculptors such as Bernini, who described the presence of a translucent lustrous brown cuprite layer as the 'natural' colour of bronze^[54]. It is perhaps interesting to note, that at the time Bernini made the observation, the lack of SO_2^- in the atmosphere probably meant that the green patination that we are used to today was something of a rarity compared with the brown/black oxide layers that form in its absence. It is rather ironic that the often termed 'natural' greening of bronze in the present environment is largely due to the presence of anthropogenic sulphur dioxide in the atmosphere.

Hydroxides: a copper hydroxide is an unstable corrosion product not found under aerobic conditions^[55] and when excavated from anaerobic conditions it is frequently transformed to atacamite (basic copper chloride) within hours^[56].

Sulphides: copper sulphides are often present on prehistoric bronze objects found in bogs as a result of H_2S produced by sulphate-reducing micro-organisms in anaerobic

conditions^[57]. Sulphides may take the form Cu_2S (chalcocite), $\text{Cu}_{1.96}\text{S}$ (djurleite), $\text{Cu}_{1.8}\text{S}$ (digenite), CuS (covellite) and $\text{Cu}_{1.6}\text{S}$ (geerite) and removal is generally favoured. Covellite and chalcocite have been occasionally found in urban areas^[58].

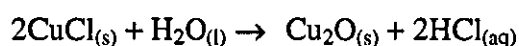
Basic sulphates: the relatively high concentrations of SO_2^- in urban areas, the insolubility* of the basic sulphate, and the extensive conditions under which it can form and remain stable makes basic copper sulphate, $\text{Cu}_4\text{SO}_4\text{OH}_6$ (brochantite), a very common corrosion product on copper and its alloys. First correctly identified by Vernon and Whitby in 1929^[31], brochantite was found to be responsible for the green coloration of most outdoor bronze sculpture previously assumed to be due to the basic carbonate. The time required to form a brochantite layer is subject to great variation: long term exposure tests performed by Mattsson and Holm^[43] on 36 varieties of copper and copper alloys showed signs of greening within seven years of exposure to marine and urban atmospheres, whereas there was no sign of greening on the rural samples. In the early part of this century, a Danish saying existed, 'When a young architect covers his roof with copper it will turn green when his hair turns grey'^[59]. Many authors have commented on the value of the protective and aesthetic qualities of uniform brochantite coatings^[31,60,61] and there is a general consensus that, if uniform, they should be retained. However, a uniform brochantite coating usually forms only on wrought copper (e.g. copper sheet) and the brochantite coatings on cast copper and its alloys (such as form the majority of outdoor sculpture) are often discontinuous and blotchy^[40]. Recently, concerns over the susceptibility of brochantite to be converted to antlerite ($\text{Cu}_3(\text{OH})_4\text{SO}_4$), a more soluble** basic sulphate offering less protection^[62], have brought into question the stability of brochantite in modern environments. Brochantite has been shown to be unstable if in direct contact with the copper metal^[63] although interfacial corrosion products often prevent this. The artistic merit and protective qualities of non-uniform brochantite layers remain a subject for discussion.

* The solubility constant, K , of brochantite is given by $\log K = -68.9$ ^[60].

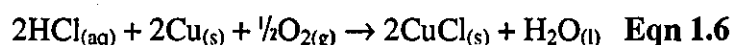
** The solubility constant, K , of antlerite is given by $\log K = -47.1$ ^[60].

Sulphate hydroxide hydrates: various hydrated basic sulphates form on copper and its alloys, but are quite uncommon^[64].

Chlorides: nantokite (CuCl) commonly forms on copper and its alloys between the oxide layer and the metal. The highly corrosive properties of chlorides is due to their high ionic and electronic conductivities^[38] as well as their ability to form soluble complexes, as in 'bronze disease'^[47,65], a self-perpetuating corrosion phenomena caused by nantokite in the presence of water that gradually eats away at the metal, see *Eqn 1.6*^[66]. The process is auto-catalytic because the acid that is liberated during the reaction is free to attack more metal.



and



Basic carbonates: although rare to form on outdoor sculpture, basic copper carbonates, such as malachite ($\text{Cu}_2(\text{CO}_3)(\text{OH})_2$), are extremely common on excavated copper artefacts^[67]. A basic carbonate layer is usually stable and often defines and retains the original surface of the artefact and therefore is rarely removed.

Basic chlorides: as with basic sulphates, the presence of chlorides in the atmosphere and the insoluble* properties of basic chlorides make them a common component of corrosion products, particularly in marine areas. Atacamite ($\alpha\text{-Cu}_2(\text{OH})_3\text{Cl}$) is especially common on copper and its alloys; less so, paratacamite ($\gamma\text{-Cu}_2(\text{OH})_3\text{Cl}$). For brass, the most common basic chloride^[68], anarakite, and has the formula $(\text{Cu,Zn})(\text{OH})_3\text{Cl}$. As with brochantite, anarakite has been shown to be unstable when formed in direct contact with the metal^[63].

* The solubility constant, K, of atacamite is given by $\log K = -69.8$ ^[60].

Iron

Oxides: wuestite (FeO), hematite (Fe_2O_3) and magnetite (Fe_3O_4) are the most common oxides of iron. Magnetite, due to its resistance to acids and black coloration, is sometimes retained as patination.

Hydroxides: iron and steels tend to form soluble hydroxides, as opposed to oxides, in the presence of water as their primary corrosion product, and this reduces their resistance to corrosion^[69]. These hydroxides precipitate oxide hydroxides on reaction with oxygen.

Oxide hydroxides: oxide hydroxides are insoluble and form as secondary corrosion products (i.e. loosely adherent rust) on iron and steel which may contain $\beta\text{-FeO(OH)}$ (akaganite), $\alpha\text{-FeO(OH)}$ (goethite) or $\gamma\text{-FeO(OH)}$ (lepidocrocite) forms of the compound^[70]. Akaganite has been known to host aggressive chlorine compounds within its structure^[71] and the removal of oxide hydroxides in general is usually desirable as they have little aesthetic or protective value and provide cathodic areas for electrochemical attack. The presence of akaganite is a strong indication that corrosion processes are still active and steps should be taken to stabilise the layer^[72].

Chlorides, chloride oxides and hydroxides: the presence of chlorides on iron is responsible for post-excavation corrosion processes that frequently destroy iron objects that have survived thousands of years of burial within a few decades^[46]. Chlorides may take the form of insoluble FeOCl , FeCl_3 and $2\text{FeCl}_3 \cdot 5\text{H}_2\text{O}$. Keller showed that the presence of chlorine is necessary for the formation of akaganite^[73]. Removal of chlorides is often the primary objective of iron conservation.

Silver

Oxides: silver does not form oxides in pure air or oxygen at room temperature and requires heating to 200°C before a film of Ag₂O forms. The oxide has little protective value and is readily converted to sulphides and chlorides.

Sulphides: under aerobic conditions, sulphides rarely form in preference to sulphates on most metals, apart from in the case of silver. Silver sulphide has a very low solubility in water and acids. Acanthite (Ag₂S) is the most common form of corrosion product on pure silver, especially in urban atmospheres, and a uniform, shiny black patina of the sulphide may be considered desirable^[74].

Chlorides: chlorargyrite (AgCl), commonly known as 'horn' silver, is often found on silver artefacts. Silver chloride can undergo photo-reduction in sunlight to produce silver metal, this being a fundamental process in photography.

Lead

Oxides: on exposure to air, lead forms insoluble oxides PbO₃ and PbO₂ in the form of dark grey patination^[75].

Hydroxides: lead has the tendency to form partially soluble hydroxides as opposed to insoluble oxides in the presence of oxygenated water^[69].

Carbonates: cerussite (PbCO₃) is occasionally found on lead and, although insoluble in water, can be dissolved by weak acids e.g. rainwater. Hydrocerrusite, basic lead carbonate (Pb₃(CO₃)₂(OH)₂), is perhaps the most common corrosion product found on lead artefacts, especially excavated objects. It is insoluble in water and dilute acids but it usually forms in a powdery form which is unsightly and accelerates the corrosion

process^[76]. The basic carbonate may also appear in a hydrated form ($3\text{PbCO}_3 \cdot 2\text{Pb(OH)}_2 \cdot \text{H}_2\text{O}$).

Sulphates: anglesite (PbSO_4) is often found on lead^[56].

Aluminium

Oxides: alumina (Al_2O_3) is the passive oxide that can often be observed on exposed aluminium structures.

Hydroxides: gibbsite (Al(OH)_3) often forms as the major corrosion product on aluminium in the presence of salt-water^[77].

Zinc

Oxides: zincite (ZnO) is commonly found on sculpture although it is easily transformed into basic compounds that are readily soluble in weak acids and thus has limited protective properties.

Sulphates: a variety of hydrated sulphates have been found on corroded zinc^[56]. Basic zinc sulphate ($\text{ZnSO}_4 \cdot 3\text{Zn(OH)}_2 \cdot 4\text{H}_2\text{O}$) has been found on pewter artefacts recovered from ship-wrecks^[56].

Tin

Oxides: cassiterite (SnO_2) is amorphous and thus escapes detection by many analytical techniques; it is the most common tin product found on bronze and pewter and is considered passivating. A partially aerobic environment may produce Sn_3O_4 and occasionally romarchite (SnO) has been found.

Hydroxychlorides: a partially aerobic environment may produce $\text{Sn}_4(\text{OH})_6\text{Cl}_2$ on pewter.

Other metals

Although the above is a fair description of the most commonly encountered corrosion products, it should be stressed that it is by no means comprehensive and the variety is far too extensive to be covered in this work. The presence of bone near the corroding metal (common in burials) may encourage phosphates to form, for example, corrosion products as complex as sampleite ($\text{NaCaCu}_5(\text{PO}_4)_4\text{Cl}\cdot 5\text{H}_2\text{O}$) have been found on excavated Egyptian bronzes^[78]. A large number of mixed metal compounds (e.g. chloroxiphite, $\text{CuPb}_3\text{Cl}_2\text{O}_2(\text{OH})_2$) are also possible, although uncommon, and are very dependent on the precise alloying characteristics of the metal.

Factors affecting the colour of corrosion products

The colour of inorganic compounds, particularly that of the transition metals, has long been exploited to produce pigments for paints and patina. Identification of compounds by colorimetry is fraught with complexity, however, due to the many factors that affect the colour of compounds, particularly those which form in impure and variable environments. Because of this, determination of corrosion compounds from their colour is an unreliable process and more sophisticated analytical methods are required, such as X-ray powder diffraction analysis, for precise identification.

Thickness of corrosion films: if a layer of corrosion is very thin (i.e. of comparable thickness to the wavelength of the light with which it is being observed) then its colour will depend fundamentally on interference effects produced by the film to such an extent that the thickness of a given compound may be estimated by its colour (see Appendix B).

Size of crystallites: even on thick films, interference effects within the crystallites of the compound can affect its coloration. For example, cuprite may appear as yellow, red, brown or black depending on the size of its crystallites.

Impurities and alloying metals: corrosion products of high purity may be produced in laboratory conditions but rarely form in an outdoor environment. Impurities need only to be present in very small quantities for significant discoloration to take place and they are rarely, if ever, completely absent. Impurities will be present in the atmosphere and in the metal itself and thwart attempts at identification through colour measurements. The complex composition of many alloys, especially those of copper, also affect the colour of corrosion.

1.3.4 The value of corrosion

Although corrosion is often regarded as detrimental and undesirable, certain corrosion products inhibit further corrosion and some also maintain an appearance that is generally considered attractive and can be highly valued.

Patination: a patina is an attractive, protective inorganic layer that has formed, naturally or artificially, on the surface of a metal. The word itself is thought to be derived from the old Italian term 'patena' that referred to a shiny dark varnish applied to shoes^[54]. Filippo Baldinucci's 'Vocabolario' of 1681 provides the first known printed reference for the word and defines patina as 'that general dark tone which time causes to appear on paintings, that can occasionally be flattering to them'. Since then, the word has been adopted by conservators to describe a thin, protective and aesthetically pleasing layer in all forms of art.

Artificial Patination

Often an artificial patina is applied at the foundry, a technique that evolved and became popular in the West between 1880-1914 in Paris by master patinuers, such as the Limet brothers^[54], although the Japanese had perfected many patination techniques centuries before^[10]. The first evidence of patination appears to be from the third millennium B.C. on Anatolian metalwork^[79]. It is generally recognised that original patina such as these should never be removed, although they rarely survive on outdoor sculpture as they are consumed by natural corrosion processes.

Natural patination

Under favourable conditions, a metal sculpture may naturally form a pleasing patina after prolonged exposure to a satisfactory environment. As the quality of a patina is primarily a function of its attractiveness, it is also highly subjective: opinions on the correct appearance of bronze vary with time^[54], culture and individual taste. No-one would want the Statue of Liberty cleaned to a shiny copper and no-one would welcome a uniform, green patination evolving on the bronze lions under Nelson's Column. Apart from protective considerations, the question 'what constitutes a patina' should be answered on an artistic basis as opposed to a scientific one and each example considered on an individual basis. To a large extent, the sculpture itself determines what type of patina is most acceptable. Often a desirable patina is accompanied by undesirable corrosion products that may form above, beneath or within the patina. In these cases, the objective of the conservator is to remove the undesirable corrosion products whilst preserving and stabilising the patina.

The quality of natural patination

Assessing the quality of patination, like assessing the quality of the art it is present on, has a certain degree of subjectivity associated with it in so far as the aesthetic considerations

are concerned. The protective qualities can be assessed on a more objective basis although even this is fraught with complexities and opinions often differ. An ideal patina has both protective and aesthetic qualities.

Aesthetic qualities

'...a sculpture painted gray is more "coloured" than a gray stone sculpture because the colour is a positive, added factor, an agent of change that disguises or regulates all other properties of the material.'^[80]

Aesthetics are dependent not only on colour, but also transparency and opacity, mattness and gloss, texture, uniformity and variegation.

Colour: colour has long been exploited by sculptors to create mood; demarcate or unify; obscure, create, oppose or distort form^[81]. It is easy to see, therefore, how leaving a sculpture to the effects of the atmosphere can alter the intended effect of a piece. The effect of coloration is also affected by the colour of the surroundings which may be either complementary or clash with that of the sculpture.

Variegation: patinas do not often form as uniform coatings. Variegation may manifest itself as a pleasing, mottled effect. Variegation may also take the form of streaks caused by run-off rainwater. Often these streaks contrast strongly with the rest of the patina and detract from the general appreciation of form, creating an overall 'camouflage' effect. Localised colour variation may also be caused by repairs, alloy variations, and the orientation of surface with respect to prevailing winds, the sun, and gravity. Worked metals (such as copper sheet) have a tendency to form uniform patination whilst cast metals usually form variegated patina.

Protective qualities

Many factors determine the protective qualities of corrosion layers. Although many of these may be a function of their chemistry, to consider chemistry alone would be oversimplistic, especially as corrosion layers are rarely homogenous and uniform.

Impermeability: the rate of corrosion is determined by the rate of positive and negative ion transfer. If the patina contains capillaries and cavities that allow for ion transport then its protective qualities are severely impaired. Such a patina may even encourage corrosion by prolonging the time of wetness of the surface of the metal through retarding the evaporation process.

Chemical stability: protective corrosion layers may be transformed into aggressive compounds if exposed to certain chemical species. A stable, protective patina is able to resist such transformation^[60].

Adherence: flaky, non-adherent corrosion products have a high permeability and are removed by the action of wind and precipitation. Friable corrosion products usually form as a secondary corrosion product and therefore are not immediately in contact with the metal surface when they form. For example, iron will pass into solution primarily as iron hydroxide and is later oxidised to form a precipitate of hydrated iron oxide or 'rust' which is only loosely adherent to the surface^[82].

Insolubility: soluble corrosion products do not offer any protective value. For protection to be effective the corrosion products have to be insoluble in the pH of whatever electrolyte is present. Areas that have high levels of acid rain may destabilise patina that are adequately protective in more neutral environments.

Hardness: areas exposed to the abrasive effects of wind-carried particulates require hard patina to retard the effects of erosion.

Uniformity: variation in the corrosion products across the surface produces areas of potential difference that encourages electrochemical corrosion processes. Such effects are particularly pronounced where a break in the protective layer has occurred and this layer becomes the cathode for ion migration from the exposed metal surface^[83].

1.4 Organic Coatings

A paint is a formulated composition, usually based on an organic resin, that dries to form a hard film adhering to the substrate. Recent developments in organic chemistry have spawned multiple paint formulations although most use the following basic components.

1.4.1 Composition of organic coatings

(1) Binder (or vehicle, medium): the binder is the (organic) resin which, once it has solidified, forms the hard, tough, adhesive surface film that is the bulk of the paint.

(2) Pigment: often in the form of fine particles of transition metal compounds, pigments not only provide colour and opacity to the coating but may provide inhibiting qualities to retard corrosion processes.

(3) Solvent: the solvent serves a transient purpose, keeping the paint liquid during application after which it evaporates to leave a solid coating. Water is a popular solvent for general purpose paints, although the solvent may also consist of one of many volatile organic compounds, including aliphatic compounds (e.g. white spirit); aromatic compounds (e.g. xylene and toluene); or oxygenated compounds (e.g. ketones, esters, ethers and alcohols).

1.4.2 Types of organic coating

Natural media

Before the availability of synthesised organic compounds that are common today, paint media relied on natural oils, such as linseed and tung oil. These oils contain unsaturated fatty acids. When they are spread thinly, the unsaturated bodies absorb oxygen, causing polymerisation and hence a rigid gel forms^[84].

Modern coatings

There are many generic classes of resins that are widely used in paints. Some of the most common are briefly outlined below^[85]. Specific formulations vary depending on the precise nature of the application. Many resins, such as polyester, polyurethane, acrylic and epoxy, have good all-round decorative and protective properties and find universal applications.

Polyester resins: include the alkyd resins that are the most widely used group of binders.

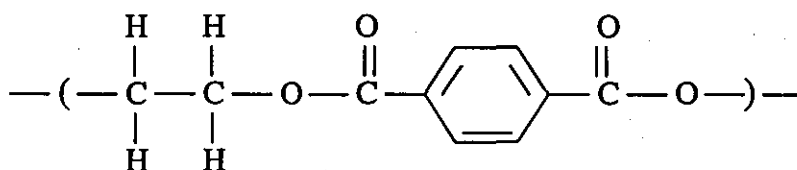


Fig. 1.4.2.a: Monomer unit of polyester resin.

Polyurethanes: are formed from the reaction of isocyanates with compounds containing an active hydrogen molecule (e.g. polyesters, acrylics, epoxies).

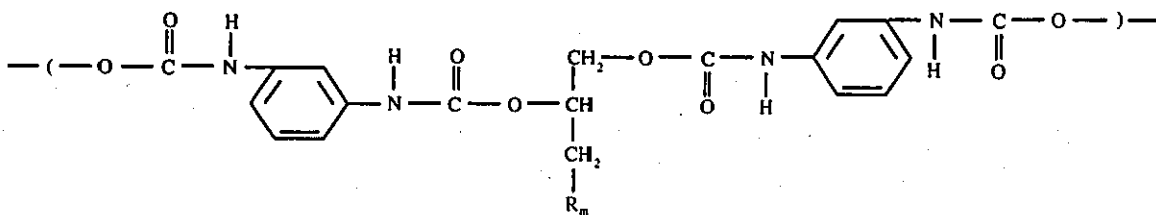


Fig 1.4.2b: Monomer unit of polyurethane resin.

Acrylic resins: are polymers that contain acrylate or methacrylate esters in their structure.

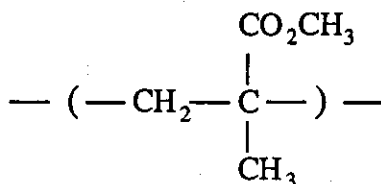


Fig. 1.4.2c: Monomer unit of acrylic resin.

Vinyl resins: are straight-chain, thermoplastic compounds prepared from vinyl monomers.

Cellulose derivatives: obtained by modifying cellulose to produce thermoplastic materials.

Epoxy resins: contain the epoxide or oxirane group, see Fig 1.4.2d.

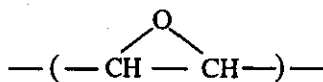


Fig. 1.4.2d: Monomer unit of epoxy resin.

Elastomeric resins: are based on natural (polyisoprene) and synthetic rubbers.

1.4.3 Methods of protection

Although paints clearly present a barrier between the metal and external environment, most paint systems allow water and oxygen to permeate faster than that required for corrosion of the bare substrate^[86]. It has been suggested that ionic conduction through the paint film is the rate determining step for corrosion although, with such a variety of paints in use today, a standard model for protection is unlikely to be applicable universally.

1.4.4 Deterioration of coatings

Despite the fact that many paints and lacquers have been formulated for the protection of metals exposed to an outdoor environment, most deteriorate over a life-time that is relatively short compared with that of the sculpture itself. A combination of effects contribute to the deterioration of protective coatings:

Thermal effects: outdoor paints are subjected to daily and annual temperature fluctuations, the range of which depends on the local climate. The difference in thermal expansion coefficients between the paint and the metal substrate induces shear stresses in the coating at the metal/coating interface (for example, acrylics have a thermal expansion coefficient approximately five times that of copper). Whilst freshly painted surfaces have sufficient elasticity to expand with the substrate, embrittlement through ageing processes (see below) leave the paint susceptible to cracking and peeling^[87].

Light effects: Solar radiation incident on the surface of the earth still contains a considerable proportion of ultraviolet light between 200 and 400nm. Photons of this wavelength have sufficient energy to cause photochemical reactions within organic molecules; scission or crosslinking reactions^[88] may take place depending on the wavelength of the radiation and the nature of the bond it is incident upon.

Oxidation effects: Prolonged exposure to air causes oxidation effects in paint films which can be responsible for cross-linking and polymerisation. The auto-oxidation process is normally initiated by homolytic bond cleavage by, for example, UV light, producing two free radicals. The reaction then propagates until the free radicals recombine and eliminate each other^[89]. The embrittlement that ensues makes the coating susceptible to cracking and failure by thermal effects.

Water or moisture: Evaporation of the solvent during the drying process often leaves the paint porous and water-absorbent. Permeation of the paint layer by water allows for electrochemical processes to act to produce corrosion beneath the paint to produce blisters and failure of the coating, see *Fig 1.4.4c*. Not only can water affect the metal substrate, but hydrolysis of the polymer chains within the medium or the pigment compounds can cause premature chalking where the pigment-polymer bonds are destroyed and the coating becomes powdery. Water droplets on the surface of the coating can act as a magnifying glass to concentrate the effect of solar radiation^[90].

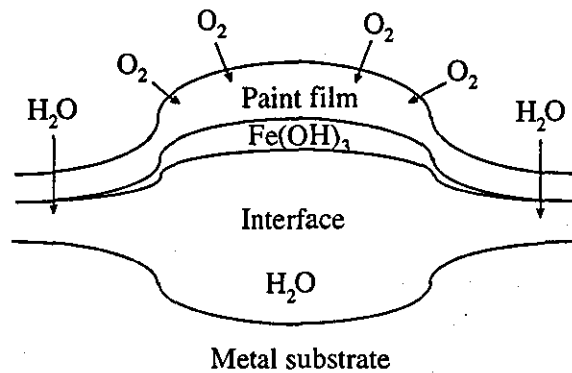


Fig. 1.4.4c: Blistering of paint film by water permeation.

Wind and airborne particles: particles borne on the wind can have abrasive effects on paint coatings causing physical damage through erosion.

1.4.5 Removal of organic coatings

If an original paint layer remains on a metal artefact then removal of that coating is seldom desirable: even remaining flecks of paint give valuable information on an object's original appearance and the painting practices of the time. There are many examples, however, particularly concerning outdoor sculpture, where paints have been used as a protective measure and have been applied within the last 30 or so years, long after the original sculpture had been cast. After a paint or lacquer is applied to a sculpture, it should be removed and repainted every few years before the coating has a chance to become aged and insoluble in organic solvents. If the sculpture is neglected, as frequently occurs, the coating becomes aged, unsightly and difficult to remove due to its embrittlement and insolubility. Even lacquers specially formulated for the protection of monuments, such as Inralac, can show signs of ageing that merit its removal after a period of only ten years^[87], a relatively short time period when compared with the durability of the sculpture itself. Damaged paint films can accelerate corrosion processes by providing cathodic regions for electrochemical attack. Corrosion phenomena that originate from cracks in the paint film are likely to be unsightly streaks and of no protective value. Repainting without removal of the old paint layer results in a loss in surface definition of the original sculpture and will produce a poor quality finish. There is at present no satisfactory method of removing aged coatings from sculpture^[91].

Organic coatings are a very common form of protection for large manufactured items, such as vehicles and buildings, and also on a smaller scale, such as wire insulation. Removal of these coatings is required when, for example, the coating has to be replaced. Many countries have recently enforced restrictions on the use of volatile solvents for removal of organic coatings due to environmental concerns^[92-95]. Alternative methods of removal include aqueous^[96], CO₂ snow (micro-particle)^[97], plasma^[98], UV ozone^[99], UV light^[100] and UV laser cleaning^[101], although these processes have severe limitations in terms of efficiency and area-processing capabilities.

1.4.6 Accelerated ageing techniques

Accelerated ageing techniques are widely used in the development and evaluation of organic coatings to assess their resilience without requiring the full duration of real-time exposure tests. For example, UV lamps emitting ultraviolet radiation in the range of 200 to 400nm may be used to imitate the effects of solar radiation at increased intensity depending on the acceleration rate required.

Unfortunately, the results from accelerated ageing studies are often unrepresentative of real-time ageing effects. The high light levels employed in accelerated ageing systems produce concentrations of free radicals that never occur in real paint systems and cause different degradation mechanisms^[89]. Accelerated ageing processes rarely model more than a single aspect of ageing (e.g. UV light effects) and neglect to account for the synergistic effects of the other factors influencing ageing as detailed above. It is generally accepted that accelerated ageing tests do not provide an accurate model for real-life ageing^[89,102].

1.5 Metal Conservation

The conservation and restoration of metal artefacts and sculpture has evolved into a highly skilled craft requiring not only artistic integrity but also scientific understanding of how metals behave and how best they can be preserved. Attitudes toward conservation vary with time, culture and personal prejudice which may often lead to a difference of opinion and a lack of clear objectives^[54]. There is, however, a fair amount of common ground that constitutes 'good, standard practice' and many of the techniques described below are employed universally.

Most metal conservation does not directly involve the metal itself, but the corrosion products and the patination layer. A stable patina is the most effective and most attractive form of protection for the underlying metal.

1.5.1 Large, outdoor sculpture

Almost all outdoor sculpture is copper alloy, normally bronze, with notable exceptions such as 'Eros', which is aluminium. Such exposed bronzes will invariably form corrosion layers and the nature of these layers determine the conservation processes^[103].

Reasons for not removing corrosion products

- (1) Detail of the original surface is present in the corrosion products and the removal of them would result in the loss of information.
- (2) The corrosion has formed an attractive and protective patina.

Reasons for removing corrosion products

- (1) The corrosion layer actively promotes further corrosion of the metal substrate.
- (2) The thickness of the corrosion layer obscures and distorts underlying detail.
- (3) Variegated coloration impairs the appreciation of form and surface texture.

Corrosion layers often possess a mixture of the above qualities and the conservator has to act at his or her discretion as to what, if any, action should be taken to improve the patina.

Divestment methods

There are a variety of methods that can be employed to remove unwanted dirt and corrosion products:

- (1) Abrasives: various forms of abrasive have been employed to remove corrosion products, such as glass beads (peening), wire-wool, sand-blasting and CO₂-snow. The use of any form of abrasive risks damage to the underlying metal, the corrosion often being

harder than the metal itself^[52] (see Appendix E). When the corrosion is uneven or the substrate has the complicated topography typical of sculpture, there is an inevitable loss of detail when abrasives are used: thin corrosion layers on elevated surfaces are rounded and flattened whilst there may be incomplete corrosion removal in the deeper recesses, see *Fig 1.5.1a*. Walnut-shell cleaning is an abrasive method that does not remove the oxide layer.

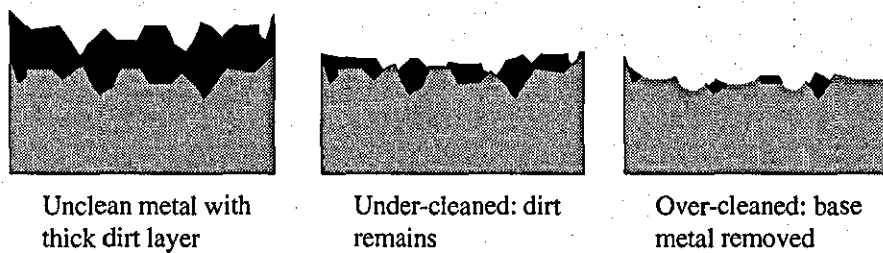


Fig. 1.5.1a: Fundamental problems of abrasive cleaning.

(2) Chemical: alkali (e.g. Rochelle salts) and acid (e.g. sulphuric, formic) are both used to treat and remove bronze corrosion products but have a tendency to leach out some of the alloying metals during treatment^[104]. Most oxides are soluble in acids and to use them can mean exposing the metal substrate.

(3) Washing: may be performed with distilled water or very dilute solutions. The addition of mild detergents aid the removal of soluble corrosion products (see Section 1.5.3).

1.5.2 Small, metal artefacts

Generally, the conservation of small artefacts deals with a far broader spectrum of metals and alloys than outdoor sculpture. Corrosion may often be so severe, especially in the case of excavated objects, that none of the original metal remains and corrosion products are all that the object consists of.

Severely corroded objects

When an object is severely corroded, the conservator tries to determine where the 'original surface' is defined by the corrosion products and therefore attempts to clean to reveal this surface. *Fig 1.5.2a* shows how the original surface might be determined in a corroded object; it may be distinguished by a change in the composition of the corrosion products, or even just their consistency and structure.

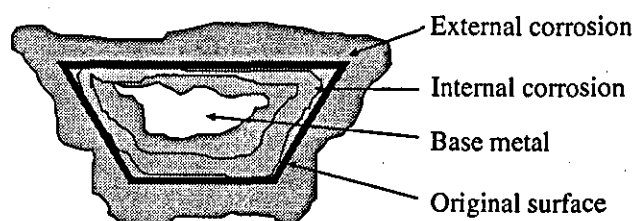


Fig. 1.5.2a: Cross-section through a corroded door nail

Divestment methods

Scalpel: the scalpel is still perhaps the most often employed tool for removing corrosion products on a small scale. A skilled operator uses it in conjunction with a microscope to gradually prise away friable corrosion products, exploiting the faults that lie between adjacent corrosion layers. Using a scalpel gives the operator tactile feedback as to the state of the location under treatment. Progress is often slow, however, and the tedious nature of the work can lead to damage to the artefact through human error.

Electrochemical reduction: the object is buried in a granulated form of base metal (e.g. zinc), covered in caustic soda (min 10%) and boiled for an hour or longer. The zinc reduces the corrosion products of the more noble metals, effectively removing them to leave bare metal.

Electrolysis: the metal object is made into a negative electrode, placed into an electrolyte (such as caustic soda) in the presence of an iron anode and an e.m.f is applied. The encrustations are reduced by this process, again leaving bare metal. The surface left by this method, and that of electrochemical reduction, is highly porous and apt to suffer further corrosion phenomena, such as bronze disease, if not extremely well rinsed after treatment.

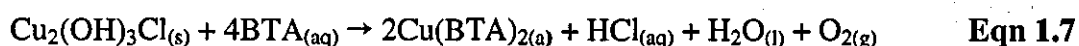
1.5.3. Patina stabilisation

Often the stabilisation of existing corrosion products is preferential to removal which may expose the metal substrate to further attack. Stabilisation is often obtained through removing the soluble elements within the corrosion layers, especially chlorides and sulphates.

Distilled or de-ionised water: Simple washing processes are often considered the safest form of treatment with little chance of damaging the patina or metal. However, they are very inefficient and treatment may extend over a period of years before all the soluble products have been removed^[105]. Also, once the soluble corrosion products have been removed the remaining patina will be porous and be susceptible to recontamination due to increased hygroscopicity.

Sodium sesquicarbonate solutions (1%-5%): The most tried and tested method for bronze stabilisation. The use of sodium sesquicarbonate is more efficient than distilled water, although it has been known to remove some of the copper metal and requires post-treatment washing to remove excess carbonates and bicarbonates. Treatments using this method have been known to extend beyond three years^[106]. As with washing in water, a porous patina may remain after treatment.

Benzotriazole (BTA) impregnation: BTA is a popular corrosion inhibitor used in many lacquers formulated for copper and its alloys. The complexing of BTA with surface copper (II) corrosion products releases chloride ions into the wash solution, see *Eqn 1.7*.



The effect of the BTA can change the appearance of the patination and, although the BTA film has good inhibiting properties, they have been known to fail after a few years^[107].

1.5.4 Re-patination

On first consideration, completely stripping the corroded object and artificially re-patinating may appear to be the most viable method of obtaining a good quality patina over which the patineur could exercise complete control. There are, however, a number of reasons why re-patination is out of favour with many conservators.

(1) Loss of base metal: a significant proportion of the patina will inevitably contain metal from the underlying object, hence a small amount of metal is sacrificed whenever an object is re-patinated. Also, there is likely to be loss of metal during the removal of the corrosion products prior to re-patination e.g., from abrasives. This pre-cleaning treatment has to be rigorous otherwise the applied patinating solution will not form a uniform, adherent layer.

(2) Inferior patination: artificial patination techniques cannot match natural patina for quality and durability. It is for this reason that original patination applied at the foundry rarely survives on outdoor sculpture^[108]. To this day, no artificial technique has been found to accelerate the formation of the desirable, uniform, brochantite patina that in nature requires numerous rain-water cycles to form.

(3) Loss of information: re-patination involves a radical change to the surface after which all historic information and evidence of antiquity present within the original patina has been lost.

The net result of these effects leaves re-patination as an option reserved for objects with little historic value and the process is applied primarily for aesthetic reasons.

Summary

This chapter has given the reader an introduction to the principles of metal corrosion and has illustrated the chemical and structural diversity of corrosion products that may be encountered and negotiated in metal cleaning and treatment in general. The main interest of this study is to investigate, by the use of a laser, metal cleaning in sculpture conservation and for this purpose it is essential that both artistic and physical criteria are met.

Contemporary problems with the removal of both organic and inorganic coatings have been described and these have provided the main incentive for this Ph.D. project. The next chapter describes how the principles of laser-physics and surface analysis techniques were combined to investigate the laser treatment of coated and corroded metal systems.

References

- [1] Martin, J. W., from *Elementary Science of Metals 1*, Wykeham Publications, London, (1969), 1.
- [2] Keen, W. R., Rogers, M. J. W., Simpson, P., from *Chemistry: Facts, Patterns, and Principles*, Addison-Wesley Pub. Ltd., London, 219.
- [3] Scott, D. A., from *Metallography and Microstructure of Ancient and Historic Metals*, The Getty Conservation Institute, Singapore (1991), 5.
- [4] Fowles G, R., from *Introduction to Modern Optics*, 2nd Ed., Holt, Reinhart and Winston, (1968), 160-3.
- [5] *Ad idem*, 168.
- [6] *Ad idem*, 162.
- [7] Prokorov, A. M., Konov, V. I., Ursu, I., Mihailescu, I. N., from *Laser Heating of Metals*, Adam Hilger, Bristol, (1990), 3-6.
- [8] *Ad idem*, p32.
- [9] Bennet, H. E., Bennet, J. M., Ashley, E. J., and Motyka, R. H., *Phys Rev*, 165, (1968), 755.
- [10] Savage, G., from *A Concise History of Bronzes*, Thames and Hudson, (1968), 119.
- [11] Mantle, E. C., *Copper and Copper Alloy Castings: Properties and Application*, Copper Development Agency, 1991.
- [12] Untracht, O., from *Jewellery Concepts and Technology*, Robert Hale, London, 51-53.
- [13] Scott, A.D., *Metallography and Microstructure of Ancient and Historic Metals*, The Getty Conservation Inst., Singapore, (1991), 27-9.
- [14] Varoufakis, G., Stathis, E. C., 'A contribution to the study of the corrosion of ancient bronzes', *Metallurgia*, (May 1971), 141-44.
- [15] Hughes, R., Rowe, M., *The Colouring, Bronzing and Patination of Metals*, Thames and Hudson, (1993) p9-23.
- [16] Plenderith, H., from *The Conservation of Antiquities and Works of Art*, Oxford University Press, London, (1966), Chapt xii.
- [17] Martin, J. W., from *Elementary Science of Metals*, Wykeham Publications (London) Ltd. (1969), 79-80.
- [18] Higgins, R. A., from *Engineering Metallurgy Pt. 1: Applied Physical Metallurgy*, 2nd Ed., The English Universities Press, London (1968), 134-44.
- [19] ASA, from *About Aluminium*, The Aluminium Stockholders Association, (1992), 7-9.
- [20] Alcan, from *Designations and Applications for Wrought Aluminium Alloys*, British Alcan Aluminium leaflet.
- [21] Canning, from *The Canning Handbook: Surface Finishing Technology*, W. Canning plc, Birmingham (1989), 293-358.
- [22] Selvaraj, M., Mohan, P. S., Chandran, K., Guruviah, S., 'Performance of paint coatings on zinc coated steel', *Bull. Electrochem.* 5(7), (1989), 502-4.
- [23] Munger, C. G., Drisko, R. W., 'A review of common failures of paint coatings. Part II, factors of uncoated and coated substrates that affect coating performance.', *Journal of Protective Coatings and Linings*, 7(5), (1990), 62-66.
- [24] No author cited, 'Options in surfacing through laser technology', *Compressed Air*, 94(10), (1989), 8-11.
- [25] Yang, D., Zhang, X., Xue, Q., 'Effects of laser treatment on the fretting wear properties of 2CR13 stainless steel'.
- [26] Henari, F., Blau, W., 'Excimer-laser surface treatment of metals for improved adhesion', *Applied Optics*, 34(3), (1995), 581-4.
- [27] Zeng, X., Tao, Z., Zhu, B., 'The development of laser surface treatment in China', from *Recent Trends in Welding Science and Technology*, ASM International, (1989), 523-7.
- [28] Canning, from *The Canning Handbook: Surface Finishing Technology*, W. Canning plc, Birmingham (1989), 840-87.
- [29] Satre, J.P. Nausea, Penguin Books Ltd, London, (1963), 47.
- [30] Evans, U. R., from *Metallic Corrosion, Passivity and Protection*, Arnold, London, (1946), 13.
- [31] Vernon, W.H.J., and Whitby, L., 'The open-air corrosion of copper. A chemical study of the surface patina', *J. Inst of Metals* 42, (1929), 181-196.

- [32] Scott, D. A., 'Copper compounds in metals and colorants: oxides and hydroxides', *Studies in Conservation*, 42, (1997), 93-100.
- [33] K. Nassau, Miller, A.E., Graedel, T.E., 'The reaction of rain with copper, copper patina, and some copper compounds', *Corrosion Science*, 27(7), (1987), 703-19.
- [34] Livingston, R. A., 'Influence of the environment on the patina of the Statue of Liberty', *Environ. Sci. Tech.*, 25(8), (1991), 1400-8.
- [35] Sherwood, S. I., 'The Greening of American Monuments: The role of atmospheric chemistry in the corrosion of outdoor bronzes'.
- [36] Graedel, T. E., 'The corrosivity of the atmosphere: Past, present and future'.
- [37] Mansfeld, F., 'Atmospheric Corrosion', in *Degradation of Metals in the Atmosphere*, ASTM STP 965, ed S.W.Dean and T. S. Lee, Philadelphia, (1988), 571-84.
- [38] Payer, J. H., Ball, G., Richett, B. I., Kim, H. S., 'Role of transport properties in corrosion products growth', *Materials Science and Engineering A198*, (1995), 91-102.
- [39] Plenderleith, J. H., from "The Conservation of Antiquities and Works of Art", Oxford University Press, London, (1966), 190-2.
- [40] Lins, A., 'Outdoor Bronzes: Some Basic Metallurgical Considerations,' from *Sculptural Monuments in an Outdoor Environment*, Ed. V.N. Naude, Philadelphia, (1985), 9-20.
- [41] Leidheiser, H. Jr., "The Corrosion of Copper, Tin, and their Alloys". The Electrochemical Society Corrosion Monograph Series. New York. John Wiley and Sons, 1971.
- [42] Shastry, C. R., Friel, J. J., and Townsend, H. E., 'Sixteen-year atmospheric corrosion performance of weathering steels in marine, rural, and industrial environments', from *Degradation of Metals in the Atmosphere*, Philadelphia, (1986), 5-15.
- [43] Mattsson, E., and Holm, R., 'Copper and copper alloys', from *Metal Corrosion in the Atmosphere*, 187-97.
- [44] Tennent, N. H., and Baird, T., 'The identification of acetate efflorescence on bronze antiquities stored in wooden cabinets', *The Conservator*, 16, (1992), 39-43.
- [45] Accardo et al, 'Stress monitoring by temperature mapping and acoustic emission analysis: A case study of Marcus Aurelius', *Studies in Conservation* 28(2), (1983), 67-74.
- [46] Patscheider, J., Veprek, S., 'Application of low-pressure hydrogen plasma to the conservation of ancient iron artifacts', *Studies in Conservation*, 31 (1986) 29-37.
- [47] MacLeod, I., 'Conservation of corroded copper alloys: A comparison of new and traditional methods for removing chloride ions', *Studies in Conservation*, 32 (1987), 25-40.
- [48] Plenderleith, J. H., from 'The Conservation of Antiquities and Works of Art', Oxford University Press, London, (1966), 216.
- [49] Collins, W.F., 'The Corrosion of Early Chinese Bronzes', 24-47.
- [50] Selwyn, L. S., Poitras, B. J., Laver, M. E., and Downham, D. A., 'Outdoor bronze statues: Analysis of metal and surface samples', *Studies in Conservation*, 41 (1996), 205-228.
- [51] Fink, C. G., 'Periodic formation of corrosion products', in *The Conservation Handbook*, Ed. H. H. Uhlig, J. Wiley, New York, (1948), 103.
- [52] Socha, J., 'Oxide coating in the conservation of metal monuments: The Column of King Sigismundus III Waza in Warsaw', *Studies in Conservation*, 25 (1980), 14-8.
- [53] Prof. Vendl, private communication.
- [54] Weil, P. D., 'Patina: Historical perspective on the artistic intent and subsequent effects of time, nature and man.', from *Sculptural Monuments in an Outdoor Environment*, Pennsylvania Institute of Fine Arts, Philadelphia, (1985), 21-7.
- [55] Scott, D. A., 'Copper compounds in metals and colorants: Oxides and hydroxides', *Studies in Conservation*, 42, (1997), 93-100.
- [56] MacLeod, I. D., 'Identification of corrosion products on non-ferrous metal artifacts recovered from shipwrecks', *Studies in Conservation*, 36, (1991), 222-34.
- [57] Hjelm-Hansen, N., 'Cleaning and stabilisation of sulphide-corroded bronzes', *Studies in Conservation*, 29 (1984), 17-20.
- [58] Graedel, T. E., Nassau, K., and Franey, J. P., 'Copper patinas formed in the atmosphere-I. Introduction', *Corrosion Science*, 27, (1987), 639-57.
- [59] Cathcart, A. N., *J. Inst of Metals*, 49, (1932), 161.

- [60] Livingston, R. A., 'Influence of the environment on the patina of the statue of liberty', *Environmental Science and Technology*, 25(8), 1991, 1400-8.
- [61] Wingerson, L., 'America cleans up Liberty', *New Scientist*, (25 Dec 1986), 31-35.
- [62] Nielsen, N. A., 'Keeping the torch lit', *Mater. Perform.*, 23(4), (1984), 78-80.
- [63] Opila, R. L., 'Copper patinas - an investigation by auger electron spectroscopy', *Corros. Sci.*, 27, (1987), 685-94.
- [64] Selwyn, L. S., Poitras, B. J., Laver, M. E., and Downham, D. A., 'Outdoor bronze statues: Analysis of metal and surface samples', *Studies in Conservation*, 41, (1996), 205-228.
- [65] Sharma, V. C., Lal, U. S., Nair, M. V., 'Zinc dust treatment - an effective method for the control of bronze disease on excavated objects', *Studies in Conservation*, 40, (1995), 110-9.
- [66] Walker, R., 'Corrosion and preservation of bronze artifacts', *J. Chemical Education*, 57(4), (April 1980), 277-80.
- [67] Pollard, A. M., Thomas, R. G., Williams, P. A., 'Mineralogical changes arising from the use of aqueous sodium carbonate solutions for the treatment of archaeological copper objects', *Studies in Conservation*, 35, (1990), 148-50.
- [68] Morales, J., Fernandez, G. T., Esparza, P., Gonzalez, S., Salvarezza, R. C., and Arvia, J., 'A comparative study of the passivation and localised corrosion of alpha, beta and alpha+beta brass in borate buffer solutions containing sodium chloride I. Electrochemical data', *Corrosion Science*, 37(2), (1995), 213-31.
- [69] Evans, U. R., *Metallic Corrosion, Passivity and Protection*, Edward Arnolds and Co, London, (1946), 2.
- [70] Biasini, V., Cristoferi, E., 'A study of the corrosion products on sixteenth and seventeenth century armour from the Ravenna National Museum', *Studies in Conservation* 40 (1995), 250-6.
- [71] Sjorgren, A., and Buchwald, V. F., 'Hydrogen plasma reduction in the D.C. mode for the conservation of iron meteorites and antiquities', *Studies in Conservation* 36 (1991), 161-71.
- [72] Zucchi, F., 'Beta-iron oxide hydroxide formation in localised active corrosion of iron artifacts' in *Corrosion and Metal Artifacts*, NBS Special Publication 479 (1977), 103-5.
- [73] Keller, P., 'Vorkommen, Entstehung und Phaseumwandlung von Beta-FeOOH in Rost', *Werk U. Korr.*, 20, (1969), 102.
- [74] Plenderleith, J. H., from *The Conservation of Antiquities and Works of Art*, Oxford University Press, London, (1966), 258-71.
- [75] Cottam, C. A., unpublished work.
- [76] Mattias, P., 'The degradation of lead antiquities from Italy', *Studies in Conservation*, 29, (1984), 87-92.
- [77] MacLeod, I. D., 'Stabilization of corroded aluminium', *Studies in Conservation*, 28, (1983), 1-7.
- [78] Fabrizi, M., Ganiaris, H., Tarling, S., Scott, D. A., 'The occurrence of sampleite, a complex copper phosphate, as a corrosion product on copper alloys objects from Memphis, Egypt', *Studies in Conservation*, 34, (1989), 45-51.
- [79] Hughes, R., Rowe, M., from *The Colouring, Bronzing and Patination of Metals*, Thames and Hudson, London, (1993), 10.
- [80] Lippard, L., 'As painting is to sculpture: A changing ratio', from *American Sculpture in the Sixties*, ed. M. Tuchman, New Graphic Society, Greenwich, (1967), 33.
- [81] Geist, S., from *Color it Sculpture*, Arts Yearbook-8, New York, (1965), 93-95.
- [82] Evans, U. R., *Metallic Corrosion, Passivity and Protection*, Edward Arnolds and Co, London, (1946), 3.
- [83] *Ad Idem*, 10.
- [84] *Ad Idem*, Chapt. 12.
- [85] Howard, J., 'Versatile Coatings', *New Scientist*, Inside Science No.88, 17th Feb, (1996), 1-4.
- [86] Walter, G. W., 'Critical review of the protection of metals by paints', *Corrosion Science* 26(1), (1986), 27-38.
- [87] Erhardt, D., Veloz, N. F., 'The durability of Inctalac: Examination of a ten year treatment', *ICOM 1984 preprints of 7th Triennial Meeting*, 84(22), 1-3.
- [88] Stevens, M. P., from *Polymer Chemistry, An Introduction*. 2nd Ed., Oxford University Press, London, (1990).

- [89] Rene de la Rie, E., 'Polymer stabilizers: a survey with reference to possible applications in the conservation field', 33, (1988), 9-22.
- [90] Holsworth R. M., 'Organic coatings failure analysis', *Journal of Coatings Technology*, 53(680), 1981, 34.
- [91] Larson, J., private communication.
- [92] Kirschner, E. M., 'Environmental, health concerns force shift in use of organic solvents', *Chemical and Engineering News*, 72(25), (20 Jun 1994), 13-20.
- [93] McIlroy, M. S., 'Investigation of laboratory methods for cleaning typical metallic surfaces using aqueous type cleaning agents', *ASTM Special Technical Publication*, 1197, (1993), 373-388.
- [94] Triplett, T., 'ABCs of VOC control', *Industrial Paint and Powder*, 72(5), (May 1996), 4.
- [95] Takahara, H., Usui, M., 'Solvent recovery technique and purification of environment in adjustment to replacing CFCs and trichloroethane', *R&D: Research and Development*, 43(2), April 1993, 41-3.
- [96] Hirota, Y., Sugii, K., Homma, Y., 'The cleaning effects of running deionised water on a GaAs surface', *J. Electrochem. Soc.*, 138, (1991), 799.
- [97] Layden, L., Wadlow, D., 'High-velocity carbon dioxide snow for cleaning vacuum-system surfaces', *J. Vac. Sci. & Tech.*, A8, (1990), 3881.
- [98] Yew, T. R., Reif, R., 'Low-temperature in-situ surface cleaning of oxide-patterned wafers by Ar/H₂ plasma sputter', *J. Appl. Phys.*, 68, (1990), 4681.
- [99] Poulis, J. A., Cool, J. C., Logtenberg, E. H. P., 'UV/ozone cleaning, a convenient alternative for high-quality bonding preparation', *Int. J. Adhesion and Adhesives*, 13(2), (April 1993), 89-96.
- [100] Sowell, R. R., Cuthrell, R. E., Maddox, D. M., Bland, R. D., 'Surface cleaning by ultraviolet radiation', *J. Vac. Sci. Tech.*, 11(1), (1974), 474-5.
- [101] Lu, Y., Aoyagi, Y., 'Laser induced dry-cleaning in air - a new surface cleaning technology in lieu of carbon fluorochloride (CFC) solvents', *Jpn. J. Appl. Phys.*, 33, (1994), 430-3.
- [102] Skerry, B. B. and Simpson, C. H., 'Accelerated test method for assessing corrosion and weathering of paints for atmospheric corrosion control', *Corrosion*, 49(8), (1993), 663-74.
- [103] Riss, D., 'Managing the care of the outdoor metal monuments by the National Park Service: Some past experience and future direction. An unofficial view by an NPS conservator', from *Sculptural Monuments in an Outdoor Environment*, Pennsylvania Institute of Fine Arts, Philadelphia, (1985), 29-38.
- [104] Ganorkar, M. C., Rao, V. P., Gayathri, P., Rao, T. A. S., 'A novel method for the conservation of copper-based artifacts', *Studies in Conservation*, 33, (1988), 97-101.
- [105] MacLeod, I., 'Conservation of corroded copper alloys: a comparison of new and traditional methods for removing chloride ions', *Studies in Conservation*, 32, (1987), 25-40.
- [106] Organ, R. M., 'Aspects of bronze patina and its treatment', *Studies in Conservation*, 8, (1963), 3-9.
- [107] Merk, L. E., 'The effectiveness of benzotriazole in the inhibition of the corrosive behaviour of stripping reagents on bronzes', *Studies in Conservation*, 26, (1981), 73-76.
- [108] Naylor, A., private communication.

CHAPTER 2

Methods and Monitoring of CO₂-Laser Treatment

2.1 Laser cleaning

John Asmus pioneered work in laser cleaning in 1972^[1]. A survey of publications on the Institute of Scientific Information Database containing the phrase 'laser cleaning' in the title or abstract reveals a marked increase in research in this area over the last 2 decades. In the 1980's only 9 publications containing the phrase were found compared with 49 in the 1990's, and 21 of those were in 1997. Laser cleaning typically finds niche applications in areas where conventional cleaning techniques are unsuitable. Perhaps the most popular lasers for cleaning are excimer lasers: these have found successful cleaning applications in areas such as semi-conductor manufacturing^[2,3,15]; the removal of mould from paper^[4,17]; the removal of organic contamination from various substrates^[5]; the removal of fingerprints from glass^[6] and the cleaning of historic oil paintings^[7,16]. Excimer laser cleaning of metals has also been reported with the successful removal of oxides from stainless steel^[8], copper and aluminium^[9] although significant heating of the surface was observed and vacuum conditions were required to prevent the surface oxidising again. Nd:YAG lasers have also found some cleaning applications, most notably in stone conservation^[10-14] where the valuable patina, that is often damaged or removed completely by conventional cleaning methods, is preserved by the laser.

Of the small amount of published research that has been conducted into the laser cleaning of metals, that which has been done has hardly touched upon the vast array of metals, corrosion products and organic coatings that may be encountered, particularly in the field of metal sculpture conservation. It is for this reason that this research was undertaken. For this study, a pulsed Transversely Excited Atmospheric (TEA) CO₂-laser was employed for the reason that the 10.6µm radiation emitted is strongly reflected by most metals and

hence damage to the metal substrate is less likely than using similar power lasers at shorter wavelengths.

2.1.1 Principles of TEA CO₂-lasers

CO₂-lasers are among the most popular and powerful lasers used in industry today. These lasers may vary widely in their internal structure and functional characteristics, but the fundamental mechanisms of their operation are basically the same.

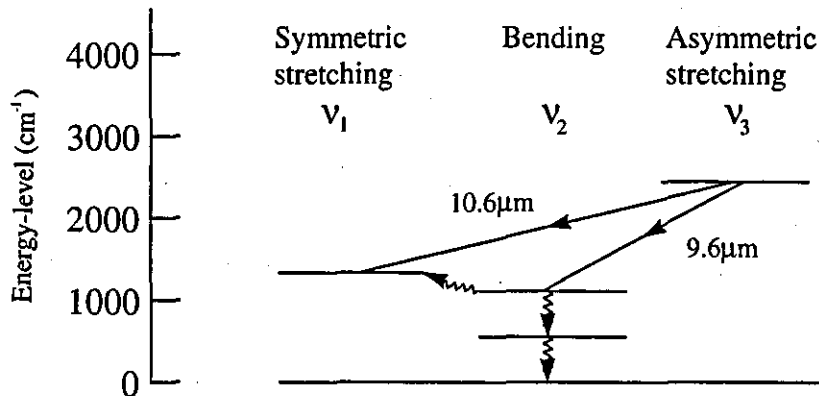


Fig. 2.1.1a: Energy-level structure in a CO₂-laser showing the relevant vibrational modes of the CO₂ molecules.

The active medium in a CO₂-laser is a mixture of CO₂, N₂, He and CO gases. The mixture is contained within a glass laser cavity containing a pair of electrodes with adjacent photo-ionising pins. Lasing is initiated when a high voltage pulse (~40kV) is applied to the electrodes thereby producing a series of intense arc discharges from the row of photo-ioniser pins, the resulting ultraviolet radiation exciting the CO₂ gas. The gas ionises and becomes conductive, allowing a current to flow through the gas between the electrodes. The resultant glow-discharge converts the supplied electrical energy into molecular vibrational energy in the CO₂ and N₂ molecules. The CO₂ molecules vibrate asymmetrically and, on losing energy, fall into one of two lower energy vibrational states resulting in either 10.6 or 9.6 μm photon emission, see *Fig. 2.1.1a*: these are the two

principal vibrational transitions of the CO₂-laser. The excited N₂ molecules excite other CO₂ molecules to the upper laser level.

Collisions with the helium gas aid the CO₂ molecules which have 'lased' to drop down from the lower energy levels to the ground state to sustain the population inversion required for lasing. Mirrors at either end of the cavity define the directional characteristics of the radiation and ensure that the infrared radiation is directed along the cavity and out through the partially reflecting mirror. Rows of fans built into the laser cavity allow for high repetition rates by ensuring that the gas between the electrodes is changed after each discharge.

CO is present in the laser mix to neutralise any 'free oxygen' produced by the breakdown of the CO₂ by the electrical discharge: a constant supply of fresh gas is required to replenish gas lost through breakdown. Temperatures inside the cavity must be kept below about 420K to maintain high gain levels so an internal water-cooled heat exchanger cools the gas as it circulates. Temperatures in excess of 420K cause significant population of the lower laser levels and hence reduce the gain of the laser cavity.

TEA CO₂-lasers, such as the one used in the experiments described in this thesis, differ from other CO₂-lasers by passing electric pulses through the gas in a direction transverse to the laser cavity axis. This arrangement produces pulsed as opposed to continuous wave radiation, and enables the laser to operate at much higher cavity pressures and extremely high powers per unit volume of gas compared with alternative arrangements^[18].

2.1.2 Laser interactions with materials

Laser ablation

Any explosive laser-material interaction is generically termed 'laser ablation'^[19]. The conditions that are required for ablation vary considerably, but typically require

microsecond (or shorter) pulses with irradiances in excess of 10^9W/cm^2 focused onto a sufficiently absorbing material, as shown in *Fig. 2.1.2a*. The vaporisation temperature of the surface is exceeded within a fraction of the pulse duration. The vaporised (blow-off) material has insufficient velocity to escape the surface before the underlying material is vaporised. Hence, temperature and pressure at the surface are rapidly increased to cause an explosion, an observable plasma or plume, and audible report. The rate of vaporisation can be so rapid that insufficient time is permitted for the significant transfer of heat into the bulk of the material by conduction, hence evidence of melting is often absent from the ablation site.

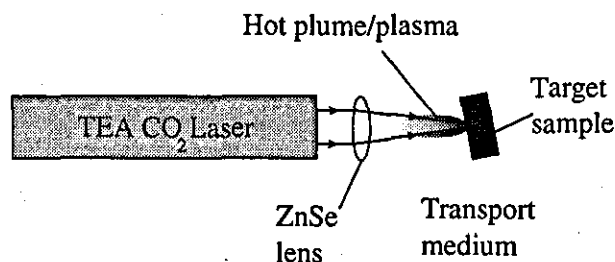


Fig. 2.1.2a: TEA CO₂-laser ablation of target material. The transport medium is usually air.

Ablation mechanisms

Depending on the wavelength of the incident radiation, one of two interaction processes are likely to dominate^[20].

Photochemical absorption: this dominates short wavelength (i.e. ultraviolet) interactions with matter. Incident photons induce electronic transitions to higher energy states within the target material. Transitions can lead to molecular dissociation by attaining an energy level above the dissociation limit or by creating an energy state that is sufficiently repulsive. Photochemical absorption of a single photon will usually be sufficient to cause dissociation in a given molecule.

Thermal absorption: individual visible and infrared photons do not usually have sufficient energy to break chemical bonds. Visible and infrared radiation is absorbed into the vibrational modes of the molecules directly or indirectly, via low-lying electronic energy states. These thermal processes raise the temperature of the target material and cause dissociation through vaporisation. Multiple photon absorption can also cause dissociation through photochemical processes, although this is unlikely due to the short lifetimes of low-lying energy states.

2.1.3 Factors affecting ablation characteristics

Laser characteristics

In many respects, it is difficult to alter the parameters of pulsed radiation for most lasers. A TEA CO₂-laser has no method of altering pulse duration or wavelength without great financial expenditure and loss of power. Apart from angle of incidence and laser fluence (controlled using a simple lens), all other laser parameters are essentially fixed.

Wavelength: determines to what extent ablation is likely to be a photochemical or thermal process. TEA CO₂-lasers emit at 10.6 μ m, in the far infrared, so the majority of the interaction is likely to be thermal.

Radiant flux density or RFD (power/area): in general, only pulsed lasers are powerful enough to deliver sufficient energy to a surface rapidly enough to prevent significant conduction to the bulk material, thereby ensuring a well-defined thermal discontinuity. The RFD can easily be varied using a simple convex lens to alter the spot dimensions. The rate of energy transfer to the surface is directly related to the RFD if interaction with the blow-off material is ignored. At an RFD high enough to exceed the plasma threshold for a given material, the blow-off material may absorb sufficient radiation to become ionised and form an opaque plasma, effectively shielding the target from the remaining laser pulse. Thus, the most efficient cleaning RFD is usually just below the plasma

threshold; using a lower RFD would expend a greater proportion of energy heating, but not vaporising, the target material.

Pulse duration: is a fixed parameter for many pulsed lasers and may vary from microseconds down to picoseconds for different lasers. A short pulse duration reduces the likelihood of thermal conduction between ablating material and the underlying material.

Angle of incidence: The reflectivity of materials is a function of the angle of the incident radiation. However, corroded surfaces have a surface roughness that presents a randomly orientated profile to the laser such that the angle of incident varies across the sample.

Spatial beam profile: all lasers exhibit intensity variation across the spatial profile of the beam. Intensity variations are caused by stable configurations of electromagnetic field within the resonant cavity, called modes, and diffraction effects at the aperture. The TEA CO₂-laser used in these experiments operated in multimode emission: this extracts the most output power from the laser cavity but produces an uneven beam with large divergence, see *Fig 2.1.3a*. Beam inhomogeneity will produce variation in the rate of ablation across the irradiated target area, and 'hot-spots' may induce undesirable plasma ignition. Beam homogenisers are available but are limited in their power handling capabilities. In general, however, when lasers are used for surface processing applications, high power beam delivery takes precedence over beam quality.

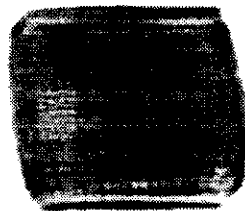


Fig. 2.1.3a: TEA CO₂-laser pulse incident on thermosensitive paper (actual size). The different modes are visible as horizontal lines.

Temporal beam profile (TBP): pulsed lasers do not deliver energy at a constant rate but have a characteristic pulse profile typically consisting of a pronounced peak with a relatively long tail, see *Fig 2.1.4c*. The laser flux is thus varying throughout the duration of each pulse and only approaches the maximum for a fraction of the overall pulse length.

Target characteristics

Although target characteristics are fundamental in determining laser-material interactions, many of the properties of the target will vary during the ablation process adding dynamic complexity to the system.

Reflectivity (R): determines what proportion of incident radiation is absorbed by the target and how much is reflected from the sample. Radiation incident on highly reflective samples may still form a plasma if the flux is sufficiently high to ionise the transport medium. The reflectivity of metals decreases as an approximately linear function of increasing temperature, as determined by the Drude model^[21]. The absorptivity (1-R) may as much as double from a temperature increase of a few hundred degrees or with a change of state from solid to liquid, for example, the absorptivity of pure silver increases from 0.0197 to 0.0374 on melting^[22].

Absorption coefficient (α): once radiation has penetrated the target, the heating effect that follows is dependent upon the rate of absorption. Metals typically have an absorption coefficient in the region of 10^6cm^{-1} for $10.6\mu\text{m}$ radiation and, although this results in the rapid absorption of radiation close to the surface, their high reflectivities at this wavelength significantly reduce any heating effects, see *Fig. 2.4.1a*.

Melting/boiling point and latent heat of fusion/vaporisation: determine whether the energy coupled with the target is sufficient to cause a change in state.

Thermal conductivity (K) and diffusivity (κ): a highly conducting target provides a heat-sink for the energy coupled to the surface thus reducing the surface temperature. For most metals, thermal conductivity and diffusivity decrease as an approximately linear function of temperature increase; brass and bronze are an exception as their thermal conductivities and diffusivities increase as a function of temperature.

Thickness: After each laser pulse is delivered to the target the heat energy is dissipated from the surface to the bulk of the sample and is gradually re-radiated into the surrounding atmosphere. Thus, successive pulses will gradually increase the temperature of the bulk material until there is equilibrium between the supplied and dissipated energy. The bulk temperature rise per pulse is therefore dependent on the thickness of the target for a given substrate.

Transport medium characteristics

Although the most convenient transport medium for laser cleaning is air, directing a flow of alternative gas^[23,24] or applying a liquid coating to the target^[25] can significantly alter the laser/surface interaction.

Density: a dense (i.e. solid or liquid), transparent medium that allows the laser beam to penetrate to the surface can accelerate the cleaning process. For example, if a thin layer of water is applied during the removal of a black crust from limestone, the laser heated crust causes an explosive vaporisation of the water which exerts sufficiently large forces on the underlying crust to loosen and eject material from it^[26].

Ionisation energy: the ionisation energy of a gaseous transport medium can provide control over the breakdown threshold for plasma formation during laser treatment. However, if a significant mass of blow-off material is produced during the treatment process, a plasma may form from the ablation products regardless of the type of gaseous environment employed.

Reactivity: will determine whether, and to what extent, there will be a chemical reaction between the transport medium and the surface of the target material. For example, the use of an inert gas transport medium will prevent the surface reacting with the atmosphere during laser-treatment. Metal surfaces may oxidise if heated by a laser in an oxygen or air atmosphere.

2.1.4 Plasma/sub-plasma cleaning effects

By varying the flux incident on a given target, the blow-off material may take one of three forms:

(i) Plume: a gaseous emission of vaporised material that may be accompanied by solid particulate matter in the form of smoke. At infrared wavelengths the plume has a very low absorption coefficient and will not significantly deprive the surface of subsequent radiation. No visible light is emitted by the plume although an audible 'click' may be produced by the rapid expansion of gas.

(ii) Hot-plume: at a higher flux, the blow-off material may absorb sufficient radiation to emit a characteristic orange/yellow glow, see *Photo 2.1.4a*. Some of the blow-off material may be ionised and increase the absorptivity of the plume to the laser radiation. Each pulse creates a loud snap.

(iii) Plasma: a plasma is a dense cloud of interacting ionised gas the formation of which requires a very high flux. The plasma may be produced from the transport medium (e.g. air-breakdown), the blow-off material from the target, or both, and appears as a bright blue spark, see *Photo 2.1.4b*, accompanied by a very loud acoustic shock. Due to the high absorptivity of the plasma, further exposure of the target surface to laser radiation is prevented for its duration.

Plasma formation

The radiation intensity that is required to initiate plasma formation is known as the plasma threshold (typically of the order of 10^{11} Wcm^{-2} for gas breakdown^[25]). The initiation of plasma formation by CO₂-lasers is not fully understood - the ionisation potential of many gases far exceeds the quantum energy of the laser. A possible mechanism of initiation may be by the process of multi-photon ionisation whereby the simultaneous absorption of many quanta by a single atom can produce an ion-electron pair. The presence of impurities, such as dust, in the transport medium can significantly lower the plasma threshold for that medium by providing sites of high absorption. Once ionisation is initiated, the free electrons absorb photons through the inverse brehmsstrahlung process in which individual photons are absorbed by an electron in the field of a heavy particle (e.g. atom or ion). The inverse brehmsstrahlung process is proportional to the laser wavelength squared and is therefore relatively large for CO₂-lasers^[19]. As these electrons gain energy they can ionise more atoms through collisions, multiplying the ionised species and the process cascades to form a body of ionised species that is the plasma.

Plasma effects

The plasma forms an opaque, absorptive and impenetrable barrier to the laser for the subsequent duration of the pulse and therefore has a shielding effect. The target surface, however, will become irradiated by the plasma itself. The spectra of plasma radiation will appear as a Plancks' curve superposed with discrete peaks at the ionisation potentials of the various incorporated ionised species, as shown in *Fig 2.4.2b*. Plasma radiation can cover the infrared, visible, ultraviolet and soft X-ray regions of the spectrum. The surface of a target may be absorptive of plasma radiation although reflective of the laser radiation and significant surface heating may ensue. Ionised species may also be incident on the surface of the sample producing chemical interactions such as oxidation.

Laser cleaning is usually carried out below the plasma threshold to avoid damage to the substrate. However, there are certain industrial applications where modification of the target by the heating and ionisation effects of the plasma can be beneficial, such as pretreatments for adhesion^[27].

2.1.4.1 Temporal Beam Profile (TBP) measurements

Experimental

Observations of the TBP of the TEA CO₂-laser required the use of infra-red detectors with a very short rise time, such as ELTEC^[28] pyroelectric devices. These devices contain a thin sheet of lithium tantalate crystal that exhibits spontaneous electric polarisation below its Curie temperature of 883K, the maximum operating temperature. Heating such a material causes the molecular dipoles within the crystal to rotate, thereby creating a measurable current. These detectors were used in conjunction with a LeCroy 9424 Quad 350 MHz digital oscilloscope as described in *Fig 2.1.4a*.

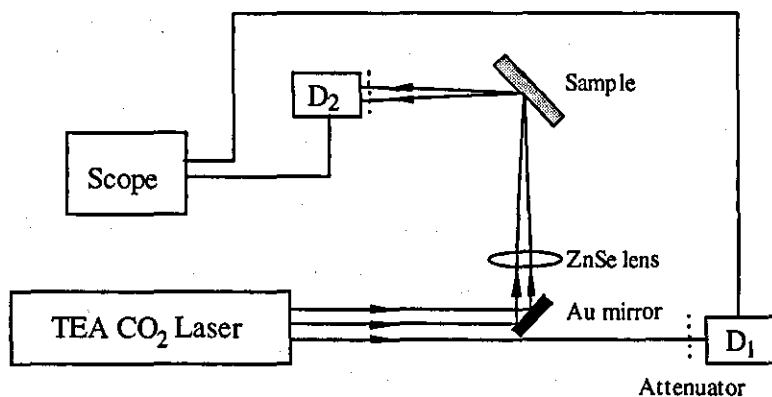


Fig. 2.1.4a: Apparatus to determine absorptive effects of laser induced breakdown on a laser pulse using pyroelectric detectors D₁ and D₂.

From the set-up described in *Fig 2.1.4a* the effect of the coupling of the laser pulse with the surface of the sample can be observed with the ELTEC detector, D₂, and compared with the pulse monitored at D₁. When the laser is fired, most of the beam is incident on

the gold mirror angled at 45 degrees. This portion of the beam is then focused onto the surface of the sample with a ZnSe lens. D₂ detects any specularly reflected radiation from the sample. A small portion of the beam avoids the gold mirror and is incident on D₁. If the incident radiation is focused onto the sample at a fluence that is insufficient to cause air-breakdown, the two detectors are expected to observe similar pulse profiles. If, however, the incident radiation is focused to a sufficient power to cause air-breakdown above the sample, the pulse profile is expected to be affected by the opacity of the plasma and should be observed by D₂. Plastic attenuators in front of the detectors were used to limit the intensity of incident radiation, thus preventing damage to the lithium tantalate crystals.

Results

Ablation below the plasma threshold had no significant effect on the shape of pulse profile of the beam reflected from the sample. Once the plasma threshold was exceeded the subsequent pulse profile was profoundly affected, the plasma effectively absorbing the entire tail of the laser pulse, as shown in *Fig 2.1.4c*.

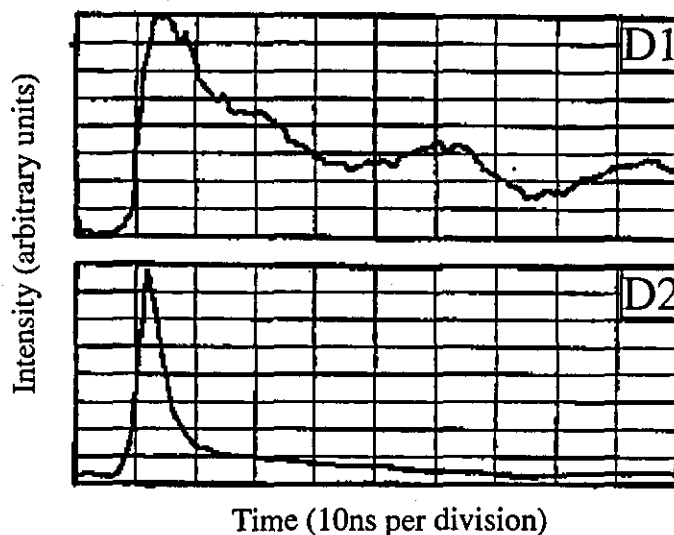


Fig. 2.1.4c: Profile of a TEA CO₂-laser radiation pulse directly incident on ELTEC detector (D₁) and incident on ELTEC detector (D₂) after plasma formation above target.

Conclusions

The initiation of a plasma occurs within the first 10ns, near the peak but on the leading edge of the laser pulse, once the plasma threshold has been exceeded. Once formed, the direct coupling of the laser with the surface is rapidly attenuated due to the opacity of the plasma. The formation of the plasma prevents approximately 70% of the incident radiation from directly coupling with the surface. Hence, the formation of a plasma greatly impairs the efficiency of laser treatment or cleaning at a specific wavelength.

2.1.5 Beam delivery

The irradiation of small samples can be achieved by keeping the laser stationary and manoeuvring the sample in the beam. Larger targets, such as metal sculpture, cannot easily be moved and require a flexible beam delivery system such that the operator may control the direction and focus of the beam on the target surface. Although fibre-optics form the most flexible and directional beam delivery systems they can be damaged by high power laser radiation^[29]. Optical-fibres for continuous wave CO₂-lasers are available up to powers in the region of 25W^[30], but none could be found that were suitable for high-powered, pulsed CO₂-lasers.

Development of a beam delivery system

The alternative to using optical fibres to manipulate the beam in three dimensions is to use a number of highly reflecting mirrors mounted in a multi-jointed tubular arm for beam delivery, as shown in *Fig 2.1.5a*. The mirrors are aligned such that the laser beam is guided along the centre of the arm regardless of its orientation.

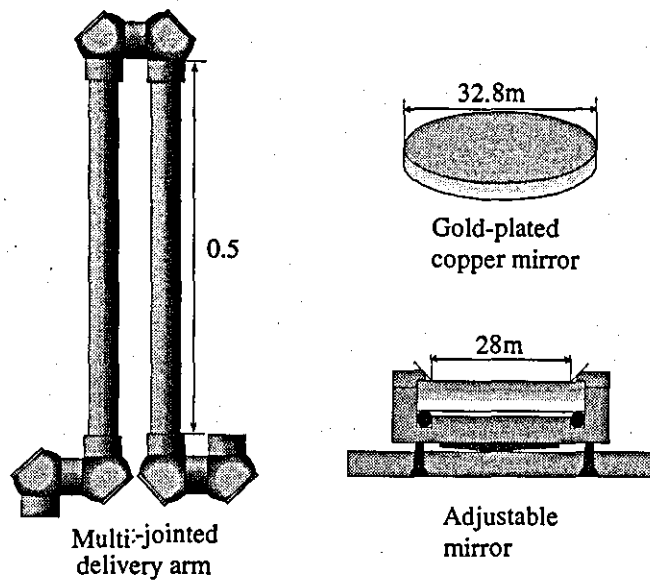


Fig 2.1.5a: TEA CO₂-laser beam delivery arm, mirrors and mirror mount.

For these experiments, an arm designed for use with a Nd:YAG laser was modified for the purpose. The glass mirrors were replaced with gold-plated copper mirrors and the arm re-aligned using a HeNe laser^[31]. The output beam from the TEA CO₂-laser had dimensions of approximately 25mm x 30mm whereas the arm had a circular aperture of only 20mm and beam reduction was attempted to reduce losses.

Beam reduction

Beam-reducers may take the form of two convex lenses or a convex and a concave lens, see *Fig 2.1.5b*. For our purposes, the latter option would have been superior because it avoids focusing the beam between the lenses which may cause unwanted air-breakdown. The former option was taken (option 1 in *Fig. 2.1.5b*) due to the availability of two convex ZnSe lenses of 38mm diameter and focal lengths of 100mm and 50mm respectively. The lenses were separated by a distance of 150mm, the sum of their focal lengths, and reduced the beam down to dimensions of approximately 12mm x 17 mm, as measured from burn-paper placed immediately after the collimating lens.

It was soon apparent that such a simple beam-reducing system was too crude to handle the output from the CO₂-laser. The beam had asymmetric divergence characteristics that prevented collimation in both planes using standard circular lenses. The diameter of the 'collimated' beam after it had traversed the length of the arm was greater than the uncollimated beam and of lower quality: even after the total length of the arm was halved, this problem remained and a further shortening of the arm would have imposed severe restrictions on the systems reach. Thus, the beam-reducer was excluded from the final set-up and the 60% losses accepted as unavoidable without considerable expenditure.

2.1.6 The CO₂-laser cleaning system

The full specification of the TEA CO₂-laser is given in Appendix D. The output of the laser is principally at the 10.6μm vibrational transition although many closely spaced, weaker rotational transitions are superimposed onto this^[32].

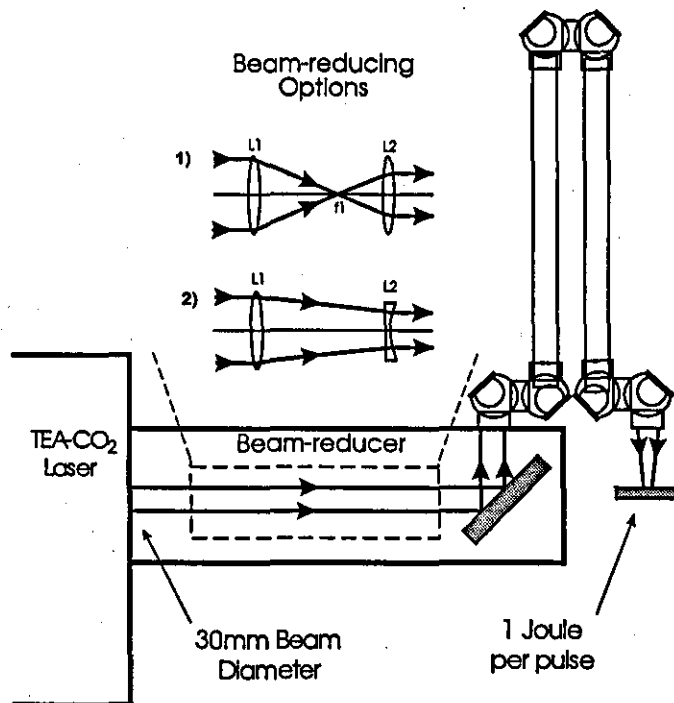


Fig. 2.1.5b: The beam delivery system attached to the TEA CO₂-laser.

The laser operates in multimode emission which optimises the total energy output from the laser cavity at the expense of beam quality (e.g. rapid divergence, large diameter and uneven intensity). The modified beam-delivery arm, as shown in *Fig 2.1.5b*, was mounted to the front of the laser when targets exceeded a convenient size for manipulation in the fixed beam. A very thin clear polyethylene sheet served as a guard against blow-off material damaging the delicate ZnSe lens.

2.2 Surface chemistry analysis

As described in Chapter 1, the chemistry of corrosion products determines, to a large extent, their quality and desirability on metal objects. A wide variety of methods of surface chemical analysis are available, each offering certain advantages and disadvantages over alternative methods. This section describes some of the methods used to obtain the results presented in Chapter 3, X-ray powder diffraction analysis was the most favoured analytical technique and shall be described in greater depth than the alternative methods.

2.2.1 X-ray powder diffraction analysis (XRD)

Principles of operation

The regular arrangement of atoms in a crystal lattice form sets of crystal planes. For a given wavelength (λ), the condition for simultaneous constructive interference for a beam of X-rays reflected from each horizontal plane is given by the Bragg equation,

$$n\lambda = 2d\sin\theta \quad \text{Eqn 2.1}$$

where d is the lattice spacing, n is an integer and θ is the incident angle measured from the crystal surface. Thus, from recording the angle of diffracted radiation from a single

crystal over a range of incident angles, the lattice spacings can be determined and the crystal identified with reference to existing diffraction patterns in the Powder Diffraction File^[33].

X-ray diffraction requires the production of a quasi-monochromatic beam of X-rays, normally achieved in diffraction apparatus by accelerating electrons from a cathode filament through a potential difference of between 10 and 300kV and allowing them to impact onto a metal-anode target, as shown in *Fig 2.2.1a*. Their rapid deceleration in the target material results in the production of brehmsstrahlung radiation in the X-ray region as well as the characteristic K_{α} and K_{β} peaks; filters and monochromators are used to select the K_{α} peak. The collimated X-ray beam is incident on the target surface at an angle θ .

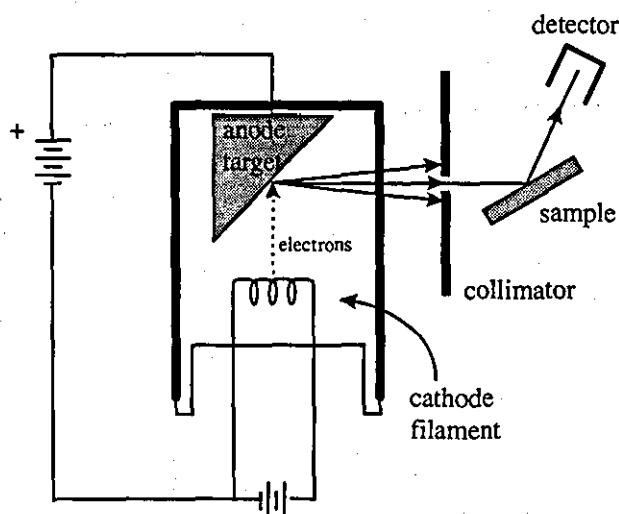


Fig. 2.2.1a: Schematic representation of XRD apparatus.

When the sample target is a single crystal, the diffracted X-rays form a pattern of spots that may be recorded on photographic film and analysed to determine the crystal geometry. When the sample target is a mass of randomly orientated crystals, as in the case of corrosion products, the diffracted rays form cones with their apex at the specimen, as shown in *Fig 2.2.1b*.

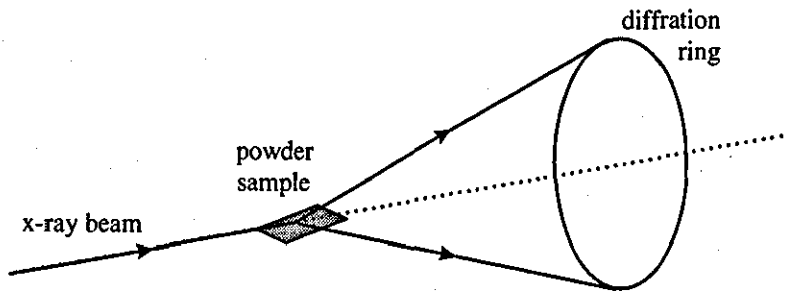


Fig: 2.2.1b: Diffraction ring formed by randomly orientated crystal powder.

As the powder sample is rotated at increments of 0.02 degrees, the detector, housed in a goniometer that rotates with the sample at an angle of 2θ (with respect to the incident beam of X-rays), records the intensity of the diffracted radiation. Strong diffraction peaks are superimposed on background radiation to give a diffraction pattern over a prescribed range of angles, as shown in *Fig 2.2.1c*.

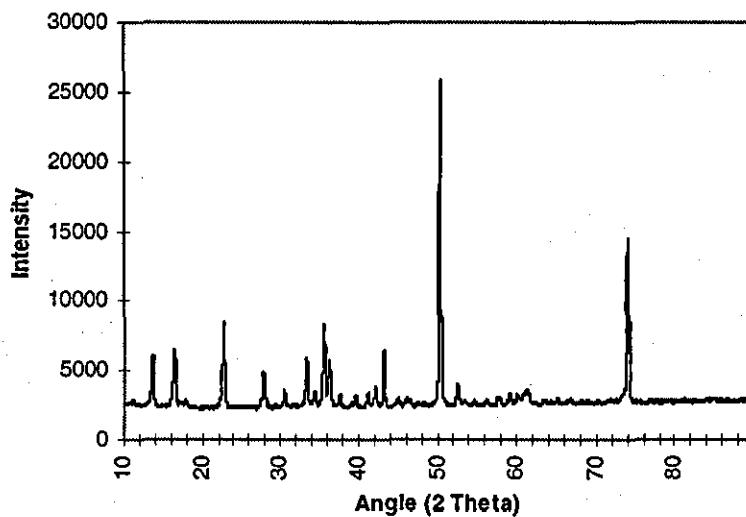


Fig: 2.2.1c: Diffraction peaks from a powder scan of corrosion products.

Eqn 2.1 can be used to find the d-spacing of the lattice planes corresponding to each diffraction peak. Identification of the sample material can then be made by comparing the d-spacing and relative peak intensities with those of known compounds.

Attributes of XRD

Compound identification: XRD provides more than just elemental analysis and can provide the full chemical formula for any of the tens of thousands of compounds already recorded. Compounds are identified by matching the strongest diffraction peaks with those listed in the powder diffraction reference catalogues. This method of analysis also allows for different phases of metals, alloys and inorganic compounds to be distinguished. Even compounds with the same chemical formula but different structures, such as PbO (litharge) and PbO (massicot), can be distinguished. When a variety of compounds are present on a sample this process becomes an arduous task as it is not often clear which peaks belong together. To take the tedium out of the process, a simple data-base was created to include the three most significant peaks of all the corresponding compounds recorded in the Powder Diffraction Files. XRD can only identify compounds that have a crystalline structure and therefore can be used on almost all inorganic compounds but few organic compounds. Completely amorphous compounds cannot be identified using XRD.

Proportions of components: semi-quantitative chemical analysis can be provided by the relative intensities of the diffraction peaks of respective compounds. Diffraction peak intensities for a given compound are not only a function of quantity, however, but also vary significantly with factors such as the size of crystallites and dimensions of the Bravais lattice*. Even if the results are properly calibrated the accuracy of quantitative analysis is generally poor.

Volume of analysis: the area of the target irradiated by the X-rays typically covers a few square millimeters which is sufficient to include all the compounds present. The X-rays have sufficient energy to penetrate through corrosion layers to the metal substrate, thereby providing information on the whole corrosive system and also the metal substrate.

* The Bravais lattice is an indefinitely repetitive arrangement of points in space that fulfils the condition that the environment of each point is identical to that of every other point. There are fourteen such arrangements in regular crystal systems.

Sensitivity: the intensity of diffracted peaks is proportional to the number of planes presented to the incident X-rays. Too few crystallites (i.e. too thin a corrosion layer) or crystallites too small to produce sufficient constructive interference may give poor peaks that will be lost in the background noise of the device. Also, corrosion layers containing large crystallites (i.e. in excess of 1 μ m) may produce a non-uniform diffraction cone and peaks will escape detection if the goniometer travels through a particularly weak section of the cone. The sensitivity will also vary depending on how effectively the structure of the compound under analysis diffracts X-rays. In general, most corrosion layers could be analysed satisfactorily and were typically a few tens of microns in thickness. The sensitivity of the instrument could be increased by increasing the scan duration or the number of passes for more difficult samples. In this way, any background noise caused by scattered X-rays could be reduced relative to the signal.

Errors: the accuracy to which each peak is resolved is determined by setting the angular increment on each scan. Although this increment remains constant, the d-spacing is proportional to the reciprocal of the sine of the diffraction angle (see *Eqn 2.1*) and, for a typical scan from 10 to 90 degrees, the interval of the d-spacing decreases as the angle increases. This was taken into account when identifying peaks by comparison with the d-spacings listed in the diffraction files: a closer match was expected as the diffraction angle increased. Low-order lines are also displaced by absorption of X-rays in the specimen to create irregular peaks. Not all diffraction patterns are unique and there are some cases where multiplicity could cause difficulties in the identification of the target material. Most minerals have complex, low-symmetry diffraction patterns which are unique to that compound but some metals and alloys produce identical diffraction patterns. Atomic replacements within the same structure are very common in minerals which results in considerable variation in the positions and relative intensities of their diffraction patterns.

2.2.2 X-ray photoelectron spectroscopy (XPS)

Principles of operation

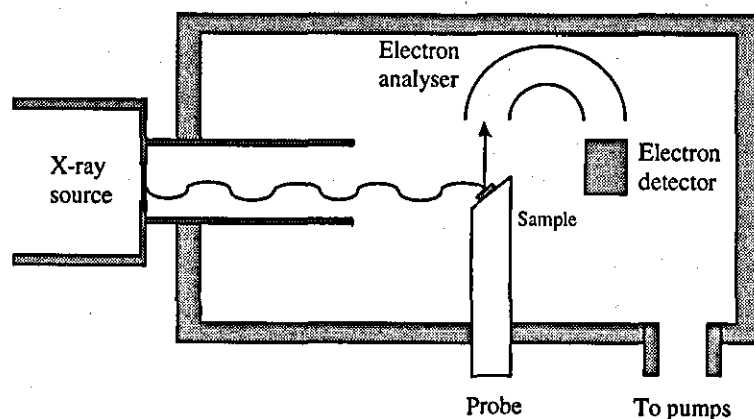


Fig: 2.2.2a: Schematic representation of XPS apparatus.

XPS uses a monochromatic beam of X-rays of known energy to eject photoelectrons from the target probe into an electron analyser, as shown in *Fig 2.2.2a*. Assuming a negligible recoil energy from the emitting atom, the kinetic energy (E_k) of the photoelectron is equal to the energy of the X-ray ($h\nu$) minus the binding energy (E_b) of the atom, see *Eqn 2.2*. The electron detector is able to determine the energy of the photoelectrons from which the binding energy can be found and the element identified.

$$E_k = h\nu - E_b \quad \text{Eqn 2.2}$$

Thus, every band in an XPS spectrum corresponds to an occupied atomic or molecular orbital of the sample substance. This provides not only elemental analysis, but also information on the oxidation states of the target compounds.

Attributes of XPS

Compound identification: XPS can provide elemental analysis of all solids, organic and inorganic, although it will not detect hydrogen or helium. The oxidation states of elements can also be determined which provides some indication as to the structure of the compounds.

Proportions of constituents: the atomic percentage of elements present can be provided to an accuracy of up to 0.1%.

Sampling depth: depending on the energy of the incident X-rays (typically below 1200eV) and the properties of the target material, the sampling depth can vary between 2 and 10nm. It is very likely that the top 10nm of a corrosion layer does not accurately represent the bulk of the corrosion layer, and XPS analysis was generally reserved for studying very thin corrosion layers or homogenous paint layers. Depth-profiling using ion-bombardment is possible on some XPS apparatus but was not available on our machine.

Errors: The sampling depth makes XPS very sensitive to surface contamination, such as dust or finger-prints, and samples were wrapped in aluminium foil between treatment and XPS analysis, which was carried out as soon as possible after treatment was completed.

2.2.3 Auger electron spectroscopy (AES)

Principles of operation

AES differs from XPS in that it uses a focused, mono-energetic electron beam to bombard the surface of the target material. The energy of the incident electrons are typically in the order of a few keV and can be sufficiently energetic to dislodge a core-level electron as a secondary electron thereby leaving a vacancy in the electron shell. One of the methods by which this excited atom can relax is via the Auger process which

results in another (Auger) electron being emitted from the surface. The energy of the Auger electron depends only upon the electron energy levels of the states involved in the Auger process and are quite independent of the energy of the impacting species (in contrast to XPS). The energy of the incident electrons is determined by a compromise between good spatial resolution (high beam energy, e.g. 10keV) and low beam damage (low beam energy, typically 1keV) with a minimum of 3keV required to excite all the atomic species that may be present. AES is performed in a near-vacuum (between 2×10^{-8} and 2×10^{-9} Torr) environment to minimise electron scatter and recontamination of the target; even at pressures as low as 10^{-6} Torr a monolayer of oxygen is laid down within 1.5 seconds^[34].

Attributes of AES

Compound identification: AES is particularly useful for studying compounds containing light atoms (i.e. $Z < 13$) because for these the ejection of Auger electrons is the major relaxation process for the induced excited states. Although AES can be used on all inorganic compounds and metals, it cannot give information on organic compounds due to surface charging effects of the incident electrons. As with XPS, hydrogen and helium cannot be detected by AES.

Proportions of components: the atomic percentage of elements present can be provided to an accuracy of up to 0.1%.

Sampling depth: depending on the energy of the incident electrons (typically between 1keV and 10keV) and the properties of the target material, the sampling depth can vary between 2 and 10nm. Depth-profiling using argon ion-bombardment was available to us although this process requires calibration with a similar sample of known thickness. Such samples were not normally available and therefore this technique could not easily be applied.

Errors: As with XPS, sampling depth makes AES very sensitive to surface contamination, such as dust or finger-prints, and samples were protected from the atmosphere between treatment and AES analysis.

2.2.4 Contact angles

The careful placement of a drop of liquid on a solid surface can elucidate considerable information as to the nature of the surface simply by measuring the angle which the boundary of the droplet makes with the surface. This angle, known as the 'contact angle', is determined by the mechanical equilibrium of the three surface tensions (i.e. free energy per centimetre square) γ_{sl} , at the interface of the solid and the liquid, γ_{lv} , at the interface of the liquid and the vapour, and γ_{sv} at the interface of the solid and the vapour, as shown in Fig 2.2.4a.

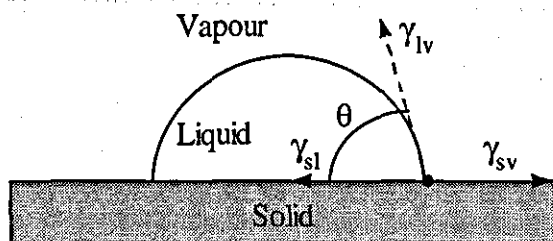


Fig. 2.2.4a: Contact angle (θ) of a water droplet.

When in equilibrium, these three parameters are related by Eqn 2.3^[35].

$$\gamma_{sv} - \gamma_{sl} = \gamma_{lv} \cos \theta \quad \text{Eqn 2.3}$$

Thus, the contact angle is a function of the surface parameters of the solid and is independent of the volume of the drop for a homogenous, flat, solid surface. The surface free energy of a solid increases with its melting point and hardness. Metals, oxides, and mineral compounds have high specific surface energies typically between 0.5 and 5 J/m². Most organic compounds are soft, with low melting points, and have low specific surface

energies below 0.1 J/m^2 . Hence, organic liquids are generally found to spread freely on solids of high surface energy, since this results in a large decrease in the surface energy of the system.

Measurement of contact angle

A simple method of measuring contact angles was to produce a magnified image of the droplet using the apparatus shown in *Fig 2.2.4b*.

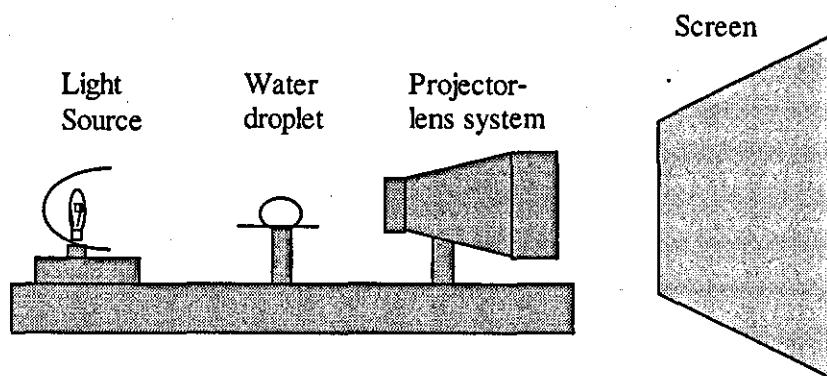


Fig. 2.2.4b: 'In-house' projector designed for the measurement of contact angles.

The image on the screen was marked out by placing a cross at the upper-most point on the droplet boundary and at the two points where the droplet came into contact with the surface. The ratio of the height (h) and diameter (d) of the water droplet was measured, from which the contact angle could be calculated using *Eqn 2.4* (see Appendix G).

$$\tan \theta/2 = 2h/d \quad \text{Eqn 2.4}$$

Uses of contact angles

Although detailed chemical and topographical information can be obtained from contact angles, this requires specialised equipment and techniques. Contact angles were of most

use in laser cleaning as a rapid test for the presence of organic contamination on the metal surface. A metal surface that was completely free of organic compounds would show zero contact angle although even the presence of an adsorbed monolayer of organic contamination produces a finite contact angle^[36].

2.3 Surface topographical analysis

2.3.1 Colour photography

Colour photography is a simple and accurate method of recording the visible effects of the laser-cleaning on surface topography. The set-up used incorporated a Pentax ME Super SLR camera with a 50mm lens and flash, as shown in *Fig 2.3.1a*. Extension tubes were used for macro-photographs and a diffuse reflector softened the effect of the flash.

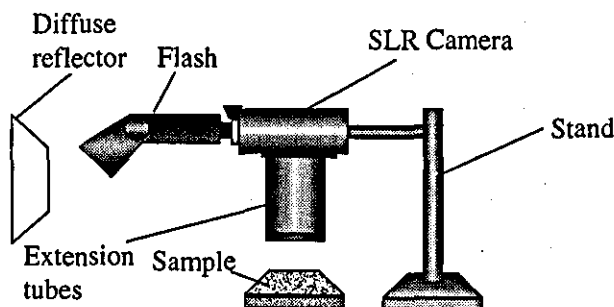


Fig. 2.3.1a: Macro-photography experimental set-up

Kodak 'Gold' film was used of 100ASA or 200ASA. Photographs were taken before, during and after cleaning. Colour photographs are displayed at the end of Chapter 3.

2.3.2 Embedded cross-section

To obtain photographs of cross-sections taken through samples they must first be embedded in a resin. The corrosion layers are thin and friable and require the support of a

surrounding resin to prevent them being damaged whilst the sample is being ground and polished.

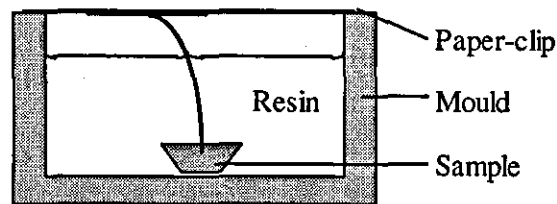


Fig. 2.3.2a: Embedding apparatus for cross-section analysis

The samples are attached to paper-clips prior to the introduction of the resin to enable positioning, as shown in *Fig 2.3.2a*. If the surface of the sample is angled slightly to the base of the resin mould a tapered cross-section can be obtained that extends its profile and presents a larger surface area to be photographed.

Once the resin has set the mould can be removed. The sample is then sanded down with consistently higher grades of silicon carbide paper until a 1000 grade finish has been obtained. The sample is then polished using a soft cloth impregnated with a high-quality metallurgical polish, or using an automated polishing machine with diamond paste, depending on the required finish. Etching may also be performed on the cross-section to provide detail of the grain structure of the metal, the etchant used being dependent upon the type of metal or alloy^[37]. The cross-section is viewed with a metallurgical microscope with a camera attachment. Photographs are taken with indoor film to compensate for the colour of the tungsten-filament lamp lighting.

Types of resin

There are various types of cold setting mounting resins commercially available, such as polyester, acrylic and epoxy resins. A suitable resin provides good edge protection with low shrinkage characteristics. 'Epofix' mounting resin was used for our studies because its low viscosity allows for impregnation of the porous corrosion layers thus consolidating any friable material and improving edge protection.

2.3.3 Scanning Electron Microscopy (SEM)

By using electrons, with de Broglie wavelengths of 0.05 angstroms or less, instead of visible light, the SEM can achieve far greater resolution than any optical microscope due to the greatly reduced diffraction effects. The linear resolution of electron microscopy is limited by lens aberrations and by scattering within the specimen, but is typically of the order of 5 to 10 angstroms, compared with the 2000 angstroms of the best optical microscopes.

The SEM is a valuable tool for detailed topographical analysis but will, of course, produce only black and white as opposed to colour pictures. SEM micrographs of laser treated metals are displayed at the end of Chapter 4.

2.4 In-line laser observations

The surface analysis procedures outlined in sections 2.2 and 2.3 are all limited in that they require a significant time for processing and sample preparation that confines their use to analysis after the laser cleaning/processing has been completed. Such methods provide accurate and useful information but do not give direct feedback to the laser operator as to the state and condition of the target. The methods outlined in this section provide the operator with pulse-by-pulse information as to changes occurring in the system during ablation.

2.4.1 Surface temperature measurement

For an opaque material, such as a metal ($\alpha = 10^5$ to 10^6 cm^{-1}) the temperature/depth profile resulting from a laser pulse (assuming no change in state) may be approximated to the following^[38]

$$\Delta T(z,t) = (2I(1-R)/K)(\kappa t)^{1/2} \text{ierfc}[z/2(\kappa t)^{1/2}] \quad \text{Eqn 2.5}$$

where ΔT is the temperature increase, I the intensity of the incident radiation, R the reflectivity of the target surface, K the thermal conductivity of the target material, κ the thermal diffusivity of the target, z is depth, t is time and ierfc is the complex error function. This equation assumes that re-radiation from the heated surface is negligible (it is typically less than 1%); that the duration of the pulse is of the order of 10ns or longer; that the thermal properties of the target material are independent of temperature and, although this is obviously not true for metals, that the thermal properties do not vary greatly over wide temperature ranges. Utilising this equation illustrates the rapid attenuation of the temperature as the bulk of the sample is approached, as shown in *Fig 2.4.1a*; almost all of the heat energy is contained within the top 10 μm of the target material after the duration of a single pulse.

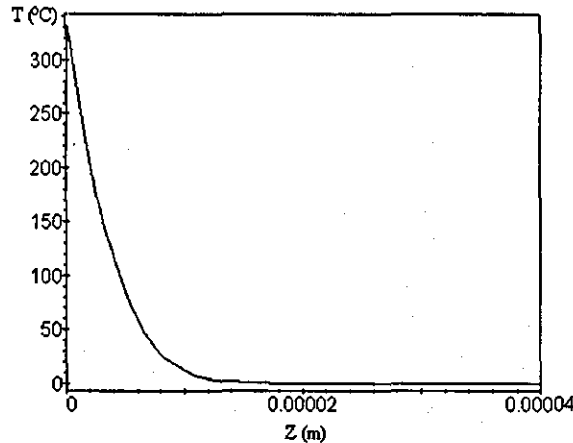


Fig. 2.4.1a: Theoretical temperature-rise/depth profile of steel immediately after a 2J, 100ns, square 10.6 μm laser pulse is incident on 1 cm^2 of surface.

To calculate the theoretical temperature rise at the surface of the sample, *Eqn 2.5* can be simplified to *Eqn 2.6* by substituting $z=0$,

$$\Delta T = (2I(1-R)/K)(\kappa t/\pi)^{1/2} \quad \text{Eqn 2.6}$$

From this equation the heating effect of the laser on various metal samples can be predicted, see Table 2.1. The reflectivities for this table have been calculated from the refractive index and absorption index^[39] of the metals at 10.6 μm and the thermal conductivities^[40] and diffusivities^[41] are given at room temperature.

Metal	Reflectivity (R)	κ (cm^2/s)	K (W/cmK)	ΔT (K)	T_m ($^\circ\text{C}$)
Ag	0.996	1.74	4.02	9.4	962
Al	0.989	0.97	2.25	33.0	660
Au	0.994	1.28	2.95	15.9	1064
Cu	0.988	1.17	4.00	22.9	1083
Fe	0.962	0.23	0.72	179	1535
Pb	0.956	0.24	0.35	438	327

Table 2.1: Theoretical temperature rise due to a 2J, 100ns, TEA CO₂-laser pulse being incident on the surface of various pure metal surfaces.

Table 2.1 shows a large variation in theoretical heating effects of a TEA CO₂-laser pulse incident on a variety of pure, clean metallic targets. Ag, Al, Au and Cu show a small increase in surface temperature, compared with their melting points, after a single laser pulse and therefore are unlikely to be damaged. Although the heating of iron is well below its melting point, it is sufficient that there could be a danger of melting after many pulses fired in rapid succession such that the effects of interpulse cooling is exceeded. It is also possible that metallic transformations occur at temperatures significantly below the melting point. Lead suffers the most pronounced surface heating and has a significantly lower melting point than the other metals such that surface damage through melting and even vaporisation (the boiling point of lead is 1740 $^\circ\text{C}$) is possible.

2.4.1.1. Bulk temperature measurement during ablation

Introduction

If the surface temperature rise after each laser pulse is insufficient to vaporise the surface of the target then the energy coupled with the surface is conducted both into the bulk of the material and into the surrounding atmosphere. If, however, surface material is ablated during irradiation, then the heated material is no longer in contact with the substrate and direct heat conduction into the substrate is prevented. Formation of a plasma above the target surface may induce secondary heating effects through absorption of the plasma radiation. Hence, the surface temperature of metals during ablation of corrosion layers involving plasma formation cannot be estimated from results such as those presented in Table 2.1 alone.

Experimental

A simple experiment was set up to monitor the temperature rise of the target material and its reflectivity during ablation, as shown in *Fig 2.4.1b*. The laser was focused to an area of 1cm^2 , sufficient to cause ablation without air-breakdown. The target samples were cut to size such that they fitted the dimensions of the focused laser beam. The temperature probe could measure with reasonable sensitivity ($\pm 0.1^\circ\text{C}$) the increase in temperature of the bulk target material due to each laser pulse. After each pulse, the target was allowed to cool to room temperature due to the temperature dependence of reflectivity (see Section 1.1.5). The reflectivity was determined from the ratio of the outputs from the ELTEC detectors (D_1 and D_2). Calibration was achieved using clean metal coupons of the target material.

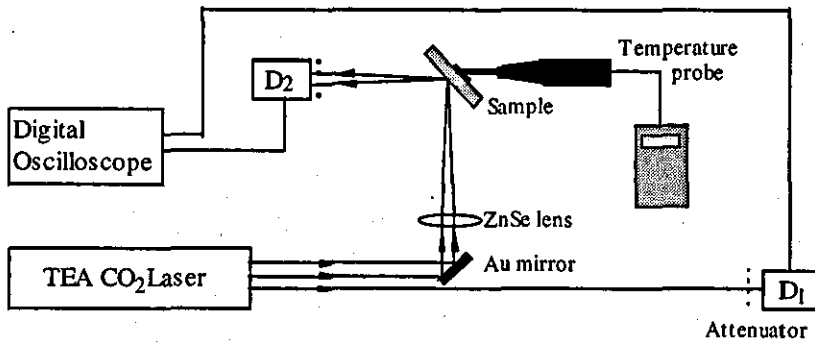


Fig. 2.4.1b: Experimental set-up for simultaneous measurement of bulk temperature and reflectivity of target sample during ablation.

Results

Fig 2.4.1c and *Fig 2.4.1d* show how, during ablation, the reflectivity of the target cannot be used to determine the bulk, and therefore the surface, temperature rise. *Fig 2.4.1c* shows how the temperature rise per pulse and reflectivity varies over the first 100 pulses.

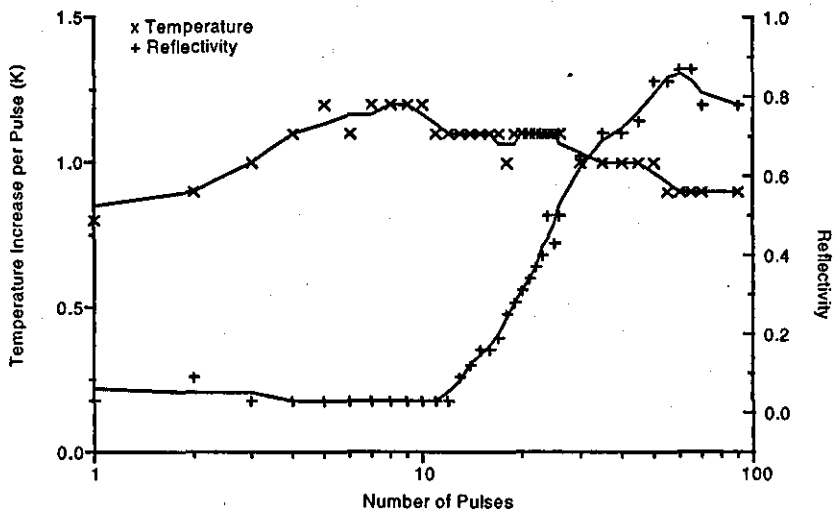


Fig. 2.4.1c: Bulk temperature rise per pulse and reflectivity of painted car body-work during ablation below the plasma threshold.

The painted car body-work consisted of a maroon top-coat with several layers of undercoat on a zinc-coated steel substrate (0.92mm thick). The thickness of the paint layer was measured, by micrometer, to be 12 μ m. For the first 10 pulses the temperature rise per pulse of the bulk material gradually increases as the metal substrate is approached. During this period, the change in the temperature rise per pulse is because of the increasing proximity of the ablation process to the surface as opposed to the change in reflectivity of the sample, which remains almost constant. The reflectivity of the sample does not start to increase until after 12 pulses, when the zinc starts becoming exposed and the temperature rise gradually starts to decrease. There then appears to be an inverse relationship between temperature rise and reflectivity as less and less paint remains to transfer heat to the substrate. Although the reflectivity of the target has increased from 0 to 0.8 over the entire process, the temperature increase per pulse has remained almost constant between 0.8 and 1.2 $^{\circ}$ C. This is, of course, not what might be expected if the reflectivity was the only factor involved.

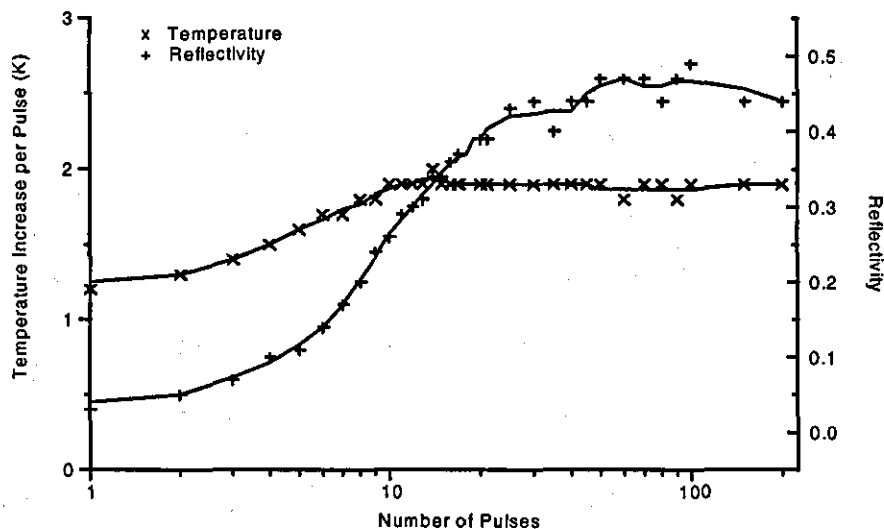


Fig. 2.4.1d: Bulk temperature rise per pulse and reflectivity of patinated copper-roofing during ablation below the plasma threshold.

The patinated copper-roofing consisted primarily of a green, brochantite layer (as determined by XRD) on a 0.6mm thick copper substrate. The brochantite is immediately blackened by the action of the laser. The temperature rise per pulse increases with the reflectivity and as the metal substrate is approached, as shown in *Fig 2.4.1d*. This again illustrates the fact that, during ablation, the reflectivity of the target alone cannot provide an accurate indication as to the temperature rise of the bulk of the material. Of course, in the absence of ablation, an increase in reflectivity would result in a decrease in temperature rise per pulse. The patina is not completely removed by the laser and a thin cuprite layer remains to transfer heat to the substrate.

Determination of surface temperature from bulk temperature

Although it was not possible to measure the temperature of the surface of the sample directly during ablation, an approximate can be obtained from the bulk temperature.

By definition,

$$\Delta T_b = \Delta E_b / cm \quad \text{Eqn 2.7}$$

Where ΔT_b = bulk temperature rise, ΔE_b = input energy, c = specific heat capacity, m = mass of target. We can define

$$\Delta E_b = A_{\text{eff}} E_i \quad \text{Eqn 2.8}$$

where A_{eff} = the proportion of the incident laser radiation absorbed by the sample, and E_i = the pulse energy of the laser. Substituting *Eqn 2.7* into *Eqn 2.8*,

$$A_{\text{eff}} = cm \Delta T_b / E_i \quad \text{Eqn 2.9}$$

Eqn 2.6 can be re-written as,

$$\Delta T_s = (2I(A_{eff})/K)(\kappa t/\pi)^{1/2} \quad \text{Eqn 2.10}$$

Therefore, neglecting heat loss from the bulk material into the atmosphere, substituting Eqn 2.9 into Eqn 2.10,

$$\Delta T_s = (2I(cm \Delta T_b / E_i)/K)(\kappa t/\pi)^{1/2} \quad \text{Eqn 2.11}$$

Using Eqn 2.11 we can obtain rough estimates for the instantaneous surface temperature rise of the painted steel and patinated copper targets. For example, a 1°C bulk temperature rise experienced by the painted steel sample, as shown in Fig 2.4.1c, corresponds to an estimated surface temperature rise of 948°C. A 2°C bulk temperature rise in the patinated copper sample, as shown in Fig 2.4.1d, corresponds to an estimated surface temperature rise of 396°C.

Conclusions

These results show that the transfer of energy from the laser pulse to the metal cannot be determined from the optical properties of the surface if ablation is taking place.

The surface temperature figures are most probably considerable over-estimates. Eqn 2.10 assumes the absorption coefficient of the surface to be between 10^6 and 10^7 cm^{-1} which is only generally valid if the surface is metallic. Inorganic species remaining on the surface are likely to have a much lower absorption coefficient and hence follow a far more gradual temperature gradient. However, these figures do indicate that the surface temperature of the metal is likely to be raised far more significantly during ablation of surface corrosion products than if the laser is incident on a clean metal (see Table 2.1). More sophisticated experimentation, such as using an InGaAs photodetector to capture

the thermal emission signal^[42], would be required to determine the surface temperature rise more accurately.

2.4.2 Laser Induced Breakdown Spectroscopy (LIBS)

Principles of operation

When the laser cleans at a sufficiently high flux the blow-off material forms a hot-plume/plasma which may contain ionised or excited species of the ablated material and the ambient gas. These excited atoms may decay through emission of photons at discrete wavelengths in the range of the near-infrared, visible and ultraviolet regions of the electromagnetic spectrum. The Laser 2000, CR-MMS 1 spectrometer, used in this investigation, uses a curved diffraction grating to split the incident radiation, with respect to wavelength, over an angular distribution and focus it onto a linear array of 256 photodiodes. The spectrometer covers the range of wavelengths from 300nm to 900nm. The data is transferred to computer where the spectra can be displayed after each laser pulse, as shown in *Fig 2.4.2a*.

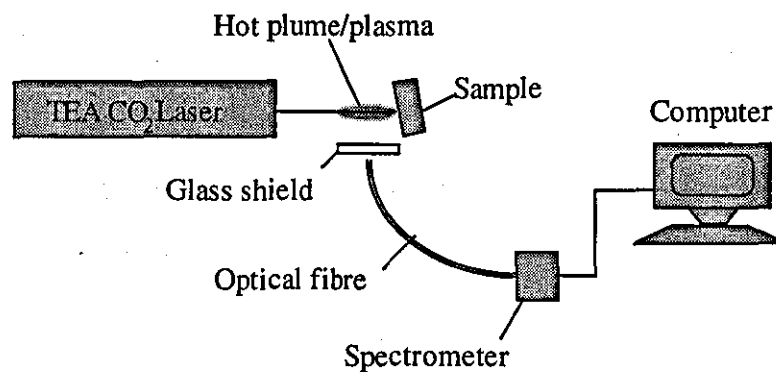


Fig. 2.4.2a: Set-up for LIBS observations of target surface.

Attributes of LIBS

Compound identification: Most elements have strong emission lines within the range of the spectrometer, but emission lines will provide only information as to the elements present in the plasma and not the molecular formulas of the compounds at the surface. The poor resolution of the spectrometer and the varying intensity of the plasma from one shot to the next prevented reliable quantitative measurements being taken.

Plume/plasma analysis: apart from chemical analysis, the spectrometer can be used to provide information on the state of the blow-off material, its temperature and the presence of ionised species.

In-line monitoring: the appeal of LIBS over other, more sophisticated and accurate forms of chemical analysis, is that through utilising the plume/plasma produced during the laser cleaning process it can provide pulse-by-pulse information. The low cost of these compact devices (less than £2500) provides the operator with a limited but useful diagnostic technique.

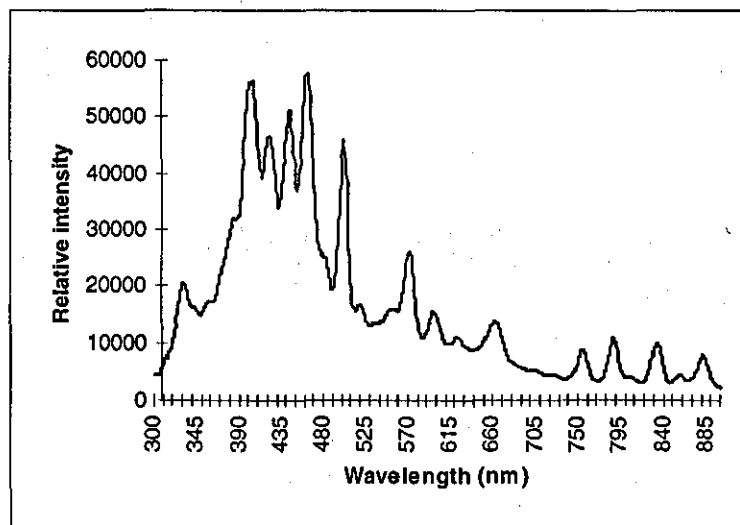


Fig. 2.4.2b: LIBS spectra of air-breakdown above an aluminium target. The peaks correspond to the presence of nitrogen and oxygen in the air. There is no evidence for aluminium atoms or ions present in the plasma.

Errors: Many problems arise from attempting to use such simple spectroscopic equipment for accurate elemental analysis. A high flux is required to produce ionised species in the blow-off material and air-breakdown often ensues producing a plethora of strong oxygen and nitrogen peaks in the emission spectra, obscuring many of the target's weaker lines, see *Fig 2.4.2b*. When a hot-plume forms that does not induce air-breakdown, the emission lines of the target material are often so weak as to go undetected but for the major components. The spatial resolution of the instrument (each photodiode covers, on average, 4nm of the spectrum) was found to be too low to resolve some neighbouring peaks and can lead to ambiguity in the results.

2.4.3 Acoustic monitoring

Method

During ablation an audible report (the 'ablative-piston signal') is produced by the rapid expansion of gases and ejection of ablated materials from the formation of the hot-plume/plasma.

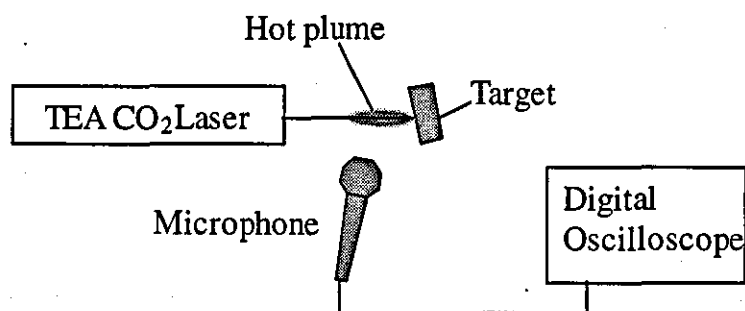


Fig. 2.4.3a: Set-up to monitor ablative-piston signal during ablation.

A simple dynamic coil microphone can be used to measure the ablative-pulse signal during ablation, as shown in *Fig. 2.4.3a*. It has been shown that the ablative-pulse signal is proportional to the etch-depth per pulse during ablation^[43]. Each laser pulse produced a strong voltage pulse on the oscilloscope that decayed as a damped harmonic oscillator

within a few hundred micro-seconds. The amplitude of the strongest peak was taken as the relative amplitude for each pulse.

Results

Fig 2.4.3b shows acoustic measurements made during the cleaning of a painted steel target. The target consisted of a maroon top-coat with several layers of white undercoat on a zinc-coated steel substrate and was exposed to laser pulses at $2\text{J}/\text{cm}^2$. There is a pronounced variation in signal amplitude, and hence etch rate, throughout the ablation process. The top-coat was removed within the first 3-4 pulses during which the pulse amplitude remains quite low. As the undercoat is exposed, the signal amplitude increases significantly between 4 and 10 pulses. After 10 pulses, the metal substrate starts to become exposed and thus the signal amplitude starts falling.

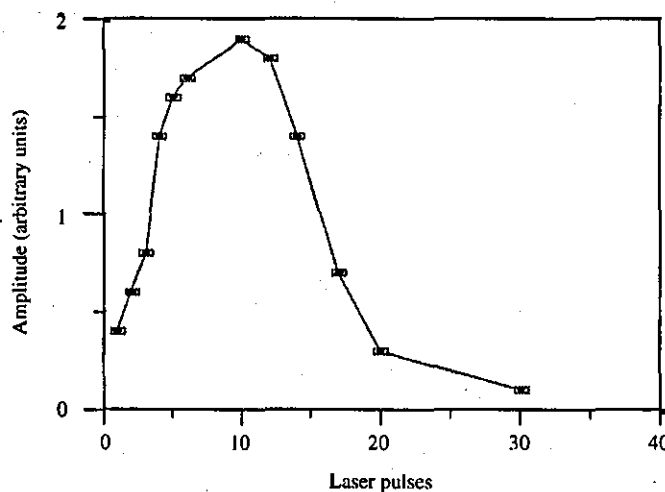


Fig. 2.4.3b: Amplitude of ablative-piston signal during laser cleaning of painted car body-work.

Clearly, the etch-depth per pulse of a given laser can vary considerably for different types of organic coating. Acoustic monitoring could provide useful feedback during the removal of one type of organic coating from another.

Fig. 2.4.3c shows acoustic measurements made during the laser treatment of patinated copper. The copper target was taken from a section of copper roofing and had a layer of brochantite corrosion products. There was an approximately linear decrease in signal amplitude with successive laser pulses. The etch rate of the laser reduced as the metal substrate was approached.

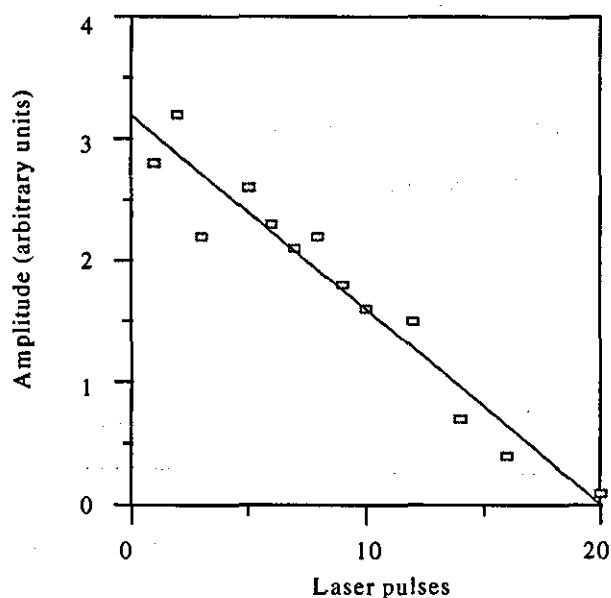


Fig. 2.4.3c: Amplitude of ablative-piston signal during laser cleaning of patinated copper.

This gradual decrease in signal amplitude would not be expected from a homogenous layer of corrosion products, the etch-rate of which would be approximately constant until the metal substrate started to become exposed. It would appear that the corrosion layer is not homogenous but varies consistently as the substrate is approached. It is reasonable to expect a greater proportion of simple corrosion products, such as oxides, near the surface of the metal whilst the external corrosion products consist of more complex compounds, such as hydrates (e.g. brochantite). The signal amplitude decreases as the proportion of the simpler compounds increases (see Chapter 5.2.1).

Conclusions

Acoustic monitoring has demonstrated how the etch rate per pulse varies for two different systems; one painted and one patinated. Both systems show a great diversity in etch rate throughout the laser treatment process. In the case of the paint, the variation in the ablative-piston signal correlated with changes in the paint coating. In the case of the patination, the linear decrease in ablative-piston signal as the metal substrate was approached implied a constant variation in composition of the coating.

Summary

This chapter has described how a suitable, self-limiting laser cleaning system has been realised and has investigated how the parameters of the laser and the properties of the target material can affect the laser treatment process. Two clearly distinguished laser treatment regimes have been identified, that of using the laser either above or below the plasma threshold. The former process is best suited to laser cleaning of metal sculpture, as described in Chapter 3, whilst the latter has application in industrial surface cleaning and treatment processes, as described in Chapter 4.

The advantages and disadvantages of various surface analysis techniques have been explored and these have been applied discriminately in the experimental work described in the following chapters.

References

- [1] Asmus, J. F., et al., 'Studies in the interaction of laser radiation with art and artefacts', *Proceedings of SPIE*, 41, (1973), 19-27.
- [2] Lu, Y. F., Song, W. D., Ye, K. D., Hong, M. H., Liu, D. M., Chan, D. S. H., Low, T. S., 'Removal of submicron particles from nickel-phosphorus surfaces by pulsed laser radiation', *Applied Surface Science*, 120(3-4), (1997), 317-322.
- [3] No author cited, 'Affordable, laser-assisted chip cleaning is effective, saves water and pollutes less', *Plating and Surface Finishing*, 84(11), (1997), 18-20.
- [4] Friberg, T. R., Zafiropoulos, V., Kalaitzaki, R., Petrakis, J., Fotakis, C., 'Excimer laser cleaning of mold-contaminated paper', *Laser in Medical Science*, 12(1), (1997), 55-59.
- [5] Park, H. K., Grigoropoulos, C. P., Leung, W. P., Tam, A. C., 'Practical excimer laser-based cleaning tool for removal of surface contaminants', *IEEE Transactions on Components Packaging and Manufacturing Technology Part A*, 17(4), (1994), 631-643.
- [6] Lu, Y. F., Komuro, S., Aoyagi, Y., 'Laser induced removal of fingerprints from glass and quartz surfaces', *Japanese Journal of Applied Physics Part 1*, 33(8), (1994), 4691-6.
- [7] Carlyle, L., Young, B., 'Report on laser interaction with paintings', unpublished report, Canadian Conservation Institute, Ottawa, Nov. 1981.
- [8] Lu, Y. F., Song, W. D., Hong, M. H., Chong, T. C., Low, T. S., 'Mechanism of and method to avoid discoloration of stainless steel surfaces in laser cleaning', *Applied Physics A: Materials Science and Processing*, 64(6), (1997), 573-8.
- [9] Lu, Y. F., Takai, M., Komuro, S., Shiokawa, T., Aoyagi, Y., 'Surface cleaning of metals by pulsed-laser irradiation in air', *Applied Physics A: Solids and Surfaces*, 59(3), (1994), 281-8.
- [10] Siano, S., Margheri, F., Pini, R., Mazzinghi, P., Salimbeni, R., 'Cleaning processes of encrusted marbles by Nd:YAG lasers operating in free-running and Q-switching regimes', *Applied Optics*, 36(27), (1997), 7073-9.
- [11] Maravelaki, P. V., Zafiropoulos, V., Kalaitzaki, M., Kowalski, R., Petrakis, J., Fotakis, C., 'Laser-induced breakdown spectroscopy as a diagnostic technique for the laser cleaning of marble', *Spectrochimica Acta Part B: Atomic Spectroscopy*, 52(1), (1997), 41-53.
- [12] Gobernadomitre, I., Medina, J., Calvo, B., Prieto, A. C., Leal, L. A., Perez, B., Marcos, F., Defrutos, A. M., 'Laser cleaning in art restoration', *Applied Surface Science*, 96-8, (1996), 474-8.
- [13] Cooper, M. I., Emmony, D. C., Larson, J., 'Characterisation of laser cleaning of limestone', *Optics and Laser Technology*, 27(1), (1995), 69-73.
- [14] Cooper, M. I., Emmony, D. C., Larson, J., 'The use of laser energy to clean polluted stone sculpture', *Journal of Photographic Science*, 40, (1992), 55-7.
- [15] Bewley, D., 'Spotless with lasers', *New Scientist*, (5 July 1997), 20-21.
- [16] Morgan, N., 'Excimer lasers restore 14th century icons', *Optics and Lasers Europe*, (Sept 1993), 36-37.
- [17] Szczepanowska, H. M., Moomaw, W. R., 'Laser stain removal of fungus-induced stains from paper', *JAIC*, 33, (1994), 25-32.
- [18] Hecht, J., from *The Laser Guidebook*, 2nd Ed., McGraw-Hill Inc., London, (1992), 159-183.
- [19] Russo, R. E., 'Laser Ablation', *Applied Spectroscopy*, 49(9), (1995), 14A-28A.
- [20] Garrison, B. J., and Srinivasan, R., 'Laser ablation of organic polymers: Microscopic models for photochemical and thermal processes', *J. Appl. Phys.*, 57(8), (1985), 2909-14.
- [21] Prokorov, A. M., Konov, V. I., Mihailescu, I. N., 'Laser heating of metals', *Adam Hilger Series on Optics and Optoelectronics*, Bristol, (1990), 30-35.
- [22] Prokorov, A. M., Konov, V. I., Mihailescu, I. N., 'Laser heating of metals', *Adam Hilger Series on Optics and Optoelectronics*, Bristol, (1990), 35.
- [23] Weisheit, A., Mordike, B. L., 'Laser Nitriding of Titanium Alloys', *Surface Engineering*, 11(2) (1995), 160-1.
- [24] Riches, S., 'An introduction to the fundamentals of laser technology', *Lasers and Power Beam Processing*, (Sept 1996), 17-9.
- [25] Ready, J. F., from 'Effects of High-Power Laser Radiation', Academic Press, London, (1971), Chapt. 5.
- [26] Cooper, M., Doctoral Thesis, 'Laser cleaning of stone sculpture', (28 April 1994), 159.

- [27] Critchlow, G. W., Cottam, C. A., Brewis, D. M., Emmony, D. C., 'Further studies into the effectiveness of CO₂-laser treatment of metals for adhesive bonding', *Int. J. Adhesion and Adhesives*, 17, (1997), 143-150.
- [28] ELTEC Instruments SA, P.O.Box 564, Neugutstrasse 4, CH-8304 Wallisellen, Switzerland.
- [29] Cooper, M., Doctoral Thesis, 'Laser cleaning of stone sculpture', (28 April 1994), 188-202.
- [30] Gurevich, V. S., Danilov, O. B., Popov, Y. G., Yachnev, I. L., 'CO₂ lasers for medical uses', *Journal of Optical Technology*, 61(12), (1994), 928-31.
- [31] *Ad idem*, 206.
- [32] Hecht, J., from *The Laser Guidebook*, 2nd Ed., McGraw-Hill, London, 171.
- [33] Mc Clune, W. F., (Chief Ed.), from *Powder Diffraction File: Alphabetical Index, Inorganic Phases 1987*, JCPDS, International Centre for Diffraction Data, Swarthmore, USA (1987).
- [34] Critchlow, G. W., private communication.
- [35] Zisman, W. A., 'Relation of the equilibrium contact angle to liquid and solid constitution', from *Contact Angles and Wettability and Adhesion*, American Chemical Society, Washington, (1964), 1-51.
- [36] Adam, N. K., 'The chemical structure of solid surfaces as deduced from contact angles', from *Contact Angles and Wettability and adhesion*, American Chemical Society, Washington, 56.
- [37] Scott, D. A., from 'Metallurgy and Microstructure of Ancient and Historic Metals', The Getty Conservation Institute, Singapore, (1991), 69-74.
- [38] Ready, J. F., from 'Effects of High-Power Laser Radiation', Academic Press, London, (1971), Chapt 3.5.
- [39] Prokorov, A. M., Konov, V. I., Mihailescu, I. N., 'Laser heating of metals', *Adam Hilger Series on Optics and Optoelectronics*, Bristol, (1990), 6.
- [40] Touloukian, Y., S., from 'Thermal Properties of Matter: Thermal Conductivity of Metallic Elements and Alloys', *The TPRC Data Series Vol. 1.*, IFI/Plenum, (1970).
- [41] Touloukian, Y., S., from 'Thermal Properties of Matter: Thermal Diffusivity', *The TPRC Data Series Vol. 10.*, IFI/Plenum, (1973).
- [42] Chen, S. C., Grigoropoulos, C. P., 'Noncontact nanosecond-time-resolution temperature measurement in excimer laser heating of Ni-P disk substrates', *Applied Physics Letters*, 71(22), (1997), 3191-3.
- [43] Leung, W. P., Tam, A. C., 'Non-contact monitoring of laser ablation using a miniature piezoelectric probe to detect photoacoustic pulses in air', *Applied Physics Letters*, 60(1), (1992), 23-5.

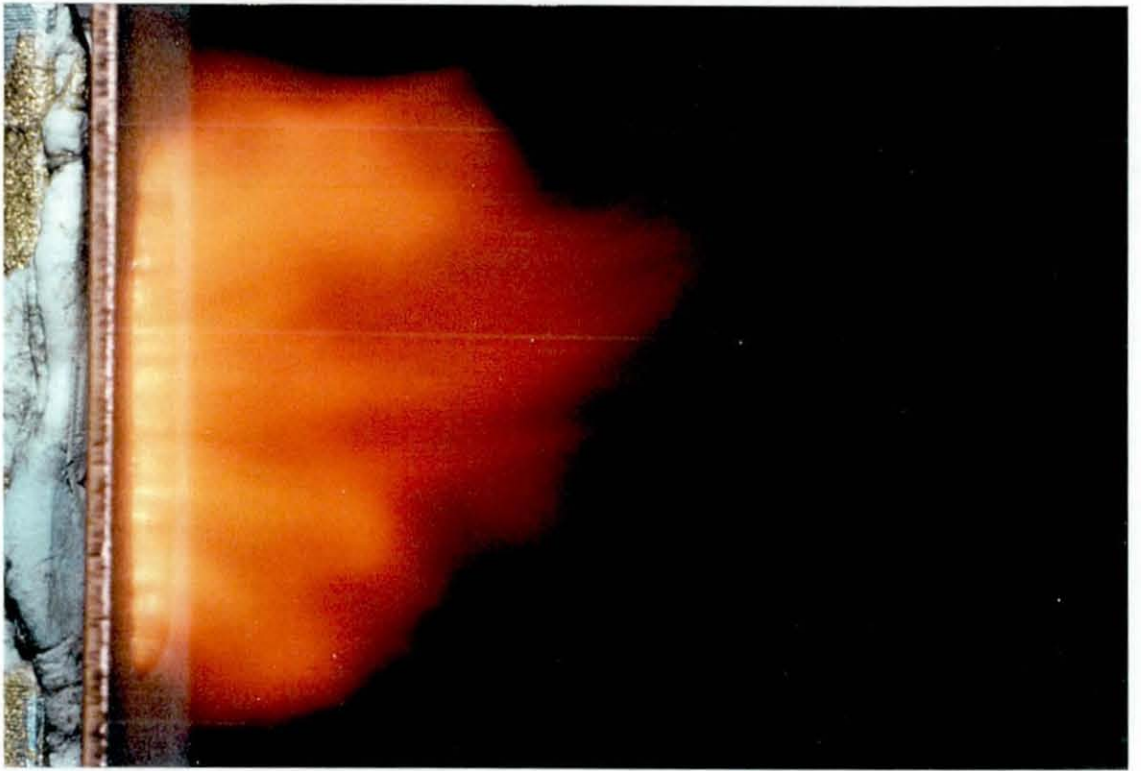


Photo 2.1.4a: Time-exposed photograph of hot-plume formation above a copper-roofing target after a single laser pulse at $2\text{J}/\text{cm}^2$. The irradiated area is approximately 10mm in height.

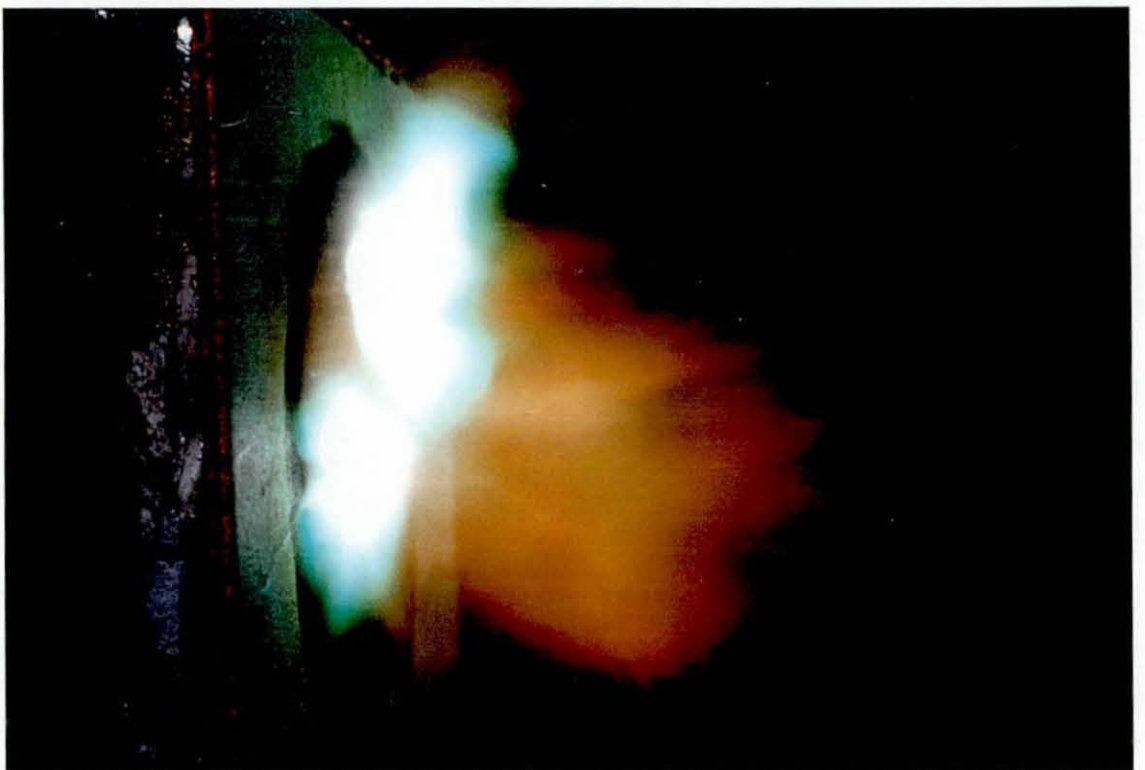


Photo 2.1.4b: Time-exposed photograph of two sites of plasma initiation above a copper-roofing target after a single laser pulse at $4\text{J}/\text{cm}^2$. The irradiated area is approximately 7mm in height.

CHAPTER 3

Sub-plasma Laser Cleaning and Treatment

3.1 Artificially patinated samples

A major obstacle in the path of much of the research into the laser cleaning of all forms of artwork and historical artefacts is the scarceness of test-samples on which new laser techniques can be tried without the risk of permanent damage to valuable objects. Even when it is considered acceptable to risk preliminary laser cleaning tests on less-valuable items there are often difficulties in bringing the objects within the vicinity of the laser due to their size. For example, the TEA CO₂-laser used in our experiments weighed 120kg and required a separate gas supply which prevented its transportation without great difficulty, whereas the outdoor sculpture that would serve as ideal test objects were equally immobile and far removed from the vicinity of the laser. Thus, artificially creating coated metal coupons within the laboratory to mimic the effects of corrosion and patination was attempted for initial cleaning tests without the danger of damaging valuable objects.

The patination recipes used by patineurs throughout history have produced coloured layers on metals that are in general chemically unrepresentative of the patination caused by prolonged outdoor exposure. Patina applied at the foundry rarely survives on outdoor sculpture without being converted or removed completely^[1] by prolonged exposure to rainwater. In this study, the artificial patination experiments were used for two reasons:

- (i) to reproduce the patination layers produced by foundry patineurs
- (ii) to mimic the corrosion/patination effects of long-term exposure

Foundry patineurs

Artificial patination was created at the foundry by application of a variety of patination solutions. The recipes of these solutions, and the method of application, varies as to the desired finish. Hundreds of tried and tested recipes are provided in Hughes and Rowe^[2] and some of these were selected for the basis of our experiments whilst others were determined by trial and error.

3.1.1 Experimental

Materials

The majority of sculpture is cast in copper alloy and for this reason metal coupons were cut from copper sheet (C106, 99.85% commercial purity) and gunmetal bronze ingot (BS 1400, see Appendix C) which is a popular alloy for casting. Some experiments were also carried out on coupons of sterling silver (precise composition not known, although sterling silver typically contains up to 10% copper). The coupons dimensions are shown in *Fig 3.1.1a*.

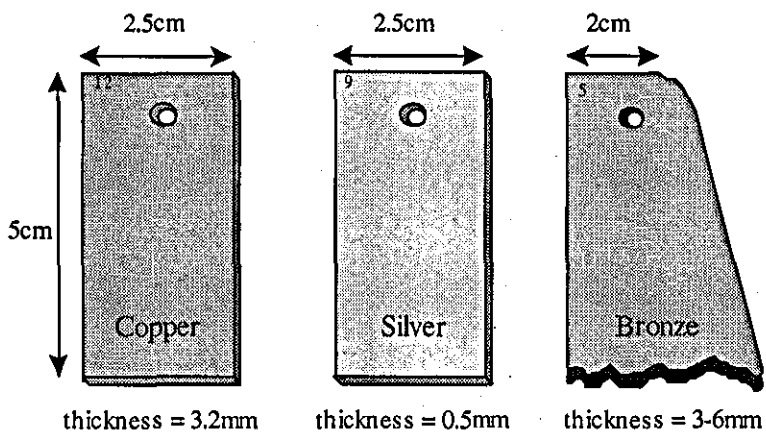


Fig 3.1.1a: Copper, silver and bronze coupons used in artificial patination experiments. Each coupon was numbered for identification purposes.

The copper and silver sheet could be cut using a guillotine whereas the bronze ingot, because of its shape, required the use of a circular saw and each coupon required a certain degree of finishing to obtain a reasonable surface for patination. Coupons were cleaned prior to patination using wire-wool and degreased with high purity acetone. The coloration process is very sensitive to the presence of surface contamination, in particular grease and oil which prevent uniform wetting of the surface. The surface of one of the bronze coupons was etched in FeCl_3 solution to reveal the grain-structure. Typically, grains had dimensions of a few millimetres with a slight reduction in size where the ingot was in contact with the mould.

Long-term exposure effects

The corrosion caused through long-term exposure usually involves the subjection of the object to cycles of wetness and temperature variation, and low-concentrations of solution, such as rainwater. To introduce a cyclic nature to the experimental set-up a simple 'dipping machine' was constructed, as shown in *Fig 3.1.1b*, to alternately dip and withdraw the metal coupon from a weak chemical solution. A fan was sometimes used to increase the rate of evaporation of the solution from the surface of the coupon which could have a significant effect on the qualities of the patina.

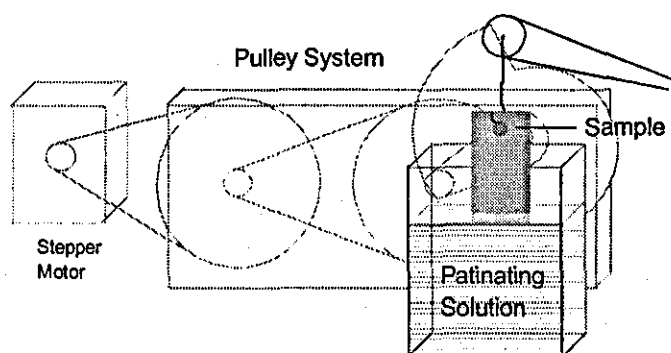


Fig. 3.1.1b: Artificial patination using a 'dipping machine'.

Laser cleaning

The specific details of the laser cleaning and the patination process will be described as a series of case-studies from *Case 1a* to *Case 9a* (the *a* represents *artificial*). In general, trial tests were made using different laser fluences on each test-piece in order to determine which produced the most desirable effect.

Surface analysis

When patina formed of sufficient thickness, XRD could be used to identify the corrosion products. Most XRD analysis was performed at a rate of 1 degree per minute (dpm) and a typical scan required about an hour and a half as the goniometer swept from 10 to 90 degrees. If a corrosion layer was very thin or particularly complex, the rate was reduced to 0.1 dpm and an overnight scan was performed to reduce the relative fluctuations in background noise that may be otherwise misinterpreted as diffraction peaks. In the results that follow in this chapter, the corrosion compounds may be referred to by their mineral names, a glossary of which may be found in Appendix H.

The diffraction pattern of gunmetal bronze, perhaps because of its complex formulation, is absent from the powder diffraction files. A cleaned gunmetal bronze coupon provided a standard diffraction pattern which could be used to eliminate bronze peaks whilst analysing corrosion on patinated bronze coupons.

When quantitative analysis was required, such as with the silver coupons in *Case 7a* and *Case 8a*, AES was used.

3.1.2 Case 1a

Introduction

A common affliction of copper and copper containing artefacts stored in wooden boxes is the formation of corrosion products from vapours emitted from the wood of the boxes or protective lacquers that have been applied to the wood^[3]. The precise nature of the corrosive vapours depend on the wood and lacquer types, although a common constituent is acetic acid. The object of this experiment was to replicate a possible corrosion layer that may form on a copper object exposed to such an environment.

Patination method

Attempts at exposing coupons to dilute acetic acid did not produce any corrosive effects other than mild oxidation and ammonium chloride was added to facilitate the reaction. The patination solution consisted of 1g NH_4Cl and 1g $\text{Cu}(\text{C}_2\text{H}_3\text{O}_2)_2$ dissolved in 250ml of distilled water at room temperature. The copper coupon was dipped over a 10 minute cycle for 48 hours. After the first 24 hours a brown patina had formed, for the last 24 hours a fan was used to accelerate the evaporation rate of the solution from the surface of the coupon.

Pre-laser treated coupon

The patination method resulted in a uniform, adherent blue patina over the surface of the coupon, under which a thin brown layer had formed. XRD of the surface revealed the major constituents of the corrosion products to be $\text{Cu}(\text{OH})\text{Cl}$ and $\text{CuC}_2\text{H}_3\text{O}_2$.

Laser treated coupon

At a fluence of 0.5 J/cm^2 the laser produced a luminous plume, but no breakdown, that completely removed the blue layer within a few pulses, leaving the brown layer unaffected, see *Photo 3.1.2a*. Further exposure to the laser at this fluence did not have any visible effect on the appearance of this layer. Increasing the fluence to 2 J/cm^2 also created a hot plume and although the blue layer was successfully removed, the underlying brown layer quickly darkened with prolonged exposure to the laser.

XRD of the laser treated area showed that the remaining brown layer was too thin to be identified, all detectable $\text{Cu}(\text{OH})\text{Cl}$ and $\text{CuC}_2\text{H}_3\text{O}_2$ had been removed.

Discussion

The laser was successful at removing the external corrosion products formed on copper in the presence of acetates and chlorides. At 0.5 J/cm^2 the laser was clearly able to selectively remove the blue corrosion without visibly altering the brown interfacial layer, although an unpleasant charring of the interfacial layer occurred at higher fluences. In the absence of XRD data it is difficult to determine the nature of the charring although it seems reasonable to assume that it is caused through the thermal decomposition of residual corrosion products to leave, for example, a black tenorite layer.

3.1.3 Case 2a

Introduction

The effect of the fan was investigated by repeating the experiment in *Case 1a*, but this time using the fan for the full 48 hours of dipping as opposed for the last 24 hours.

Patination Method

As in *Case 1a*, with the fan used for the full 48 hours.

Pre-laser treated coupon

The patination method resulted in a patina of greater thickness and different coloration than in *Case 1a*. The colour gradually varied between blue and green over the surface of the coupon and an underlying red layer was evident, see *Photo 3.1.3a*. XRD identified the compounds to be primarily $\text{Cu}_2\text{Cl}(\text{OH})_3$, CuCl and $\text{CuC}_2\text{H}_3\text{O}_2$.

Laser treated coupon

The laser removed the blue/green surface layer within a few pulses at a fluence of $2\text{J}/\text{cm}^2$ whilst leaving a uniform red layer underneath that did not discolour with further irradiation, see *Photo 3.1.3b*. XRD of the laser-treated area detected only CuCl , hence all detectable $\text{Cu}_2\text{Cl}(\text{OH})_3$ and $\text{CuC}_2\text{H}_3\text{O}_2$ had been removed. It is very likely, however, that significant levels of compounds other than CuCl were present as pure CuCl is usually white in appearance. Over the period of a few months, the red surface started to blacken and XRD detected the presence of CuCl and Cu_2O .

Discussion

The sensitivity of the patination process to a slight variation in method is illustrated when this case is compared to *Case 1a* and the difference in corrosion products considered. Again, we see the laser capable of removing the external corrosion products whilst a resilient interfacial layer remains. Unfortunately, CuCl remained on the surface of the laser cleaned sample and observations of the surface, which had blackened after a period of a few months, showed the remaining layer to be unstable. The formation of Cu_2O in the CuCl layer is a strong indication of bronze disease (see Section 1.3.3).

3.1.4 Case 3a

Introduction

The rainfall in urban areas contains many species of chemicals, such as nitrates, sulphates and chlorides, that act synergistically to accelerate the corrosion of copper sculpture. In *Case 3a* a copper coupon is patinated in the presence of such chemicals.

Patination method

The patination solution consisted of 1g NaCl, 1g CuSO₄.5H₂O, 1g CuNO₃.3H₂O dissolved in 250ml of distilled water at room temperature. The coupon was dipped over a 10 minute cycle for 72 hours and continuously fanned.

Pre-laser treated coupon

The patination solution produced a very rough corrosion layer; the coloration varying between blue, green and white over the surface. There is evidence of an underlying, thin red layer beneath the bulk of the corrosion products. XRD identified a variety of chlorides including two forms of Cu₂Cl(OH)₃ (one being atacamite), Cu(OH)Cl and CuCl (nantokite).

Laser treated coupon

At 2J/cm² the laser removed most of the blue/green/white layer to reveal the underlying red layer, see *Photo 3.1.4a*. However, some filiform corrosion products, blackened by the action of the laser, remained resilient to removal at sub-plasma fluences, see *Photo 3.1.4b*. XRD identified the remaining corrosion to be CuCl (nantokite) and Cu₂Cl(OH)₃. From the coloration and location of the corrosion products, it is reasonable to assume that

the red layer consists mostly of CuCl whereas the blackened remains contain a high proportion of $\text{Cu}_2\text{Cl}(\text{OH})_3$.

Cross-sectional analysis clearly shows the existence of a red interfacial layer between the copper metal and bulk corrosion products, see *Photo 3.1.4c*, prior to laser treatment and this red layer remaining post-treatment.

Discussion

The patinating solution contained a mixture of sulphate, nitrate as well as chloride compounds, but the corrosion layer consisted purely of chlorides of various forms. This was not surprising because chloride ions in solution have the ability to convert otherwise stable corrosion products, such as brochantite, into chloride compounds^[4]. Although the concentration of the patination chemicals were far in excess of any natural rainfall, the patina consisted of compounds commonly observed on naturally corroded copper in marine environments. The active nature of chloride compounds in corrosion layers makes their removal almost always desirable. The bulk, external corrosion products were completely removed except in the case of the filiform $\text{Cu}_2\text{Cl}(\text{OH})_3$, which was blackened but not removed. The blackening is due to the thermal decomposition of $\text{Cu}_2\text{Cl}(\text{OH})_3$ to solid black CuO and the expulsion of gaseous HCl and H_2O . The tenorite that remains forms a thin black layer on the surface of the $\text{Cu}_2\text{Cl}(\text{OH})_3$ fibrils of insufficient thickness to be detected by XRD. The cross-section shows that the resilient, interfacial red layer existed prior to laser cleaning and has not formed from the action of the laser on the metal substrate or external corrosion products. Again, the laser has been successful at removing the bulk of the corrosion products whilst leaving a resilient interfacial layer, but in this case laser-transformed corrosion products, such as tenorite, also remain on the surface. The high proportion of chlorides remaining on the surface indicates that this layer, resilient to laser ablation, is unstable and unprotective.

3.1.5 Case 4a

Introduction

Cu_2O (cuprite) is a very common corrosion product which occurs on copper and copper alloys as an interface between the metal substrate and the external corrosion products. The coupon used in *Case 4a* replicates the brown cuprite layers that may be found, for example, on modern copper coins after a few years of use. Cuprite coatings have been known to be applied by patineurs^[5].

Patination method

A patinating solution of 5g $\text{CuNO}_3 \cdot 5\text{H}_2\text{O}$ in 25ml of distilled water was made up and boiled. The copper coupon was immersed in the boiling solution for 20 minutes then removed and rinsed first in hot water, then cold distilled water.

Pre-laser treated coupon

The coupon had formed a thin, uniform and adherent, brown patina. XRD identified only Cu_2O (cuprite) to be present.

Laser treated coupon

The laser had no visible effect upon the brown surface layer at sub-plasma fluence, nor was there any visible plume formed or audible shock. Increasing the fluence above the plasma threshold caused non-uniform blackening of the patina radiating across the surface from the area of irradiation.

Discussion

Oxides often form interfacial corrosion layers between the metal substrate and external corrosion products and usually form a passivating film during the initial corrosion process. Removal of the oxide would leave the metal substrate exposed to further corrosion and is seldom desirable. Thus, the fact that the laser left the oxide layer unchanged at sub-plasma fluences is generally desirable.

3.1.6 Case 5a

Introduction

Gunmetal bronze is commonly used in outdoor sculpture and hence the patina formed is often a product of the action of chlorides, sulphates and nitrates. The patination of bronze in the presence of such chemicals is investigated in this case.

Patination method

The patination solution consisted of 1g NaCl, 1g CuSO₄.5H₂O and 1g CuNO₃.3H₂O dissolved in 250ml of distilled water at room temperature. The coupon was dipped over a 10 minute cycle for 72 hours and continuously fanned whilst out of the solution. The patination process was identical to that of the copper coupon described in *Case 3a*.

Pre-laser treated coupon

The bronze formed an adherent, smooth, deep blue patina which varied slightly in tone over the surface. Some visibly large crystallites of corrosion, up to a millimeter in diameter, had formed near the jagged surface that would have been exposed whilst the ingot was being cast. There also appeared to be a brown underlying corrosion layer. XRD

revealed the presence of $\text{CuCl}_2 \cdot 3\text{Cu}(\text{OH})_2$ (basic copper chloride), CuCl (nantokite) and $\text{Cu}_2\text{Cl}(\text{OH})_3$ in the corrosion layers.

Laser treated coupon

The coupon was irradiated with a fluence of $2\text{J}/\text{cm}^2$ which removed the external, blue corrosion layer within several pulses, see *Photo 3.1.6a*. A brown layer remained that was not visibly effected by the laser at sub-plasma fluences. The thickness of the brown layer varied considerably over the area of the treated coupon, in some areas the etched surface of the granular bronze is clearly visible, whereas in other areas the layer obscures the metal surface completely. X-ray spectra of the brown layer did not elicit any clear information as to its nature, probably due to its thinness.

Discussion

Although the bronze in *Case 5a* was patinated under the same conditions as the copper in *Case 3a*, the resulting corrosion products were significantly different. The most pronounced difference between the two systems was the visual appearance of the laser treated areas, red in the case of the copper and dark brown in the case of the bronze. Although the dark brown coloration of the treated bronze was attractive and the bulk of the aggressive chlorides had been removed, the protective qualities and stability could not be determined due to the lack of chemical information.

3.1.7 Case 6a

Introduction

$(\text{Cu,Zn})_2(\text{OH})_3\text{Cl}$ (anarakite) is a corrosion product that may commonly appear on brass^[6,7] from exposure to chloride species. Anarakite has been known to appear on gunmetal bronze which also has a high zinc content.

Patination method

Concentrated $\text{HCl}_{(\text{aq})}$ was dropped by pipette onto the surface of a bronze coupon and allowed, over the period of a few days and in the confines of a fume-cupboard, to evaporate.

Pre-laser cleaned coupon

The patinating solution produced a uniform, relatively thick, adherent, pale turquoise patina. XRD produced strong peaks for the presence of anarakite and atacamite in the patina, and also some evidence for the presence of $\beta\text{-ZnOHCl}$.

Laser cleaned coupon

The laser was used at a fluence of $2\text{J}/\text{cm}^2$, sufficient to remove the external corrosion products within a few pulses. The remaining surface retained a thin uniform brown layer, through which the grain structure of the etched bronze surface could be observed, see *Photo 3.1.7a*.

XRD detected the presence of CuCl and SnO_2 in the remaining brown layer. A cross-section taken through the coupon shows that the brown layer existed prior to the laser treatment process, see *Photo 3.1.7b*.

Discussion

Again, the cleaning process has been limited by a thin, resilient surface layer that existed on the original patinated coupon. The presence of chlorides in this layer implies that it is unstable although the colour is not unpleasant.

3.1.8 Case 7a

Introduction

The most common form of tarnish on silver is Ag_2S . This tarnish is simple to create by exposing the silver to H_2S and water in an oxygen-rich environment^[8]. Silver does not naturally form bulk oxide layers, therefore, by investigating the effects of the laser on the sulphide layer, any oxidising effects caused by the laser can be readily identified. In the previous cases, any evidence for laser-induced oxidation was difficult to identify because there were already oxides present.

Patination method

A sterling silver coupon was suspended above a solution containing 4g of $\text{Na}_2\text{S}\cdot 9\text{H}_2\text{O}$ dissolved in 100ml of distilled water. The solution was kept at a temperature of 60°C by use of a hot-plate and the coupon was left for a period of two hours. The coupon was then rinsed thoroughly in running water.

Pre-laser treated coupon

The sterling silver had formed a thin, dark grey, adherent coating. The coating was too thin to determine its formulation through XRD analysis. AES was used to determine the composition of the corrosion products (see Table 3.1).

Area	Etch(s)	Cl (at%)	Na (at%)	C (at%)	Ag (at%)	S (at%)	Cu (at%)	O (at%)	Ag/Cu	Ag/S
A	0	10	4	20	20	33	5	8	3.8	0.6
B	0	14	2	20	21	27	8	9	2.8	0.8
B	60	1	1	0	42	47	10	0	4.3	0.9

Table 3.1: AES surface scan of sterling silver prior to laser treatment.

AES was performed on two areas which shall be called A and B respectively. The depth of the analysis was estimated to be between 2 and 4nm. The untreated corrosion layer has a large amount of atmospheric organic contamination that accounts for the high levels of Cl, Na, C and O present. The O may also be due to an Ag₂O layer that has been known to form to the depth of a few angstroms on silver in the presence of oxygen. A 60 second argon ion etch was performed to give information about the bulk of the corrosion products and reveals the presence of only Ag, S and Cu in significant quantities and no evidence of oxygen at all. Clearly, the copper and silver are present as sulphides only.

Laser treated coupon

Laser treatment was performed at both sub-plasma (Sample 1) and plasma (Sample 2) fluences (see Table 3.2).

Sample	Area	Etch(s)	Cl (at%)	Na (at%)	C (at%)	Ag (at%)	S (at%)	Cu (at%)	O (at%)	Ag/Cu	Ag/S
1	A	0	1	1	2	46	35	10	5	4.6	1.3
1	B	0	2	2	1	35	41	11	7	3.2	0.9
2	A	0	0	1	0	52	32	9	5	5.5	1.6
2	B	0	1	0	1	50	28	13	6	3.8	1.8

Table 3.2: AES surface scan of sterling silver after sub-plasma (Sample 1) and plasma (Sample 2) laser treatment.

Sample 1

The visual appearance of the sub-plasma treated coupon was virtually indistinguishable from the untreated coupon, the dark layer remained but had a slightly more diffuse appearance. The laser produced a weak, hot-plume for one or two pulses at 2J/cm² after which there was no visible interaction. The sub-plasma treated coupon shows a radical decrease in surface organic contamination; the low levels of detected C, Na and Cl

probably being due to recontamination from exposure to the laboratory atmosphere between the time of laser treatment and AES analysis. Ag, Cu and S levels are of similar value as the pre-laser treated etched sample.

The presence of oxygen in the absence of significant organic contamination suggests that the laser has converted some of the sulphides to oxides. It is interesting to note the Cu/O ratio is typically 2:1, suggesting the conversion of copper sulphides to cuprite.

Sample 2

The plasma treated coupon shows a further reduction in the levels of Cl, Na and C. There is no significant change in the Ag, S, Cu and O levels with respect to the sub-plasma treated coupon. Again, there was little visible difference between the plasma treated and untreated coupons.

Discussion

At both plasma and sub-plasma fluences the laser has reduced the level of organic contamination on the surface of the tarnish layer. The laser has also induced some oxidation at the surface of the tarnish which is absent from the bulk corrosion products. The high levels of Cu in the tarnish is due to its presence as a sacrificial component in sterling silver.

3.1.9 Case 8a

Introduction

The experimental method of *Case 7a* was repeated, but with the sterling silver coupon replaced with a high purity (99.95%) silver coupon. It was hoped that by almost eliminating the copper component that reaction chemistry would be simplified.

Patination method

See Case 7a.

Pre-laser treated coupon

Area	Etch(s)	C (at%)	Ag (at%)	S (at%)	Cu (at%)	O (at%)	Ag/S
A	0	39.4	23.1	15.5	4.1	17.9	-
B	0	27.8	30.3	15.2	6.9	19.8	-
B	20	0	66.7	33.3	0.0	0.0	2

Table 3.3: AES surface scan of high-purity silver prior to laser treatment.

In Table 3.3, the non-etched, pre-laser treated coupon shows the expected high levels of C due to atmospheric contamination. There is also a significant copper peak that was unexpected in such high purity silver, although the Cu does not appear to be present in the bulk of the tarnish layer. After etching the only elements detected are Ag and S in the expected 2:1 (i.e. Ag₂S) ratio.

Laser treated coupon

Laser treatment was performed at both sub-plasma (Sample 1) and plasma (Sample 2) fluences, see Table 3.4 (overleaf).

Sample 1

The non-etched coupon shows a large reduction in C after sub-plasma laser treatment at 2J/cm² although high levels of O remain. There is little change in the levels of Ag, S, Cu. After a 20s etch, the only elements detected are Ag and S, although the ratio has increased to 2.48 in comparison to 2.00 in the untreated sample.

Sample	Area	Etch(s)	C (at%)	Ag (at%)	S (at%)	Cu (at%)	O (at%)	Ag/S
1	A	0	11.2	44.9	21.2	8.1	14.6	-
1	B	0	12.4	36.2	15.8	6.5	29.2	-
1	B	20	0	71.3	28.7	0.0	0.0	2.48
2	A	0	3.4	20.8	4.0	10.9	60.7	-
2	B	0	4.0	33.2	8.7	4.6	49.4	-
2	B	20	0	66.9	24.1	0.0	9.1	2.78

Table 3.4: AES surface scan of high-purity silver after sub-plasma (Sample 1) and plasma (Sample 2) laser treatment.

Sample 2

The non-etched coupon shows a further reduction in C after plasma treatment. Whilst Ag and Cu levels remain about the same, O levels have increased greatly and S levels have been significantly reduced. The action of the plasma has been apparently to convert the surface sulphides to oxides. After a 20s etch, the Ag:S ratio has increased to 2.78 and the presence of O remains significant.

Discussion

Although the non-etched silver coupons exhibited strong copper peaks, copper was not present in the bulk of the tarnish, unlike in the case of the tarnish layer on sterling silver (see *Case 7a*). This indicates a duplex system with copper corrosion products forming a layer on top of silver corrosion products. The high levels of copper compounds at the surface of the tarnish implies that there is migration of copper ions to the surface during patination giving the top 15nm or so a copper concentration far in excess of that of the bulk material. Copper is generally the most common impurity in commercial silver because native silver ore often has a high copper content, some of which remains after the refinery process. The estimated etch rate of the ion-bombardment system is 45nm/min (based on a silver standard). The 20s etch would therefore have penetrated to a depth of

approximately 15nm, after which no copper was detected in the pre-laser treated coupon. The fact that copper remains after sub-plasma and plasma fluences shows us that the laser has removed less than 15nm of tarnish, if it has removed any at all.

As in *Case 7a*, the laser plasma is more effective at removing organic contamination than the sub-plasma beam. Although there is some evidence for the conversion of sulphides to oxides at sub-plasma fluences, this effect is far more pronounced at plasma fluences to the extent that the sulphide peaks were almost eliminated. The oxide peaks after plasma treatment remained significant even after a 20s etch.

In conclusion, the laser cannot be used to remove tarnish from silver. The hot-plume created by the laser during the first couple of pulses is due to the ablation of organic contamination from the surface of the tarnish layer. At plasma fluences, some evidence of surface oxidation was found although after a 20s etch (i.e. just a few tens of nanometers) the oxide level was reduced to 20% of that at the surface. Hence, even at plasma fluences the oxidising effect of the laser on silver tarnish is quite superficial.

3.1.10 Case 9a

Introduction

Much of the past and contemporary research on iron conservation has been focused on the removal of chlorides from the corrosion layer^[9-13]. In *Case 9a*, a mild steel coupon is rusted in a saline solution to cause corrosion containing a mixture of oxides and chlorides. To investigate whether a complex topography might affect the laser cleaning process, the coupon was punched with numerals to create features on the surface. Real iron objects will often present a complex relief, especially if they are significantly corroded.

Patination method

4g of NaCl was dissolved in 250ml of distilled water. The mild steel coupon was dipped into the solution over a ten minute cycle for 24 hours.

Pre-laser treated coupon

The mild steel coupon had a fairly uniform, orange/brown corrosion layer over its surface. The corrosion of the punched numerals appeared identical to that of the rest of the surface. XRD analysis revealed most significant peaks for β - $\text{Fe}_2(\text{OH})_3\text{Cl}$ and also strong peaks for ϵ - Fe_2O_3 and FeOOH . The metal substrate appeared as α -Fe.

Laser treated coupon

Laser treatment was performed at a fluence of $2\text{J}/\text{cm}^2$. After 2-3 pulses, all visible evidence of rust had been removed from both the surface and the punched numerals, see *Photo 3.1.10a*. The exposed steel had a pitted appearance due to the affects of corrosion. XRD was not performed on the cleaned area because the technique is not sensitive enough to detect corrosion layers too thin to be seen with the naked eye.

Discussion

The rust layer was unsightly and, due to the presence of chloride compounds, aggressive. Therefore, its removal could be warranted even though the metal substrate has been exposed, but the steel may require further treatment to prevent the corrosion process re-starting. The ability of the laser to penetrate into the fine detail of the numerals illustrates a clear advantage of laser cleaning over some more conventional cleaning methods.

3.2 Naturally Patinated Samples

The results from the artificially patinated coupons give some indication as to how certain metal/corrosion systems respond to laser treatment but they cannot be relied upon to accurately represent real-life corrosion systems. Fortunately, sculpture is not the only form of metal structure exposed to long-term, atmospheric effects and a number of naturally patinated samples were obtained from alternative sources. Through the kindness of National Museums and Galleries on Merseyside (NMGM) and Newarke Housing Museums, Leicester, some tests were also made on genuine sculpture and artefacts.

3.2.1 Case 1n

Introduction

Of all the corrosion products found on outdoor copper and copper alloys, brochantite, the basic copper sulphate, is probably the most written about^[14-18]. Attempts to form a brochantite patina on copper and bronze under laboratory conditions were unsuccessful and the author knows of no reference to how this may be formed artificially. Fortunately, due to some re-roofing to the halls of residence around the university campus, patinated copper roofing became available to us which contained a high percentage of brochantite in the corrosion layers. Part of the roofing, positioned at a slight angle to the horizontal, had formed a uniform, green patination layer and it is from this section that coupons were cut for our investigation for *Case 1n*. Another part of the roofing was positioned vertically and had patinated very differently with a very dark under-layer over which green speckles were scattered.

Pre-laser treated coupon

The 0.6mm thick copper roofing was cut into coupons of 80mm x 30mm for ease of laser processing and surface analysis. The pale green patina that had formed was uniform,

adherent and smooth. XRD produced very strong peaks for the presence of $\text{Cu}_4\text{SO}_4(\text{OH})_6$ (brochantite) and some $\text{Cu}_2\text{Cl}(\text{OH})_3$. Some evidence for CuO_2 (cuprite), CuCl (nantokite), Cu_2SO_4 and $\text{Cu}_2\text{O}(\text{SO}_4)$ (dilerophantite) was also found. Identification of the substrate was complicated by the fact that copper-metal and $\text{Cu}_{3,8}\text{Ni}$ (an alloy commonly used in roofing) have virtually indistinguishable powder diffraction patterns: SEM spot-analysis failed to detect any nickel in the cleaned copper sample and therefore the roofing material was taken to be copper. Cross-sectional analysis of the coupon did not reveal any evidence of an interfacial layer between the green patina and the metal substrate, see *Photo. 3.2.1b*.

Laser treated coupon

The laser interacted with the patina at low fluences of $0.5\text{J}/\text{cm}^2$ to produce a browning/blackening effect without any significant ablation. A much stronger interaction occurred around $2\text{J}/\text{cm}^2$ producing a hot-plume, see *Photo 2.1.4a* (previous chapter). At this higher fluence the blackening of the patina that remained was very pronounced. XRD of the blackened patina revealed a significant increase in the presence of cuprite. After about 15 pulses the laser treatment was complete (i.e. there was no more laser interaction) and a grey layer remained, see *Photo 3.2.1a*. XRD, performed at 0.1dpm , identified strong cuprite peaks in the remaining layer, with some evidence for CuCl (nantokite) and Cu_2S (chalcocite).

Cross-sections taken of the laser treated samples were unsuccessful due to the remaining surface layer having a tendency to dissolve in the embedding resin.

Laser-induced breakdown spectroscopy

LIBS spectra were taken at three different fluences during the laser treatment of the copper roofing, see *Fig 3.2.1c*. At the normal cleaning fluence of $2\text{J}/\text{cm}^2$ the ablation plume was absent of any ionisation peaks. A slight increase in fluence ('low plasma')

allowed for some ionisation to be observed without significant alteration in the appearance of the ablation plume. The five significant peaks observed at this fluence all correspond to copper ions showing that ionisation of the blow-off material can occur prior to air-breakdown. A further increase in fluence to $4\text{J}/\text{cm}^2$ ('plasma') radically changes the colour of the plume from orange to bright blue, see *Photo 2.1.4b* (previous chapter). The spectra shows very strong copper peaks (1, 5, 8, 10, 14 and 18); the other peaks were identified as nitrogen and oxygen from the air. No other elements could be identified from the spectra.

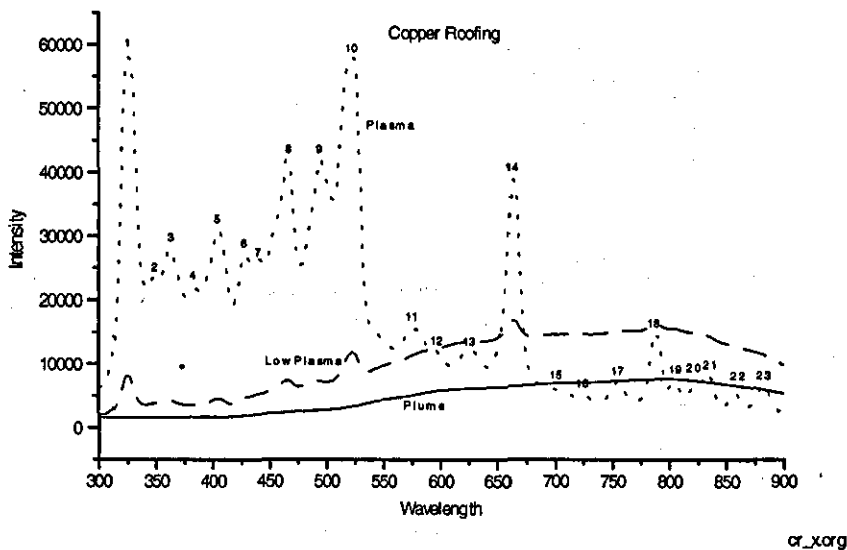


Fig. 3.2.1c: LIBS spectra of copper roofing irradiated at three different fluences.

FT-IR spectroscopy

The resilience of the cuprite layer compared to the brochantite layer can be explained by their IR absorbance spectra. *Figs 3.2.1d* and *3.2.1e* show the absorbance spectra for brochantite and cuprite respectively. As can be seen, brochantite has some broad, high absorbance bands from 500 to 4000cm^{-1} , one occurring between 600 and 1200cm^{-1} (i.e. between 8.3 and $16.7\mu\text{m}$). Cuprite, however, does not show significant absorptivity between 5 and $16.7\mu\text{m}$. Hence, the $10.6\mu\text{m}$ radiation is absorbed far more significantly by the brochantite layer as opposed to the cuprite layer.

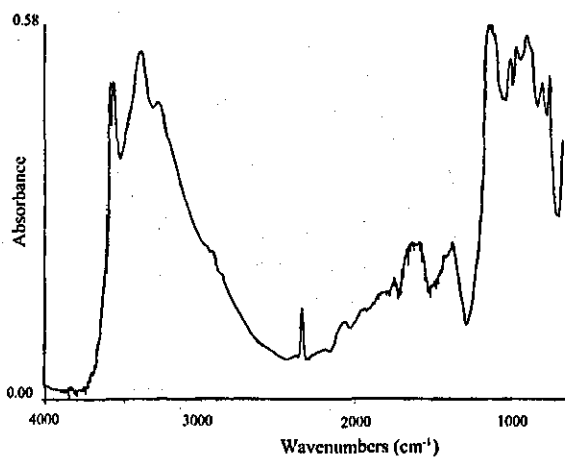


Fig 3.2.1d FT-IR Absorbance spectra of brochantite layer.

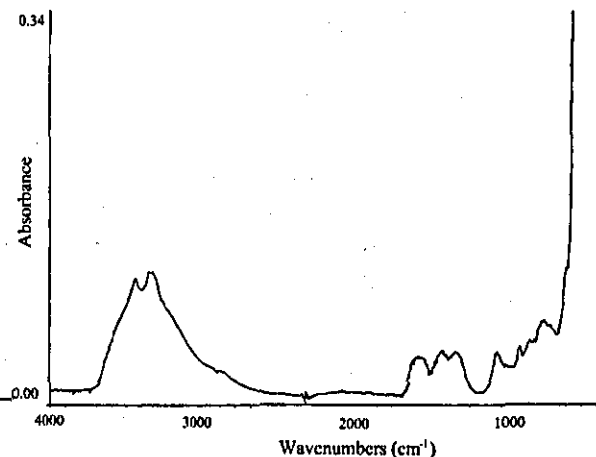
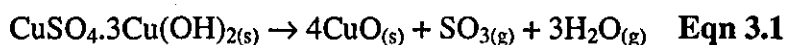


Fig 3.2.1e: FT-IR Absorbance spectra of cuprite layer.

Discussion

After each pulse, the surface of the underlying patina is blackened, apparently due to thermal effects that decompose the brochantite to tenorite (brochantite decomposes at 573K^[19]). The lack of evidence for a grey layer prior to laser treatment implies that the cuprite layer that remains after laser treatment is complete is formed from the decomposition of brochantite in contact with the surface of the metal substrate. This two stage process is initiated by the decomposition of brochantite to tenorite, *Eqn 3.1*, followed by the subsequent reduction of the tenorite to cuprite due to its proximity to the copper metal, *Eqn 3.2*. This is evidence of an indirect oxidation of the metal substrate due to laser irradiation and results in an undesirable, although slight, loss of the base metal. The grey appearance of the remaining layer could be due to optical effects of a thin black layer on a very rough, corroded surface. The application of a beeswax layer to the grey layer improves its appearance significantly, see *Photo 3.2.1a*, to produce a black surface. The passive qualities of the remaining cuprite layer may be compromised by some evidence of nantokite also remaining.





There is no doubt that brochantite is a valuable form of patination on many forms of sculpture and removal is generally undesirable, especially when it has formed such a uniform layer as in this example. However, when brochantite forms unsightly, streaky corrosion products its removal may be warranted. Also, it has been shown that when brochantite is in direct contact with the metal substrate, as it appears to be in this case, the patina is unstable^[7]. The blackening of the patina implies that surface contamination could not be removed from an underlying brochantite patina without unsightly damage to the patina and a 'layer-by-layer' technique for removing brochantite would be unsuccessful using this laser-cleaning system.

3.2.2 Case 2n

Introduction

Old coins are a convenient source of copper, bronze and silver that have, over the period of hundreds or even thousands of years of burial, formed a patina. A Roman coin has been used in this case that has been dated around the first or second century B.C.^[20] and, although little is known of its history, most of that time has probably been spent in the earth. The interaction of the laser with the surface is of particular interest, not only because of the age of the coin but also because its patina will differ significantly from corrosion products formed in the air.

Pre-laser treated coin

The coin had a diameter of approximately 2.5cm, a thickness of 2-3mm, and a roughly circular shape, see *Photo 3.2.2a*. A human head is clearly embossed on one side with lettering around the edge. The dark green patina that has formed has a polished

appearance and there is some evidence of an underlying, light brown interfacial layer. Despite the fact that the patina was of considerable thickness, XRD, even at 0.1 dpm, produced an extremely noisy diffraction spectra that contained few distinguishable peaks. The problems with the XRD analysis were ascribed to the small size of the crystallites in the polished surface because the spectra were consistent with those produced by amorphous materials or materials with only short-range crystalline order. Cuprite was the only compound identified with XRD although, from the colour of the surface, it is quite clear that the majority of the patina consisted of other compounds and most peaks could not be accounted for. Spot-analysis on the SEM identified a strong phosphorus peak; phosphates have been known to form the major corrosion products on objects buried in the vicinity of bones^[21]. Other peaks identified by SEM spot-analysis included calcium, silicon, iron and aluminium, the presence of which is likely to be due to embedded soil particles; small chlorine and sulphur peaks were also detected.

Laser treated coin

The laser was used at a fluence of $2\text{J}/\text{cm}^2$; ablation was accompanied by a blackening of the substrate. After between 40 and 50 shots there ceased to be further interaction at a given spot, the remaining corrosion products having a purple/brown appearance, see *Photo 3.2.2a*. XRD of the treated surface detected only cuprite and copper and no peaks were unaccounted for. Apart from copper, SEM spot-analysis detected a small phosphorus peak and significant tin peaks. The tin probably originated from the copper alloy but corroded in preference to the copper. The remaining surface is copper enriched and accounts for the copper detected by XRD. SEM photography reveals, on the micro-scale, a far rougher surface existing after laser treatment than the surface of the patina, see *Photo 3.2.2b*.

Discussion

From the general appearance of the coin after cleaning, it was clear that some surface definition had been removed through the laser treatment process. As is often the case with very old objects, much of the information that existed in the original metal now only exists in the patina as the metal surface has retreated. The patina appeared to be of high quality, there were no flaky/powdery areas that could indicate instability, and its preservation would normally be desirable. Furthermore, the removal of valuable surface information from the coin is undesirable and the laser process, in this case, was clearly harmful to the coin.

3.2.2 Case 3n

Introduction

As a source of naturally corroded brass, a blowtorch was purchased from a second-hand shop. The blowtorch could be considered to have three distinct areas of metallurgical interest; the body, which was covered with a green/black corrosion layer; the head, on which the patina was distinctly different due to the extremes of heat it had endured; and the handle/head bracket, both of corroded iron or steel. Each will be considered in turn.

(i) Body

Pre-laser treated body

The body of the blowtorch was completely covered in an opaque green/black corrosion layer, see *Photo 3.2.3a*. Some areas showed white spots of corrosion indicative of bronze disease (see Section 1.3.3). XRD of a sample taken from the body (1.06mm thick) showed it to be of CuZn brass: evidence for β -Cu_{0.61}Zn_{0.38} and pure copper was also detected. The only corrosion product identified was (Cu,Zn)₂(OH)₃Cl (anarakite).

Laser treated body

A fluence as low as $0.5\text{J}/\text{cm}^2$ had a whitening effect on the corrosion layer. Cleaning was found to be most efficient at a fluence of $2\text{J}/\text{cm}^2$ which removed the corrosion layer within a few pulses. XRD of the laser-whitened corrosion layer did not significantly differ from XRD of the untreated corrosion layer. The visible appearance of the $2\text{J}/\text{cm}^2$ laser treated surface was as if all the corrosion products had been removed and the metal substrate had been exposed and it had the appearance of copper, see *Photo 3.2.3b*. XRD of the cleaned surface detected copper and CuZn brass only, although some small peaks were present that could not be accounted for.

The needle valve on the blow-torch presented an opportunity of using the laser on an object of considerable complexity that may present a conservator with some difficulty, see *Photo 3.2.3c*. The laser successfully removed all visible corrosion products from around the embossed lettering and the screw-thread, see *Photo 3.2.3d*.

A cross-section taken through the blowtorch body shows the extent to which cleaning has been achieved, see *Photo 3.2.3i*. The untreated area shows the apparent lack of an interfacial layer between the anarakite and the metal substrate. The cross-section also shows no damage to the metal.

Discussion

The zinc had corroded selectively from the brass surface ('dezincification') and had left a thin, copper enriched surface under a layer of corrosion products. Although XRD did not provide evidence for the formulation of the white corrosion spots, they are likely to be white nantokite which is often found in the presence of anarakite as a product of bronze disease. Anarakite dehydrates to white nantokite at 623K which accounts for the whitening caused by the laser at low fluences. XRD could not identify any remaining corrosion products on the surface of the laser-treated brass.

Anarakite has been shown to be unstable when in direct contact with copper alloys^[7] and the appearance of the corrosion layer was generally unattractive. There are, however, dangers in exposing the metal substrate to further corrosive species and the treated body would probably require a protective coating, such as a lacquer.

(ii) Head

Pre-laser treated head

The head of the blowtorch had a more blackened appearance than the body and a thickness of 0.85mm. 'Rust' from the supporting steel bracket had added some orange/brown discoloration to the corrosion layer, see *Photo 3.2.3e*. XRD of the head revealed the brass composition to be identical to that of the body, with some evidence for enriched copper through the action of dezincification. The corrosion layers were identified to be cuprite and tenorite (CuO), the black tenorite layer forming on top of red cuprite from the oxidation of the cuprite due to the heat of the blowtorch.

Laser treated head

Laser treatment at $4\text{J}/\text{cm}^2$ visibly altered the appearance of the corrosion layers, see *Photo 3.2.3f*; the black layer now appeared grey and any of the exposed red layer was browned. XRD still only detected the presence of cuprite and tenorite, although the ratios of their respective peaks had altered such that there appeared to be a clear increase in the proportion of cuprite to tenorite on the surface (the relative intensities of the tenorite peaks on the treated sample were consistently higher than selected cuprite peaks whereas the converse was true on the untreated sample.)

Discussion

From the appearance of the surface and the XRD analysis, some of the tenorite had been ablated whilst some had been melted and became resilient to laser ablation. The presence of tenorite is common on copper alloys that are exposed to extremes of heat but is otherwise quite rare; it is a stable compound in neutral conditions although it is more soluble in dilute acids, such as rainwater, than cuprite. The laser did not have a pronounced effect on the head, although it did remove the discoloration from the rusty bracket and gave a more uniform appearance.

(iii) Handle

Pre-laser treated sample

The iron based appendages of the blowtorch had the typical orange/brown/black appearance of rust over the surface, see *Photo 3.2.3g*, and an overall thickness of about 2.5mm. In some areas, significant metal loss had almost eaten through the bracket completely and the rust was, in general, quite powdery. XRD of the rust detected the presence of β -FeO(OH) (akaganite) and Fe₃O₄ (magnetite); no indication was provided as to the nature of the metal substrate because the corrosion was too thick for the x-rays to penetrate.

Laser treated sample

The laser was used at a fluence of 2J/cm² and, although there was significant interaction, there appeared to be very little ablation. The colour of the surface was altered to a uniform dull grey, see *Photo 3.2.3h*. XRD revealed a considerable alteration in the composition of the corrosion, only γ -Fe₂O₃ (maghenite) was detected. The substrate was identified as α -Fe with Fe₃C (cohenite).

Discussion

Although there was no direct evidence for chlorides in the corrosion layers on the handle, Keller^[13] has shown that the presence of chlorine is necessary for the formation of akaganite, which has been known to hold aggressive chloride compounds within its structure. This fact, together with the abundance of chlorides in the corrosion over the body of the blowtorch, strongly suggests that the blow-torch has been exposed to a chlorine-rich environment. The formation of maghenite from the treatment process will have enhanced the passive qualities of the layer, maghenite having the protective qualities associated with metal sesquioxides. The appearance of the layer has also been improved from the unpleasant rust colour to a more uniform, dull grey.

3.2.4 Case 4n

Introduction

The restoration of a piece of sculpture under the care of NMGM provided an opportunity to test the laser on an authentic, naturally corroded object. The model of the Liverbird had been cast, unusually, in brass and was only 1.2m in height so that it could be transported, without too much difficulty, to our optics laboratory. Little of the sculpture's history was known, other than it had originally been painted completely white and had been exposed to a combined urban and marine environment in the centre of Liverpool for many years.

Corrosion analysis

There remains little visible evidence of the white paint that had been originally applied to the sculpture; exposed areas are covered in a pale green corrosion layer whereas on sheltered areas and depressions a thick, black crust has formed, see *Photo 3.2.4b*. Closer examination reveals that the black crust obscures some of the remaining white paint. It is

interesting to note that the various sections from which the sculpture has clearly been constructed have slightly differing forms of corrosion.

Samples large enough for XRD or laser tests could not be cut directly from the sculpture without incurring significant damage. Instead, XRD samples were obtained by using a scraper to remove corrosion products from both the pale green and black areas. The powders were glued, using Copydex, to glass slides to provide a flat surface for XRD analysis; both Copydex and glass are amorphous compounds that will not produce diffraction peaks themselves. Both the pale green and black powders provided X-ray spectra with such a high peak density that, even at 0.1dpm, it was impossible to resolve some of them. The most significant peaks from the pale green powder were from $\text{Cu}_4\text{SO}_4(\text{OH})$ (brochantite) and $\text{Cu}(\text{OH})\text{Cl}$, with strong peaks for $\text{Cu}_2\text{O}(\text{SO}_4)$ and $\text{Cu}_2\text{Cl}(\text{OH})_3$, and also evidence for $\text{C}_2\text{CuO}_4 \cdot x\text{H}_2\text{O}$ (copper oxalates have been known to form from pigeon excrement). The black powder had most significant peaks for $(\text{Cu,Zn})_2(\text{OH})_3\text{Cl}$ (anarakite) and $\text{Cu}_2\text{Cl}(\text{OH})_3$ (atacamite), with strong peaks for $\epsilon\text{-Zn}(\text{OH})_2$, $\text{Cu}(\text{OH,Cl})_2 \cdot 2\text{H}_2\text{O}$ (calumetite) and $\text{Cu}(\text{OH})\text{Cl}$.

A cross-section carefully cut from a discrete area of the sculpture clearly shows that the black corrosion is present on top of the pale green layer, which in turn is separated from the brass substrate by a red layer which may be cuprite, see *Photo 3.2.4d*. However, XRD did not detect the presence of cuprite in the scrapings taken from the surface. The scrapings contained a far higher proportion of the external corrosion products and these may have swamped the cuprite peaks.

Laser treated areas

The size of the Liverbird required the use of the beam delivery system to effectively couple the laser radiation with the surface. Furthermore, the Liverbird was mounted on a wheeled base to facilitate positioning. Laser treatment was performed over a discrete area

near the base of the tail feathers at a fluence of approximately $2\text{J}/\text{cm}^2$. The thick corrosion required upwards of 40 pulses before laser interaction ceased.

The fully-treated surface, see *Photo 3.2.4c*, had a uniform brown/purple coloration similar in appearance to the tests performed in *Case 2n*. It was clear from the treated areas that the corrosion layers obscured much of the underlying detail of the sculpture and the laser had done much to expose this detail. The treated area also appeared to be badly pitted through corrosive processes.

The layer remaining after treatment was thin enough to present difficulties in providing enough powder for reliable analysis. XRD of the powder was performed at 0.1dpm and produced most significant peaks for cuprite and zinc oxide (ZnO), with some evidence for the presence of ZnSO_4 and $\text{C}_2\text{CuO}_4 \cdot x\text{H}_2\text{O}$.

Discussion

The complexity of the corrosion products and paint remnants on the surface of the Liverbird makes it hard to determine what the optimum level of cleaning would be. There is evidence that a pale green corrosion layer exists beneath the black crust and paint, and it is likely that this extends over the whole of the surface. The black crust and paint are clearly unsightly and, from the high proportion of chlorides present in the black crust, it probably contributes to the corrosion process. An attractive solution would be to remove the black crust and leave the pale green layer; this would not only leave an attractive, uniform patina, but reveal much of the hidden detail. However, the XRD peaks detected for the pale green layer were as significant for $\text{Cu}(\text{OH})\text{Cl}$ as they were for the passive brochantite, so the passive qualities of the layer as a whole are unknown.

The laser was successful in removing unwanted corrosion products and did not expose the metal substrate to the atmosphere, but the removal of the pale green layer, in this case, was questionable. A clear improvement to the cleaning system would be to have the

option of cleaning down to the pale green corrosion layer without damaging it. The layer that remained consisted of mostly oxides and was of a colour that was not appealing. The application of a beeswax coating considerably improved its appearance by producing a deep brown gloss, see *Photo 3.2.4a*. Brown oxide coatings are not unknown as forms of patination for copper alloys^[5], but was not considered acceptable by NMGM for this particular example.

3.2.5 Case 5n

Introduction

The treatment of rust is a common problem in the conservation of iron and steel. In this example, an old 'homeguard' helmet from World War II had lost most of its original paint to severe corrosion.

Pre-laser treated helmet

Although a significant amount of dark green paint still remained on the surface of the helmet, what did remain was blotchy and discontinuous; over half of the surface was covered with orange/brown/black rust. The helmet was of a thickness of just 1mm such that samples could be easily cut from it for XRD analysis. Evidence for γ -Fe₂O₃ (maghenite), Fe₃O₄ (magnetite), FeOOH and α -FeO(OH) (goethite) were found in the corrosion products.

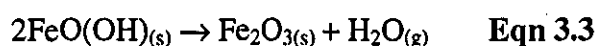
Laser treated helmet

The laser was used at a fluence of 2J/cm². All visible paint was removed at this fluence to reveal a shiny, metal substrate, see *Photo 3.2.5a* and *3.2.5b*. The laser did not appear to induce significant ablation of the rust, although the colour changed radically to slate grey. XRD of the laser treated sample did not detect a significant difference in the chemical

species present compared to the untreated area, although there was a noticeable increase in the ratio of maghenite and magnetite to the hydroxides.

Discussion

The diffraction patterns for maghenite and magnetite are very similar and distinguishing between them is very difficult. Fortunately, both maghenite and magnetite are passive oxides that form on iron. The effect of the laser on the rust appears to be to induce thermal decomposition of the hydroxides to oxides which takes place at 136°C, see *Eqn 3.3*.



However, once the oxides have formed on the surface they impair the ability of the laser radiation to couple with deeper layers and therefore hydroxides beyond the influence of the laser remain unchanged. The effectiveness of the laser to convert all hydroxides to oxides therefore depends on the thickness of the rust. For example, the thinner rust layer on the blowtorch handle (*Case 3n(iii)*) had all hydroxides converted to maghenite.

The slate-grey colour of the laser-treated rust could be considerably improved by the application of a bees-wax coating which caused a pleasant darkening of the layer, see *Photo 3.2.5a*.

3.2.6 Case 6n

Introduction

A more severe example of rusting was provided by a nail that had been donated by NMGM from a site of archaeological interest. Laser treatment was attempted because no conventional conservation techniques could be successfully applied.

Pre-laser treated nail

The rust had considerably altered the appearance and form of the nail, see *Photo 3.2.6a*. The original surface lay beneath a thick and friable corrosion crust. Although only a fragment of the original metal remained, the original surface was clearly defined in the dark corrosion layer (typically magnetite) beneath the rust in which the original rectangular form could be seen. The nail itself was far too rough for XRD analysis and a sample of the rust was cut from the surface, powdered in a mortar and pestle, and analysed separately. Strongest peaks were observed for the presence of β -FeOOH (akagenite), FeOOH and η -Fe₂O₃, with some evidence for the presence of ϵ -Fe₂O₃.

Laser treated nail

At a fluence of 2J/cm² the laser interacted with surface of the nail but there was little evidence of ablation and the laser just blackened the surface, see *Photo 3.2.6b*. After the surface was completely blackened, all interaction ceased.

Discussion

The blackening of the rust, as we have seen in previous examples, is probably due to the thermal decomposition of the hydroxides to maghenite. The laser treatment could not be considered beneficial to the object in this case. Ideally, the external rust should be removed to reveal the original surface of the nail.

3.2.7 Case 7n

Introduction

Before the development of stainless steels, cutlery was made from alloys that were more susceptible to the corrosive environment to which they were subjected. The spoon in this

case was obtained from a jumble-sale and displays an unsightly and discontinuous corrosion layer.

Pre-laser treated spoon

Although the spoon was significantly corroded, bare metal was exposed over a considerable portion of its surface. The thickness of the bowl of the spoon was measured to be just 0.45mm. The majority of the corrosion was of an orange/brown appearance and had formed a thin, adherent layer: in some areas a blue/green layer had formed over the top of this, see *Photo 3.2.7a*. The corrosion was too thin to provide good XRD spectra, even at 0.1dpm, although there was clear evidence for the presence of Zn_2O and some suggestion for the presence of $Ni(NO_3)_2 \cdot 6H_2O$ and $NiCl_2 \cdot 2H_2O$. The alloy was clearly identified as $\delta-Ni_3Zn_{22}$.

Laser treated spoon

The spoon required just two pulses from the laser at $2J/cm^2$ to remove all visible evidence of the corrosion products, see *Photo 3.2.7b*. The laser treated surface still appeared discoloured, however, although XRD provided no indication of corrosion products remaining. The discoloration could have been due to surface enrichment of either of the alloying metals due to the corrosion process, although this was not evident from XRD analysis. The laser did not produce any discoloration of the uncorroded metal.

Discussion

Sometimes corrosion products are not removed during the conservation of cooking utensils as they provide information about how, and with what, they were used^[22]. Otherwise, the laser was successful at removing the unsightly corrosion products from the spoon without any visible damage to the metal substrate.

3.2.8 Case 8n

Introduction

A corroded, excavated lead artefact was borrowed from Newarke Housing Museums for laser cleaning tests. The lead object was a flat band 15cm long and 10cm in diameter with a raised ridge along its centre and had been buried for a sufficient period to form a significant corrosion layer.

Pre-laser treated artefact

The artefact had a thin, powdery, creamy white corrosion layer over the entire surface. Encrusted clay and soil were removed by rinsing with distilled water as the laser was incapable of removing such deposits. Surface scrapings of the corrosion products were taken for XRD analysis. The most significant peaks from XRD analysis were for basic lead carbonate, $(3\text{PbCO}_3 \cdot 2\text{Pd}(\text{OH})_2 \cdot \text{H}_2\text{O})$; many lesser peaks could not be identified and were probably due to contamination from soil and clay.

Laser treated artefact

Although the corrosion layer was thin, removal required 5-10 laser pulses at a fluence of 3-4 J/cm². The laser exposed the metal substrate that was shiny and smooth in places, see *Photo 3.2.8*. Microscopic examination confirmed the suspicion that the metal surface had been melted by the laser from the presence of small, metallic globules on the surface. Corrosive effects usually roughen a metal surface to the extent that it has a diffuse appearance even when completely clean whereas exposed, shiny metal after laser treatment is usually a sign of melting.

Discussion

The corrosion layer was unsightly and unprotective and therefore required removal. The laser was successful at removing the corrosion layer but clearly damaged the metal substrate. Damage to the substrate is clearly unacceptable. The laser was also tested on a clean lead coupon and was found to cause oxidation at fluences as low as 0.5 J/cm^2 . Thus, the laser shows little potential in the area of lead conservation, as predicted from the theoretical calculations in Table 1.1 (see Chapter 1).

3.2.9 Summary of Results

Tables 3.5 and 3.6 show a summary of the effects the laser had on the various artificial and naturally patinated metals. It is immediately apparent that the influence of the laser radiation very much depends on the precise nature of the corrosion products. However, phenomenologically, the laser treatment process can be fitted within five categories.

(i) Complete removal of inorganics, exposing a bare metal substrate

Cases 9a, 3n(i) and 7n had all evidence of inorganics removed by the laser to the extent that none could be detected using the XRD apparatus. The exposed substrate was of matt appearance due to the high degree of micro-roughness resulting from the corrosion process; no evidence of melting was apparent on these samples which would have produced regions of shiny, solidified metal.

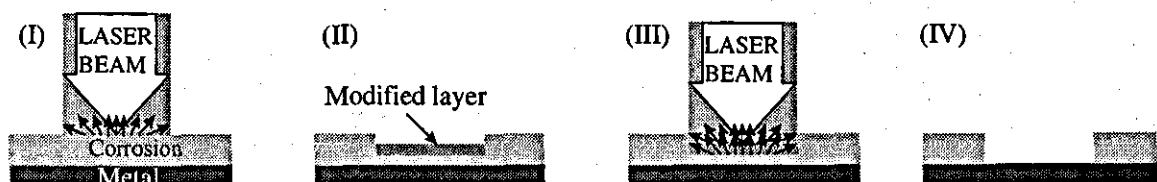


Fig. 3.2.9a: Complete cleaning to expose metal substrate

Fig 3.2.9a shows a possible model for the cleaning process. The laser is strongly absorbed by the surface (I), induces ablation and may leave a thin modified layer of decomposed corrosion products (II). Successive laser pulses are absorbed by the modified layer and the underlying corrosion products (III) until the metal substrate is exposed (IV).

The results do not show any clear indication as to why these three cases should be the only cases where complete cleaning has been realised. For example, the rusted mild steel in Case 9a did not react to laser treatment in the same way as the rusted steel in Cases 3n, 5n and 6n. Case 9a had a high proportion of hydroxychlorides, absent in the other cases, which could have increased the susceptibility of the rust to ablate, although this is purely conjecture.

These examples illustrate the danger of generalising the effects of laser irradiation on real systems; the effect of the laser on two steel coupons that have rusted under different conditions could be completely different.

(ii) Removal of surface inorganic layers whilst leaving an interfacial layer unaffected

This was the most common affect that the laser had on the targets and was apparent in Cases 2a, 3a, 5a, 6a, 2n and 4n.

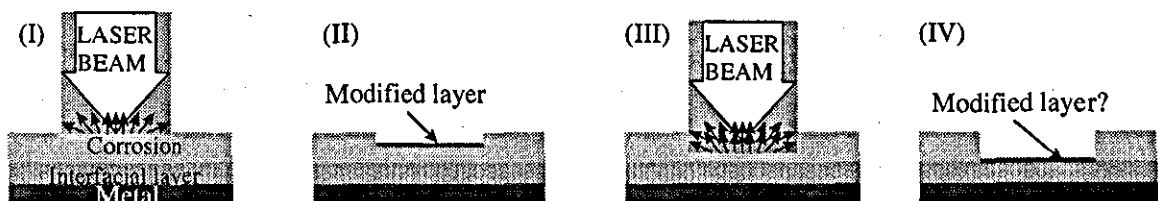


Fig. 3.2.9b: Laser ablation limited by an interfacial layer. After interactions have ceased, it is possible that a thin modified layer remains on top of the interfacial layer.

Fig 3.2.9b shows a possible model for the laser treatment process. The laser interacts with the surface corrosion (I) to cause ablation and leaves a modified layer of thermally decomposed corrosion products (II). Further irradiation is absorbed in both the modified and underlying corrosion layers (III) and ablation continues until the interfacial corrosion layer is reached. Once the treatment is complete, it is difficult to determine whether a modified layer remains on the surface or whether the interfacial layer is exposed (IV). The problem lies in the potential for the external corrosion products to decompose to chemical species (such as oxides) that are likely to be present in the interfacial layer. Cross-sections taken of the laser treated coupons support the view that no modified layer remains on the interfacial layer.

(iii) Little or no effect on the target material

Cases 4a, 7a, and 8a show that the laser has little or no effect on Ag_2S or Cu_2O . A weak plume may form during irradiation for the first few pulses, but this is due to the removal of organic contamination from the surface of the inorganic layer.

(iv) Modification of an inorganic layer without significant removal of material.



Fig 3.2.9c: Laser modification of surface corrosion products without causing significant ablation.

It was sometimes the case that the laser could raise the temperature of the target material sufficiently to cause some thermal decomposition whilst leaving a residue that prevented any further interaction. Examples are given in *Cases 3n(iii), 5n* and *6n*, all of which are

various forms of rust on steel. The rust in all cases consisted of a mixture of oxides and hydroxides. When the laser heated the surface, the hydroxides decomposed to form oxides. The result was to enrich the surface of the rust in oxide products that were resilient to laser ablation and hence stifled any further reaction, as shown in *Fig 3.2.9c*. Although the depth to which the laser decomposed the hydroxide is not known, there was clear evidence for hydroxides remaining below the surface layer in *Cases 5n* and *6n*.

(v) *Ablation of surface inorganic layers combined with modification of underlying material.*

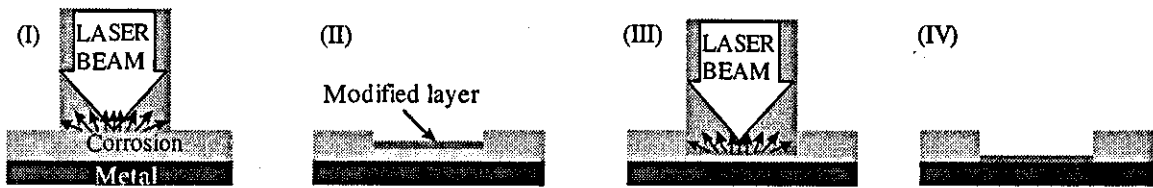


Fig 3.2.9d: Laser cleaning leaving resilient layer of modified corrosion products.

Fig 3.2.9d shows how the laser behaves on targets such as that presented in *Case 1n*. The leading edge of the pulse produces rapid heating of the corrosion surface (I) and ablation through the rapid thermal decomposition of the target, in this case, brochantite. However, heated material remains on the surface in the form of a thin, modified layer, i.e. the brochantite has decomposed to tenorite and remained at the surface (II). Clearly, a significant amount of heat is penetrating into the bulk of the corrosion layer during the ablation of the surface. This could be due to the length of the pulse, in particular the extended tail of the pulse which could provide a heat source after ablation had ceased. The next laser pulse (III) passes through the thin tenorite layer without much effect (the tenorite layer of *Case 3n(ii)* was unaffected by the laser at this fluence) but is absorbed by the underlying brochantite, causing ablation. By this process, a thin tenorite layer appears to propagate toward the metal substrate with successive laser pulses until all the brochantite has been removed (IV). However, if the tenorite is heated by the laser during contact with the substrate, as in *Case 3n*, it is reduced to cuprite.

Case	Metal substrate	Chemical treatment or description	Corrosion before laser	Corrosion after laser	Fluence (J/cm ²), pulses
1a	copper	1g of NH ₄ Cl, 1g of C ₂ H ₃ CuO ₂ , 250 ml water, 10 min dip cycle for 48hrs, partially fanned.	Uniform, blue layer on top of brown layer. XRD: Cu(OH)Cl and C ₂ H ₃ CuO ₂ .	Blue layer removed without damage to the underlying brown layer.	0.5, 2-3
2a	copper	1g of NH ₄ Cl, 1g of C ₂ H ₃ CuO ₂ , 250 ml water, 10 min dip cycle for 48hrs, fanned.	Uniform, blue/green layer on top of red layer. XRD: Cu ₂ Cl(OH) ₃ , C ₂ H ₃ CuO ₂ , CuCl.	Blue/green layer removed, red layer remained. XRD: CuCl.	2, 1-2
3a	copper	1g of NaCl, 1g of CuSO ₄ .5H ₂ O, 1g of CuNO ₃ .3H ₂ O, 250ml water, 10 min dip cycle for 72 hrs.	Variable, blue and white, thick corrosion layer on top of red layer. XRD: Cu ₂ Cl(OH) ₃ , Cu(OH)Cl and CuCl.	Blue/white layer removed, red layer remained with some fibrillose black corrosion products. XRD: CuCl and Cu ₂ Cl(OH) ₃ .	2, 5-10
4a	copper	5g of CuNO ₃ .5H ₂ O in 25ml water, boiled for 20mins.	Thin, uniform, brown layer. XRD: Cu ₂ O.	No change.	4, 10
5a	bronze	1g NaCl, 1g CuSO ₄ .5H ₂ O, 1g CuNO ₃ .5H ₂ O, 250ml water, 10min dip cycle for 72hrs.	Blue layer on top of dark brown layer. XRD: CuCl ₂ .3Cu(OH) ₂ , CuCl and Cu ₂ Cl(OH) ₃ .	Blue layer was removed, brown layer remained. XRD: no clear identification.	2, 3-5
6a	bronze	Conc. HCl was left to evaporate from the surface of the coupon.	Thick, uniform pale torquoise layer on top of brown layer. XRD: (Cu,Zn) ₂ (OH) ₃ Cl, Cu ₂ Cl(OH) ₃ , β-ZnOHCl.	Uniform brown layer remained. XRD: CuCl and SnO ₂ .	2, 3-5
7a	Sterling silver	Coupon suspended above a solution of 4g Na ₂ S.9H ₂ O in 100ml water at 60°C for 2hrs.	Very thin, dark grey tarnish. AES: copper and silver sulphides.	Very thin, dark grey tarnish. AES: copper and silver sulphides.	2,2-3
8a	Silver	Coupon suspended above a solution of 4g Na ₂ S.9H ₂ O in 100ml water at 60°C for 2hrs.	Very thin, dark grey tarnish. AES: Ag ₂ S.	Very thin, dark grey tarnish. AES: Ag ₂ S.	2,2-3
9a	mild steel	4g NaCl, 250ml water, 10 min dip cycle for 24hrs.	Uniform layer of orange/brown 'rust'. XRD: β-FeOHCl, ε-Fe ₂ O ₃ and FeOOH.	Metal substrate exposed, all corrosion removed.	2, 2-3

Table 3.5: Summary of the laser treatment of artificially patinated metal coupons.

Case	Metal substrate	Description	Corrosion before laser	Corrosion after laser	Fluence (J/cm ²), pulses
1n	copper	Copper roofing that had been replaced after 30 years of exposure to the atmosphere of a university campus.	Uniform, pale green layer. XRD: Mostly Cu ₄ SO ₄ (OH) ₆ and Cu ₂ Cl(OH) ₃ . Also, Cu ₂ O, CuCl, Cu ₂ SO ₄ and Cu ₂ O(SO ₄).	Dull grey layer. XRD: Mostly Cu ₂ O, some evidence for Cu ₂ S.	2, 10-20
2n	copper	Roman coin, patina has formed during burial for a couple of thousand years.	Polished, dark green patina with brown underlying layer. Chemical composition undetermined.	Purple/ brown layer remained. XRD: mostly Cu ₂ O.	2, 40-50
3n(i)	brass	Brass blowtorch, badly corroded but unknown history. Sample taken from the body.	Uniform green/black layer with spurious occurrences of white spots. XRD: (Cu,Zn) ₂ (OH) ₃ Cl.	All corrosion removed to expose the dezincified, copper coloured substrate.	2, 5-10
3n(ii)	brass	Same blowtorch as above, sample taken from the nozzle.	Uniform, black layer on top of red layer. XRD: CuO and Cu ₂ O.	Slight discoloration, dull grey layer remained. XRD CuO and Cu ₂ O.	4, 5-10
3n(iii)	steel	Rusted handle of the blowtorch.	Variable, orange/brown rust layer. XRD: β-FeO(OH) and Fe ₃ O ₄ .	Rust was discoloured to a slate grey. XRD: γ-Fe ₂ O ₃ only.	2, 5-10
4n	brass	A Liverbird sculpture that has been exposed to the marine and urban environment of Liverpool for many years. Originally painted white, little evidence of the paint remains.	Uniform, pale green layer on top of which a thick black crust had formed spuriously and underneath was a red layer. XRD (green): Mostly Cu ₄ SO ₄ (OH) ₆ and Cu(OH)Cl; XRD (black): Mostly (Cu,Zn) ₂ (OH) ₃ Cl and Cu ₂ Cl(OH) ₃ .	Most corrosion was removed, a thin brown/purple layer remained. XRD: Mostly Cu ₂ O and ZnO.	2, 20-30
5n	steel	Rusted 'home-guard' helmet.	Variable, friable orange/brown rust layer. XRD: γ-Fe ₂ O ₃ , Fe ₃ O ₄ , FeOOH and α-FeO(OH).	Rust was discoloured to a slate grey. XRD: γ-Fe ₂ O ₃ , Fe ₃ O ₄ , FeOOH and α-FeO(OH).	2, 5-10
6n	iron	Extremely corroded nail from excavation site, almost none of the original metal remained.	Thick, partially friable orange/brown rust. XRD: β-FeOOH, FeOOH, η-Fe ₂ O ₃ , ε-Fe ₂ O ₃ .	Surface was blackened.	2, 5-10
7n	zinc alloy	Spoon.	Thin blue/green corrosion on orange/brown layer. XRD: Zn ₂ O with possible presence of nickel nitrates and chlorides.	All detectable traces of corrosion removed to leave exposed metal substrate.	2, 3-5

Table 3.6: Summary of the laser treatment of naturally corroded and patinated metal objects.

3.3 Organic Coatings

Introduction

Organic coatings, in the form of paints and lacquers, are often applied to outdoor sculpture as a form of protection from corrosion. However, the coatings themselves suffer from degradation and inevitably breakdown creating an unsightly exterior that encourages localised corrosion which may gradually spread over the whole sculpture, for example, on the Liverbird in *Case 4n*. For this reason, it is important to investigate whether the laser is successful at removing not only fresh organic coatings, but also aged and deteriorated coatings.

Method

Surface analysis of the coatings could not be performed using XRD methods due to the amorphous nature of the organic compounds. Also, due to electromagnetic noise from surface charging effects, AES could not produce good quality spectra from organic compounds. Therefore, the only method available to us for observing these coatings was XPS. This technique could be used for quantitative elemental analysis and, with the use of high-resolution spectra, could identify the effects of ageing and weathering in the coatings.

3.3.1 Fresh paint

Introduction

Laser cleaning tests on organic coatings were started with some simple tests on copper coupons painted with a selection of different, common paints. Both modern (acrylic and cellulose) and traditional (linseed oil based) paints were tried.

Method

The three copper (C106, 99.85% pure) coupons were cleaned with wire-wool and rinsed in high-purity acetone. Each was painted with a different black paint; one with cellulose spray paint (two coats), one with Halford's 'Ford Black' acrylic spray paint (two coats), and one with Winsor and Newton's 'carbon black' oil paint (one coat). The coupons were left to dry for one week before laser cleaning.

Laser Cleaning

The laser was used at a fluence of $2\text{J}/\text{cm}^2$. All visible traces of paint were removed from all three coupons, see *Photo 3.3.1*. Although the coupons at first appeared completely stripped of paint within 5-10 pulses, the surface of the coupon felt as though some of the coating still remained. If some paint remained on the surface, then it was in the form of a very thin layer as there was no evidence of interference fringes or pigment and the copper appeared clean to the eye. However, final confirmation of an organic layer remaining was revealed using contact angles; values in the region of ninety degrees were observed whereas an atomically clean surface would have provided a zero contact angle. Extending the sub-plasma cleaning to more than 100 pulses did not eliminate the contact angle and, therefore, the remaining organic layer.

Discussion

Although these three paints were all susceptible to laser ablation, they all left some residue after laser-treatment at sub-plasma fluences that could not be removed, even after subjection to excessive radiation. The origins and nature of these residues are explored in more detail in Section 3.3.4.

3.3.2 Fresh lacquers

Introduction

Section 3.3.1 showed how a variety of paints were susceptible to laser ablation. From these results alone, it is not obvious whether it was the pigment, the medium, or a combination of the two that rendered the coatings susceptible to ablation. Lacquers are essentially paints that lack pigment and those tested here show that pigments are not necessary for TEA CO₂-laser ablation to be effective. The three lacquers tested in this section are all commercially available and specially formulated for the protection of outdoor sculpture and therefore have direct relevance to sculpture conservation.

Method

The three copper coupons were cleaned with wire-wool and rinsed in high-purity acetone. Each was painted with a different type of lacquer; one with Incralac, an acrylic based lacquer consisting of a solution of methyl methacrylate copolymer incorporating benzotriazole and specially formulated for the protection of copper and bronze (two coats); one with Ercalene, a cellulose based lacquer with plasticizer for all metals, particularly copper and brass (two coats); and one with Covalac, another lacquer specially formulated for the protection of copper and copper alloys (two coats). The coupons were left to dry for one week before laser cleaning.

Laser cleaned coupons

The laser was used at a fluence of 2J/cm². All visible traces of lacquer were removed from all three coupons, see *Photo 3.3.2*. As with the painted coupons, although the coupons at first appeared completely stripped of paint, the surface of the coupon felt as though some of the coating still remained and this was confirmed using contact angles; values in the regions of ninety degrees were observed. Extending the sub-plasma cleaning

to more than 100 pulses did not eliminate the contact angle and, therefore, the remaining organic layer.

Discussion

All the lacquers were susceptible to laser ablation but, like the paints, a very thin organic layer remained after sub-plasma cleaning that could not be removed, even after excessive laser irradiation. It would appear that the presence of pigment is not required for ablation to occur and significant absorption occurs in the medium of the coating.

3.3.3 Aged and weathered coatings

Introduction

The results from sections 3.3.1 and 3.3.2 show that the laser has potential to remove fresh organic coatings. However, with the exception of graffiti, fresh organic coatings rarely require removal and it is only after a period of ageing and weathering that a coating has degraded to an extent that it needs to be replaced. The effects of ageing usually alter the absorption spectrum of the coating, as shown in *Fig. 3.3.3a*^[23], as well as its chemical and physical properties in general. It would be inaccurate to draw conclusions from results obtained from the laser cleaning of fresh organic coatings and apply them to similar coatings that have been outdoors for a number of years.

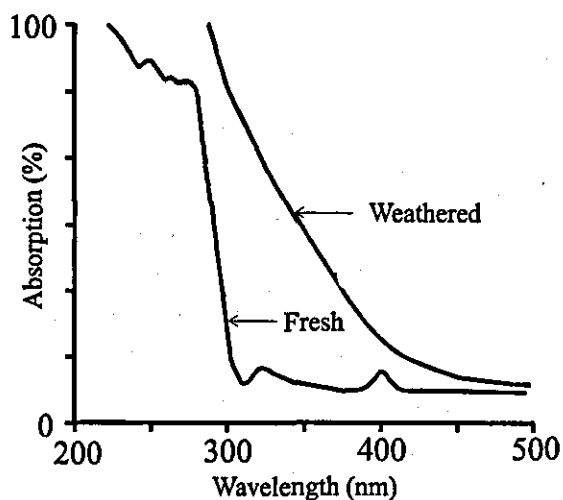


Fig. 3.3.3a: The effect of ageing on the absorption spectrum of Incralac.

The investigation into aged coatings started with a series of attempts to use accelerated ageing techniques to imitate the effects of many years of outdoor exposure within a few weeks in the laboratory.

The first ageing experiments were tried on copper with an Incralac coating. Ultraviolet fluorescent tubes were used that were active at 185 and 254nm, regions of high absorptivity in the Incralac absorption spectrum. The lacquered coupons were placed at distances between 1 and 5cm from the UV source and solubility tests were performed at daily intervals over a period of five days. UV exposure did not induce any significant alteration in the solubility of Incralac in acetone although, after a period of five days, the coupons placed closest to the UV-tubes had had all the lacquer removed. The UV radiation appeared to be causing scission as opposed to crosslinking reactions in the polymer coating and hence the experiment was abandoned and an alternative UV source sought.

The second ageing experiment used a UV source that was active at 340nm, within the emission spectra of solar radiation. The coupons were placed at 25mm from the UV-tubes and exposed for a duration of 4 hrs, 1 day, 1 week, 1 month, and 3 months. After the 3

month test period, a slight decrease in solubility of the Inralac coating in acetone was observed although the extent of deterioration fell far short of what would represent a degraded coating on an outdoor sculpture.

After the accelerated ageing techniques proved to be unsuccessful and unrepresentative of real ageing phenomena^[24], it was decided to use naturally aged paint samples for experiments. This meant losing a certain amount of knowledge as to the precise nature and composition of the coating whilst retaining an authentically aged sample.

Method

Body-work samples were cut from a dilapidated automobile. They were painted both sides, one side formed the external, exposed panel, and the other formed the internal, protected panel of the car. The internal side (IS) had not been exposed to the ageing effects of the weather and thus provided a control for the ageing effects observed on the external side (ES). The paint thickness was measured for the ES and IS using a micrometer and were found to be 8 and 13 μm respectively, the ES having a thicker coating to provide additional protection. The number plate indicated the age of the vehicle to be approximately ten years.

The body-work was cut into 1 cm^2 squares of 0.92mm thickness for laser treatment and XPS analysis. Cross-sectional analysis revealed various off-white paint layers between the metal substrate and the maroon coloured top-coat. Laser cleaning was performed at a fluence of 2J/ cm^2 .

XPS analysis was performed with a VG ESCALAB Mk I using Al K α X-rays of energy 1486.6 eV at a residual pressure of 10^{-7} Torr. Broad scan spectra were used to determine atomic composition and high resolution spectra were used to provide more detailed information on bond energies such that ageing effects could be identified. The estimated depth of analysis was about 10nm and elements from Li through to U could be identified.

Surface compositions were determined after the subtraction of a Shirley-type background spectra^[25]. For the broad-scan spectra, three spectra of three one-minute scans were taken for each of the samples and the results averaged. The high resolution spectra are accumulations of twenty scans.

Pre-laser cleaned samples

The samples were cleaned with distilled water prior to analysis of the original surface. Visual evidence of ageing was observed in the loss of gloss and slight yellowing of the ES with respect to the IS surface. Both the ES and IS contain the same four elements, C, O, N and Si (and, of course, a significant proportion of undetected H) as shown in Table 3.7. C and O are typical components of organic coatings. The O/C ratio in the ES coating is significantly higher than the IS coating, indicative of oxidation and ageing. The significant levels of N could also be part of the coating medium, or be present within chromophore compounds that give the top-coat its maroon coloration (there was no evidence of inorganic compounds to provide pigment). The Si could be present in the form of polysiloxanes which are used as surfactants in modern paints.

Sample	C (at%)	O (at%)	N (at%)	Si (at%)
ES	65.6	24.2	6.8	3.5
IS	75.6	18.2	5.8	0.5

Table 3.7: Broad scan spectra of original paint layer.

High-resolution spectra support the evidence for weathering of the top-coat found using the broad-scan spectra. *Fig 3.3.3b* and *c* show the C1s and N1s spectra respectively for the top-coat samples. In *Fig 3.3.3b*, the most significant peak at 285eV represents C/H and C/C bonds, the smaller peaks at higher bond energies are due to C/heteroatom bonds. The smaller peak is far more pronounced in the ES than the IS samples due to the greater abundance of functionalities such as C-N, C=N, C-O, C=O groups in the ES sample. Similarly, *Fig 3.3.3c* shows the most significant peak at 399eV due to C/N bonds. There

is also a smaller peak for the ES sample at 403eV due to N/O bonds which is absent from the IS sample. The O1s spectra for both samples showed a single, symmetrical peak around 532.9eV ascribable mainly to C-O bonds with no appreciable difference between the samples. Differences between samples due to ageing can be expected to be more pronounced in the C1s and N1s spectra than in the O1s spectra where the relative changes are smaller.

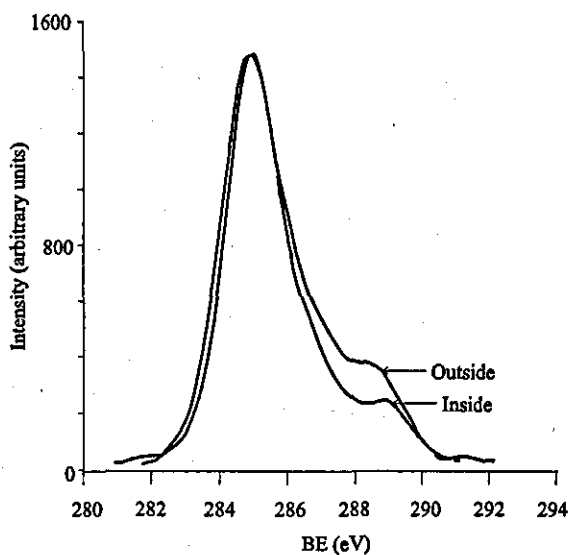


Fig. 3.3.3b: C1s spectra of weathered (outside) and fresh (inside) top-coat.

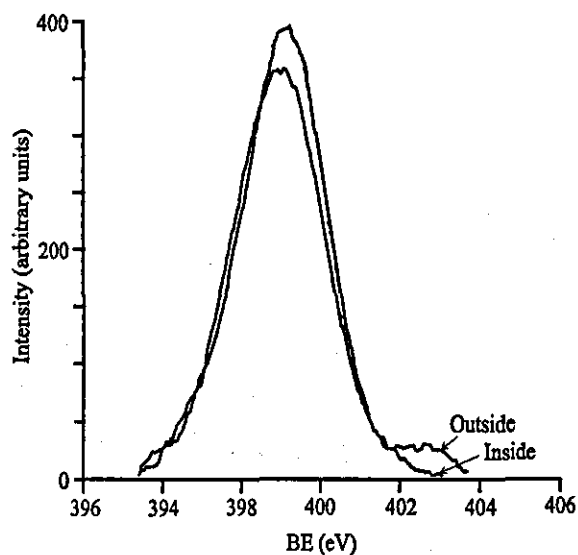


Fig. 3.3.3c: N1s spectra of weathered (outside) and fresh (inside) top-coat.

Partial laser cleaning

The partial laser cleaning tests were performed by firing a single shot at the surface of the sample. The composition of the surface of the remaining paint is shown in Table 3.8. The partially cleaned surface had a faded appearance with respect to the original maroon colour: this could be due to the roughening effect that the laser may produce, or due to the decrease in chromophore species present, as shown by the N decrease in Table 3.8. The decrease in Si can also be expected as the surfactant will be most concentrated at the surface. There is a striking similarity between the two sides; both have almost identical C/O ratios and there is no evidence of ageing from comparing the atomic compositions.

Sample	C (at%)	O (at%)	N (at%)	Si (at%)
ES	78.8	19.1	1.6	0.5
IS	78.5	19.7	1.5	0.2

Table 3.8: Broad scan spectra of paint layer after single laser pulse.

The high resolution spectra shown in *Fig 3.3.3d* confirms the fact that the aged layer has been removed to leave identical surfaces for the ES and IS samples. The ES and IS peaks for the C1s spectra are clearly resolved and almost identical; the intermediate shift zone of the ES spectra has decreased to the level of the IS spectra due to the removal of the mildly oxidised species originating from ambient exposure.

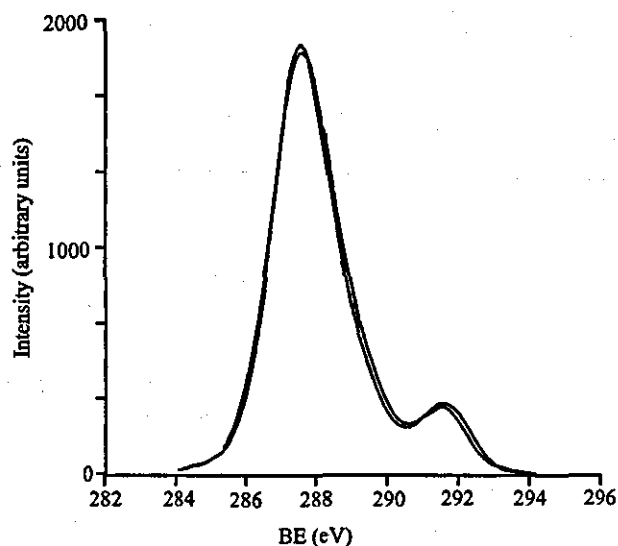


Fig. 3.3.3d: C1s high-resolution spectra of fresh and aged paint layers after a single laser pulse.

Discussion

The effects of ageing on the properties of the paint layer did not appear to significantly influence the effectiveness of the laser cleaning process and all effects of ageing had been removed after a single laser pulse. It is typical for ageing effects to alter the visible and

ultraviolet end of the absorption spectrum of organic coatings (e.g. yellowing effects) whilst leaving the infrared portion of the spectrum relatively unchanged. FT-IR spectroscopy of the IS and ES samples prior to laser treatment shown in *Fig 3.3.3e* confirm that their infrared spectra are virtually identical.

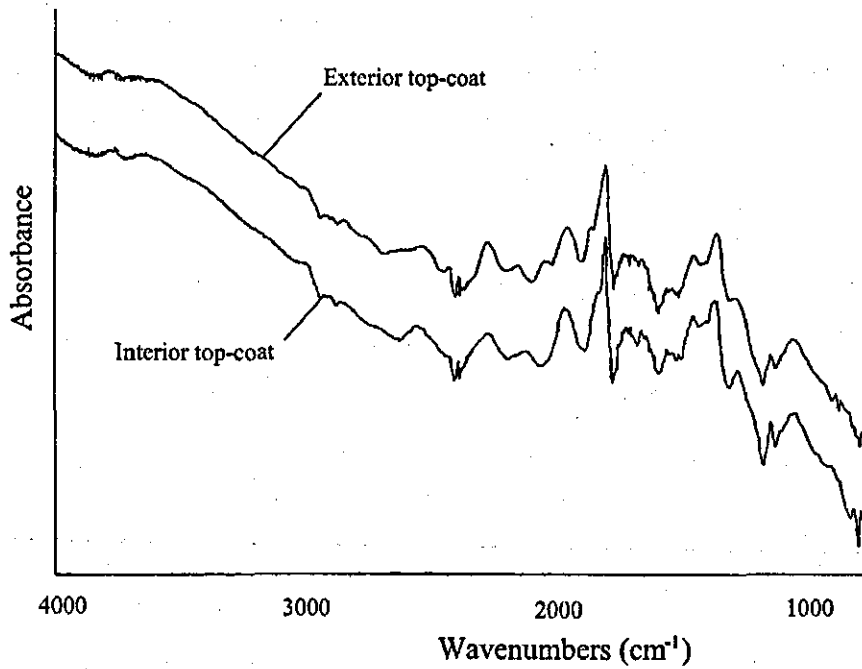


Fig. 3.3.3e: FT-IR absorbance spectra for interior (fresh) and exterior (aged) top-coat paint samples. The scans have been vertically shifted for comparison purposes.

Although the infrared absorption spectra of the coating is not significantly altered by ageing, there is likely to be an increase in boiling point due to cross-linking of the polymer chains. Cross-linking would impair the efficiency of the thermal ablation process to a certain extent. At present, there is no satisfactory method of removing aged organic coatings from metals. The laser shows great potential in this area.

3.3.4 Residual layers

Introduction

Although the laser has shown itself to be an efficient and effective remover of organic coatings at sub-plasma fluences, the cleaned surface invariably shows a large contact angle that is evidence of organic products remaining on the surface. Excessive cleaning at sub-plasma fluences does not remove these compounds although they form a layer too thin to be seen with the naked eye.

To investigate the nature of these residual layers and determine the reason as to why they remain, XPS analysis was utilised on sub-plasma laser cleaned samples.

Method

The painted body-work samples from Section 3.3.3 were cleaned at sub-plasma fluences until no more laser interaction took place. XPS analysis was performed using the same machine and method described in the previous experiment; high resolution and broad scan spectra were obtained. The full cleaning process required between fifteen and twenty laser pulses at a fluence of $2\text{J}/\text{cm}^2$.

Results and Discussion

The fully cleaned samples had a dull grey appearance, see *Photo 3.3.3g* and *3.3.3h*. The metal substrate was mild steel with a zinc coating.

Table 3.9 (overleaf) shows the broad scan spectra of the samples. The high levels of P are due to the presence of a phosphate coating on the zinc substrate. These coatings are applied for corrosion resistance and for their adhesive qualities^[26] and can contain both

Zn and Sn anions^[27]. As can be expected, the IS and ES samples show no significance difference in their composition at this depth of analysis.

Sample	C (at%)	O (at%)	N (at%)	Si (at%)	P (at%)	Zn (at%)	Sn (at%)
ES	59.4	25.9	2.4	-	8.1	3.0	1.2
IS	62.2	23.9	2.7	-	8.3	2.1	0.8

Table 3.9: Broad-scan spectra of fully cleaned samples at sub-plasma fluences

The most striking observation from this analysis is that approximately 60% C exists on the surface. Zinc and tin phosphate groups are typically of the form PO_3^- or PO_4^- such that the majority, if not all, the oxygen remaining on the surface is likely to be associated with the P and not the C. Thus, the carbon could only be associated with a very small amount of N or O, insufficient for paint formulations. It would appear, from these results, that the source of C is not from paint remaining on the surface. *Fig 3.3.4a* shows a high-resolution spectrum that enforces the results from the broad-scan spectrum.

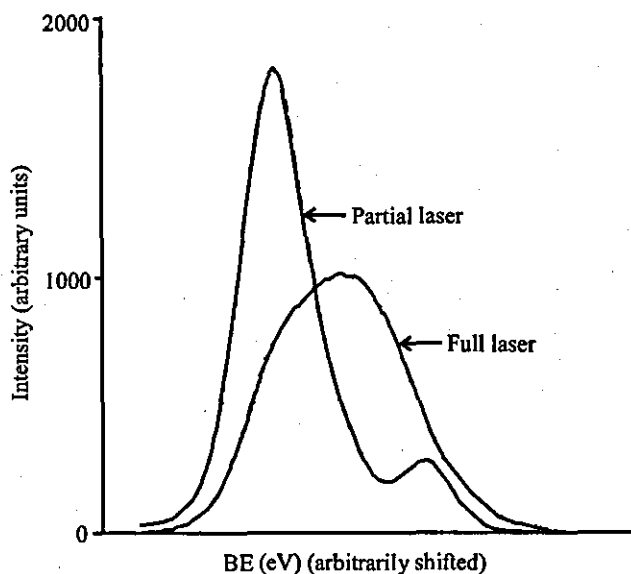


Fig. 3.3.4a: High-resolution C1s spectra of part-cleaned paint and residue on fully cleaned surface.

The C1s spectrum of the fully cleaned sample has a single, almost symmetrical peak compared with the two peaks of the C1s paint spectrum of the partially cleaned sample. The remaining C on the fully cleaned sample has only C/C and/or C/H bonds with no evidence of functional groups attached. When these residual layers were first observed on the cleaned painted samples we assumed them to be simply remaining paint. It seemed feasible that the proximity of the metal substrate would sink the heating effect of the laser and prevent ablation close to the metal surface. However, XPS analysis has identified the remaining layer to be either simple hydrocarbons or elemental carbon, but not paint.

A possible explanation for the presence of a residual layer could be from re-deposition of the ablated paint products. The species evolved from the pyrolysis of polymer compounds depends on the polymer and the temperature to which they are raised. In general, polymers raised to a temperature below 500°C will evolve species of monomer compounds or larger; above 500°C and degradation of the monomers produce smaller molecular products and atoms^[28]. The temperature of the hot-plume during paint ablation has been estimated to be spread over the region of 2000-6000K from LIBS observations. The presence of ions in the plume indicates that little, if any, of the ablated material exists as monomers or even molecules, but as atoms and ions. Whatever its origin, the residual layer is more resilient to ablation than the original paint and thus cannot be removed under similar conditions of irradiation.

References

- [1] Naylor, A., 'Developments in the conservation of coloured metal surface treatments to outdoor sculpture', unpublished work.
- [2] Hughes, R., and Rowe, M., 'The Colouring, Bronzing and Patination of Metals', Thames and Hudson, London, (1991).
- [3] Tennent, H. N. and Baird, T., 'The identification of acetate efflorescence on bronze antiquities stored in wooden cabinets', *The Conservator*, 16, (1992), 39-43.
- [4] Livingston, R. A., 'Influence of the environment on the patina of the Statue of Liberty', *Environ. Sci. Technol.*, Vol. 25, No. 8, (1991), 1400-8.
- [5] Sochja, J., 'Oxide coating in the conservation of metal monuments: The column of King Sigismundus III Waza in Warsaw', *Studies in Conservation*, 25, (1980), 14-8.
- [6] Morales, J., Fernandez, G. T., Esparaza, P., Gonzalez, S., Salvarezza, R. C., Arvia, J., 'A comparative study of the passivation and localised corrosion of alpha, beta, and alpha + beta brass in borate buffer solutions containing sodium chloride I. Electrochemical data', *Corrosion Science*, 37(2), (1995), 213-31.
- [7] Opila, R. L., 'Copper patinas - an investigation by auger electron spectroscopy', *Corros. Sci.*, 27, (1987), 685.
- [8] Sneed, M. C., Maynard, J. L., Brasted, R. C., from *Comprehensive Inorganic Chemistry Vol. II*, D. Van Nostrand Company Inc., London, (1954), 142-3.
- [9] Biasini, V., Cristoferi, E., 'A study of the corrosion products on sixteenth and seventeenth century armour from the Ravenna National Museum', *Studies in Conservation*, 40, (1995), 250-6.
- [10] Sjorgren, A., and Buchwald, V. F., 'Hydrogen plasma reduction in the D.C. mode for the conservation of iron meteorites and antiquities', *Studies in Conservation* 36, (1991), 161-71.
- [11] Zucchi, F., 'Beta-iron oxide hydroxide formation in localised active corrosion of iron artifacts' in *Corrosion and Metal Artifacts*, NBS Special Publication 479 (1977), 103-5.
- [12] Patscheider, J., Veprek, S., 'Application of low-pressure hydrogen plasma to the conservation of ancient iron artifacts', *Studies in Conservation*, 31, (1986), 29-37.
- [13] Keller, P., 'Vorkommen, Entstehung und Phaseumwandlung von Beta-FeOOH in Rost', *Werk U. Korr.*, 20, (1969), 102.
- [14] Vernon, W.H.J., and Whitby, L., 'The open-air corrosion of copper. A chemical study of the surface patina', *J. Inst of Metals*, 42, (1929), 181-196.
- [15] Livingston, R. A., 'Influence of the environment on the patina of the statue of liberty', *Environmental Science and Technology*, 25(8), 1991, 1400-8.
- [16] Wingerson, L., 'America cleans up Liberty', *New Scientist*, (25 Dec 1986), 31-35.
- [17] Lins, A., 'Outdoor Bronzes: Some Basic Metallurgical Considerations,' from *Sculptural Monuments in an Outdoor Environment*, Ed. V.N. Naude, Pennsylvania Academy of Fine Arts, Philadelphia, (1985), 9-20.
- [18] Nielsen, N. A., *Mater. Perform.*, 23(4), (1984), 78.
- [19] Weast, R.C., (Chief Ed.), from *CRC handbook of Chemistry and Physics*, 70th Ed., CRC Press Inc., Florida, (1989).
- [20] from Newarke Housing Museums.
- [21] Fabrizio, M., Ganiaris, H., Tarling, S., Scott, D.A., 'The occurrence of sampleite, a complex copper phosphate, as a corrosion product on copper alloys objects from Memphis, Egypt', *Studies in Conservation*, 34, (1989), 45-51.
- [22] Steve Newman, private communication.
- [23] Erhardt, D., Veloz, N. F., 'The durability of Inralac: Examination of a ten year old treatment, ICOM 1984 Preprints of the 7th Triennial Meeting, 84.22.1-3.
- [24] Skerry, B. S. and Simpson, C. H., 'Accelerated test method for assessing corrosion and weathering of paints for atmospheric corrosion control', *Corrosion*, 49(8), (1993), 663-74.
- [25] Shirley, D. A., *Physics Review B*, 5, (1972), 4709.
- [26] Weng, D., Jokiell, P., Vebleis, A., Boehni, H., 'Corrosion and protection characteristics of zinc and manganese phosphate coatings', *Surface Science and Technology*, 88, (1996), 147-56.
- [27] Nomura, K., Ujihira, Y., Kojima, R., Yoshida, M., 'Characterisation of converted tin phosphate coating on iron and steel by conversion Moessbauer spectroscopy (CEMS)', *Journal of Material Science*, 27, (1992), 2449-57.

[28] Madorsky, S. L., from *Thermal Degradation of Organic Polymers*, John Wiley and Sons, Inc. London, (1964) 3.



Photo 3.1.2a: *Case 1a*. The surface shows the results of three laser treatment tests; on the left, 2 pulses at $0.5\text{J}/\text{cm}^2$; at the top right, 2 pulses at $2\text{J}/\text{cm}^2$; at the bottom right, 10 pulses at $2\text{J}/\text{cm}^2$.

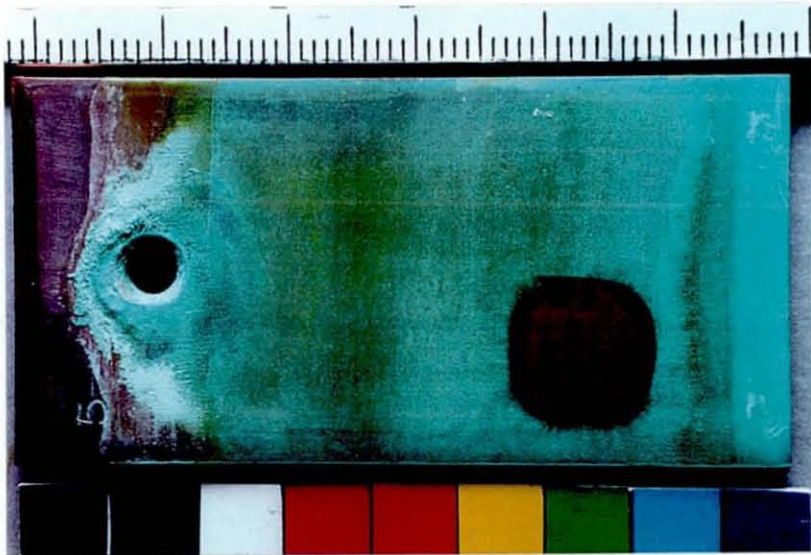


Photo 3.1.3a: *Case 2a*. The laser treatment on the bottom, right-hand side was performed at a fluence of $2\text{J}/\text{cm}^2$ and required 4-5 pulses to reveal the underlying red layer.

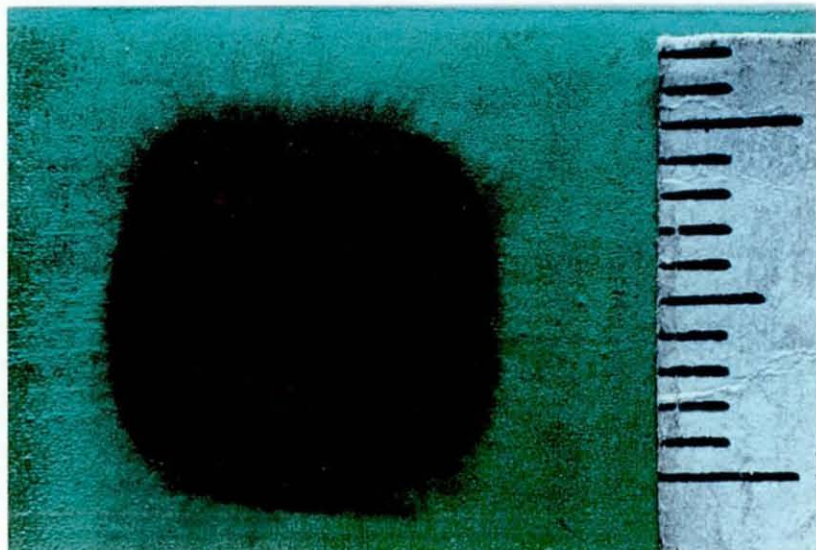


Photo 3.1.3b: Detail of the laser treated area of *Case 2a*.

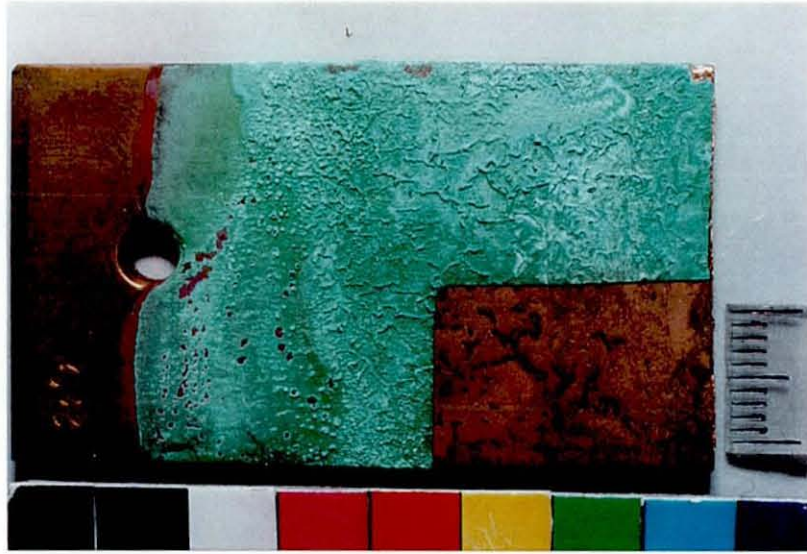


Photo 3.1.4a: *Case 3a*. The laser treatment on the bottom, right-hand side was performed at a fluence of $2\text{J}/\text{cm}^2$ and required 9-10 pulses to reveal the underlying red layer.



Photo 3.1.4b: Detail of the laser treated area of *Case 3a*.



Photo 3.1.4c: Cross-section through the copper coupon from *Case 3a*. The left-hand side shows the untreated corrosion layers, the right-hand side the laser treated area. The red interfacial layer is clearly visible on both sides and represents the limit of the cleaning process.

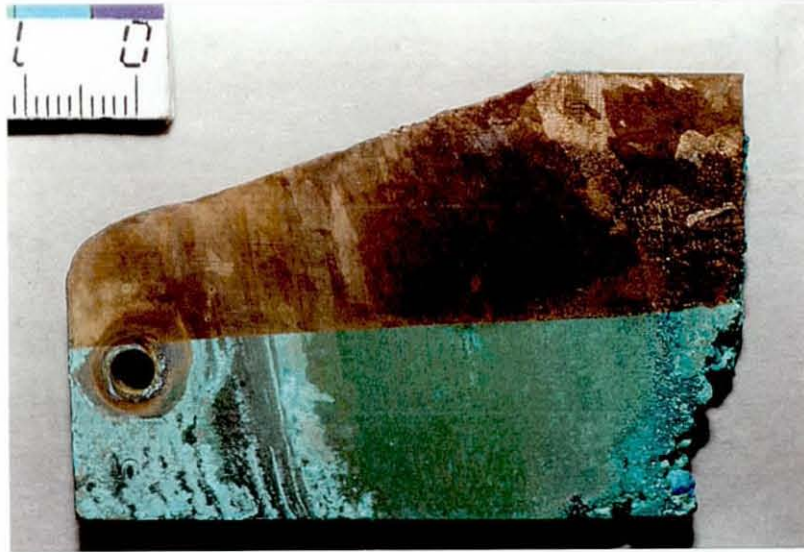


Photo 3.1.6a: *Case 5a.* The top half of the coupon was subjected to 4-5 laser pulses at $2\text{J}/\text{cm}^2$. The grain structure of the metal is clearly visible in the etched surface.



Photo 3.1.7a: *Case 6a.* The right-hand side of the coupon was subject to 7-8 laser pulses at $2\text{J}/\text{cm}^2$. The grain structure of the metal is visible under a thin, brown oxide layer.

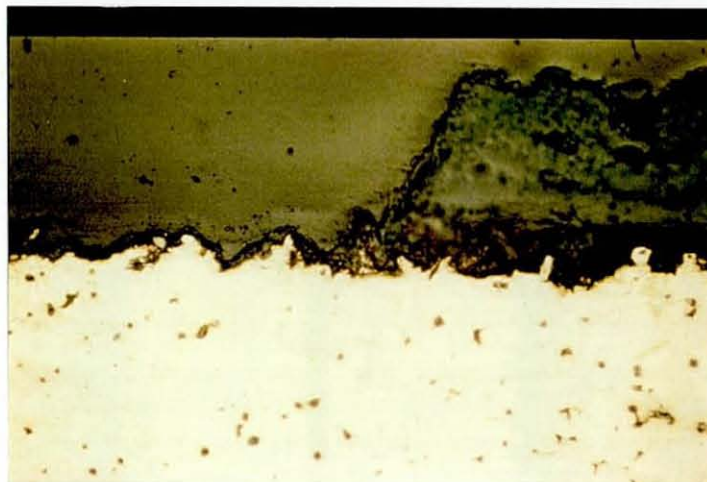


Photo 3.1.7b: Cross-section through the bronze coupon from *Case 6a*. The right-hand side shows the untreated corrosion layers, the left-hand side shows the laser treated area. The dark brown interfacial layer is clearly visible on both sides and represents the limit of the cleaning process.



Photo 3.1.10a: *Case 9a.* The mild steel surface has been exposed after 2-3 laser pulses at $2\text{J}/\text{cm}^2$.

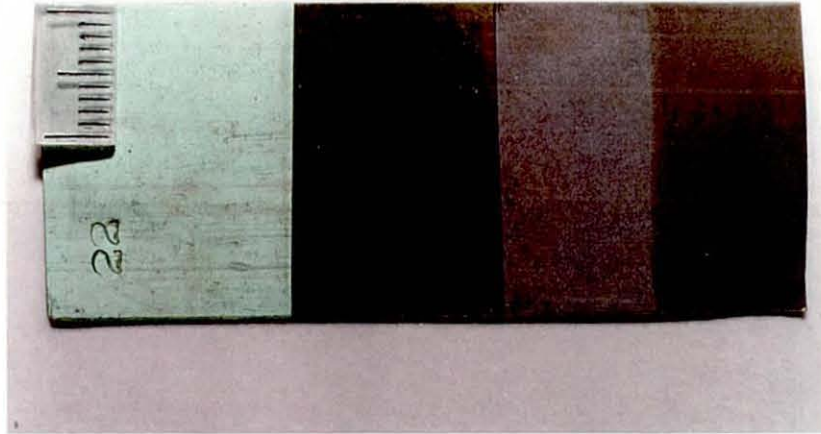


Photo 3.2.1a: *Case 1n.* From left to right is the untreated coupon; the blackening effect after two, $2\text{J}/\text{cm}^2$ laser pulses; the fully treated sample after 10-15 pulses at $2\text{J}/\text{cm}^2$; and the fully treated sample after a beeswax coating has been applied.

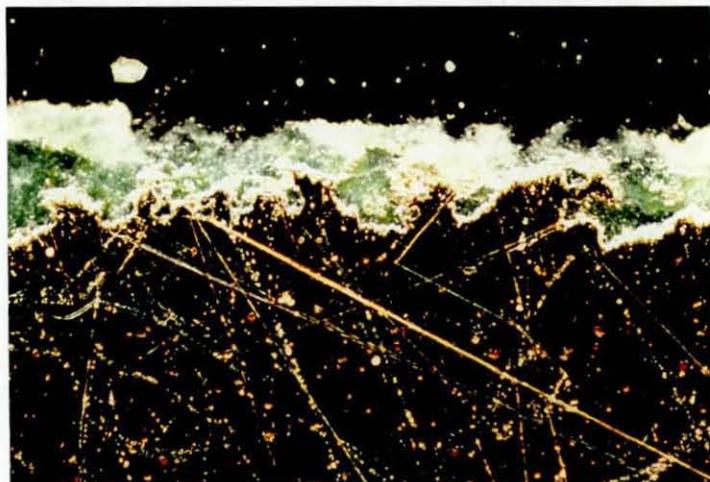


Photo 3.2.1b: Cross-section taken through the roofing of *Case 1n*. There is no visible interfacial layer between the green corrosion and the copper substrate.



Photo 3.2.2a: *Case 2n*. The top half of the coin has been subjected to 20-30 laser pulses at $2\text{J}/\text{cm}^2$. There has been some loss of detail due to the laser.

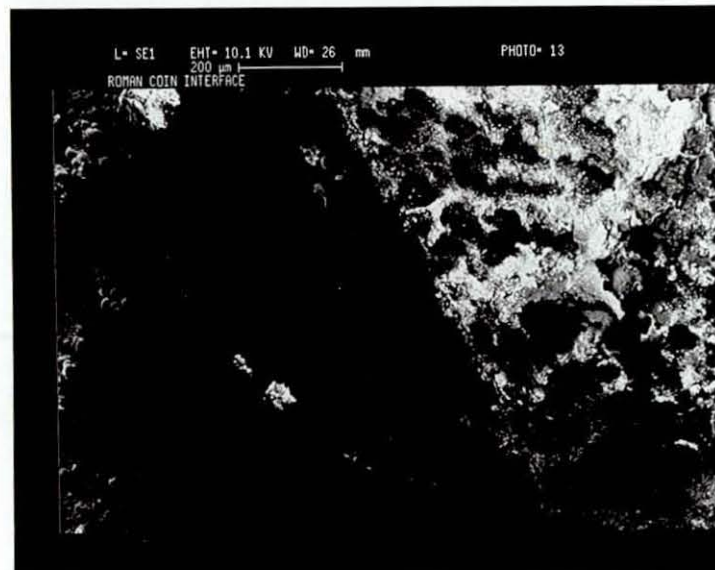


Photo 3.2.2b: SEM photograph of the interface of the treated (left) and untreated (right) areas of the coin. Some corrosion products, especially near the border of the two areas, are similar in appearance to stalagmites and have been melted by the laser interaction.



Photo 3.2.3a: Naturally corroded blowtorch of *Case 3n*, as received.



Photo 3.2.3b: The blowtorch after laser treatment at a fluence of $2\text{J}/\text{cm}^2$. Part of the steel bracket and head-piece have been removed for surface analysis.



Photo 3.2.3c: The untreated needle valve from the blowtorch in *Case 3n*.



Photo 3.2.3d: The needle valve after laser treatment at a fluence of $2\text{J}/\text{cm}^2$. Note how the laser has penetrated into the thread and clarified the embossed writing.

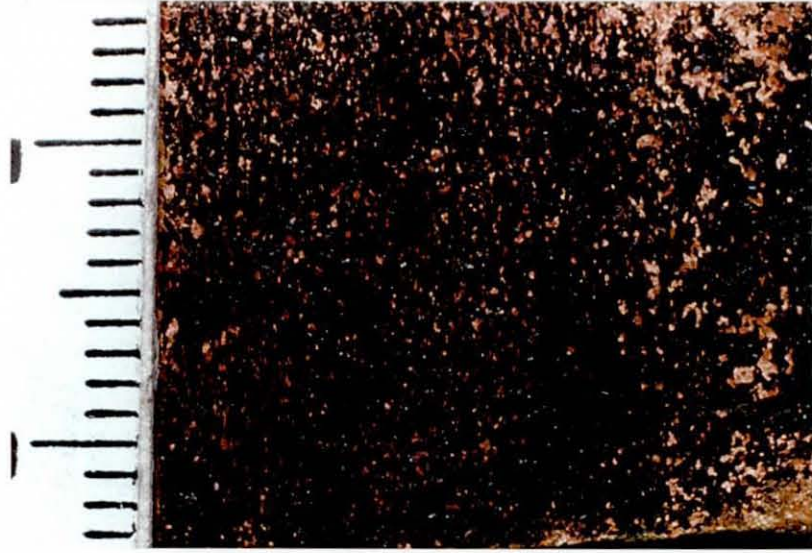


Photo 3.2.3e: Untreated sample taken from the blowtorch head in *Case 3n*. Some of the powdery black layer fell away as the sample was removed to reveal an underlying red layer.

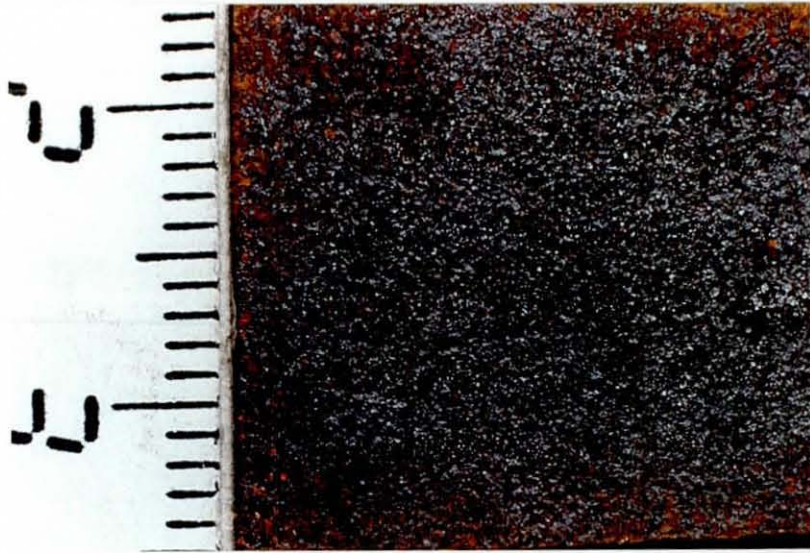


Photo 3.2.3f: Laser treatment of the surface of the blowtorch head at a fluence of $4\text{J}/\text{cm}^2$ which has altered the coloration.



Photo 3.2.3g: Untreated sample taken from the blowtorch bracket in *Case 3n*.

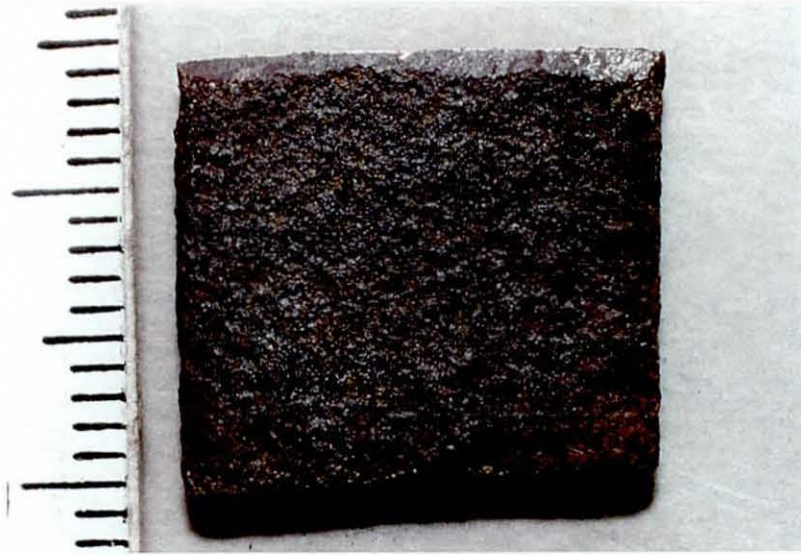


Photo 3.2.3h: Laser treatment of the blowtorch bracket at a fluence of $2\text{J}/\text{cm}^2$ caused a change in coloration.



Photo 3.2.3i: A cross-section through the blowtorch body in *Case 3n*. The right-hand side is untreated and the left-hand side has been laser treated. There is no evidence of a remaining corrosion layer on the laser-treated side, and the metal surface has retained its roughness with no evidence of melting.

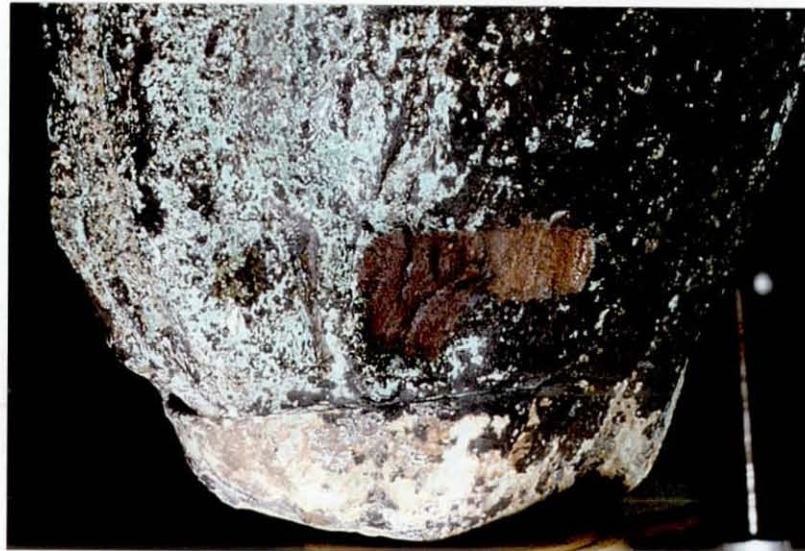


Photo 3.2.4a: The green patination, the white paint, and the black crust are all apparent in this photograph of the Liverbird's tail-feathers. The dark brown area in the centre has been laser cleaned and also beeswaxed. The brass area to the right is where a sample was



Photo 3.2.4b: *Case 4n*, as received. Laser treatment was initiated on the sheltered region of the tail-feathers.



Photo 3.2.4c: A larger area of treatment, this time without any beeswax coating. If this photograph is compared with *Photo 3.2.4a*, there has been a clear improvement of surface definition.

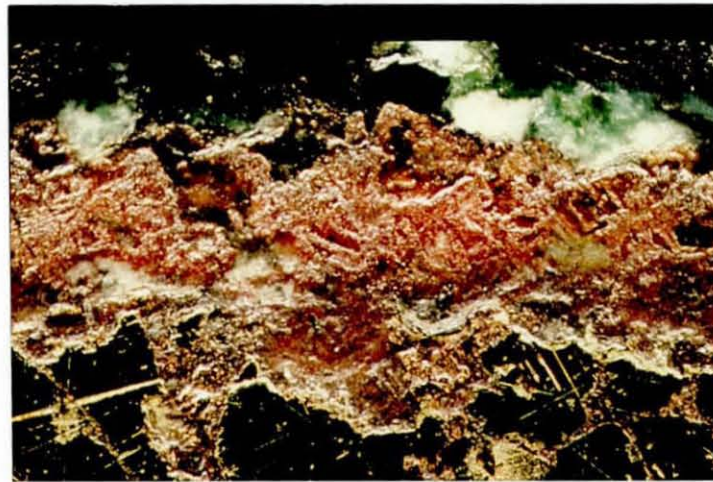


Photo 3.2.4d: A cross-section taken from one of the claws of the Liverbird. The bottom of the photograph shows the brass substrate, on top of which the red layer, then green layer, then black layer can be distinguished.



Photo 3.2.5a: *Case 5n*. The untreated, rusted surface is shown on the right, the laser treated surface in the middle, and the laser treated surface after a beeswax coating has been applied, on the left.

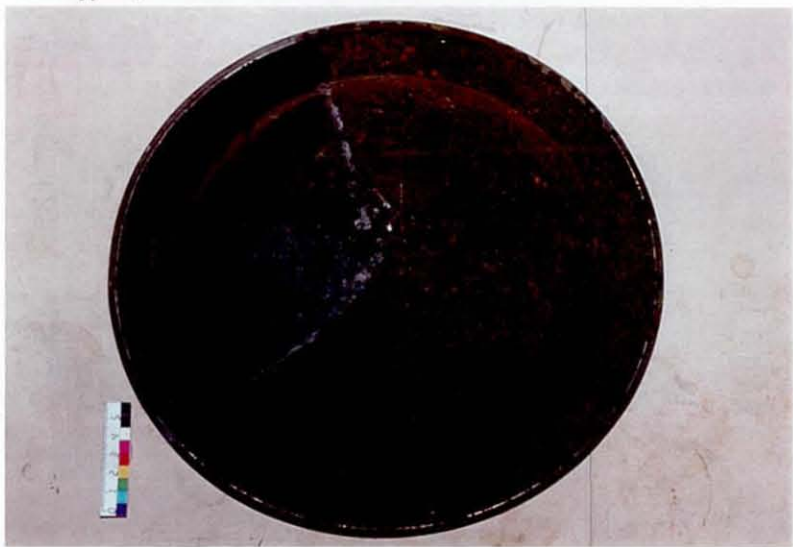


Photo 3.2.5b: *Case 5n*. The same helmet shown from above.



Photo 3.2.6a: The rusted nail from *Case 6n*. The shape of the original surface is completely obscured by corrosion products.



Photo 3.2.6b: Laser treatment of the nail at a fluence of $2\text{J}/\text{cm}^2$ caused blackening of the corrosion products.



Photo 3.2.7a: The bowl of the untreated spoon from *Case 7n*.



Photo 3.2.7b: The corrosion was removed from the spoon after just a couple of pulses at $2\text{J}/\text{cm}^2$. The source of the discoloration was not identified.

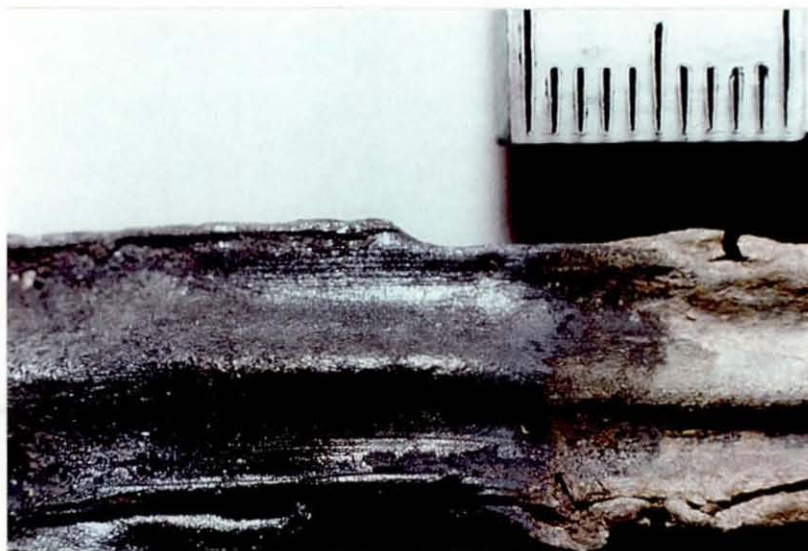


Photo 3.2.8a: *Case 8n*. Left-side shows laser treatment after 5-10 pulses at $3\text{-}4\text{J}/\text{cm}^2$.

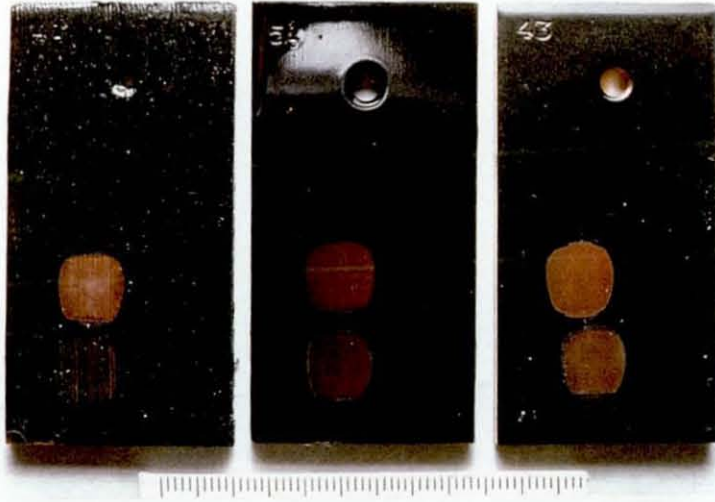


Photo 3.3.1: From left to right, the laser removal of oil-base, acrylic and cellulose paint. The bottom tests were due to 1 pulse at $2\text{J}/\text{cm}^2$, the top were 5 pulses at $2\text{J}/\text{cm}^2$.

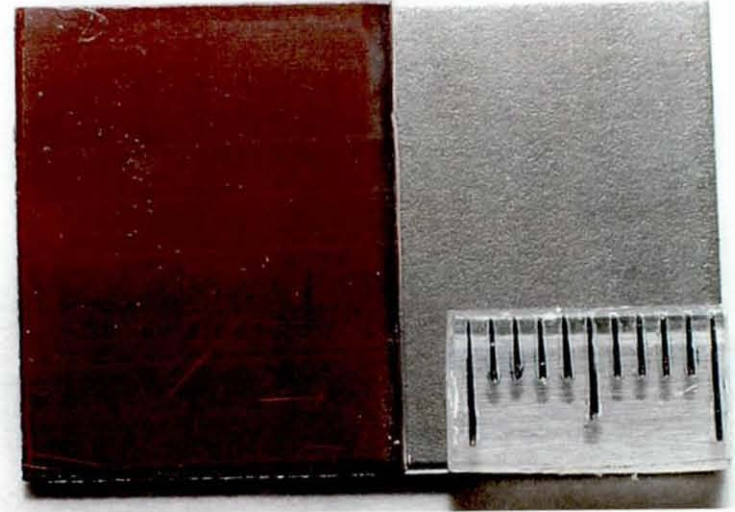


Photo 3.3.3g: Laser paint removal from a zinc-coated mild steel substrate.

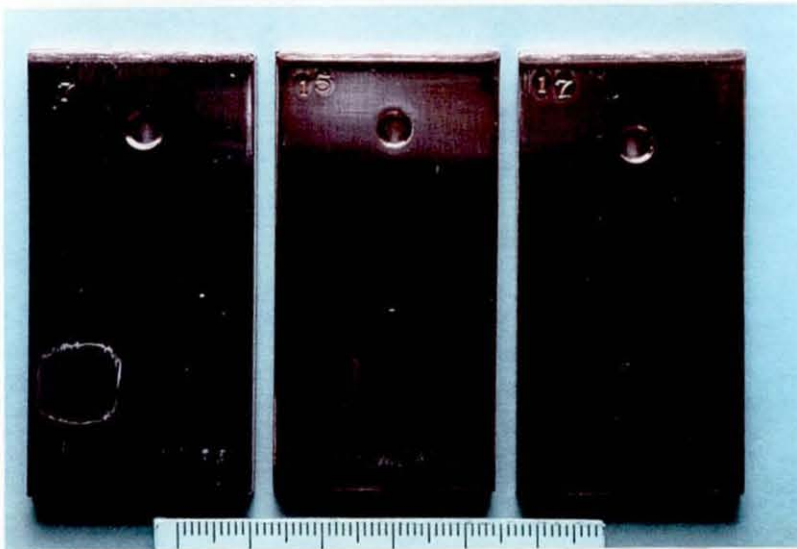


Photo 3.3.2: From left to right, the laser removal of Inralac, Covalac and Ercalene. The tests were carried out at between 1 and $2\text{J}/\text{cm}^2$ for 2 to 3 pulses.

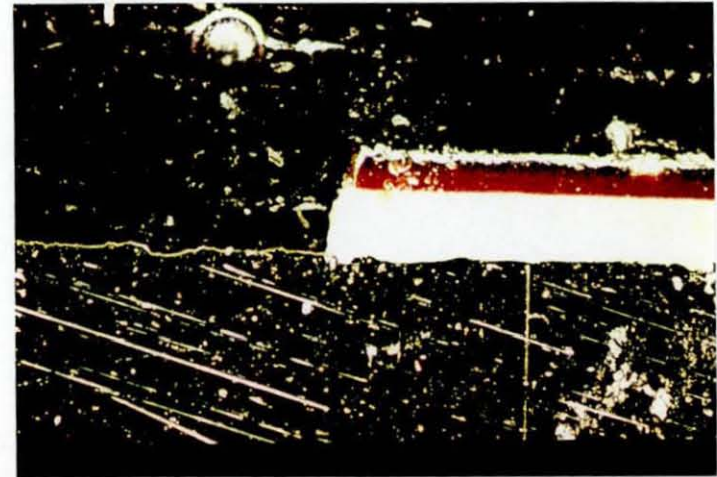


Photo 3.3.3h: Cross-section showing the painted substrate on the right and the laser treated substrate on the left.

CHAPTER 4

Plasma Laser Cleaning and Treatment

The use of the TEA-CO₂ laser at plasma-inducing fluences offered another facet to the laser's cleaning and treatment ability. Research into plasma laser cleaning was driven by the need for an effective, environmentally-friendly alternative to the use of volatile organic solvents for the pretreatment of metals prior to adhesive bonding: this will be explained in more detail in Section 4.2 where the effect of the plasma on specific metal targets is investigated.

4.1 Plasma Effects

TEA CO₂-laser treatment of materials using a fluence in excess of 4Jcm⁻² can partially ionise the air directly above the target sample. The resultant plasma will invariably interact with the surface of the material and therefore its presence is unwanted in the field of metal conservation. However, the effects of the plasma can be beneficial when extreme surface cleanliness is required and slight modification of the metal substrate is not so important or may even be desirable.

4.1.1 Plasma cleaning mechanisms

Plasma-fluence radiation incident on a metal surface will clean the surface in two steps:-

(i) As described in section 2.4.1, the laser pulse couples with the surface of the metal for approximately 10ns prior to the formation of the plasma. During this period, there is no shielding of the surface to the incident radiation and there is some ablation of surface contamination by direct interaction with the laser pulse.

(ii) At some point on the leading edge of the laser pulse, ionisation will be initiated and a plasma will rapidly form. Once formed, practically all the subsequent laser pulse is shielded from the target surface and is absorbed by the plasma itself. There is no further direct coupling of the laser radiation with the surface for the duration of the pulse. The plasma forms as a bright blue/white spark that re-radiates energy in the blue/near-UV portion of the spectrum. The plasma emits a significant amount of ionising radiation that can remove organic compounds from the surface of the metal. Metals are generally absorbing in this region of the spectrum and may experience significant heating through exposure to the plasma. Also, ionised atoms of air and blow-off material may be incident on, and interact with, the surface of the metal.

4.1.2 Initiating and sustaining plasma

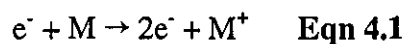
Creation of initial electrons

There are several mechanisms involved with initiating and sustaining plasma. In the first instance, electrons have to be produced from the ionisation of matter. Single photons of visible or infrared radiation have insufficient energy to ionise most gases. Hence, multi-photon ionisation (MPI) has been proposed as a possible mechanism for initial electron production. For example, photons from an Nd:YAG laser have a wavelength of 1060nm and energy of 1.2eV and thus the MPI of N₂ would require the absorption of 10 such electrons. Baravian *et al*^[1] have shown MPI to be an acceptable model for plasma initiation in this case. However, CO₂-laser photons have one tenth the energy of those of Nd:YAG lasers; more than 100 of the 0.12eV photons from CO₂-lasers would be required to ionise most gas atoms (ionisation potentials for most gases exceed 10eV). The high number of impacts required for MPI at CO₂-laser wavelengths are highly improbable and the mechanism does not sufficiently explain the low breakdown thresholds in pulsed CO₂-laser irradiated gases^[2].

At 10.6 μm , air-breakdown occurs quite sporadically and the definition of threshold intensity is taken to be that at which the probability of breakdown is greater than 50% for a given pulse^[3]. Under normal laboratory conditions, breakdown at 10.6 μm is initiated by aerosols in the atmosphere absorbing laser radiation and releasing electrons through thermionic emission^[4]. If the laser is incident on a partially absorbing surface then blow-off material from the surface itself can become absorptive aerosols to fuel the breakdown process.

Maintaining a plasma

Once electrons have been generated by thermionic emission, absorption of radiation by these electrons lead to further heating and thermionic emission; i.e. thermal runaway proceeds for the duration of the pulse. Furthermore, if the electrons gain sufficient energy they can ionise the gas or solid through the reaction



which leads to cascade breakdown and the electron concentration increasing exponentially with time^[5]. Electrons in the laser field gain energy through the inverse brehmsstrahlung (IB) process. Brehmsstrahlung combines the words 'brehmsen', meaning slow-down, and 'strahlung', meaning radiation. Electrons may emit radiation through deceleration and, conversely, absorb energy through acceleration. The IB process is proportional to the wavelength squared^[6], and is therefore far more significant at the relatively long wavelengths of CO₂-laser radiation than most other lasers.

In summary, therefore, we can expect plasma formation using a CO₂-laser beam in air and focused onto a target material to be initiated by thermionic emission of electrons from the absorption of radiation by aerosols in the atmosphere and blow-off material from the target. The plasma is expanded and maintained by thermal runaway in which electrons

gain energy through the IB process and ionise blow-off material, aerosol matter and transport medium gases, which leads to cascade breakdown.

Factors affecting plasma threshold

For a TEA CO₂-laser focused above a metal target, the following factors can influence the plasma threshold fluence.

(i) 'Air quality': breakdown thresholds can be increased many fold by removal of aerosol particles from air^[7], especially when the target is clean and highly reflective so as not to contribute blow-off material to the process. The size, abundance and optical-properties of the aerosols will also influence the breakdown threshold. The air quality can be expected to decrease during laser cleaning as blow-off material contributes to the level of aerosols in the immediate surroundings.

(ii) Target material: clean metals are generally highly reflective of CO₂-laser radiation, although some may suffer surface vaporisation at high fluences. Hence, metals susceptible to laser ablation may contribute matter to the breakdown process. The surfaces of metals will almost invariably possess some degree of surface contamination through exposure to adventitious material (e.g. hydrocarbons) from the air and this material may be vaporised and contribute to the breakdown process. Corroded and coated metals are liable to contribute a large amount of blow-off material during laser irradiation at significantly lower threshold levels than clean metals. Also, metals generally reflect such a large proportion of incident radiation that the region directly above the surface of the metal effectively doubles in flux density due to overlap of both incident and reflected beams.

(iii) Focusing lens: the laser beam focused by a lens with a long focal length will form a radiation field of a more acute angle than that of a lens with a short focal length. Hence, for a given fluence, the region directly above the target material will have a higher flux

density for the weaker lens and will therefore be more conducive to plasma formation. However, the minimum spot-size for coherent radiation in a given focal system with a circular aperture is the Airy disk, given by^[8]

$$R \sim 1.22f\lambda/D \quad \text{Eqn. 4.2}$$

where R is the spot radius, f the focal length of the lens, λ the wavelength of laser radiation and D the diameter of the aperture. Hence, for a given system, the more powerful lens can focus the beam to a smaller spot-size and thus provide a higher obtainable fluence. Taking these two considerations into account, the more powerful the lens, the higher the possible incident fluence and the earlier in the laser pulse breakdown could be initiated. However, once breakdown had been initiated, the less powerful lens system would provide a greater flux to sustain the plasma for the remainder of the pulse. From these two opposing factors it is not clear whether a long or short focal length is desirable for efficient plasma production and detailed experimental observations would be required to assess the effects focal length has on plasma formation.

4.1.3 Plasma observations

Laser-induced breakdown can be defined as the generation, by a laser pulse, of a highly ionised gas (plasma). When breakdown occurs in air, it usually takes the form of a bright blue/white spark and should not be confused with the hot plume of gas and blow-off material that forms during sub-plasma irradiation. *Photo 2.4.2b* (see Chapter 2) shows a time-exposure photograph of the breakdown above a copper-roofing target. The plasma has started to form at two different sites and is surrounded by the hot plume of heated blow-off material.

The distinction between the plasma and hot-plume can also be seen using Laser Induced Breakdown Spectroscopy (LIBS). *Fig 3.2.1c* (see Chapter 3) shows 3 spectra from using the laser at different fluences. At the lowest fluence, no peaks are detected and therefore

there is no evidence for ionised matter. At this fluence, the plume had an orange/yellow appearance. At a higher fluence, several peaks are detected although the appearance of the plume has not visibly altered. The peaks that are observed at this fluence are due to the ionised blow-off material and not air-breakdown which supports the theory that the electrons are initially produced by the thermionic emission of heated aerosols (in this case, from the blow-off material) and not directly from ionisation of the air. The highest fluence produces a spectra with many peaks from ionised blow-off material, and nitrogen and oxygen from the air and is accompanied by the characteristic blue/white flash.

4.1.4 Plasma cleaning

The surface interaction of the laser just below the plasma fluence appears to vary significantly from that of the laser just above the plasma fluence and it would appear that it was the plasma itself, as opposed to the slight increase in fluence, that was responsible for the differences.

In section 3.3.4 it was discussed how metal coupons with organic coatings on them still produced a large contact angle after prolonged irradiation with sub-plasma laser pulses. Further experiments on the same coupons revealed that the contact angle could be reduced to zero if the intensity of the radiation was increased above the plasma threshold. Even a sub-monolayer of organic contamination will produce an observable contact angle^[9], hence, cleaning at plasma fluences appears to remove all traces of organic compounds.

Laboratory exposure tests

To illustrate the effectiveness of plasma cleaning and the influence of organic contamination on contact angles, a simple laser cleaning and laboratory exposure test was performed. Coupons of degreased mild steel were subjected to laser pulses, each exceeding the plasma threshold. The contact angle was measured throughout the

treatment, as shown in *Fig 4.1.4a*. It is interesting to note that even after a thorough double-degreasing there is still sufficient adsorbed or strongly bonded carbon-based molecules on the surface to give a contact angle of almost 70°. The contact angle initially decreases rapidly with laser treatment and is reduced to 10° after just five pulses. However, at this point a plateau is reached and it requires another 10 pulses to reduce the contact angle to zero, at which point the surface can be considered atomically clean and completely free of organic contamination. AES was carried out to confirm that the surface could be considered atomically clean after 15 pulses.

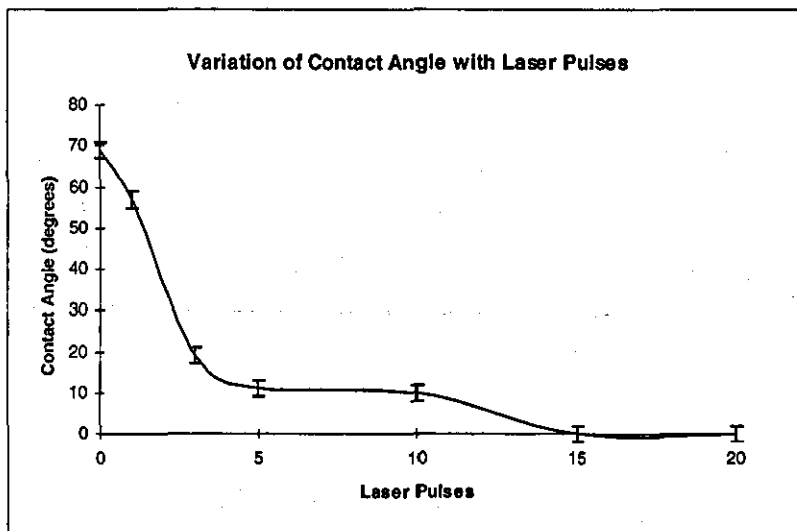


Fig. 4.1.4a: Decrease in contact angle with laser pulses exceeding the plasma threshold incident on a degreased mild steel target.

Laboratory exposure tests were performed with coupons of mild steel, laser-cleaned with 20 pulses above the plasma threshold such that a zero contact angle was measured at the surface. The coupons were then left exposed to the atmosphere of the laboratory and the contact angles measured over a 24hr period using triply distilled water, as shown in *Fig 4.1.4b*.

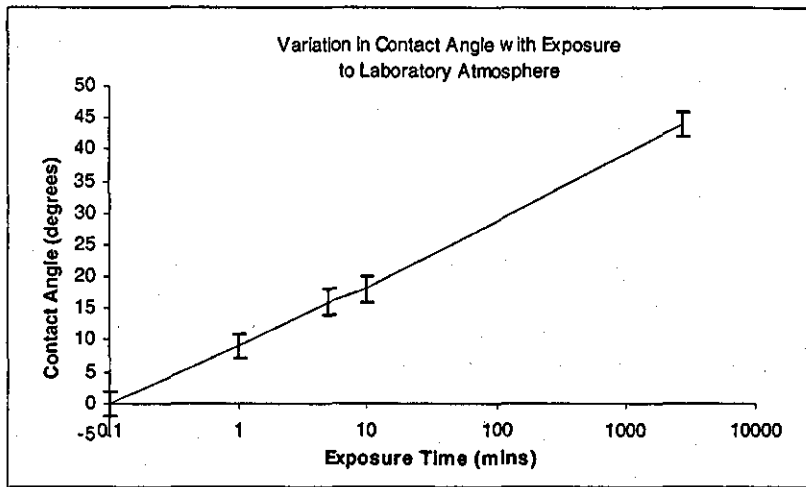


Fig 4.1.4b: Variation in contact angle with time during the laboratory exposure of laser cleaned mild steel coupon.

There is a clear logarithmic relationship between the contact angle and the exposure time with significant contamination levels even after just a minute of exposure.

Plasma spectroscopy

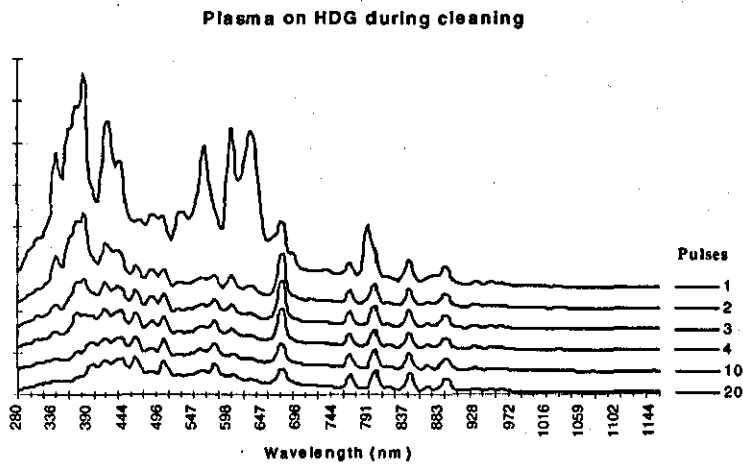


Fig 4.1.4c: LIBS spectra of plasma during laser treatment of degraded HDG at a fluence of 12Jcm^{-2} . After 10 pulses, only N and O peaks remain. Spectra have been shifted vertically for comparison.

The laser required several pulses above the plasma threshold fluence to achieve zero-contact angle. It was possible to use LIBS to observe the cleaning effect of the laser at plasma fluences. Degreased hot-dip galvanised (HDG) mild steel coupons were subjected to laser pulses above the plasma threshold. *Figs 4.1.4c and 4.1.4d* show the spectra obtained after a given number of pulses at 12Jcm^{-2} and 6Jcm^{-2} respectively.

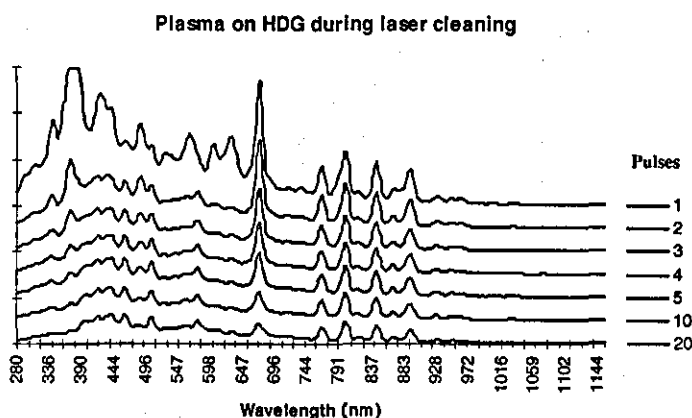


Fig. 4.1.4d: LIBS spectra of plasma during laser treatment of degreased HDG at a fluence of 6Jcm^{-2} . After 10 pulses, only N and O peaks remain. Spectra have been vertically shifted for comparison.

In both cases, the first laser pulse produces a plasma of greatest intensity and also the largest number of peaks. The second laser pulse has a similar appearance to the first, although some of the peaks have decreased significantly in size. The gradual elimination of these peaks continues with an increasing number of pulses until both examples exhibit consistent spectra after 10 and 20 pulses.

It appears that a clean metal surface remains after 10 and 20 pulses, and that the peaks that are still evident are due to ionisation of oxygen and nitrogen in the air. No evidence of zinc, the metal substrate, is observed in any of the spectra. When the initial spectra are compared with the final spectra, it is simple to identify the peaks which exist due to surface contamination and observe their decline throughout the treatment process.

The intensity of the plasma on the whole decreases throughout the cleaning process, this is especially apparent when the first pulse is compared to the second. The surface contamination provides blow-off material for thermionic emission of electrons and thus expedites the initiation of the plasma. Hence, there appears to be a direct correlation between the intensity of the plasma radiation and the cleanliness of the surface.

4.2 Cleaning and adhesion

Introduction

There are several advantages of using adhesives on metals compared with other, more conventional methods of joining, such as brazing, welding, riveting and welding. These include: the ability to join thin sheets efficiently; improvements in stress distribution in the joint; increases in design flexibility; and also, adhesives are often the most convenient and cost effective technique^[10].

The failure of joints incorporating metal adherends can often be attributed to inadequate surface preparation^[11] and suitable surface pretreatment is an 'extremely important factor^[12] in creating reliable, durable joints. During the manufacture of metals there is plenty of opportunity for contamination of the surface with various organic and inorganic substances^[13] such that the surface will typically resemble that shown in *Fig 4.2a*; even cleaned metal surfaces will pick up contamination from the atmosphere if left exposed, see section 4.1.4. The removal of surface contamination, loosely bound oxides etc., will usually ensure a joint with a high initial bond strength. However, to produce a highly durable joint will usually require the presence of an adherent, passive oxide layer on the surface of the adherend which is receptive to the adhesive and have good environmental resistance^[14].

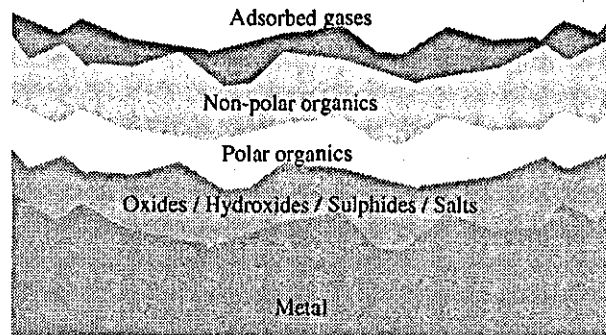


Fig. 4.2a: Adsorbed layers on a metal surface, typically to a depth of 10-300nm.

A wide range of surface treatments are available for metal adhesion which procure some or all of the aforementioned features to facilitate a strong and durable bond. These include mechanical treatments, e.g. abrasion or grit-blasting; chemical treatments, e.g. chromic-sulfuric acid etching or conversion coating; and electrochemical treatments, e.g. chromic or phosphoric acid anodising. It is widely accepted that the most effective surface treatments for aluminium are chromic and phosphoric acid anodising for a broad range of exposure conditions^[15-18]. Although there can be no doubt as to the effectiveness of these treatments, their application can be complicated, involving many stages and invariably produce excessive quantities of highly toxic effluent.

Recently, a new method of surface treatment has been developed that involves the use of high powered laser radiation. Lasers can alter the chemical properties of the surface, and hence influence the interaction of the adhesive with the adherend and also the adherend's resistance to environmental degradation. Lasers can also alter the surface morphology, effecting the degree of physical interlocking between adhesive and adherend. To date, most work has concentrated on the use of excimer lasers to clean the surface and increase its roughness and porosity, thereby enabling a higher degree of mechanical interlocking and hence adhesion^[19,20]. The following investigation into metal surface pretreatments using the TEA CO₂-laser combines the ablative effect of the laser incident on the surface of the metal together with the subsequent formation of a plasma above the surface.

4.2.1 Aluminium

Introduction

In order to investigate the potential for TEA CO₂-lasers to be used as a pretreatment process for metals in adhesive bonding, a comparative study was carried out comparing this with a number of established, effective pretreatment processes on aluminium. Aluminium was chosen because this metal is already widely used with adhesives, in particular, in the aerospace industry where it has lead to advantages that include 'weight saving, improved aerodynamics, and reduced cost of manufacture'^[21]. In this case, laser treatment was compared with three other treatment methods as detailed below. Bonded joints were created with each pretreatment method using a standard adhesive and tested to measure the initial joint strength and stressed durability performance.

Experimental

Aluminium 5251 alloy (nominal composition by weight, 0.1-0.5% Mn, 1.7-2.4% Mg, 0.15% Cu, 0.4% Si, 0.5% Fe, Al balance) was cut into coupons measuring 25mm x 60mm by 2mm thickness. The coupons were subjected to the following treatments:

(i) Degrease only: achieved by two separate 10min ultrasonic submersions in 'Super Purity' acetone. This process is repeated as part of the treatments (ii) and (iii) below.

(ii) Degrease plus laser treatment: laser treatment was performed at an energy density of approximately 20Jcm⁻². The laser was rastered over the surface such that each point received 5 pulses each. This was sufficient to reduce the contact angle to zero and hence produce a surface free from organic contamination. Joints were assembled within 30 seconds of laser treatment to minimise recontamination from the atmosphere.

(iii) Degrease plus grit-blast: grit-blasting was carried out using 80/120 grade alumina grit. The coupons were again degreased after grit-blasting.

(iv) Conversion coating: performed with Bonderite 705 (a chromate-phosphate based process) and a treatment time of 5 minutes.

Bonding was performed using a single lap-shear (SLS) configuration and Araldite 2007 (AV119), a 120°C curing, single-part adhesive, mixed with 1%, "Ballotini" 250µm glass spheres. The joints were assembled in a jig to give an overlap of 10mm and were held together with bulldog clips until the adhesive had fully cured.

Initial joint strengths were tested using a Lloyd 2000R tensometer fitted with a 10kN load cell. Stressed durability results were obtained using Maddison-type tubes^[22] with applied loads of 1 and 1.5kN and the mean time-to-failure recorded. These tubes contain two pre-calibrated springs that are attached to one end of a given joint, the other end being fixed, and thus a constant load is applied to the joint. All tests were performed on three replicate joints.

Surface compositions and depth profiles of degreased-only and laser treated samples were obtained using AES with sequential argon-ion bombardment. The instrument was a Varian spectrometer operating with a primary beam energy of 3keV, a current of 0.7µA into an analysis area approximately 100µm in diameter; the ion-gun operated with Ar⁺ ions of 3keV energy and current density of 75µAcm⁻². Surface morphology was recorded using SEM on a Cambridge Stereoscan 360 instrument using a primary beam energy of either 10 or 20keV.

Results and discussion

Table 4.1 shows the results of the AES surface survey scans of degreased only (DO) and laser-treated (LT) regions of the same coupon. Even after the rigorous degreasing process

the DO region still retains a high degree of organic contamination which may be strongly adsorbed or bonded to the surface. The laser-treatment process appears to have removed all traces of organic contamination (the detection limit for carbon in this matrix is approximately 1at%). This result was confirmed by the zero degree contact angle obtained from the LT region compared with the DO region which gave a contact angle in excess of 50°.

Sample	C(at%)	O(at%)	Al(at%)	Cl(at%)	Mg(at%)
Degreased only	29.6	48.7	8.5	0.9	12.4
Laser-treated	0.0	56.4	34.1	0.0	9.6

Table 4.1: AES surface scan of DO and LT aluminium.

The high levels of magnesium detected at the surface compared with the proportion of magnesium in the bulk constituents implies that surface enrichment with respect to magnesium is evident in the alloy; the Mg:Al ratio is significantly lower in the laser treated adherend than the degreased only adherend.

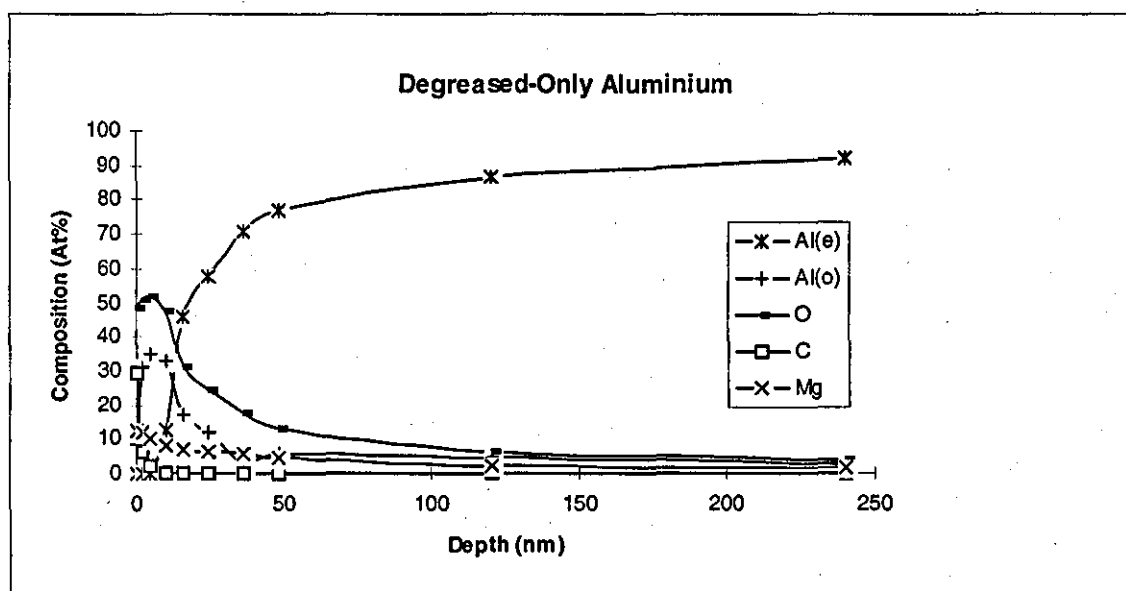


Fig. 4.2.1a: AES depth profile of DO aluminium.

A high Mg:Al ratio has been associated with poor joint durability for aluminium alloy adherends by a variety of authors^[23-25]. Fig. 4.2.1a and Fig 4.2.1b show the depth profiles of DO and LT areas respectively. The DO area shows that the organic layer exists at the very surface of the coupon in the top 10nm.

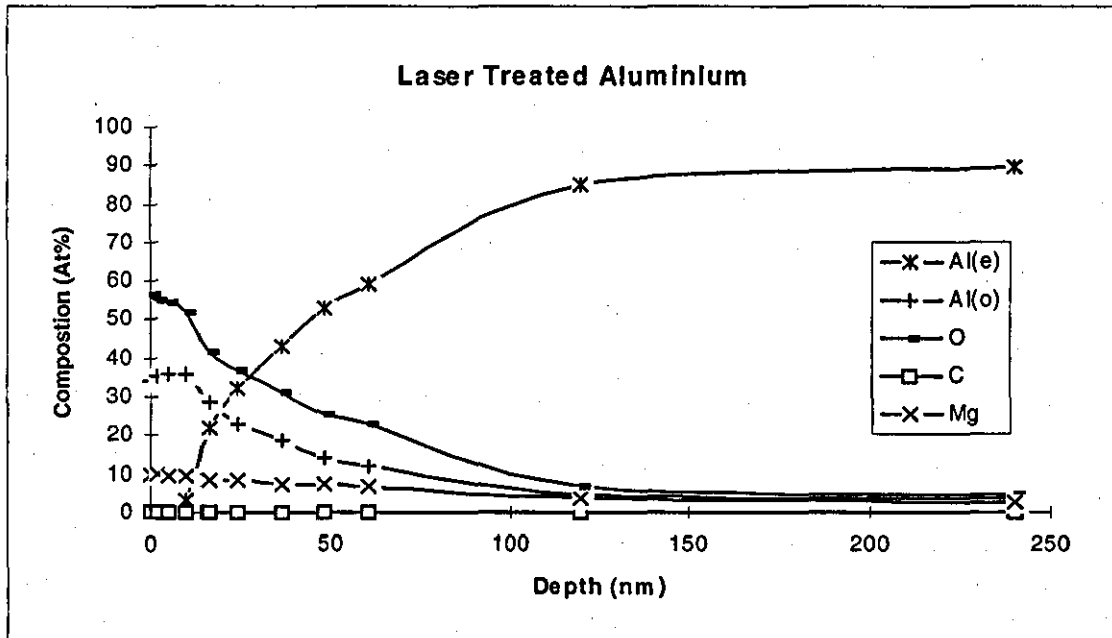


Fig. 4.2.1b: AES depth profile of LT aluminium after 5 pulses at 20Jcm^{-2} .

The organic layer on the DO Al extends for only a few nanometers below the surface, although no carbon at all is detected on the laser treated surface. Beneath this organic layer, there are significant differences in the composition of the surface oxide layer. The ratio of metal aluminium (Al(e)) to oxidised aluminium (Al(o)) increase was more gradual with depth in the LT region than the DO region, evidence for the significant increase in oxide thickness introduced by the laser treatment. Surface oxidation due to laser treatment could be due to the heating effect of the laser plasma in an oxidising medium or ionised oxygen from air-breakdown impacting on the surface. However, there is no evidence for the presence of nitrides on the surface from the impact of ionised nitrogen which would also be present in the plasma.

Photos 4.2.1c to f show SEM micrographs of the DO and LT surfaces at low and high magnifications. Both magnifications show little visible disparity between the surfaces and there is clear evidence of loosely bound material, particulates and rolling lines on both examples.

Bond Testing

Tables 4.2 and 4.3 show initial joint strengths and stressed durability results for DO and LT, SLS aluminium joints.

Treatment	Initial joint strength (N) [1 Standard Deviation]
Degrease only	1895 [184]
Laser treated	4876 [845]
Grit-blast	4687 [160]
Conversion coating	4057 [313]

Table 4.2: Comparative study of initial aluminium joint strengths after various pretreatments. Each value is the mean derived from three replicate joints.

Table 4.2 shows how the various surface treatments performed under initial joint strength tests. All treatments give an increase in initial joint strength improvement in excess of 100% with respect to the DO treatment, with the laser treated coupons performing most effectively with a 150% improvement.

Table 4.3 shows how the various surface treatments affected the stressed durability of the aluminium joints. For an applied load of 1kN, all the treated coupons show similar improvements with mean time-to-failures (MTF) increasing by a factor of approximately 25 with respect to the DO treatments. Again, the LT coupons perform well, falling just short of the MTF's observed with conversion coating. There is greater disparity, however, for an applied load of 1.5kN. Although all treatments show a large improvement

compared with the DO coupons, the LT coupons perform worst out of the two alternative treatments.

Treatment	Mean time to failure (hrs) (1kN applied load) [1 Std. Dev.]	Mean time to failure (hrs) (1.5kN applied load) [1 Std. Dev.]
Degrease only	19 [4]	<1 [<1]
Laser treated	532 [35]	158 [10]
Grit-blast	465 [22]	223 [54]
Conversion coating	547 [25]	367 [24]

Table 4.3: Comparative study of stressed durability performance of aluminium joints after various pretreatments. Each value is the mean derived from three replicate joints.

It would appear that the performance of the LT joints depends greatly on the conditions under which they are stressed. Apart from the high-load durability performance, the LT joints were comparable with the best of the alternative surface treatments studied.

The improvement of the adhesive properties due to LT in comparison to DO appears to be principally due to the removal of the organic layer and extreme cleanliness of the treated surface. The presence of a thin organic layer could prevent the formation of interatomic or intermolecular bonds which form over a distance of a few angstroms or nanometers. No significant change in the surface topography of the aluminium is evident from the SEM micrographs of the LT area and AES depth profiles show only a slight thickening of the oxide layer, hence it is unlikely that adhesive properties have significantly improved through a change in surface features and structure.

4.2.2 Steel

Introduction

The potential of the laser for use in metal adhesion pretreatment processes prompted further research into different adhesive systems. It was decided to conduct a comparative study for steel coupons to see how the laser treatment process performed against some of the most effective modern methods. In this case, the degreasing stage was omitted prior to laser treatment as it proved to be unnecessary; in the previous study it was concluded that the laser effectively degreased the surface during treatment.

Experimental

CR1 mild steel (a cold-rolled, low-carbon steel) was cut into coupons measuring 25mm x 60mm by 2mm thickness. The coupons were subjected to the following treatments:

- (i) Degrease only: achieved by two separate 10min ultrasonic submersions in 'Super Purity' acetone. This process is repeated as part of the treatments (iii) and (iv) below.
- (ii) Laser treatment: laser treatment was performed at an energy density of approximately 20Jcm^{-2} and, as the laser was rastered over the surface, each point received 40 pulses. This was sufficient to reduce the contact angle to zero and hence produce a surface free from organic contamination. Joints were assembled within 30 seconds of laser treatment to minimise recontamination from the atmosphere. No degreasing was attempted prior to laser treatment.
- (iii) Degrease plus grit-blast: grit-blasting was carried out using 80/120 grade alumina grit. The coupons were again degreased after grit-blasting.

(iv) Grit-blast plus silane application: grit-blasting as described in (iii) followed by application of 1% aqueous solution of Union Carbide A187 silane* . Silane treatment has been shown to increase bond durability through increasing interface stability^[26].

Bonding tests and surface analysis were carried out using identical methods and equipment as described in Section 4.2.1. In addition, two different surface exposure times (SETs) were used prior to bonding the laser treated coupons to investigate the effect of organic contamination on the bond quality. As a method of assessing bond durability, the strength of three replicate joints for each pretreatment were also measured after 12 weeks immersion in deionised water at 60°C.

Results and discussion

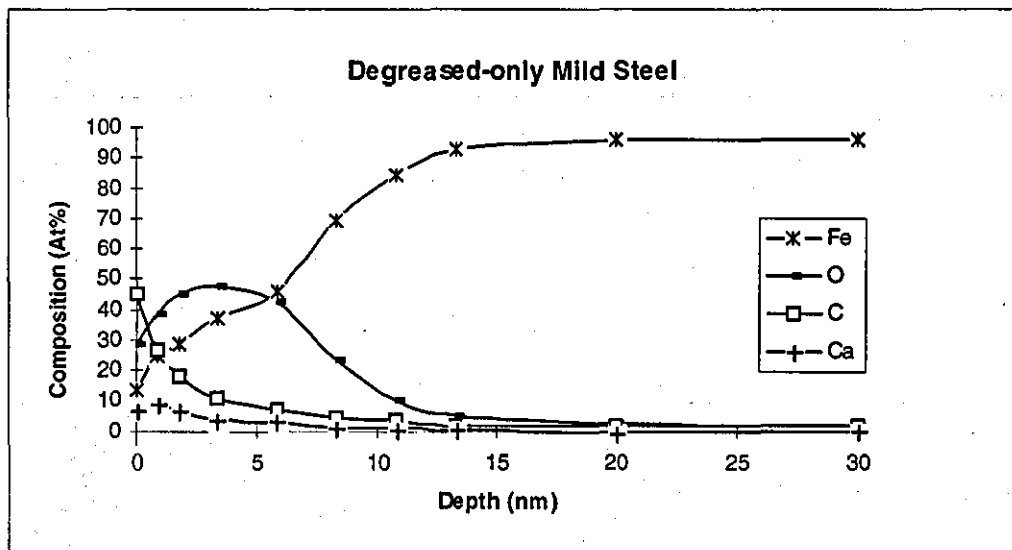


Fig. 4.2.2a: AES depth profile of a DO mild steel coupon.

Fig 4.2.2a shows the AES depth profile of the DO mild steel coupon. As with the aluminium alloy coupons, the degreasing process has left a thin, organic layer, extending to a depth of 5-10nm, on the surface of the metal. There is also evidence of oxygen and

* A187 Silane is the commercial name for γ -glycidoxypropylmethoxysilane.

calcium on the surface although beyond approximately 20nm there is a homogenous iron/carbon alloy.

The LT areas of the steel coupons showed considerable variegation in the surface appearance. Considerable areas of oxidation were apparent that varied in colour from shiny grey to dark blue. *Fig 4.2.2b* shows an AES depth profile of a grey area of laser-treated mild steel. The very small levels of carbon can be accounted for within the composition of the alloy and no organic surface contamination is evident. The significant levels of calcium have remained on the surface and the oxide layer has been extended from approximately 8nm (DO) to about 30nm.

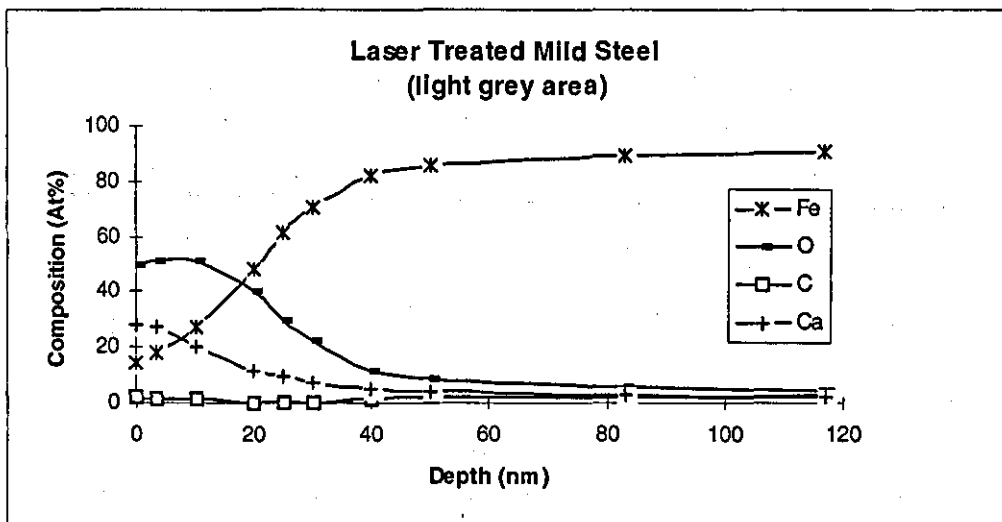


Fig 4.2.2b: AES depth profile of the 'grey-area' of mild steel surface after 30 laser pulses at a fluence of 20Jcm⁻².

Fig 4.2.2c shows the AES depth profile of the LT dark blue area. Again, there is no evidence of organic surface contamination. The oxide layer has been extended further and is between 80nm and 100nm thickness. The colours of the oxide films correspond well with those cited in Appendix C, the light grey area being too thin to form interference fringes.

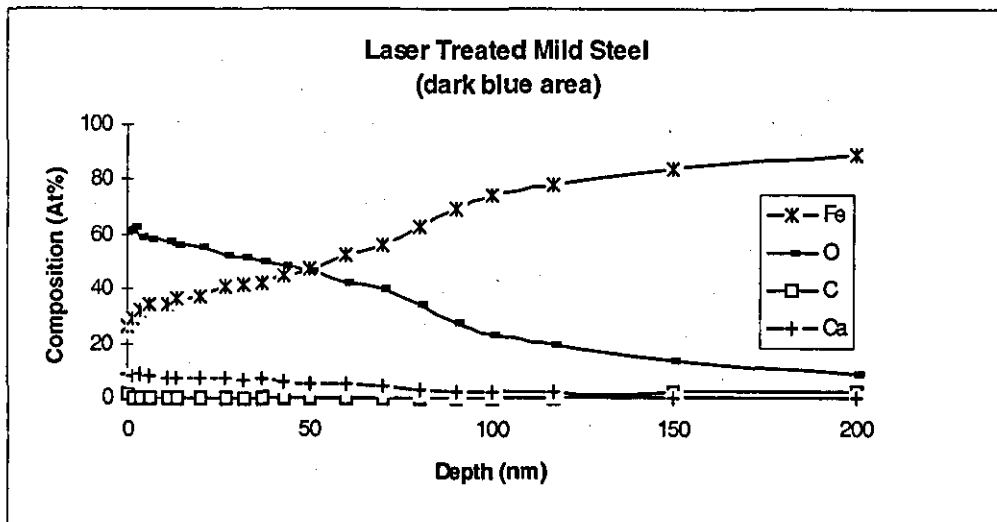


Fig 4.2.2c: AES depth profile of the 'blue-area' of mild steel surface after 30 laser pulses at a fluence of 20Jcm⁻².

The oxidising effect of the laser is far more pronounced on the mild steel than the aluminium. SEM micrographs show that there is also considerable change in surface topography due to the effects of the laser on the mild steel samples.

Photos 4.2.2d and 4.2.2e show the DO mild steel surfaces under low (x270) and high (x6800) magnification respectively, both show a patchy surface with prominent cracks visible. SEM micrographs of the laser-treated grey area on the same scale, as shown in Photos 4.2.2f and 4.2.2g, show a significant change in surface topography with respect to the DO surface; there is evidence for surface melting and globules of molten metal or oxide are apparent. There also appears to be a rippling effect caused in the LT grey area that is best seen in Photo 4.2.2f. Such rippling effects can often be observed on laser treated surface and are termed non-resonant periodic structures^[27-29] and although the exact mechanisms that contribute to their formation are not fully understood, they do require surface melting followed by a rapid cooling process to 'freeze' the structures. The dark blue, laser treated area is different still with a surface texture that appears much smoother than the other two areas, as shown in Photos 4.2.2h and 4.2.2i. The extent of

surface melting of the dark blue area has given it a "glassy" appearance absent from cracks and friable material.

Bond Testing

Table 4.4 shows the initial joint strengths and unstressed durability data for the CR1 mild steel SLS joints bonded with the aforementioned single-part epoxide after different treatment processes.

Treatment	Initial joint strength (N) [1 Std. Dev]	Joint strength (N) after 12 weeks exposure [1 Std. Dev]
Degrease-only	3552 [700]	3073 [732]
Laser-treated (30s SET)	5203 [138]	3920 [309]
Laser-treated (2760m SET)	4938 [307]	3979 [622]
Grit-blast	5240 [350]	5410 [120]
Grit-blast plus silane	5160 [260]	5610 [270]

Table 4.4: Comparative study of initial joint strengths of mild steel joints after various pretreatments and exposure conditions. Each value is the mean derived from three replicate joints.

If the initial joint strengths are considered, the laser treated (30s SET) and the two grit-blast treated coupons all give the same level of improvement on the DO coupons within a difference of 2%. However, after a period of 12 weeks exposure, both laser treated joints have suffered significant weakening whilst the alternative grit-blast treatments have not lost any of their strength. The percentage strength retention for the laser treated joints are the worst of all the treatments, including DO, implying a low-resistance of the LT joints to degrading mechanisms in laboratory exposure tests. This gives a strong indication that, on mild steel, although the laser treatment ensures a good initial joint strength through removal of surface contamination, the bond durability is compromised through the growth

of an oxide layer that is not passive and hence fails over the long-term on exposure to aggressive environments.

There was no significant difference in joint strength between the SETs of 30s and 2760 mins for both initial and durability tests. A SET of 2760 mins allowed a significant build up of organic contamination on the surface of the coupons which resulted in a radical decrease in the wettability of the surface, see *Fig 4.1.4b*. This organic layer did not appear to affect the joint quality in this case, possibly because the high-cure temperature could have caused the contaminant to be adsorbed into the adhesive.

4.2.3 Hot-dip galvanised (HDG) mild steel

Introduction

The use of adhesive bonding for HDG mild steel is of particular interest in the automotive industry where the use of adhesives have been found to increase structural stiffness and mechanical durability whilst reducing unwanted riding vibrations^[30]. Thus, it was considered worthwhile to continue the laser treatment investigation on HDG mild steel and, again, compare it with other popular adhesion pretreatments. It would also offer the opportunity to observe how the laser treatment process interacts with a thin metal coating.

Experimental

The HDG mild steel sheet was cut into coupons measuring 55mm x 20mm by 1.2mm thickness using a guillotine. Each coupon was subjected to one of the following surface treatments prior to adhesive bonding. All the conversion coating treatments were performed by Chemetall UK, Aylesbury.

(i) Degrease-only: using 'Super Purity' acetone in an ultra-sonic bath for two separate 10 minute periods.

- (ii) TEA CO₂-laser treatment: at a power density of approximately 20Jcm⁻². The laser was rastered over the surface of the coupon. Three treatment levels were used such that each point received 5, 10 or 30 laser pulses.
- (iii) Phosphate-based conversion coating: Gardobond 250.
- (iv) Chromate-based conversion coating: Gardobond 4504.
- (v) Phosphate and Chromate based duplex conversion coating: Gardobond 250 followed by Gardobond 4504.

Bonding

The adhesive used was XB5315, a single part, 180°C curing epoxide supplied by Ciba Polymers. The joints were bonded in a single lap-shear configuration with 10mm overlaps and were held together using bulldog clips throughout the 30min duration of the cure stage.

A Hounsfield H50KM tensometer was used to determine initial joint strengths and Maddison-type tubes at loads of either 0.2kN or 0.5kN were used to determine stressed durability ranking. All tests were performed with three replicate joints for each set of conditions.

Surface analysis equipment and method was identical to that described in 4.2.1.

Results and Discussion

Fig 4.2.3a shows the AES depth profile of the DO, HDG mild steel surface. There are a significant amount of oxides evident near the surface of the coupon. The oxide levels decrease with depth such that they fall beneath 10% after just 60nm. The carbon, in common with the DO metals in Sections 4.2.1 and 4.2.2, is only evident in the top 20nm.

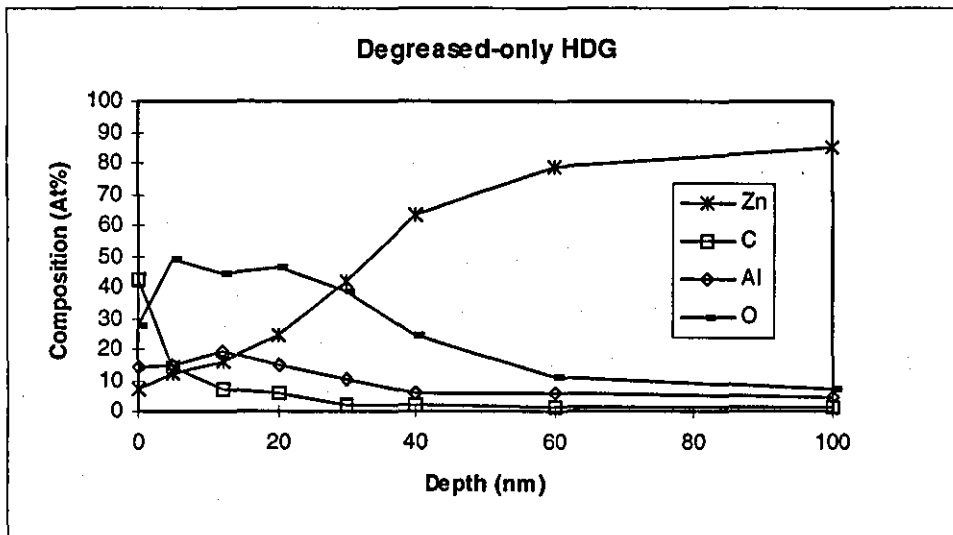


Fig 4.2.3a: AES depth profile of degraded only HDG surface.

Fig 4.2.3b shows the AES depth profile of the HDG mild steel coupon after 5 laser pulses.

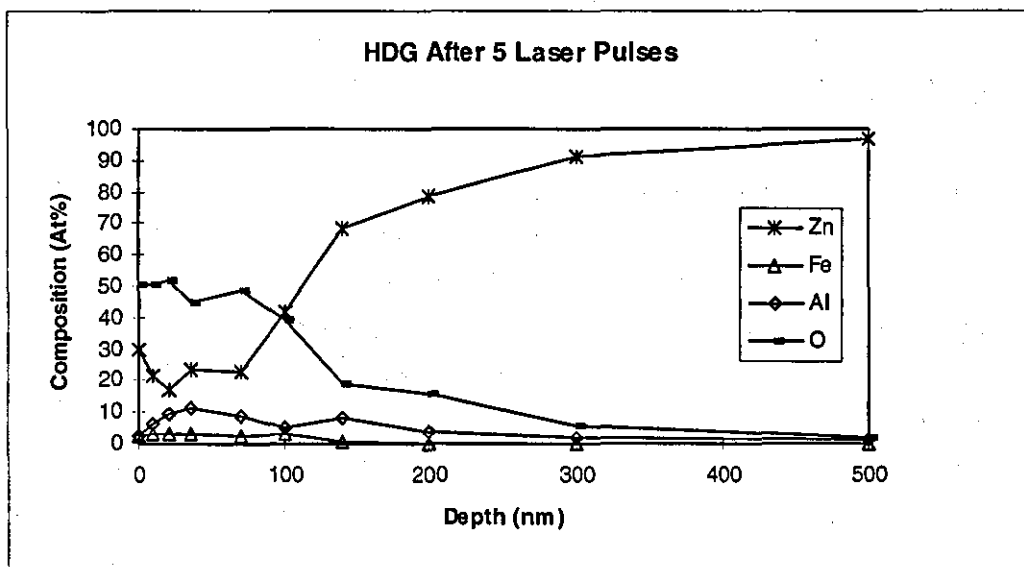


Fig 4.2.3b: AES depth profile of laser treated HDG after 5 pulses at 20Jcm⁻².

There is a general increase in the depth of the oxide on the laser treated coupons compared with the DO coupon. After 5 laser pulses, oxide levels exceed 10% for almost 300nm compared with just 60nm for the DO coupon. There is no evidence of carbon remaining after 5 laser pulses and all organic compounds have been removed. The most surprising result is the presence of iron at the surface of the coupon. There appears to have been migration of the iron from underneath the zinc coating to its surface. However, there is no evidence of iron in the bulk of the zinc coating.

Fig 4.2.3c shows the AES depth profile of HDG mild steel surface after 10 laser pulses. The oxide layer extends to about the same depth as after 5 laser pulses. As could be expected, there is no evidence of carbon at the surface. There is a significant increase in iron at the surface compared with the 5 pulse coupon.

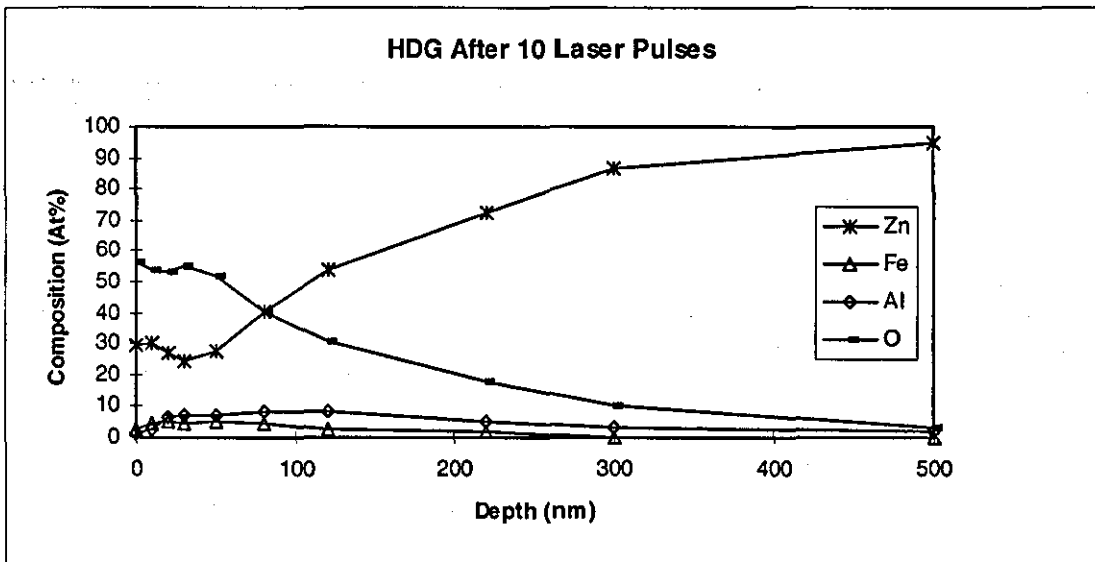


Fig 4.2.3c: AES depth profile of laser treated HDG surface after 10 pulses at 20Jcm^{-2} .

Photo 4.2.3d shows an SEM micrograph of the 5 pulse, laser treated surface at a magnification of about x1000. The surface has considerable micro-roughness with a lot of loosely bound oxide globules and flakes. After 10 laser pulses, Photo 4.2.3e shows the surface at the same scale. There is still some evidence for loosely bound oxide material,

but there also appears to be an adherent oxide layer forming over the surface. *Photo 4.2.3f* shows the surface at the same scale after 30 pulses. All the loosely bound material has been removed and the oxide layer has formed a uniform coating.

Bond testing

Initial joint strength of the laser treated coupons were slightly worse than DO and Gardobond 4504 treated coupons, although these three pretreatment methods all performed within 10% of each other. Table 4.5 shows the narrow range of initial joint strengths as a result of the different pretreatment processes. Increasing the number of laser pulses from 5 to 30 had little effect on the initial joint strength.

Treatment	Joint strength (kN) [1 standard deviation]
Degrease only	4.4 [0.8]
Laser treated (5 pulses)	3.9 [0.31]
Laser treated (10 pulses)	4.0 [0.56]
Laser treated (30 pulses)	4.1 [0.22]
Gardobond 250	4.5 [0.22]
Gardobond 4504	4.5 [0.03]
Gardobond 250 + 4504	3.6 [0.11]

Table 4.5: Comparative study of initial joint strengths of SLS, HDG joints after various pretreatments. Each value and standard deviation is determined from three replicate joints.

Table 4.6 shows the stressed durability performance of the various pretreatments under applied loads of 0.2 and 0.5kN. Under an applied load of 0.2kN, the 10 pulse laser treated coupons performed within 10% of the Gardobond 4504, the best of the alternative pretreatments, and out-performed the DO joints. Laser treatment did not perform as well at the higher load, falling just short of the DO joints and far short of the

Gardobond 4504 treatment that out-performed all other treatments by a factor of 2 or greater.

Treatment	Mean time-to-failure (hrs) with 0.2kN applied load [1 Std. Dev.]	Mean time-to-failure (hrs) with 0.5kN applied load [1 Std. Dev.]
Degrease only	163 [32]	85 [12]
Laser treated (5 pulses)	177 [38]	37 [11]
Laser treated (10 pulses)	217 [30]	79 [30]
Laser treated (30 pulses)	162 [30]	58 [18]
Gardobond 250	90 [16]	27 [7]
Gardobond 4504	235 [36]	172 [6]
Gardobond 250 + 4504	198 [53]	27 [7]

Table 4.6: Comparative study of stressed durability performance of SLS, HDG joints in DI water at 60°C after various pretreatments. Each value is the mean derived from three replicate joints.

Surprisingly, the 10 pulse laser treatment out-performed both the 5 and 30 pulse laser treated joints in both stressed durability tests. Stressed durability has been shown to be dependent on the quality of the inorganic coating present on the adherend surface as opposed to the surface cleanliness. There is a marked difference between the uniform oxide coating formed after 30 pulses, *Photo 4.2.3f*, and the patchy oxide formed after 10 pulses, *Photo 4.2.3e*. It would appear that the increase in surface roughness, and therefore surface area, of the 10 pulse treated surface accounts for the improvement in bond durability. It should be noted, therefore, that increasing the number of pulses during the laser pretreatment of metal adherends may not necessarily improve the bond quality.

4.2.4 Summary of Results

Table 4.7 compares the laser treatment process with the best of the commercial processes and the degrease only treatment. For all the target materials, the laser treatment

consistently produces the best, or close to the best results for initial joint strength. This can be expected as the initial joint strength is determined by the removal of surface contamination and general cleanliness of the adherends at which the laser has been demonstrated to be very effective. The laser treatment gives more variable data for the durability results where alternative treatments show a significant improvement under certain conditions. For small applied loads, the laser treatment still performs almost as well as the best commercial treatments. However, when the larger loads are used the best commercial treatments perform significantly better.

Treatment	Initial joint strength (N)			Mean time to failure with small applied load (hrs)			Mean time to failure with large applied load (hrs)		
	Al	Steel	HDG	Al	Steel	HDG	Al	Steel	HDG
Degrease only	1895	3552	4400	19	-	163	<1	-	85
Laser treatment	4876	5203	4100	532	-	217	158	-	79
Best Commercial	4687	5240	4500	547	-	235	367	-	172

Table 4.7: Summary of results from comparative studies of pretreatment processes for metal adhesion.

Joint durability is not so dependent on the surface cleanliness of the adherends as on the presence of a passive, adherent and receptive oxide/hydroxide layer on the adherend. As indicated on the mild steel, if the laser forms an oxide layer that is not stable then the joints will perform poorly under long-term exposure to aggressive environments. Results from the HDG joints showed that increasing the number of laser pulses did not necessarily improve bond durability. For this initial investigation it was assumed that the optimum laser treatment was the minimum number of pulses to produce a zero contact angle (i.e. complete removal of organic compounds) at the surface. Further investigation is required to determine the effect of extended laser treatment on bond durability and there appears to be potential for significant improvement and optimisation of the treatment.

References

- [1] Baravian, G., Godart, J., and Sultan G., 'Multiphoton ionisation of molecular nitrogen by a Neodymium-glass laser', *Phys. Rev.*, A25, (1982), 1483-95.
- [2] Weyl, G. M., 'Physics of Laser-Induced Breakdown: An Update', from *Laser Induced Plasmas and Applications*, Eds L. J. Radziemski and D. A. Cremers, Marcel Dekker Inc, New York, (1989), 2.
- [3] Hill, G. A., James, D. J., and Ramsden, S. A., 'Breakdown thresholds in rare and molecular gases using pulsed 10.6 micron radiation', *J. Phys. D. Appl. Phys.*, 5, (1971), L97-99.
- [4] Lencioni, D. E., 'The effect of dust on 10.6 micron laser induced air breakdown', *Phys. Rev. Lett.*, 23, (1973), 12-14.
- [5] Weyl, G. M., 'Physics of Laser-Induced Breakdown: An Update', from *Laser Induced Plasmas and Applications*, Eds L. J. Radziemski and D. A. Cremers, Marcel Dekker Inc, New York, (1989), 2.
- [6] Russo, R.E., 'Laser ablation', *Applied Spectroscopy*, Vol 49, No 9, (1995) 14A-28A.
- [7] Yablouovitch, E., 'Self phase modulation of light in a laser breakdown plasma', *Phys. Rev. Lett.*, 32, (1974), 1101-4.
- [8] Hecht, E., from 'Optics', 2nd Ed., Addison-Wesley Publishing Company, Reading, (1987), 419.
- [9] Adam, N. K., 'The chemical structure of solid surfaces as deduced from contact angles', from *Contact Angles and Wettability and Adhesion*, American Chemical Society, Washington, 56.
- [10] Kinloch, A. J., from *Durability of Structural Adhesives*, Applied Science Publications, London, (1983), 2.
- [11] Arnold, D. B., and Carter, C. S., *Proceedings of the 27th National SAMPE Symposium*, (1982), 769.
- [12] Kinloch, A. J., from *Durability of Structural Adhesives*, Applied Science Publications, London, (1983), 20.
- [13] Minford, J. D., from *Durability of Structural Adhesives*, Ed. J. A. Kinloch, Applied Science Publications, London, (1983), 149.
- [14] Kinloch, A. J., from *Durability of Structural Adhesives*, Applied Science Publications, London, (1983), 19.
- [15] Thrall, E.W. and Shannon, R.W., (Eds) 'Adhesive Bonding of Aluminium Alloys', Marcel Dekker Inc., New York, (1985).
- [16] Venables, J. D., 'Adhesion and durability of polymer bonds', *J. Mater. Sci.*, 19, (1984), 2431-53.
- [17] Parker, B. M., 'Adhesive bonding of fibre-reinforced composites', *Int. J. Adhes. Adhes.*, 13(1), (1993), 47.
- [18] Hennemann, O. D., and Brockmann, W., 'Surface morphology and its influence on adhesion', *J. Adhes.*, 12, (1981), 297.
- [19] Gendler, L., Rosen, A., Bamberger, M., Rotel, M., Zahavi, J., Buchman, A., Doduik, H., 'Improvement of the adhesive bonding strength in sealed anodised aluminium through excimer laser prebond treatment', *Journal of Materials Science*, 29, (1994), 1521-6.
- [20] Sancaktar, E., Babu, S. V., Zhang, E., D' Couto, G. C., 'The effects of laser radiation at 248nm on the surface characteristics and joint properties of aluminium adherends', *J. Adhesion*, 50, (1995), 103-33.
- [21] Reynolds, B. L., *Proc. Army Mater. Conf.* 4, (1976), 605.
- [22] Brewis, D. M., Critchlow, G.W., 'The influence of surface-treatment on the durability of aluminium epoxide lap joints', *Trans. IMF*, 74(6), (1996), 198-201.
- [23] Bishop, H., Smart, N. R., and Kinloch, A. J., 'Surface-analysis and bonding of aluminium-magnesium alloys', *J. Adhesion*, 14, (1982), 105-18.
- [24] Sun, T. S., Chen, J. M., Venable, J. D., and Hopping, R., 'Effects of chemical and thermal treatments on the composition of 2024 aluminium adherend surfaces', *Appl. Surf. Sci.*, 1, (1978), 202-14.
- [25] Kinloch A. J., in *Adhesion-6*, ed. K. W. Allen, Applied Science Publishers, London, (1982), 95.
- [26] Gettings, M., Baker, F. S. and Kinloch, A. J., 'The use of Auger and X-ray photoelectron spectroscopy to study the locus of failure of structural adhesive joints', *J. Appl. Polym. Sci.*, 21 (1977), 2375.
- [27] Prokhorov, A.M., Konov, V. I., Ursu, I., Mihailescu, I. N., 'Laser Heating of Metals', Adam Hilger, New York, (1990), 115-7.
- [28] Emmony, D. C., Howson, R. P., Willis, L. J., 'Laser mirror damage in germanium at 10.6 μ m', *Appl. Phys. Lett.* 23, (1973), 598-600.

[29] Emmony, D. C., Phillips, N. J., Toyer, J. H., Willis, L. J., 'The topography of laser irradiated germanium', J. Phys. D: Appl. Phys, 8, (1975), 1472-9.

[30] Coduti, P. L., Proc. 20th Anniversary Meeting of the Adhesion Soc., Hilton Head S.C., U.S.A., (23-26 Feb. 1997), 347.

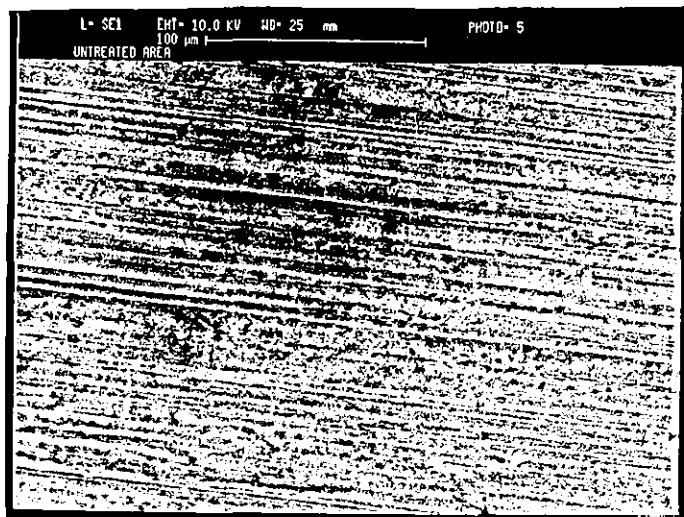


Photo 4.2.1c: SEM micrograph of degreased aluminium (magnification approx. x400).

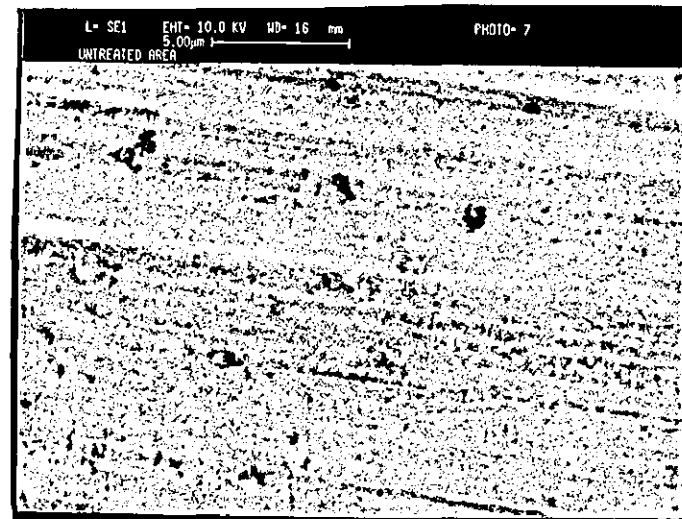


Photo 4.2.1e: SEM micrograph of degreased aluminium (magnification approx. x8000).

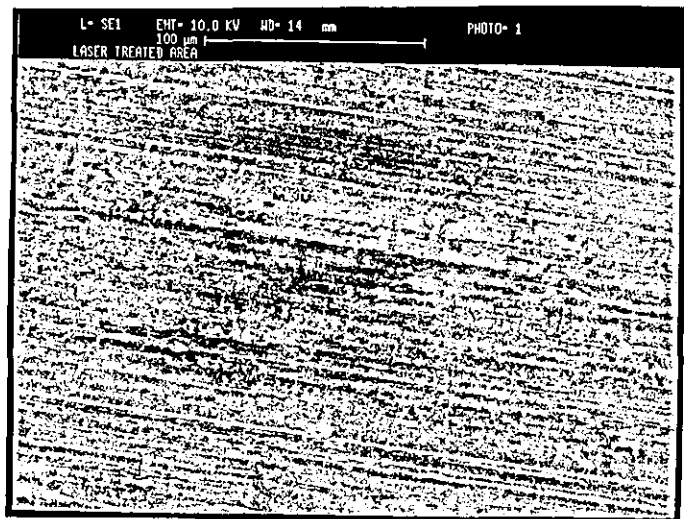


Photo 4.2.1d: SEM micrograph of laser-treated aluminium (magnification approx. x400).

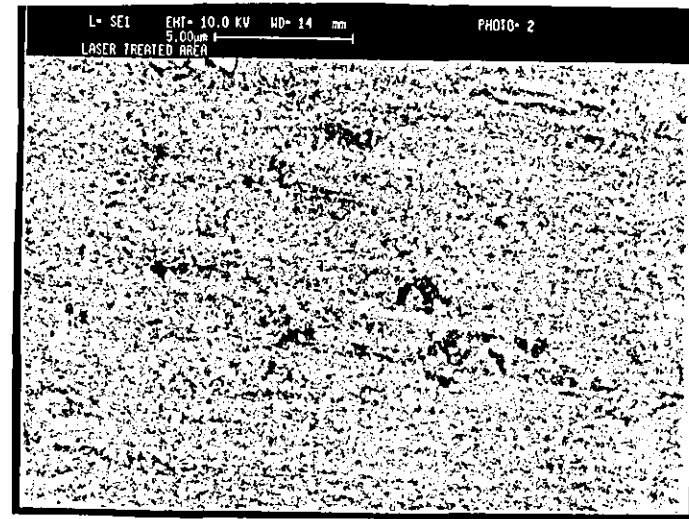


Photo 4.2.1f: SEM micrograph of laser-treated aluminium (magnification approx. x8000).

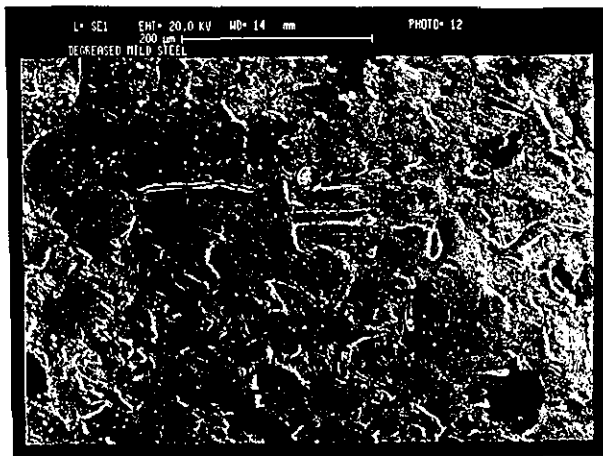


Photo 4.2.2d: SEM micrograph of degreased steel (magnification approx. x175).

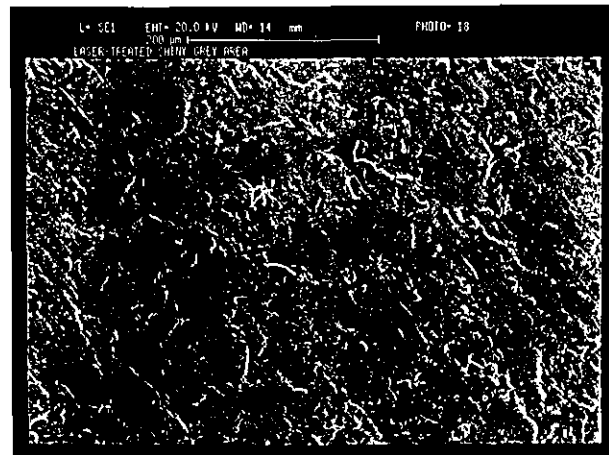


Photo 4.2.2f: SEM micrograph of grey area of laser treated steel (magnification approx. x175).

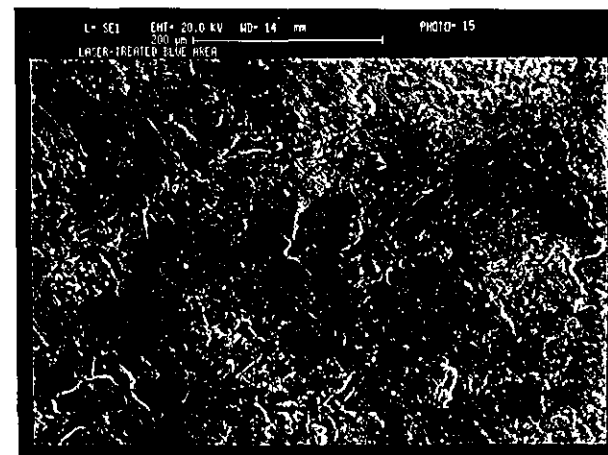


Photo 4.2.2h: SEM micrograph of blue area of laser treated steel (magnification approx. x175).

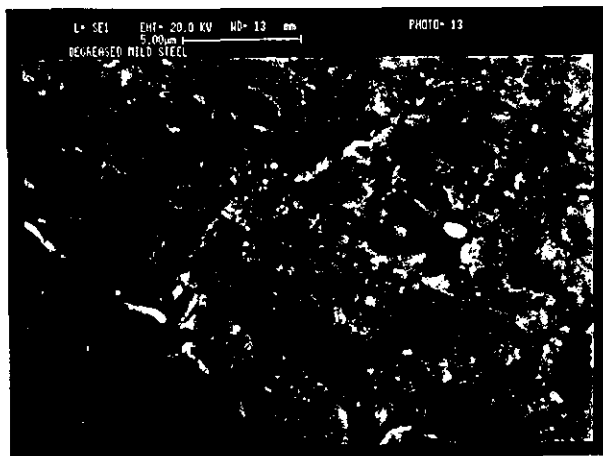


Photo 4.2.2e: SEM micrograph of degreased steel (magnification approx. x7000).

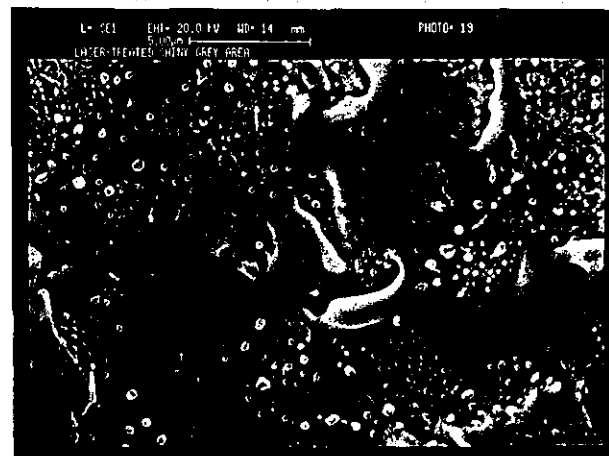


Photo 4.2.2g: SEM micrograph of grey area of laser treated steel (mag. approx. x7000).

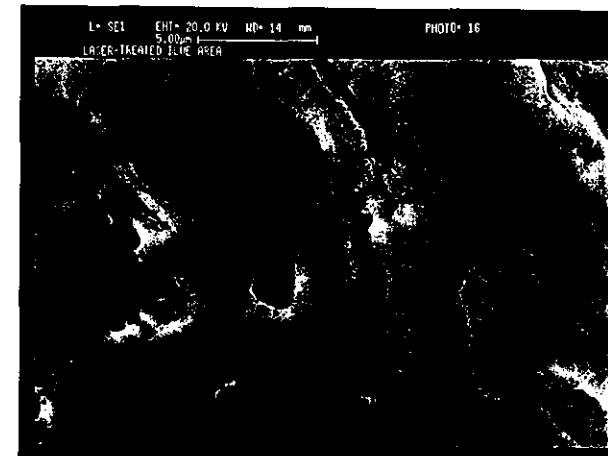


Photo 4.2.2i: SEM micrograph of blue area of laser treated steel (magnification approx. x7000).

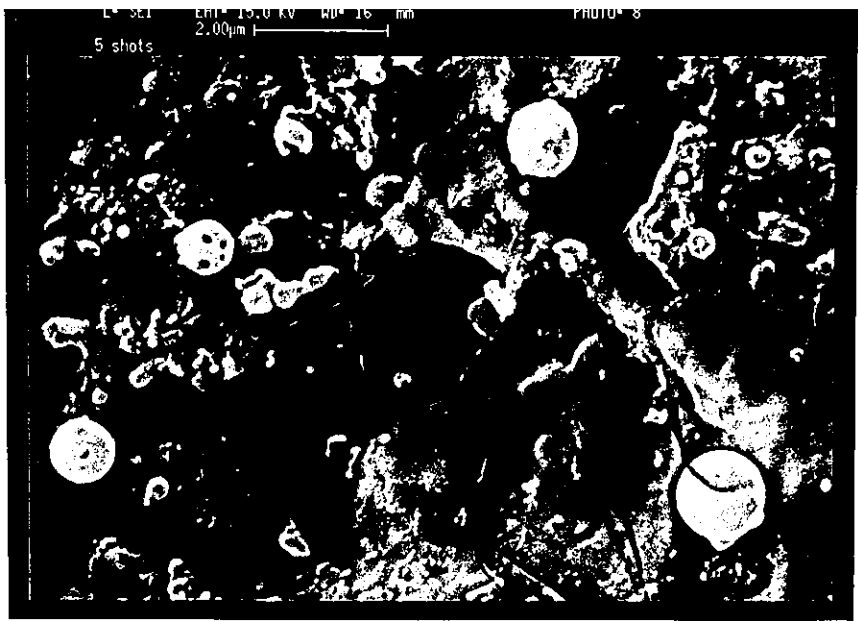


Photo 4.2.3d: SEM micrograph of laser treated HDG steel after 5 shots (magnification approx. x10000).

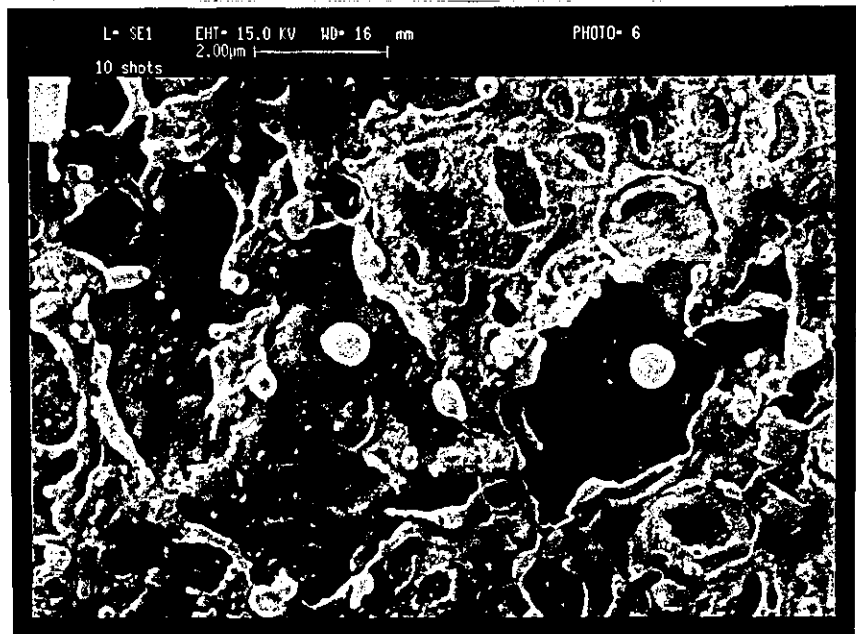


Photo 4.2.3e: SEM micrograph of laser treated HDG steel after 10 shots (magnification approx. x10000).

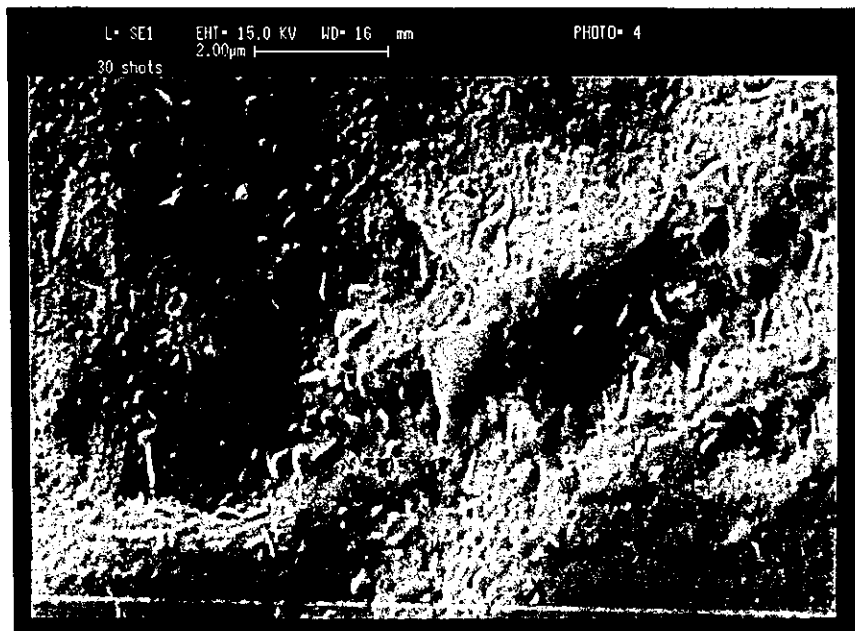


Photo 4.2.3f: SEM micrograph of laser treated HDG steel after 30 shots (magnification approx. x10000).

Chapter 5

Conclusions and Further Work

5.1 Conclusions

This thesis has considered the use of the TEA-CO₂ laser in many different metal cleaning and treatment applications. Throughout the experimental investigation an emphasis has been placed on the accumulation of broad-ranging empirical data to give a realistic impression of how the TEA-CO₂ laser will perform in different scenarios. This chapter presents the conclusions of this work and suggestions for further work where, due to limited time and resources, there still remains much to be done.

5.1.1 Metals without a coating.

Sub-plasma laser fluences

Metal cleaning applications that should not affect the metal substrate, such as those suitable for sculpture cleaning, require the use of sub-plasma laser fluences to avoid damage if the laser is the chosen method of cleaning. However, even at sub-plasma fluences, the TEA CO₂-laser was capable of either melting or oxidising certain metals, such as lead, or could potentially cause a temperature rise at the surface sufficient to induce phase changes in metals such as iron and steel (see Table 2.1). With other metals tested, however, no damage to the metal surface ensued from laser treatment and the laser could be considered as a self-limiting cleaning tool. These metals included copper, bronze, brass and silver which are all commonly used in sculpture and historic artefacts.

Plasma fluences

Although the production of a plasma above the surface of the metal target has been shown to induce oxidation on aluminium^[1], iron^[2] and galvanised mild steel^[3], to various

degrees, this may be advantageous in certain applications. Although the formation of the plasma prevents the majority of the laser beam from coupling directly with the metal surface, it achieves the complete removal of organic contamination, including the chemisorbed polar molecules that are not removed by sub-plasma laser treatment and normal degreasing processes.

In terms of using the laser in metal adhesion pretreatments, the high levels of surface cleanliness combined with the added effect of oxidation can produce an adhesive-receptive, passive layer that assists initial bond strength and bond durability. Again, however, we find this form of treatment is very much dependent on the target material.

Apart from performing consistently well on different adhesive systems, the laser treatment process has the following advantages over various other forms of commercial processes:

- **Simplicity:** the laser treatment is a simple, single step process that could be easily automated, monitored and optimised.
- **Economy:** there are no raw materials consumed in the LT process and, once the laser has been purchased, overheads are very low.
- **Cleanliness:** the LT process needs no chemical treatments at all. Other processes often require hazardous chemicals such as environmentally damaging volatile solvents used for initial degreasing and the unpleasant acids used in the conversion coatings. Recently imposed restrictions on the industrial use of volatile solvents^[4-7], such as the Montreal Protocol^[6] and the Clean Air Act^[7], are making laser cleaning technologies an attractive alternative.
- **Versatility:** although the three different metals used in these experiments did show some material dependency for the effectiveness of the LT process, the LT did not produce poor results under any of the conditions and it is likely that all metals will respond well to laser treatment. For example, TEA CO₂-laser treatment has been studied for use in dental applications where an improvement in shear strength by a

factor of 40 has been observed in Ti/PMMA joints compared with untreated controls^[8].

- Selectivity: the directionality of the beam and simple masking methods provide the user with control over precisely which area of the target is treated.

Other, less attractive attributes of laser treatment include the processing rate, typically varying from between 0.25 and 1 cm²/s for the present system depending on the condition of the substrate. For this reason, the current laser could not be considered a viable tool for large scale pretreatment processes although the ability to focus, mask and direct the laser may be useful for certain precision bonding requirements^[9].

The laser pre-treated adherends were shown to perform consistently well in comparative studies with popular alternatives in terms of initial joint strength and bond durability under small loads. SEM and AES analysis showed how the surface topography and surface chemistry altered due to the action of the laser. Visible spectroscopy provided an in-line method of monitoring and optimising the treatment process.

5.1.2 Metals with inorganic coatings

Although it was very difficult to predict how the laser would perform on different corroded targets, there did appear to be a clear difference in the laser's interaction with the complex corrosion products on the surface and the simple compounds that often form in contact with the metal.

It is usual for top-layer corrosion products to contain a high proportion of complex molecules, such as basic sulphates, nitrates, and carbonates, whereas the interfacial corrosion products are usually simple oxides, hydroxides, sulphides and chlorides. There is a clear tendency for the laser to remove the more complex corrosion products whilst the simple compounds remain. There are several reasons why this might be so:

- Complex molecules have far more vibrational energy states than simple molecules. Radiation in the region of that emitted by the CO₂-laser is absorbed primarily by the vibrational energy states of molecules which makes these complex molecules, in general, far more absorptive at a given wavelength, thus increasing their susceptibility to ablate. To illustrate this point, *Figs 3.2.1d and e* show the absorption spectrum of brochantite and cuprite for comparison.
- Surface corrosion products often contain hydrated or hydroxide groups. Water is well known for its strong absorption of CO₂-laser radiation and hence molecules containing hydrated or hydroxide groups can also be expected to exhibit strong absorptive properties in that region.
- Many complex compounds, such as basic sulphates, chlorides and carbonates, decompose at relatively low temperatures compared with the melting and boiling points of simple corrosion products. Thermal decomposition of these compounds is invariably accompanied by the expulsion of gaseous products such as water vapour and oxygen. Due to the rapid heating rates that can be achieved by laser ablation, the rapid discharge of gases from the thermal decomposition process can produce an explosive effect that could actively dislodge material.
- Simple compounds are less likely to be affected by the laser due to their typically higher transparency and their high melting and boiling points: simple inorganic compounds, such as NaCl, KCl and ZnSe, are commonly used for CO₂-laser windows and lenses. The proximity of the compounds to a metal heat-sink could impair the efficiency of the heating process by thermal conduction into the substrate.

Homogenous and heterogeneous coatings

There has been a tendency in this discussion, and also in other literature, to treat different corrosion layers as homogenous, discreet and uniform layers of single or mixtures of chemical compounds. XRD only provides evidence of the most abundant, crystalline chemical species and gives no indication as to how these species are distributed throughout the corrosion layers. This thesis has shown how corroded metals of very

similar chemical composition can react very differently to laser treatment. For example, a corrosion layer that may be unaffected by the laser may become susceptible to ablation if dispersed with just a small amount of absorptive chemical species.

There is a large, although finite, number of possible corrosion products that can form on metals, but there is an infinite number of possible mixtures and variations for the precise composition of the corrosion layers. As a result of this fact, the effect the laser will have on a given target can only be predicted with a limited degree of confidence and empirical results from representative samples would be very worthwhile to ensure the required effects are achieved on a given object.

Sculpture coatings

A possible application of the laser treatment process is in sculpture conservation. The laser cannot be considered as a panacea for corrosion problems and is unsuitable for many areas of work. These include

- Extreme corrosion: if the corrosion products contain information and detail of the original surface then it is likely that these will be removed by the laser as in *Case 2n*, the Roman coin. If surface corrosion is susceptible to ablation then its removal will usually proceed until the metal substrate is reached or a necessary change in the corrosion chemistry is encountered.
- Certain metals: lead has been shown to be oxidised or, at higher fluences, melted, by the laser. Fortunately, none of the other clean metals subjected to laser treatment showed any signs of damage.
- 'Layer-by-layer' corrosion removal: during the removal of external corrosion products, the laser invariably left a modified layer at the surface due to the thermal decomposition of the layer. For example, the brochantite layer in *Case 1n* (the copper roofing) could not be partially removed by the laser without leaving behind an unsightly, brown/black modified layer.

- Selective removal of complex corrosion products: the susceptibility of desirable, uniform patina, such as brochantite, to decompose at relatively low fluences negates the possibility to use the laser to remove unwanted corrosion products from such underlying layers as in *Case 4n*, the Liverbird sculpture.

However, there are also certain areas particularly suited to the laser treatment process.

These include

- Removal of organics: many outdoor sculptures have been painted or lacquered at some point and the remnants of these deteriorated coatings have become integrated with the rest of the corrosion products. The laser has been shown to be successful at the removal of all the fresh and aged organic coatings tested. The laser also has the potential to be used for the removal of graffiti.
- Removal of complex corrosion products: the laser can remove aggressive, external corrosion products to leave a bare metal substrate as in *Case 3n(i)*, the body of the blowtorch; or a passive interfacial layer as in *Case 4n*, the Liverbird sculpture.
- Treatment of localised corrosion effects: the directional aspect of the laser beam allows for the treatment of localised areas without risk of damage to the surrounding area.
- Passivation of corrosion products: in some cases, the laser may modify the corrosion products to increase their passive qualities as in *Case 5n*, the home-guard helmet.

This work presents the first detailed investigation of the use of CO₂-lasers to clean and treat various corrosion phenomena in the field of metal conservation^[10]. The process was applied to a wide variety of corrosive systems to provide a representative sample on which to make an evaluation. A variety of surface modification and cleaning effects have been identified using XRD, XPS, AES, colour photography and cross-sectional analysis^[11,12].

To a large extent, this work is inconclusive. Although throughout the investigation a detailed study was carried out on each object and a significant variety of objects were laser treated, there still requires a large amount of work to be done before the general capabilities of the laser in metal conservation can be assessed accurately. However, even within this small cross-section of cases, the laser has produced some promising results. A self-limiting cleaning regime has been demonstrated for the large majority of corrosive systems on most of the metal substrates considered in this study. Damage to the metal substrate was absent in all cases other than on lead targets. Undesirable exposure of the metal substrate due to laser cleaning occurred only in a minority of cases and often a passive, uniform interfacial layer became exposed and remained after laser treatment. The laser was also successful at removing all tested organic coatings, both paints and lacquers. The laser's ability at removing aged organic coatings is especially significant due to the problems these present in modern conservation.

Although the laser produced a variety of effects on corroded and patinated surfaces, by far the most common effect was the removal of external inorganic layers to reveal interfacial inorganic compounds. These layers were often oxides which were protective and typically stable, adherent, insoluble, hard and uniform. It is important to remember that the heating effect of a CO₂-laser pulse on a thin corrosion layer is likely to heat the metal far more significantly, due to absorption within the corrosion layer, than if it were incident on a clean metal surface. Although this didn't appear to present any problems in our investigation, it was clear that the surface temperature was elevated far in excess of those predicted by Table 2.1.

Various in-line observations have indicated possible methods of providing feedback to the conservator during the laser-treatment process. A flexible beam delivery system offers control and directionality for the user and would be a necessary appendage for regular conservation work.

The final assessment of the abilities of the laser as a cleaning system rests with the requirements of the individual conservator and is largely a matter of taste and experience. Although it is doubtful that the laser should replace any conventional conservation techniques, it could provide a useful alternative and become another weapon in the conservator's armoury against corrosion, and could also be used in conjunction with other conservation tools.

5.1.3 Metals with organic coatings

All organic coatings exposed to the CO₂-laser were susceptible to ablation^[13]. We can conclude:

- Organic coatings in general are likely to be susceptible to CO₂-laser ablation.
- Significant absorption takes place within organic media and allows for both paints and lacquers to be removed.
- Artificial and natural organic media were both removed by the laser.
- The effect of ageing and weathering does not prevent organic coatings being removed by the CO₂-laser.
- A very thin layer (not visible to the naked eye) frequently exists after the CO₂-laser removal of organic coatings. This layer is either carbon or hydrocarbon and is resilient to ablation at sub-plasma fluences, but can be removed at plasma fluences. It is not clear, at present, whether the layer is the remnants of the original coating or due to the re-deposition of blow-off material.
- Acoustic monitoring of the ablative-piston signal can provide feedback for the monitoring of layer-by-layer removal of laminated coatings.
- LIBS can provide an in-line monitoring technique for assessing the cleanliness of the metal surface during cleaning above the plasma threshold. Plasma fluences can remove organic residues that remain after sub-plasma cleaning.

5.2 Further Work

The potential exists for a great deal of research to be done in the field of the laser surface treatment of metals, in areas of both industry and conservation.

Adhesion pretreatments

Our initial work into the use of CO₂-lasers in metal adhesive pretreatments has shown very promising results although there has been little opportunity to optimise the process. There is plenty of scope to improve the efficiency and the effectiveness of the process, and also to expand the research to other metals not considered in this thesis. Where high-yield manufacturing processes are required, the automation of the laser treatment process would be desirable.

Conservation

The use of lasers in the field of metal sculpture conservation has even more possibilities. Our research concentrated on the use of CO₂-lasers due to the high reflectivity of metals at that wavelength; there are no other lasers capable of emitting high-powered pulses in that region. Current trends in laser technology have resulted in the development of pulsed mid-infrared lasers such as Q-switched Er:YAG, pulsed Holmium:YAG, and Q-switched CTE:YAG lasers emitting radiation at 2.9 μ m, 2.1 μ m and 2.7 μ m respectively and with power capabilities approaching those of the TEA-CO₂ laser used in our experiments. These lasers have found applications principally as medical lasers^[14-16] but may also have potential to produce good results in metal cleaning applications due to the high reflectivity of most metals in that region although, it should be noted, that these lasers are considerably more expensive than equivalent power TEA CO₂-lasers. Q-Switched Nd:YAG lasers, already popular in stone cleaning applications, emit radiation at 1.06 μ m at which metals are significantly more absorbing. Q-switched Nd:YAG lasers have been shown to melt copper, brass and aluminium at fluences required to remove

corrosion^[17,18], although they have produced good results on aluminium sculpture^[19] when used with care. Using lasers that emit radiation in the region of 1 μ m or shorter will result in a loss of the self-limiting nature of the cleaning process due to the decrease in reflectivity of metals as wavelength decreases. There is, however, research being carried out at these shorter wavelengths for the treatment of specific corrosion products, for example, the removal of corrosion products from green patina on copper using frequency doubled, Q-switched Nd:YAG lasers emitting radiation at 503nm^[20]. Furthermore, if in-line monitoring techniques can be developed to provide accurate feedback to the conservator, it may be possible to achieve good, controlled results for lasers of shorter wavelengths.

Of the metals investigated in this thesis, perhaps gold is the most significant omission. Gilding is present on a significant number of sculptures, is highly valued, but presents many problems for the conservator. Often the gilding is damaged and becomes sandwiched between corrosion products, making it very delicate. Gold is one of the best reflectors of 10.6 μ m radiation and CO₂-lasers would appear to have potential in removing corrosion products from gilding.

Perhaps the largest obstacle to the acceptance of lasers in conservation is the high cost of lasers in general. For the purchase of a laser to be economically viable it needs to be used frequently and offer considerable improvements on existing conservation methods. If in-line monitoring techniques could be developed to a high degree of reliability then it could be possible to use a single type of laser for all forms of cleaning and conservation.

Portability is an important factor if CO₂-lasers are to be a pragmatic method for conservation of outdoor sculpture. Although the TEA CO₂-laser used in our experiments is bulky, heavy and required an external gas supply, equivalent lasers are now available with far greater manoeuvrability. Laser Lines Ltd.^[21] provide large, but portable TEA CO₂-lasers capable of delivering 1-2J per pulse at 20Hz or greater. Sharplan Lasers^[22] can

provide highly-portable, pulsed CO₂-lasers that provide 400mJ per pulse at an average power of 150W, normally used for medical purposes.

5.3 Laser Safety

There are certain precautions that should be acknowledged during the use of high-powered lasers for ablation, especially if the laser is to be used in a public place.

Laser radiation

Body-tissue is significantly absorbing of CO₂-laser radiation. High-power laser radiation can damage the surface of the skin or the cornea of the eye. A simple method of reducing the range over which the laser beam is dangerous is by using a powerful focusing lens. A powerful lens increases the rate of divergence of any radiation reflected from the target material (once laser treatment is complete, the target is likely to be highly reflective) and hence the potential for the laser to do damage is reduced over distance. The user should wear appropriate laser goggles during operation and should work in a suitable enclosure in isolation from those without appropriate protection.

Noise

When the laser is used above the plasma-fluence, a considerable report is produced by the expanding plasma after each pulse. Ear protection is advisable for the comfort of the user.

Ablation products

Different materials will produce different ablation products, some will be dangerous and are unpleasant if the user is working in a confined area with poor ventilation. For example, acidic sulphur compounds were detected during the treatment of the copper roofing in *Case 1n*; Excimer laser treatment of fluoropolymers has been shown to

produce HF^[23,24]; polymer ablation in general can produce short-chain molecules that adhere to the lungs and oesophagus causing respiratory problems; copper alloys frequently contain small quantities of arsenic and antimony that have been known to concentrate near the surface^[25]. In general, it is advisable to use an efficient vacuum nozzle situated close to the target irradiation area to remove blow-off material as it is produced and to ensure that good ventilation is provided. If there is any reason to suspect that the ablation products could be especially dangerous, then further precautions, such as masks, should be considered. Anyone in doubt of the potential danger of ablation products should bear in mind the story of some unfortunate doctors who employed lasers for the removal of warts. After they experienced breathing problems it was discovered that warts had lined the walls of their breathing canals^[26].

References

- [1] Critchlow, G. W., Brewis, D. M., Emmony, D. C., Cottam, C. A., 'Initial investigation into the effectiveness of CO₂-laser treatment of aluminium for adhesive bonding', *Int. J. Adhesion and Adhesives*, 15(4), (1995), 233-236.
- [2] Critchlow, G. W., Cottam, C. A., Brewis, D. M., Emmony, D. C., 'Further investigation into the effectiveness of CO₂-laser treatment of metals for adhesive bonding', *Int. J. Adhesion and Adhesives*, 17(2), (1997), 143-150.
- [3] Critchlow, G. W., Bedwell, K. H., and Cottam, C. A., 'The effectiveness of CO₂-laser ablation for the treatment of HDG mild steel prior to adhesive bonding', submitted to the Transactions of Institute of Metal Finishing.
- [4] Takahara, H., Usui, M., 'Solvent recovery technique and purification of environment in adjustment to replacing CFCs and trichloroethane', *R&D: Research and Development*, 43(2), April 1993, 41-3.
- [5] Kirschner, E. M., 'Environmental, health concerns force shift in use of organic solvents', *Chemical and Engineering News*, 72(25), 20th June 1994, 13-20.
- [6] McIlroy, M. S., 'Investigation of laboratory methods for cleaning typical metallic surfaces using aqueous type cleaning agents', *ASTM Special Technical Publication*, 1197, (1993), 373-388.
- [7] Triplett, T., 'ABCs of VOC control', *Industrial Paint and Powder*, 72(5), May 1996, 4.
- [8] Buchman, A., Doduik, H., Rotel, M., and Zahavi, J., *J. Adhes. Sci. Technol.* 8(10), 1994, 1211-1224.
- [9] Muller, W. D., Seliger, K., Meyerand, J., and Gilbert, J. L., *J. Mater. Sci.: Mater. Med.*, 5, (1994), 692-4.
- [10] Cottam, C. A., Emmony, D. C., 'Laser cleaning of metals at infra-red wavelengths', *Proceedings of the Oct. 1995 LACONA I conference, Restauranterblatter, Verlag-Mayer*, (1997).
- [11] Cottam, C. A., Emmony, D. C., 'Practical assessment of the cleaning effect of CO₂-laser radiation on corroded metal', submitted for publication in the refereed proceedings of the 1997, LACONA II conference.
- [12] Cottam, C. A., Emmony, D. E., 'Exploratory observations of the TEA-CO₂ laser irradiation of corroded metals', submitted for publication to *Corrosion Science*.
- [13] Cottam, C. A., Cuesta, A., 'XPS monitoring of the removal of an aged polymer coating from a metal substrate by TEA-CO₂ laser ablation', accepted for publication in the *Journal of Material Science*, 5th April 1998.
- [14] Merberg, G. N., 'Current status of infrared fiber optics for medical laser power delivery', *Lasers in Surgery and Medicine*, 13(5), (1993), 572-6.
- [15] Parel, J. M., Ren, Q. S., Simon, G., 'Noncontact laser photothermal keratoplasty :1. Biophysical principles and laser-beam delivery', *Journal of Refractive and Corneal Surgery*, 10(5), (1994), 511-8.
- [16] Kermani, O., Lubatschowski, H., Ertmer, W., Krieglstein, G. K., 'Internal ablative sinostomy using a fiber delivered Q-switched CTE-YAG laser', *International Ophthalmology*, 17(4), (1993), 211-5.
- [17] Cottam, C. A., unpublished work.
- [18] Choe, Y., from *Nd:YAG Laser Cleaning of Metals*, MSc project, (1996).
- [19] Dalton, M., from *Q-Switched Nd:YAG Laser Cleaning of Gilbert's Eros Statue*, MSc project, (1993).
- [20] Berry, A., Lynton Lasers Ltd., unpublished work.
- [21] Laser Lines Ltd., Beaumont Close, Banbury, Oxon, OX16 7TQ, England.
- [22] Sharplan Lasers Europe Ltd., Merit House, Edgeware Road, Colindale, London NW9 5AF, England.
- [23] Berman, M. R., 'Excimer laser darkening of ETFE polymer films', *Journal of Applied Polymer Science*, 45, (1992), 111-7.
- [24] Wright, W. W., from *Degradation in Polymer Degradation-6*, Ed. N. Grassie, Elsevier, New York, 1985, 1-19.
- [25] Hughes, R., and Rowe, M., from *The Colouring, Bronzing and Patination of Metals*, Thames and Hudson Ltd., London, (1991), 10.
- [26] Friberg, T., 'Excimer laser removal of mould from paper: sterilisation and environmental considerations', presentation at the 2nd Lacona conference, April 1997.

Appendices

A: Electrochemical series

Metal	Electrode Potential (V)
Platinum	+1.20
Silver	+0.80
Copper	+0.35
Hydrogen	0.0
Lead	-0.13
Tin	-0.14
Nickel	-0.25
Cadmium	-0.42
Iron	-0.44
Zinc	-0.77
Aluminium	-1.34
Magnesium	-1.80
Sodium	-2.72

B: Colour of thin oxide films

Copper Oxide		Nickle Oxide		Iron Oxide	
Colour	Thickness (nm)	Colour	Thickness (nm)	Colour	Thickness (nm)
Dark brown	38	Pale brown	49	Straw	46
Red brown	42	Dark brown	54	Orange	52
Dark purple	45	Purple	57	Red brown	58
Dark violet	48	Dark violet	60	Purple	63
Dark blue	50	Dark blue	76	Violet	68
Blue green	83			Blue	72
Silvery green	88	Silvery green	112		
Yellow green	97	Yellow green	120		
Yellow	98	Yellow	126		
Old gold	111	Straw	135		
Orange	120	Yellow brown	162		
Red	126	Dark brown	172		

C: Gunmetal bronze formulation

LG3 BS 1400 (GUNMETAL BRONZE)	% by weight
Copper	Balance
Tin	6.210
Zinc	5.029
Lead	2.938
Iron	0.146
Nickel	0.450
Phosphorous	0.020
Arsenic	0.020
Antimony	0.136
Bismuth	0.001
Silicon	0.001
Aluminium	0.001
Manganese	0.002
Sulphur	0.030

D: Laserbrand 450 specification

Laser pulse energy (max) (J)	5.0
Laser pulse energy (min) (J)	4.25
Pulse width at half height (nS)	90
Pulse repetition frequency (max) (Hz)	10.0
Beam divergence (max) (mrad)	3
Beam divergence (min) (mrad)	2
Height of beam at output (min) (mm)	23
Width of beam at output (min) (mm)	27
Wavelength of laser radiation (nm)	10600
Dimensions (m)	0.7 x 0.57 x 0.75
Weight (kg)	120
Power consumption (max) (W)	900
Cooling system flow rate (min) (l/min)	2.0
Laser gas mix	He/CO ₂ /N ₂ /CO
Laser gas pressure at input (psig)	35-45

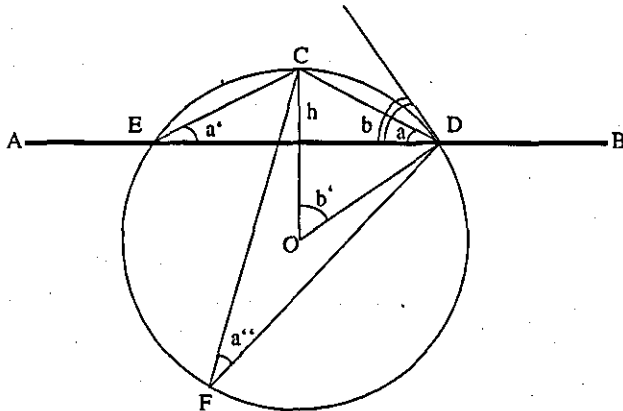
E: Hardness of materials

Material	Micro-hardness kg/mm ²
CuO	120-135
CuS	29-30
Green patina	46-115
Black patina	91
Copper	73
Bronze	91
Brass	121

F: Composition of Loess

Compound	Quantity	Compound	Quantity	Compound	Quantity
SiO ₂	59%	Fe ₂ O ₃	trace	Na ₂ O	trace
Al ₂ O ₃	11.5%	FeO	trace	K ₂ O	trace
CaCO ₃	15%	MgO	trace	H ₂ O	trace
MgCO ₃	5%	CaO	trace	P ₂ O ₅	trace

G: Derivation of the contact angle formula $\tan(\theta/2) = 2h/d$



If the water droplet is small, it can be represented as a segment, ECD of a circle about its centre, O, where AB represents the sample surface. The contact angle, b , is the angle between the tangent to the circle at point D and the surface. As this tangent is at right-angles to OD, and OC is perpendicular to AB, b and b' are equal. A geometric principle of circles is that the angle subtended at the centre of a circle by a given chord is twice that of the angle subtended at the circumference by the same chord, ie. b' is twice a'' . Another principle states that all angles subtended at the circumference from a given chord are equal, and hence a'' and a' are equal. From symmetry, a and a' are equal and hence it has been shown that b is twice a . From the diagram, $\tan a$ is equal to the height of the droplet divided by half the diameter and so, therefore, is $\tan b/2$, where b is represented as θ in the equation. This derivation is valid only if the drop is small since gravitational forces distort the shape of large drops. In this work, drop sizes were always less than 2mm in diameter and hence valid.

H: Glossary of common corrosion compounds and their mineral names

Name	Formula	Name	Formula	Name	Formula
Acanthite	Ag ₂ S	Chloragyrite	AgCl	Hydrocerussite	Pb ₃ (CO ₃) ₂ (OH) ₂
Akaganite	β-FeO(OH)	Cohenite	Fe ₃ C	Lepidocrocite	γ-FeO(OH)
Anarakite	(Cu,Zn) ₂ (OH) ₃ Cl	Covellite	CuS	Maghenite	γ-Fe ₂ O ₃
Antlerite	Cu ₃ (OH) ₄ SO ₄	Cuprite	Cu ₂ O	Malachite	Cu ₂ (CO ₃)(OH) ₂
Atacamite	α-Cu ₂ Cl(OH) ₃	Digenite	Cu _{1.8} S	Magnetite	Fe ₃ O ₄
Battlachite	Cu ₂ Cl(OH) ₃	Dilerophanite	Cu ₂ O(SO ₄)	Melanothallite	Cu ₂ OCl ₂
Brochantite	Cu ₄ SO ₄ (OH) ₆	Djurleite	Cu _{1.96} S	Nantokite	CuCl
Calumetite	Cu(OH,Cl) ₂ .2H ₂ O	Geerite	Cu _{1.6} S	Paratacamite	γ-Cu ₂ (OH) ₃ Cl
Cassiterite	SnO ₂	Gibbsite	Al(OH) ₃	Tenorite	CuO
Cerussite	PbCO ₃	Goethite	α-FeO(OH)	Romarchite	SnO
Chalcocite	Cu ₂ S	Hematite	Fe ₂ O ₃	Wuestite	FeO

